

R



*Research and Development
Annual Report
1992*

Research and Development Annual Report 1992

National Aeronautics and Space Administration
Lyndon B. Johnson Space Center
Houston, Texas

August 1993

Foreword

The NASA Johnson Space Center (JSC) primary research and development thrusts include: human spacecraft development, human support systems, and human spacecraft operations. We have invested significant resources in developing infrastructures such as facilities and partnerships that will enable us to address major technologies and cost-effective approaches for present and future Agency missions. We have already reported progress made in some of our projects in the 1992 Research and Technology Annual Report (RTAR). Only efforts pursued under Research and Operating Plans (RTOPs) are reported in the RTAR in a format suggested by NASA Headquarters. In consultation with academia, research institutions, industry, and JSC organizations, the need for reporting progress made on many of our projects in support of human spacecraft design, development, and operation was established last year. As a result, we are issuing for the first time this Research and Development Annual Report (RADAR) as a complement to the RTAR.

In all of our efforts, we actively seek and foster collaboration with other NASA centers, government agencies, academia and research communities, and industry. I believe sharing the knowledge through this report is crucial to the continued growth of this collaboration. Our goal is to provide reports which are responsive to the needs of our partners in industry, academia, and government communities. To this end, your comments and suggestions will be highly appreciated and should be mailed to Dr. Kumar Krishen, Code IA4, NASA Johnson Space Center, Houston, Texas 77058, or faxed to 713-244-8589.



Aaron Cohen
Director, Johnson Space Center

Contents

Acronym List	vii
Introduction	xi

Computer and Software

The Flight Analysis and Design System	3
Real-Time Data System	9
Extended Real-Time FEAT: A Tool for Real-Time Automated Failure Identification in the Control Center Complex	23
Consolidated Communications Facility	27
Improved FEAT Computation Times	33
Failure Environment Analysis Tool Applications	39
Application of Automation and Intelligent Software to Analysis of Engineering Space Shuttle Systems	47
A Monitoring System with Tolerance for Real-Time Data Problems	53
Integration of Advanced Teleoperation Technologies for Control of Space Robots	57
An Intelligent, Free-Flying Robot for Crew Help and Crew or Equipment Retrieval in Space	67
The Space Station Freedom Reliability and Maintainability Assessment Tool and Its Use for Prediction of Maintenance Demand	75
A Dynamic RMAT Model: A Method for Assessing the Space Station Freedom Program Functional Capability During Assembly Phase	79
Verification and Validation (V&V) of Knowledge Based Systems	83
NETS: A Tool for the Development and Delivery of Neural Networks	87
NASA Electronic Library System	91

Mission Operations

Optical and Photo Equipment Bracket for the Shuttle Starboard Overhead Window	3
Shuttle Orbiter Repackaged Galley (SORG)	7
Space Station Maintenance Studies Using Plaid Graphics	11

Medical and Life Sciences

Image Analysis and Flow Cytometric Measurements of Urokinase in Metastatic Cancer Cells	3
Time to Detection of Circulating Microbubbles as a Risk Factor for Decompression Sickness	15
Verification of Methods to Permit Flying after Diving in Neutral Buoyancy Facilities	17
The Effect of Gravitational Acceleration on Ventricular Filling: Diastolic Ventricular Function in Microgravity and 1g	19
Validation of the Clavicle/Shoulder Kinematics of a Human Computer Reach Model	21
A Preliminary Comparison and Validation of Computer Lighting Simulation Models for Space Applications Using Empirically Collected Data	25

Habitation Development Tool	31
Human-Computer Interaction Issues in Geographic Information Systems	35
Loads Produced by a Suited Operator Performing a Tool Task Without the Use of Foot Restraints	41

Space Systems Technology

Tunable Plasma Rockets with RF-Heating and Superconducting Thrust Chambers	3
Improved Power Tool Development	9
EMU Fuel Cell and Metal Hydride Hydrogen Storage System In-House Evaluation	13
Metal Oxide CO2 and Humidity Remover	17
Air-Bearing Fan	21
A Hybrid Regenerative Water Recovery System for Lunar/Mars Life Support Applications	25
Two-Phase Pressure Drop of Ammonia in Small Diameter Horizontal Tubes: Experimental Results	31
Two-Phase Flow Characterization for Fluid Components and Variable Gravity Conditions	37
Electromagnetic Probe Development for Fluid Flow Measurements	41
High Temperature Superconductivity Communications Flight Experiment	45
Computer Antenna Pointing for Space Station Freedom	51
A Mobile Communications Space Link Between the Space Shuttle Orbiter and the Advanced Communications Technology Satellite	55
Hybrid Vision's Eye Tracking	61
Spacecraft Gliding Parachute Autoland Project - Status	65
Avionics Reference Model	71

Acronym List

A

AC alternating current
 ACCT advanced control center technologies
 ACFM actual cubic feet per minute
 ACRV assured crew return vehicle
 ACTS advanced communications technology satellite
 AGL above ground level
 AI artificial intelligence
 AIS automated information security
 ANOVA univariate analysis of variance
 AOS acquisition of signal
 APFR adjustable portable foot restraint
 ADIC application specific integrated circuit
 ata atmospheres absolute pressure
 ATCS active thermal control system

B

BLSS bus loss smart system
 BPSK biphas shift keying
 Btu British thermal unit

C

CCC Consolidated Control Center
 Control Center Complex
 CCF Consolidated Communications Facility
 CCSDS consultative committee for space data systems
 CDROM compact disk read only memory
 CDRS consolidated data recording subsystem
 CDS consolidated distribution subsystem
 CDSS consolidated data select switch
 CETA crew and equipment translation aid
 CO₂ carbon dioxide
 COOPES cooperative expert systems
 COTS commercial off the shelf

D

D/L downlink
 DARPA Defense Advanced Research Projects
 DART dexterous anthropomorphic robotic test bed
 DDS digraph data system
 DDT direct drive test
 DESSY decision support system
 DFS depth first search
 DHM dexterous hand masters
 DLL dynamic link library
 DNA deoxyribonucleic acid
 DDE dynamic data exchange

DPSK differential phase shift keying
 DSP digital signal processor
 DTIC Defense Technical Information Center
 DTO Development Test Objective

E

EAM exoskeleton arm masters
 ECLSS environmental control and life support system
 EECOM electrical, emergency, and consumables manager
 EEI external entity interface
 EMI electromagnetic interface
 EMU extravehicular mobility unit
 EP equivalent person
 ERF extended real-time FEAT
 ESE + T EVA stowage of equipment and tools
 ESTL Electronic Systems Test Laboratory
 EVA extravehicular activity

F

FADS flight analysis and design system
 FCESS fuel cell energy storage system
 FCM flow cytometry
 FCMS fuel cell monitoring system
 FCR flight control room
 FDCF Flight Design Computation Facility
 FDHB Flight Design Handbook
 FDI fault detection and identification
 FDIR fault detection, isolation, and recovery
 FDM fault detection and management
 FDWS flight director weather system
 FEAT failure environment analysis tool
 FEPS front-end processor subsystem
 FMEA failure mode effect analysis
 FT/RM fault tolerance analysis and redundancy management
 FY fiscal year

G

GFAP glial fibrillary acidic protein
 GIS geographic information systems
 GNC guidance, navigation, and control
 GPS global positioning system
 GSE ground support equipment

H

H/W hardware
 HCIL Human - Computer Interaction Laboratory
 HDT habitation development tool

HDTV high-definition television
 HGA high-gain antenna
 HMD head-mounted display
 HMW high molecular weight
 HRWRS hybrid regenerative water recovery system
 HTSC high temperature super conductors
 HST Hubble Space Telescope

I

I/F interface
 IC inorganic carbon
 Isp specific impulse
 ICM image cytometry
 IEEE Institute of Electrical and Electronic Engineers

IR information retrieval
 ISO OSI International Organization for Standardization Open Systems Interconnection
 IVA intravehicular activity

JIN JSC information network
 JPL Jet Propulsion Laboratory
 JTC joint transform correlator

L

L/D lift-to-drag
 LAN local area network
 LEO-GEO low Earth orbit to geostationary orbit
 LeRC Lewis Research Center
 LESCC Lockheed Engineering and Sciences Corporation
 LiOH lithium hydroxide
 LMW low molecular weight
 LOS loss of signal
 LTS lunar transportation system

M

MANOVA multivariate analysis of variance
 MBS mobile based servicer
 MCC Mission Control Center
 MCCU Mission Control Center upgrade
 MDSSC McDonnell Douglas Space Systems Company
 MEL minimum equipment list
 MER mission evaluation room
 MICOM Missile Command (U.S. Army)
 MIDAS MER Intelligent Diagnostic and Analysis System
 mmHg millimeters of mercury
 MMIC monolithic microwave integrated circuit
 MOC mission operations computer
 MOCHR metal oxide CO₂ and humidity remover
 MOD Mission Operations Directorate
 MPM Manipulator positioning mechanism
 MPSR multipurpose support room
 MR mixture ratio

mrad milliradians
 MRL manipulator retention latches
 MTBF mean time between failure
 MTTR mean time to repair

N

NELS NASA electronic library system

O

OAFE Orbiter/ACTS flight experiment
 OMS orbital maneuvering system
 ORVs on-orbit retrievable units

P

PAs plasminogen activators
 PBT playback trainer
 PC personal computer
 PDRS payload data and retrieval system
 PFR portable foot restraint
 PI propidium iodide
 PLSSB portable life support system breadboard
 PLSS portable life support system
 PRS procedural reasoning system
 PRSD power reactant storage and distribution systems
 psi pounds per square inch
 psia pounds per square inch absolute
 psig pounds per square inch gauge
 PSPA phase shift/power amplifier
 PWP portable work platform

R

R&M reliability and maintainability
 RCS reaction control system
 RF radio frequency
 RFP request for proposals
 RGA rate gyro assembly
 RMAT reliability and maintainability assessment tool
 RMS remote manipulator system
 root mean square
 reverse osmosis
 RO Rockwell Palo Alto Laboratory
 RPAL
 rpm revolutions per minute
 RTDS real-time data system
 RTOP Research and Technology Objectives and Plans

S

SIRA Shuttle Integrated Risk Assessment Project
 SMS Shuttle mission simulator
 SORG Shuttle Orbiter repackaged galley
 SOW statement of work
 SSCC Space Station Control Center
 SSEIC Space Station Engineering Integration Contractor

SSEOP Space Shuttle Earth Observation Project
SSF Space Station Freedom
SSP Space Shuttle Program
STIG Space Technology Interdependency Group
STS Space Transportation System

T

TCS test and checkout subsystem
TDRS tracking data and relay system
TDS total dissolved solids
TiO₂ titanium dioxide
TMIS technical management information system
TOC total organic carbon
TRASYS thermal radiation analyzer system
TRIP teleoperated robot
TSS tethered satellite system

U

U/L uplink
ULC unpressurized logistics carrier

uPA urokinase
USAF United States Air Force
UV ultraviolet

V

VEXO voltage controlled crystal oscillator

W

WAIS wide area information server
WSTF White Sands Training Facility
WWCTS waste water collection and transport system

Z

ZOE zone of exclusion

INTRODUCTION

The decision to publish the Johnson Space Center (JSC) Research and Development Annual Report (RADAR) was made through a detailed process involving industry, academia, research institutions, and JSC organizations. These groups identified the need for a method of reporting significant JSC accomplishments which are not funded by Research and Technology Operating Plans (RTOPs). That work which is funded through RTOPs is currently reported in the Research and Technology Annual Report (RTAR); RADAR will serve as a complement to that report. Concurrent with identifying a need for the RADAR, a more detailed format than the one used on the RTAR was developed. The enthusiastic support of JSC organizations produced a number of submissions, from which we selected a variety of papers that illustrate the substantial accomplishments JSC achieved in 1992.

This report describes projects that support the primary mission of JSC and focus on human spacecraft design, development, and operation. Also of prime importance to JSC mission success are support systems that are essential to human spacecraft safety and reliability. As a consequence of the emphasis at JSC on human spacecraft research and technology, the results of our activities have found and continue to find wide applications in civil and commercial areas. In a recent review, the JSC Technology Coordinating Committee Action Team¹ developed a list of JSC technologies and markets which could potentially benefit from our research and development. A summary of these technology development activities is listed in table 1.

The emerging technologies at JSC include advanced materials, superconductors, advanced semiconductors, digital imaging, high density data storage, high performance computers, optoelectronics, artificial intelligence, flexible computer integrated manufacturing (robotics and automation), sensor technology, biotechnology, medical devices and diagnosis, life

support, extravehicular and intravehicular activity (EVA and IVA) and human factors. JSC is expending substantial effort in developing interdependent research and technology programs with the Department of Defense, the Advanced Research Projects Agency, the Ballistic Missile Defense Organization, and the Department of Energy. The principal goals of these programs are to promote communication, share lessons learned, and realize cost savings through shared facilities and resources. Also being developed are partnerships with universities and research institutions to address critical research and development that will require their participation. Finally, we are promoting the transfer of our knowledge and technology to academia and industry to strengthen America's industrial competitiveness. We have an impressive record of achievements in technology transfer and are redoubling our efforts in this area.

We are eager to communicate the results of our research and development in all areas. To this end, we decided to issue the first RADAR to complement the RTAR. We deliberately chose a format which gives more detailed descriptions of the projects than the RTAR. In the years to come, we believe RADAR will become the Center's unique report which highlights our yearly research and development accomplishments.

Your feedback and comments will be crucial in making this report valuable to the community of managers, researchers, academicians, and developers it serves. Should you have any comments or suggestions, I can be reached via fax at (713) 244-8589.


Kumar Krishen, Ph.D.
Chief Technologist

¹ Robert Ried, Bill Eggleston, Kumar Krishen, Audrey Schwartz, Earle Crum, Dick Ramsell, Bob Savely, James Villarreal, Phil Deans of JSC and Robin Lineberger of KPMG.

Table 1. JSC Technology Development Activities

EMERGING TECHNOLOGY/JSC TECHNOLOGIES	INTERNATIONAL COMPETITIVE POSITION	LIKELY MARKETS	COMMENTS
Advanced Materials <ul style="list-style-type: none"> • Ceramic Composites • Space Durable Coatings • Entry Thermal Protection Systems • Hypervelocity Impact Shield • Fracture Mechanics Analysis Tools 	<p>Certainly competitive and probably leading in all areas.</p>	<ul style="list-style-type: none"> • Aerospace/Defense/Space • Construction Industry • Consumer Products • Manufacturing • Engineering (Fracture Analysis) 	
Superconductors <ul style="list-style-type: none"> • Antenna System Applications • Magnetics Systems Applications 	<p>Applications are in a leading position.</p>	<ul style="list-style-type: none"> • Aerospace • Manufacturing • Energy 	<ul style="list-style-type: none"> • JSC coordination with high temperature superconductor researcher on antenna applications. • Magnetic systems may have later applications to spacecraft docking and payload handling.
Advanced Semiconductor <ul style="list-style-type: none"> • Vertical Stack Devices • X-Ray Lithographic • Gallium Arsenide • Etching • Ebeam, Epitaxial Bonding • Analog Devices, DSP • Bio Sensors 		<ul style="list-style-type: none"> • Telecommunications • Satellites • Microwave • IR Detectors • Fiber Optics 	
Digital Imaging <ul style="list-style-type: none"> • Pattern Recognition • Virtual Reality • Video Rate Image Warping • DSP • High Definition Television • Chromosome Analysis • Digital Image Compression • Retinography • Electronic Still Camera 	<p>JSC requirements are drivers of technology for space specific applications.</p> <p>Available US technology is about even with the Japanese.</p>	<ul style="list-style-type: none"> • Medical/Health Care • Computer/Communications • Law Enforcement • Nuclear Industry • Environment • Photo Industry • IC Industry • Mapping • Aerospace/Defense/Space 	<ul style="list-style-type: none"> • Strong benefit from existing Technology Utilization program and from ties with military partners, DARPA and national labs.
High Density Data Storage <ul style="list-style-type: none"> • Ferroelectric • CD ROM • Gigabyte Storage 		<ul style="list-style-type: none"> • Computer • Aerospace/Defense/Space • All Industry Users of Computers 	<ul style="list-style-type: none"> • JSC is currently applying these technologies.
High Performance Computers <ul style="list-style-type: none"> • Parallel Processing • Neural Networks 		<ul style="list-style-type: none"> • Computer • Aerospace/Defense/Space • All Industry Users of Computers 	

Table 1. JSC Technology Development Activities (Continued)

EMERGING TECHNOLOGY/JSC TECHNOLOGIES	INTERNATIONAL COMPETITIVE POSITION	LIKELY MARKETS	COMMENTS
Optoelectronics <ul style="list-style-type: none"> • Spatial Light Modulators • Fast Joint Transformation Correlators • Optimal Filter Theory 	JSC conducts and supports state of the art work in filter theory.	<ul style="list-style-type: none"> • Medical • Manufacturing 	<ul style="list-style-type: none"> • The JSC program has benefited more from military funding and cooperation than from NASA funding.
Artificial Intelligence <ul style="list-style-type: none"> • Expert Systems • Fuzzy Logic • Neural Networks • Automation of Operations • Automation of Eng. Analysis • Human-Computer Interaction 	<ul style="list-style-type: none"> • Overall competitive: application of high performance computing to AI and Expert systems. • Lagging: advanced software engineering, fuzzy logic, and neural networks. 	<ul style="list-style-type: none"> • AI can be applied to virtually any industry. 	
Flexible Computer Integrated Manufacturing (Robotics/Telerobotics) <ul style="list-style-type: none"> • Telescience • Virtual Reality • Remote Operator Interaction • Integrating SSF Robots for Assembly and Maintenance • Dextrous End Effector • Evaluating Robotic Technologies • Fault Tolerant Robots 	<ul style="list-style-type: none"> • As far as space robotics is concerned, the JSC program is the best in the world. With respect to robotics in general, JSC is competitive. 	<ul style="list-style-type: none"> • Medical Technology • Automotive • Chemical • Environmental Cleanup • Petrochemical • Manufacturing • Telerobotics • Aerospace/Space/Defense 	
Sensor Technology <ul style="list-style-type: none"> • Types/Categories (Infrared, Nuclear Magnetic Resonance, Magnetic, Ultrasonic, Temperature, Chemometric) • Impedance Imaging • Smart Sensors • Plasma Grid Detector • Backwater Mossbauer Spectrometer (BAMS) • Thermal Analysis Analyzer • Ultra Sensitivity Instrumental Neutron Activation Analysis 		<ul style="list-style-type: none"> • Most industries will benefit from this technology development area, especially the medical and health care industries. 	Benefits of JSC sensor technology include <ul style="list-style-type: none"> • Noninvasive Monitoring • Reduction in Size of Equipment • Decrease Cost of Health Care
Biotechnology <ul style="list-style-type: none"> • Bioreactor • Tissue Equivalent Proportional Counter (TEPC) • Cell Support Systems • Understanding of Osteoporosis, Immunology, Cell Biochemistry 		<ul style="list-style-type: none"> • Aerospace/Defense/Space • Nuclear Power • Pharmaceutical • Biotechnology • Health Industry 	<ul style="list-style-type: none"> • SSF will play a major driving/applying role in this area. • JSC Bioreactor is being marketed by Synthecon, Inc. through a JSC technology utilization program.

Table 1. JSC Technology Development Activities (Continued)

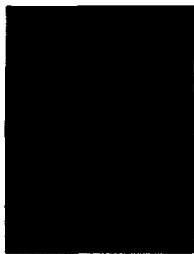
EMERGING TECHNOLOGY/JSC TECHNOLOGIES	INTERNATIONAL COMPETITIVE POSITION	LIKELY MARKETS	COMMENTS
<p>Medical Devices and Diagnosis</p> <ul style="list-style-type: none"> • Image Warping and Patterned Sensors • Joint Transformation Correlation • Data Reduction and Analysis Algorithms for Sensors • Dried Blood Collection/Analysis Techniques • Behavioral Performance Devices/Algorithms • Echocardiography • Electrical Muscle Stimulation • Robust Exercise Equipment • Medical Equipment Computer • Advanced Life Support (Training, Equipment, Supplies and Layout) 	<ul style="list-style-type: none"> • Competitive for the category • Leading in the development of an integrated portable medical computer system, and in innovations on training 	<ul style="list-style-type: none"> • Medical/Health Care • Education • Sports • Aerospace/Defense/Space • Law Enforcement • Consumer Products • Environmental 	<ul style="list-style-type: none"> • Strong benefit from existing technology utilization program • Working with University of Texas Medical School and Baylor University Medical School in medical devices/diagnosis areas
<p>Life Support</p> <ul style="list-style-type: none"> • Air Revitalization • Water Recovery • Food Storage and Preparation • Waste Management and Processing • Resource Recovery • Thermal Control • Long Duration Testing (Testbed) • Environmental Quality Monitoring Technology • Closed Environment Requirements and Microbiology and Toxicology 	<p>In general terms, those systems/requirements in the US are similar to the Russians; the technologies are roughly equivalent. The Russians are ahead of US in regenerative life support technologies because of their utilization of those technologies on the MIR space station.</p>	<ul style="list-style-type: none"> • Aerospace/Space • Environmental • Medical • Construction/Building • Agriculture/Food Processing 	<ul style="list-style-type: none"> • JSC efforts in biological life support very closely parallel the natural environment and may have potential for helping environmental problems on Earth.
<p>EVA</p> <ul style="list-style-type: none"> • Air Revitalization • Thermal Control • Power/Batteries • Displays and Control • Weight Reduction • High Mobility • In-Suit Monitoring • Mobility/Ease of Work • Protection from Decompression Sickness 	<p>Generally ahead of the Russians in that the US uses a combination of throw-away, low logistics systems, and regenerative systems, whereas Russia generally uses only throw-away systems. The Europeans are expected to use American technology.</p>	<ul style="list-style-type: none"> • Aerospace/Defense/Space • Nuclear • Environmental Cleanup • Medical/Health Care • Hazardous Environments • Manufacturing 	

Table 1. JSC Technology Development Activities (Concluded)

EMERGING TECHNOLOGY/JSC TECHNOLOGIES	INTERNATIONAL COMPETITIVE POSITION	LIKELY MARKETS	COMMENTS
<p>Human Factors</p> <ul style="list-style-type: none"> • Anthropometry and Biomechanics • Computerized Human Modeling (Animation, Lighting) • Human-Computer Interfaces • Virtual Reality for EVA • Personal Emergency Provisions • Tools and Diagnostic Equipment • Escape Systems • Crew Health Care Systems —Countermeasures • Display Panels • Computer Input Devices • Instrument Noise Abatement • Instrument Vibration Isolation • Performance Evaluation • User Friendly Science Monitoring Workstations • Crew Systems 		<ul style="list-style-type: none"> • Aerospace/Defense/Space • Architecture • Medical Technology • Education • Sports (Equipment and Training) • Law Enforcement • Manufacturing and Design • Consumer Products • Environmental • Mapping • Software and Hardware Development • Subsea Exploration • Nuclear Plant Operation • Food Industry 	<ul style="list-style-type: none"> • Animation Software and Human Modeling Available to Public • Research Products Passed on to Industry and Universities; Will Benefit Consumers and Quality of Life • SSF and Advanced Programs Important Drivers in This Area



*Computer
and
Software*



The Flight Analysis and Design System

Charles F. Deiterich
Johnson Space Center/DC

Abstract

The flight and analysis system is a computational environment, including application software, that supports the Space Shuttle Program in the area of flight design. This system was developed to replace several specialized and separate systems which mainly evolved from engineering tools. FADS is an integrated system which provides electronic data sharing, increased throughput for both production and analysis and high productivity for the flight designer.

Introduction

The Flight Design Computational Facility (FDCF) systems have been the cornerstone of the flight analysis and design efforts at JSC for the Shuttle Program; they have supported all Space Shuttle Program (SSP) flights through 1992. A flow evaluation team (1986-1988) determined that the support environment could not prepare for the expected flight rates by 1992 without an unacceptable increase in either personnel or program risk. It was also determined that the flight design (FD) process was computer resource limited, not manpower limited. The flight analysis and design system (FADS) development effort (1989-1992) responds to this identified need of safing the FD support system by 1992.

FADS is intended to increase system safety by reducing manual data entry and increasing designer efficiency. These results are expected through the use of:

- Electronic transfer of both internal and external products
- Archiving of products for later use or analysis
- Common and automated services for input processing and output processing, including data checking
- A data base to allow sharing of data between applications
- Reduced turnaround times

Description

The flight design and analysis system is a computer environment that provides the computational base of the highly complex and critical FD process. Flight design is the process of integrating payload requirements and mission objectives into a mission and trajectory design that satisfies SSP and Orbiter constraints, ground capabilities, and crew procedures and constraints. Flight design supports the following:

- Mission reconfiguration of ground facilities, such as the Mission Control Center (MCC) and the Shuttle mission simulator (SMS)

- Flight software reconfiguration for the Shuttle onboard computer systems, both the primary avionics software system and the backup flight system
- Plans and procedures used by the flight crew and flight control team
- Direct mission support that, on flight day, updates the onboard computer ascent guidance profile and provides entry/landing analyses prior to deorbit of the Shuttle
- Analyses and special studies

Approach

Flight design is a highly critical element of spaceflight from several points of view.

Products from the FD process are necessary to support complex training activities for both the ground controllers and flight crew. Mission success is very dependent upon trajectory design, maneuver targeting, and other FD products that directly support vehicle rendezvous, payload deploy/retrieval, consumables utilization, etc. From a safety aspect, the ascent guidance information (called I-loads or computer initialization loads) provided to the onboard computer is most critical for control of the Shuttle during powered ascent, followed by the guidance, navigation, and targeting parameters for deorbit, entry, and landing execution.

Of special note is the direct mission support activity that recalculates the ascent profile to update the Shuttle computer based on launch day-measured winds. Vehicle structural loads and ascent performance are predicted based on the flight day-measured environment received electronically by FADS. Ascent targets are modified as required to eliminate any loading violations and are tested via computer simulation. After review, these values or I-loads are electronically transferred to the Shuttle onboard guidance computer. Additionally, atmospheric flight analyses based on actual winds are used to support landing site selection and subsequent Shuttle flights through landing and rollout.

The FD process is supplied with a vast amount of input data from a variety of sources. Generally, the source of flight-specific input data is the Space Shuttle Program Office. Input include requirements, constraints, and characteristics. The data describe the Orbiter vehicle and configuration rules and guidelines, mission objectives (i.e., payloads, experiments, and test objectives), ground facilities (including capabilities and use criteria for launch and landing sites, control rooms, relay satellites, and ground-based communication sites), status and schedules of resources, special analyses and studies, and public affairs functions.

PRECEDING PAGE BLANK NOT FILMED
PAGE 2 INTENTIONALLY LEFT BLANK 3

The outputs consist of analysis, design, reconfiguration, and flight support products and services. The primary flight design output is a mission trajectory baseline that is used in Orbiter software, MCC operations, vehicle launch loadings, and program commit-to-flight activities. Alternate and contingency plans and data are also produced.

This FD process includes a feedback loop from the FD activities back to the source of input data, making it an iterative process between FD and the data sources. The major objective of this loop is to be able to redefine input so that all incompatible mission-related objectives, requirements, and constraints can be resolved.

There are many FD interfaces. Flight design receives input data and direction from the Flow Process Panel, from the Space Shuttle Program Office, and from the various configuration control boards.

Products and services of FD support crew activity planning, flight software generation, flight software verification, and mission development for other NASA and military centers.

Three general types of functions are performed by FD: analysis, flight product generation, and mission support. Singularly or in combinations, these functions are performed to achieve the objectives of FD.

- Analysis is an engineering investigation of various plausible options to determine which, if any, option achieves a pre-defined mission objective.
- Production is the preflight generation and dissemination of pertinent operational data and information for selected options.
- Direct mission support is the provision of experienced FD support to the real-time operational flight support team during actual or simulated flights. The majority of this support is related to trajectory topics.

The functions of FD can be characterized by an integrated system of generic models that converts various input data into FD output products. Output data are generally produced through the use of software tools installed on a computer or other hardware facility. By using established methods and procedures, the flight designer guides the process that translates input data into the desired output.

Some FD functions are iterative. That is, the results of the process are submitted back into the function for subsequent processing. Often, the use of output data is the major determining factor of the number of processing iterations necessary to complete the objective.

Many FD processes involve several functions. Each function performs a task that provides data to one or more other functions. The sum of the process structure—that is, the process network of functions—produces one or more objective output or products.

Each task performed within a network of functions is the responsibility of a single FD discipline (e.g., ascent). To satisfy the objectives, however, one or more FD disciplines may be called upon to perform discipline tasks. The final output of the process may be produced as a cooperative effort of many different elements of FD. Details of various

tasks performed by FD are documented in the Flight Design Handbook (FDHB).

An outcome of performing FD functions is that a number of data products are produced or services are rendered. The information contained in the data or the services rendered may be one or more of the following general types:

- Techniques are developed through analysis and are usually required when new or unique situations are encountered in a flight profile. Examples of this type of product include targeting methods for propulsive maneuvers, sequence of trajectory events in orbit operations, and propellant dump sequences.
- Design is the use of accepted techniques to develop standard flight products; for example, the nominal or unchanging trajectory in a flight path.
- Reconfiguration data and information are delivered to operational elements and facilities for those elements and facilities to reconfigure for the upcoming flight.
- Flight support is an FD service that supplies FD data and information in support of operational flight control elements either during simulation or actual flights.

Within the list of product categories, we find a variety of product properties. This is because of the varied use and required media of the receiving facilities. FADS has been designed and implemented to support the following product properties:

- Product complexity - Some FD products are simple values that represent some state or condition. Other products may contain information with complex and interactive relationships that will require a high degree of specific knowledge to comprehend fully.
- Product form and format - Products are produced in a variety of forms and formats. These forms and formats include tables, charts, drawings, text, etc.
- Volume of information - The FD product volume varies from a few data values to thousands of pages of printed tables and reels of magnetic tape. A few products are extremely voluminous and require massive storage methods.
- Product category - Each FD product is categorized by its potential or actual effect on the mission. At one end of the spectrum are those products that influence crew and vehicle safety and mission success. At the other end of the spectrum are those products that are generated for other purposes, such as public relations.
- Product media - Product media used within FD include electronic and magnetic tape, paper, microfiche, and other photographic means. The media are determined by the product user and flight designer facilities (e.g., hardware), the product's use (e.g., in support of a meeting), the proximity of the user to the flight designer, etc.

FADS is the primary computational capability for FD activities for the SSP.

Flight-specific information and mission requirement parameters are collected within FADS, are assessed, and are used to initialize and support FD computations and resulting products for SSP flight preparation. The open systems

design and the use of commercially available system service and user interface software have deemed FADS to be the platform of the future. Although Shuttle flight design was the initial FADS objective, Space Station Freedom (SSF) flight planning, design, and direct mission support are being implemented on FADS. The SSF capability will provide premission (pre-increment) planning for trajectory, vehicle consumables, power, logistics, maintenance, and crew activity scheduling, as well as for mission controller analyses and planning during the conduct of the actual SSF mission. Thus, this is the first step in demonstrating the ability of FADS to support future planning applications of yet to be defined programs.

Results

A description of FADS use and a system description follows:

- FADS provides the capability to produce detailed SSP FDs. Input to these flight designs are mission manifest requirements, payload operations constraints, MCC flight rules, and data that describe the Space Shuttle and its payloads (e.g., mass properties, aerodynamics, etc.). Detailed FD output include launch windows, predicted trajectories, onboard computer guidance parameters, groundtrack and communication coverage information, attitude profiles, consumables usage, payload deploy conditions, rendezvous and/or docking sequences, etc. This information is provided to the Software Production Facility, the MCC, the Shuttle Mission Training Facility, the Shuttle Avionics Integration Laboratory, other NASA centers, the Range Safety Office at Patrick Air Force Base, payload organizations, etc.
 - The platform is a totally networked system with 270 workstations, 27 file servers, 4 compute nodes, 2 data nodes, an archive server, and associated peripherals such as printers and plotters. Across the system there will be 412 Gbytes of storage, not including the unlimited storage of the archive server. About 2.4 million lines of code (ANSI C, FORTRAN 77, and commercial off the shelf (COTS) fourth-generation language) are contained within FADS which is a total of 553 programs that represent menus, scripts, and trajectory applications.
 - The system is menu-driven and supports batch, demand, and interactive jobs. Electronic data handling eliminates most manual input; turnaround time and system access are greatly improved over the current system. All of these things help the flight designer do a better and more precise job. As for the software developers, computer-aided software engineering tools, documentation, and other associated utilities reside on FADS to assist in the software developers' activities.
- Increases the safety of the FD process through reduction of errors inserted by the manual data handling needs of the former system. FADS provides for electronic data transfer, predefined or boilerplate data preparation scripts, a data management system for storage and control of all official data, and increased data management tools and processes.
 - Affords flight designers vastly increased productivity through the use of preset menus, the automation of data manipulation processes, the ability to retrieve archived analyses rather than recreating them, better and hands-on training for new flight designers, and a standard look and feel for the user interface across the entire user community.
 - Increases capacity and throughput by an order of magnitude. The flight designer can now turn around a large simulation of the Shuttle vehicle dynamics in a matter of a few minutes instead of the 2 to 3 days previously required. This will allow the design of Shuttle flights within a shorter template and with a minimum of user wait time.
 - Improves reliability and maintainability through the use of standard designs for system services, instead of multiple vendors with multiple operating systems. There is also an endless variety of graphics and reporting services to maintain, common approaches to software design across disciplines rather than 13 different ways of doing things, the use of COTS products instead of custom software developments, and the use of an open systems approach to the architecture and components provided with FADS.
 - Will simplify any modification to the system that is required in the future and will afford future savings as well. FADS is designed to be modular in all hardware and software aspects. Increased capacity can be achieved by the addition of small increments in workstation population. Reductions are also simplified if flight designer productivity increases to the point where equipment can be excessed. Individual workstations or entire suites of workstations, file servers, and compute nodes can be deleted from the system without loss of service for the remaining functions.

The significance to NASA is described in the objectives and associated accomplishments. Objectives of the FADS are to:

- "Safe" the Space Shuttle flight design system by providing a modern computer system that would minimize the manual data entry requirements in support of the hundreds of flight products required each year by the SSP flight rate.
- Solve the problem of the long user computer run turnaround time that existed with the flight design computer facility (FDCF) system.
- Provide a more efficient computing capability that would allow the flight design manpower requirements to be reduced by 50 equivalent persons (EP) per year.
- Consolidate and improve the over 3M lines of computer code that were part of the FD process.

Significance

Implementation of the FADS program provides significant improvement for flight design efforts at JSC in support of the SSP. FADS:

- Provide an electronic media for the FDHB (a desirable but not mandatory requirement) that would allow the flight designers easy access to process documentation.

To accomplish these objectives we must:

- "Safe" the Space Shuttle flight design system. With the workstation, compute node, and data node capability of the FADS system, an enormous amount of manual data entry requirements has been eliminated. With the electronic storage capability of FADS, almost all of the old system requirements for paper or microfiche products have been eliminated. This capability to eliminate microfiche was a significant factor in a separate Mission Operations Directorate initiative to reduce costs by deleting most of the microfiche facility. All of the objectives were met in "safing" the FD process.
- Solve the problem of the long user computer run turnaround time. With the compute power of the FADS system, the turnaround time problem has been completely eliminated. Computer runs that took hours to execute and days to get output on the FDCS system are being processed in a matter of minutes on the FADS system.
- Provide a more efficient computing capability. As a result of the FADS system design, the goal of reducing the flight design manpower requirements by 50 EP has been met and is effective as of FY93. In addition, the operating cost for the FADS system as compared to the FDCS system has allowed a reduction of approximately \$2.5M per year. This cost savings is effective as of April 1993. As a result of the application software consolidation effort, the Space Transportation System Operational Contract materials and maintenance budget is being reduced by 7 EP starting in FY94.
- Consolidate and improve. At the beginning of the FADS project, the FDCS contained 851 configuration items and had a code count of 3,694,600 lines. Most of this code was obsolete FORTRAN code. At the end of September 1992, the FADS system contained 258 application configuration items and had a total application code count of 1,951,215 lines (a reduction of 1,743,385 lines). All of the code had been upgraded to modern FORTRAN or to C code. As a result of the electronic interface capability of FADS, 117 configuration items of scripts and menus had been added to FADS. With this new code, the total FADS code count is 2,376,547 lines. This represents a net code savings of 1,318,053 lines.
- Provide an electronic media. The FADS system has delivered a capability for electronic display of the FDHB through the Framemaker COTS package. With this capability, the flight designer can use the windowing capability to display the product and process procedures at the same time the product is being executed on the FADS system.

Assessment of Use

FADS is now fully operational and is being employed by all disciplines for all phases of FD activity. This has

allowed us to eliminate the UNIVAC system, the Pyramid system, the Alliant systems, and the Perkin-Elmer systems from our inventory, thus reducing our operations costs in the maintenance of multiple systems. Development of new flight designers has been vastly improved with hands-on training of the FD processes. The engineering change cycle has been greatly reduced, which is a direct effect of the new structured software development environment. And, most importantly, the automation of data preparation processes has eliminated manual data manipulation and entry and has provided a measure of safety that was sorely needed.

FADS was developed to address some specific safety, capacity, and productivity concerns. Definite improvement in efficiency and productivity has already been seen. The existence of FADS, however, will foster a revolution in our approach to flight design for the SSP, thus providing tremendous potential for further and greater improvements. As designers and users become familiar with the benefits afforded by the FADS distributed environment, they will devise new approaches to their tasks. Anticipated improvements include conversion of batch applications to interactive processors, increased use of direct graphical interfaces instead of selection menus to simplify the user interfaces, consolidation of some serial functions into strings of processors that run together, and possibly even consolidation of disciplines or the generation of end-to-end FD applications.

FADS has been implemented to provide a long-term FD computation capability. Much of the design is based on allowing hardware, systems software, and COTS services to be replaced with minimal impact. As SSP support to the SSF and other advanced programs commences, the role of FADS in the flight preparation function will increase. In addition, the capability for SSF preflight preparation and direct mission support for trajectory control and flight planning is being added to FADS. FADS access is being expanded to provide support in the SSF preincrement area and in the Control Center Complex for actual mission control.

The FADS platform is a distributed processing environment with high-powered workstations interconnected to compute with data facilities. These will meet the basic needs of most NASA systems, which means the FADS design can service the needs of programs stretching from SSF support requirements (locally at JSC) to any administrative, engineering, or scientific tasks at any NASA facility. The FADS software design can provide FD simulation and trajectory planning needs for most NASA vehicles.

Creativity

The primary design approach to FADS is based on the concept of "open systems." This approach precludes a dependency on proprietary products and customized system elements, and it allows open competition for component replacement with minimal impact. The portable operating system interface for computer environments operating

system standard, ANSI "C," and ANSI FORTRAN 77 are specified.

The use of COTS hardware and software is to be maximized with only a minimum of custom software for mandatory system services. This approach has a smaller development cost and reduces the in-house sustaining engineering support.

A "bundled" acquisition process was used to procure COTS hardware and software. This new process involved the integration of all of the platform requirements and design constraints into one procurement. Bundled acquisition reduced the time required for procurement and greatly reduced the risk for the integration of COTS hardware and software instead of focusing on the technical accountability for platform implementation.

A distributed system is defined. Workstations are the user interface to FADS and, as such, allow immediate response for input and output data processing. Interactive trajectory and small to medium batch applications are executed on the workstation; however, the powerful compute nodes provide excellent throughput for large and highly iterative programs.

To gain the necessary background to produce adequate design requirements, a time-consuming and extremely difficult task of analyzing the evolving and very complex FD process would have been needed. In lieu of this study, workload reference models based on current system were developed and transformed into performance sizing needs. Similarly, data models were developed to determine mass storage sizing and specifications for centralized data storage for shared data.

A menu-driven system and a standardized user interface using COTS and common utilities were designed, which resulted in a user-friendly and productive tool.

With the advent of the increased standards for automated information security (AIS), significant new ground has been covered to assure a system that is fully compliant.

- Network hardware and software for a distributed system have been specified to meet the required AIS access and controls requirements.
- The capability to review input data and to provide virus checking prior to transfer to the main FADS has been implemented via a controlled external interface.
- Account and password controls have been designed to prevent unauthorized access.
- System activity is logged to provide an audit trail to assure data integrity.

Trajectory applications are being developed to a standard application model. Input and output file protocols are standardized to allow use of common system services. COTS packages are specified for the menu builder, graphics processor, and data management system tools.

Strict configuration management for critical and controlled application software has been implemented to assure quality and traceability results.

FADS resource usage and system performance monitoring are provided to manage the FD process properly.

Tangible Value

The following savings will be accrued:

- Increased productivity and efficiency have avoided a required increase of 50 EP (equivalent person) for flight designer staffing.
- A savings of \$2.5M/year is anticipated for FD computer systems operations.
- Consolidation and streamlining of the application software have resulted in an overall reduction of code. This reduction will decrease the required software maintenance effort by 7 EP.
- The FADS training environment for the associated MCC operators will reduce the simulation requirements placed on the MCC and support facilities.
- As originally planned in 1989, the project was completed in FY92 and was on schedule and within budget. Considerable efficiency in the FD process, production error elimination, improved software manageability, and user satisfaction are expected.

References

- ¹Flight Analysis and Design System Level A Requirements," Revision B, JSC 23683B, September 21, 1990.
- ²Project Management Plan for the Flight Analysis and Design System," JSC 23995, February 1990.

Acknowledgments

I would like to thank Rockwell and LORAL and their associates for their support. I would also like to thank all the NASA personnel for their contributions.

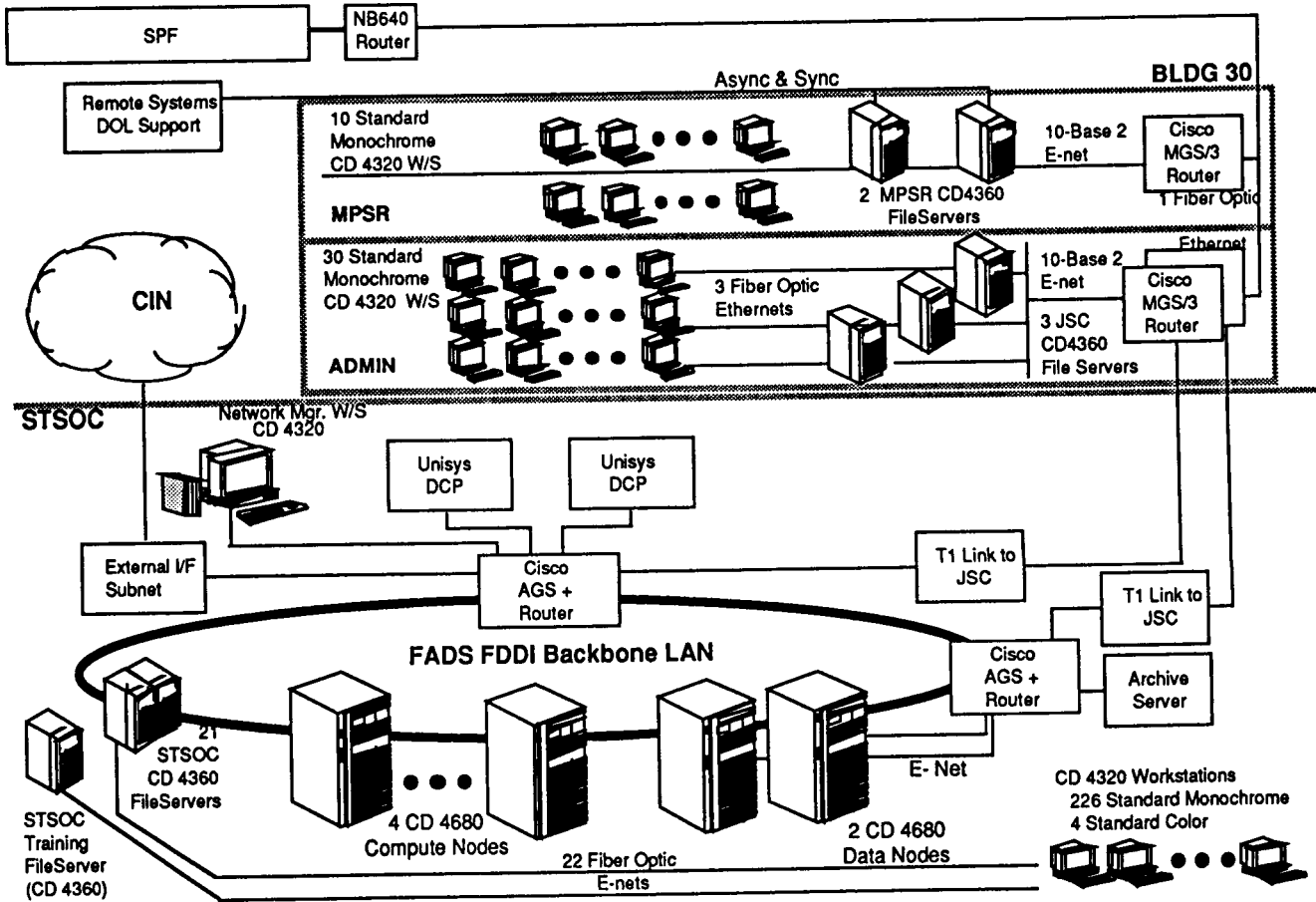


Figure 1. FADS High Level Architecture.

Real-Time Data System

Linda A. Perrine
Johnson Space Center/DF

Abstract

The real-time data system (RTDS) project is in its seventh year of operations within the Mission Operations Directorate (MOD) at JSC. RTDS continues to lead by example in the introduction of new technologies to the dynamic environment of Space Shuttle Mission Control Center (MCC) operations. RTDS also continues to sponsor a number of projects in the form of funding, manpower, and a development platform that allows for rapidly developed prototypes to be introduced into MCC operations on a noninterference basis. Many of the projects that RTDS has sponsored over the years have resulted in significant cost reduction and improvements in MCC operations efficiency. In this report we will summarize the highlights of RTDS accomplishments in 1992 and the current projects being worked in 1993.

Introduction

In the past year, significant changes have been made in the plans for the future of manned spacecraft control center development, plans that are affecting the future of the RTDS project. With the completion of the new Space Station Control Center (SSCC) (building 30S), plans were begun immediately to implement a new architecture for the new control center that could accommodate modern-day technology that would last for the 30-year life span of Space Station Freedom (SSF). The original plans for the SSCC called for it to act independently from the original MCC and for minimal communications to be possible between the two facilities owing to the 30-year difference in technologies between the two facilities. In June 1992, the decision was made to upgrade the MCC using the planned architecture for the SSCC, and this upgrade created what is known today as the Consolidated Control Center (CCC). The rationale supporting this decision factored in the improvement in communications between the two facilities and the reuse of the SSCC architecture in the MCC, thus showing substantive cost savings were possible after upgrading the MCC facility to newer, more sustainable technologies.

The CCC architecture consists of consoles built from commercial UNIX workstations and file servers, a fiber optic (FDDI) network backbone, a distributed common front-end system that will replace the current mission operations computer, and commercial software applications that exploit today's graphical user interface technologies. This will give a new, modern look and feel to the control center that will give JSC's control centers a

much needed face-lift and will allow for the introduction of tomorrow's technologies with a new approach to development and integration.

The technologies just described show that what RTDS has been demonstrating was possible for years. The RTDS project has played a significant role over its lifetime, proving that today's technologies can meet the requirements of our control centers and can improve the efficiency and safety of Space Shuttle operations. Although the RTDS project has succeeded in its original goal of moving the control center in the direction it is headed today, the project also has an important goal for the future: to continue introducing tomorrow's technologies to CCC mission operations. With NASA and MOD budgets being stretched to their limits, the only means of accomplishing control center technology research and development within MOD will be through money provided by the Research and Technology Objectives and Plans (RTOP) process. This is the role the follow-on project to RTDS intends to fulfill. We plan to refer to the successor of RTDS as Advanced Control Center Technologies (ACCT) and will be submitting FY94 and subsequent years funding requests using this project title.

Project Objectives

The RTDS project objectives continue to be consistent with those of past years. Among these are to:

- Inexpensively introduce new technology into real-time Space Shuttle operations
- Transfer applicable technology and applications into Space Station operations
- Improve the quality of flight controller real-time decisions using applied artificial intelligence and expert system technologies
- Improve the quality and efficiency of training for flight controllers using new technologies
- Provide a flight controller development platform externally from the control center for the purpose of exposing the end users of new technologies that RTDS explores as soon as possible, thus reducing development costs and discontinuing development quickly if it has no applicability to the particular discipline

The process by which RTDS accomplishes these objectives has been centered around a real-time telemetry processing and distribution system that was developed in the early years of the project. This feature of the RTDS platform has been essential to achieving the goals of the

project until now. With control center development moving towards a platform very similar to the one developed by RTDS over the years, the same necessity no longer exists to distribute our own real-time telemetry to the RTDS console workstations. Also, plans are being worked within MOD to locate all workstation-console development off the flight support workstations and into other facilities both inside and outside of the CCC facility. These are key factors for the change in project focus as the project transitions from the RTDS project to the ACCT project.

Several RTDS 1993 projects focus on planning for the change from providing our own telemetry distribution system to becoming a recipient of the new CCC telemetry distribution system. The first of these is the Gateway project, which is being managed and developed by RTDS personnel with support from Computer Sciences Corporation contractors. Gateway is developing an automated information security bridge between the level 3 CCC networks and the external, level 1 JSC information network (JIN). This will allow real-time CCC telemetry to be distributed around the Center to any building that has access to the JIN, and will allow limited authorized access from the JIN into the CCC networks. The second project, referred to as common data interface, is transferring the lessons learned from the RTDS approach to data distribution and acquisition to Loral contractors supporting the CCC implementation of telemetry acquisition. The final step for leaving the RTDS telemetry processing system will come towards the end of 1993, when the project will install several more workstations into the MCC side of building 30 on the RTDS network and will connect the RTDS network to the existing early commercial off-the-shelf (COTS) platform network that runs between the SSCC and the MCC. This last installation of RTDS-provided workstations will support many of this year's RTDS applications and will act as a transition platform for the Shuttle workstation software to be converted to the CCC platform. This is being presented to MOD management as an MCC-to-CCC workstation transition plan and is currently being reviewed by the various flight control organizations in MOD.

FY92 Accomplishments

The following summarizes the highlights of RTDS accomplishments in FY92. RTDS provides support and services to many organizations both inside and outside MOD in addition to its role as developer of new applications and technologies. RTDS also acted as MCC VIP host to a number of visitors during 1992, including the NATO AGARD committee (4/92), the Navy F-16 AI researchers (8/92), and the NASA Administrator Dan Goldin (9/92). What follows are the most significant successes for the past year of the project. (Note: The associated NASA photo number is listed with the project title in parentheses.)

Flight Director Weather System (FDWS) (S92 47203, S92 47200)

At the request of the flight director's office, the FDWS was developed to provide automated, real-time weather information at the flight director console in the main flight control room. A key element of safe and efficient conduct of Shuttle missions is an awareness of and a response to weather conditions at the primary landing sites, Kennedy Space Center, Florida; Edwards Air Force Base, California; and White Sands Missile Test Range, New Mexico. Prior to FDWS, the primary source of weather information for the flight director was through an audio voice link with weather office personnel. This required that the flight director absorb data by listening and jotting down sets of numbers describing wind directions, speeds, and runway designators. During periods such as prelaunch and deorbit preparation (when the flight director is occupied with many tasks), this form of data transmission was deemed unacceptably slow and distracting. The FDWS is now fully operational and is supporting all Space Shuttle missions. It has proved to be of great benefit for "situation at a glance" and history information that had been unavailable prior to its deployment. Its direct, simple set of displays and easy-to-use configuration selection have allowed it to be easily integrated into the flight director's regimen. The ready acceptance and continued use of the FDWS are the best testimonials to its success, and it now contributes to safer and more effective missions.

Remote Manipulator System (RMS) Position Monitor (S92 47198, S92 47197)

The RMS position monitor application represents the first step in MCC operations towards a graphical presentation of the physical relationship between the Shuttle, the RMS, and the payload that is attached to the RMS. This expert system makes significant progress in presenting telemetry to the flight controller in a manner that is much more meaningful than the tabular information presented on the current console hardware in the MCC. The RMS operator in the MCC traditionally has relied on digital presentation of RMS joint angles (arm, elbow, wrist) and live video downlinked by the crew to interpret current RMS positioning. The position monitor application provides pictorial views of the RMS, payload, and Shuttle payload bay in X, Y, Z axis views together with other telemetry and alert messages that can be arranged in four quadrants on one screen. When live video is unavailable, the RMS position monitor application often is used as a substitute on NASA Select TV to give the audience a picture of current onboard activities in real time.

The position monitor application has supported all 1992 missions that included RMS operations. Highlights included Space Transportation System (STS)-49, which featured a three-crewmember extravehicular activity

(EVA) in conjunction with RMS/Intelsat operations. STS-46 saw the RMS used to deploy the Eureka-1 satellite. Each new mission that requires that payloads be maneuvered by the RMS has a graphical model of the payload developed in the RMS flight planning system, which then provides the model of the payload used within the position monitor. The position monitor application is currently undergoing an upgrade to a Silicon Graphics surface model representation of the Shuttle, RMS, and payloads that will bring state-of-the-art, real-time graphics technology to MCC operations.

Playback Trainer (PBT) (S92 47180)

The PBT is a training facility developed for flight controller training in the Space Shuttle Program. The PBT was rapidly developed by reusing already established RTDS hardware and software to allow three DEC workstations to emulate green console displays and event indicator light panels. A series of Shuttle mission simulator (SMS) sessions was run to allow RTDS personnel to record a pre-scripted set of nominal and failure signatures for a variety of flight control disciplines. These recorded failure signatures were then organized into a set of lessons for each flight control discipline that is targeted to use this trainer. The intent is to off-load failure recognition type training objectives to a facility outside the expensive integrated MCC-SMS environment. Prior to the PBT, all training objectives required for flight controller certification had to occur in the integrated environment because no other facility existed to accomplish this aspect of each controller's training. The PBT is now operational in most of the targeted disciplines with a few recording sessions required for the remaining disciplines.

Booster Expert System (S92 47190, S92 47202)

The booster expert system continued operational flight support on the RTDS system in 1992. The series of displays that comprises this application has been formatted to present as much data in the most meaningful format possible. The system combines tabular data with plotted data and takes advantage of the color capabilities of the workstation to present limit violations. The booster application is the most flight tested of all RTDS applications, and support from RTDS is considered an essential backup system to the MOC and consoles. Another opportunity arose during the STS-50 ascent phase where the MOC lost some of the key booster computations and RTDS was able to act in place of the MOC for several minutes during ascent. These occurrences are not as infrequent as most people would like to believe.

The booster discipline is pressing ahead in its goal of becoming the first console position to operate completely from workstations. Within the next few months, the booster expert system will place a total of five

workstations behind the multipurpose support room (MPSR) consoles (3 Suns and 2 DEC's provided by RTDS) and will begin supporting simulations in the MPSR from a workstation-only configuration. After a simulation test period, a flight-following period, and, eventually, flight support from this configuration in the MPSR, we intend to replace the flight control room (FCR) console with a CCC workstation console configuration in 1994. Because the FCR console is shared by both the booster and payload data and retrieval system (PDRS) disciplines, the PDRS (RMS) console operators are making the same plans to be ready to operate from the same CCC console configuration in 1994.

Fuel Cell Monitoring System (FCMS) and Bus Loss Smart System (BLSS) (S92 47192, S92 47193)

The FCMS and BLSS applications are being developed using Gensym's G2 product and will complete the operational application in March 1993. These applications debut expert system technology at the electrical power system MPSR console position. The application represents a series of graphical displays that are organized in a hierarchy of information presentation and that provide real-time data via RTDS. The highest level display shows a pictorial representation of the Shuttle electrical distribution system. This display is fed by each of three separate displays that depict each fuel cell schematic. The two applications are tied together such that a fault in a particular fuel cell, which affects its ability to provide power to the main direct current bus associated with it, will be reflected in the bus loss series of displays. An early attempt at incorporating rules that reflect crew procedure malfunction flow diagrams has also been incorporated to assist the operator in assessing the impacts of any particular bus failure.

Procedural Reasoning System (PRS) (S92 47186)

The PRS operational evaluation project is running on schedule, with completion anticipated in April 1993. At that time, the SRI International and Australian AI Institute project team will meet at JSC to perform demonstrations of the system running against flight controller trainer simulator malfunction cases (and possibly RTDS data). The demonstrations will be performed on RTDS-provided workstations. The final report, which will describe the suitability of this technology to MCC-related tasks, will be provided shortly thereafter.

Recent efforts have demonstrated the robustness of the PRS inference engine against MOD-provided Shuttle orbital maneuvering system/reaction control system (OMS/RCS) malfunction cases. The current version of PRS handles all of the malfunctions, appropriately using the OMS/RCS knowledge base developed directly by PROP flight controllers. This knowledge base has been

improved recently to cope with most of the fault diagnosis and isolation activities anticipated for the system, and it is being further improved to handle the fault-recovery tasks necessary to bring redundant systems on-line. Recent work also has focused on the design of a run-time user interface that provides the user with a real-time status of PRS activities, permits the user to control system goals and behaviors, and enables the user to perform hypothetical reasoning.

Upon successful completion of this project, it is expected that MOD will request purchase through appropriate channels of a commercial version of the PRS inference engine and user interface.

VISTA

The VISTA project also is running on schedule, with anticipated completion in April 1993. At that time, the Rockwell Palo Alto Laboratory (RPAL) team will meet at JSC to perform demonstrations of the project ideas on RTDS-provided workstations.

The project intends to demonstrate the feasibility of applying decision-theoretic reasoning techniques to the problem of managing flight controller displays. At the same time, the project is demonstrating the feasibility of applying belief networks to the problem of monitoring and diagnosing the performance of Orbiter systems under uncertainty (including missing data). The PROP group is building workstation data displays for VISTA to control, through collaboration with the workstation window manager, at various levels of granularity. The RPAL group continues to improve display management ideas while establishing an interprocess communication protocol. Additionally, RPAL and PROP continue to collaborate on the development and improvement of belief network models for various OMS operations contexts.

Procurement of the Hugin belief network reasoning system, which will provide the inference engine for the reasoning system, has been completed and the product has been delivered and installed on the appropriate RTDS workstations. Procurement of the additional COTS tools has been completed at RPAL, and these tools are being used for software and interdisplay communication protocol development.

IDEA - INCO DataCOMM Expert Application

IDEA is an expert application that performs flight recorder logging. This application was specifically built to reduce the number of man-hours required to monitor and log Shuttle recorder information. With IDEA performing recorder logging, the instrumentation officer would perform commanding of recorders. The application emulates the recorder management displays and associates each recorder bit with its Greenwich mean time. In this manner, the application is cognizant of the data on the recorders. The application monitors the

quality of data provided by the RTDS. The quality is actually the number of frames per second that the RTDS telemetry processor is receiving. During acquisition of signal (AOS), the quality should score 100. The quality should be less than 100 when the data quality is degraded. Whenever the quality is not 100 for 5 or more seconds, IDEA records these data as loss of signal (LOS) by coloring the recorder bit red and by creating an LOS list. The application keeps track of LOS, AOS, and playback lists. AOS recorder bits are colored black. All recorder lists are printed to UNIX files as an archive.

PILOT - Workstation Process Monitor

The PILOT and autopilot applications are being developed with Gensym's G2 product to monitor the RTDS telemetry SEND and RECEIVE processes that are resident on the workstations that are distributing data and receiving data across the RTDS network. The autopilot software is resident on all client RTDS workstations; this software may act in either a send/receive mode. The PILOT application operates singularly at the RTDS operations management workstation, which presents to the RTDS operator a graphical presentation of the RTDS client and server workstations in a hierarchy view. PILOT tracks the client workstations send/receive processes and notifies the operator of problems at a particular console workstation after which the operator has the option of clicking on an icon of that workstation to bring up a window that will show activities on that node. The autopilots running on each client workstation have the ability to determine when a particular send/receive process has gone bad, has dropped data, or is no longer receiving data across the network; the autopilots can take action on their own to kill the bad process and restart a new process to regain normal send/receive processing.

PILOT debuted during the last Shuttle mission, STS-54. The RTDS operations staff was provided with opportunities to recommend improvements in user interface and functionality. The autopilot application has been in use since STS-47, and the application continues to be improved with each flight. Once these applications have reached an operational support capability, they will be demonstrated to the control center workstation LAN [local area network] controller operators, who will manage the operational workstations, to determine further development that could eventually be used in the management of the CCC console workstations.

Office MPSR (S92 47181)

The office MPSR project plans to explore the potential of running UNIX, X-Window applications natively on a UNIX workstation but also of presenting the application on a personal computer (PC) class computer. This project has the potential of allowing an inexpensive means of monitoring control center applications, with

real-time data, from flight controller office PCs. In 1992, commercial software was purchased that is required to be running on the PC to communicate to a UNIX workstation. Several products were evaluated and 31 licenses of Hummingbird Communication's HCL-eXceed X-server software were purchased by RTDS. In addition, Locus Computing Corporation's TCP/IP for DOS product was required to allow the PC to process TCP/IP network protocols between the UNIX workstation and the PC. The end result is the PC can act as an X-server that processes a client application's windows locally at the PC together with the real-time data RTDS provides over the JIN. The booster and maintenance management and control system disciplines currently make regular use of this function for a combination of SIM and flight-following opportunities for training in the office. No communication is provided between the office and actual MPSR support personnel, so no direct involvement of control center activities takes place in the office. In 1993, RTDS will bring on line the remaining licenses for the remaining Systems Division flight control disciplines.

1993 Activities

A primary objective of 1993 RTDS activities is to begin new development in the console disciplines that have not had an opportunity in the past to be involved with RTDS. To accomplish this, several 1992 activities were considered completed and the RTDS developers were moved over to new tasks. These new tasks include the completion of FDWS, PBT, and RMS position monitor, thus allowing for new development in the EVA and electrical, emergency, and consumables manager (EECOM) disciplines. RTDS continues to follow the philosophy of bringing new development to an operational capability and then transitioning it to appropriate sustaining personnel outside the project staff.

Several of the previously mentioned 1992 applications are continuing development into 1993. They include: FCMS and BLSS, PILOT, PRS, VISTA, and office MPSR. These applications will not be mentioned here again. Refer to the previous text for future development planned on these tasks.

EVA Expert System

The EVA expert system project was started in November 1992 and will bring the EVA flight control operations into the workstation development activity that has been ongoing in the other disciplines for years. This application is targeted at improving all aspects of monitoring EVA crewmember extravehicular mobility unit (EMU) suit data. The current EVA real-time data system processes all crewmember biomedical data together with suit data into one long bit stream that must be deciphered by the current system, calibrated, and presented in ~25 different parameters for each suit. The development planned for the EVA expert system

application will acquire data via RTDS, parse the data, and apply pseudo-measurement stimulation identifications to each of the 25 parameters before presenting unique parameters for each suit to the graphical user interface. A combination of tabular, plotted, and schematical views of EMU suit data is planned for 1993 development. This project has the ambitious goal to provide EVA flight controllers with a complete application in time for the start of the STS-61/Hubble space telescope (HST) revisit mission simulations (September 1993). It is anticipated that this application will provide the EVA operators with a chance to perform flight-following of the HST EVA activities from the CCC operations control room workstations during the flight planned for December 1993.

The EMU data processing module of this application was used for the first time in the MCC during the EVA on STS-54. The goal during STS-54 was to acquire the EMU suit data via RTDS and to verify its correctness against the current EVA flight data system that are residing on an HP-9000 computer. Postflight validation of the RTDS version of the EMU data is ongoing. During the flight, EVA section management, flight surgeons, and EVA flight controllers all had an opportunity to become familiar with the project and to make inputs for future development.

EECOM Expert System

The EECOM expert system project will be the first introduction of RTDS data and expert system development for the EECOM flight control discipline. This application will reflect EECOM flight control requirements for the display design and development that are planned for use in the CCC in December 1994. These displays will combine tabular, plotted, and schematical views of the data to generate follow-on requirements for data presentation in a more efficient manner. At the beginning of this project development, Talarian's RTworks product was selected as the graphical user interface builder tool and rule development environment. Recently, the CCC selected a different graphical display builder tool, Sammi, which was developed by a local Houston company, Kinesix. The remaining work for the EECOM application will be done using this Sammi product.

This project is expected to provide a lead-in application for follow-on work in FY94 as part of a joint project with the Control Center Systems Branch (DJ2). A joint Code C Ops Cost Reduction Proposal was submitted by DJ2/Janet Lauritsen and RTDS/Linda Perrine to explore the Jet Propulsion Laboratory's (JPL's) SELMON tool. This project will be referred to as DREMON, and it will evaluate the selective monitoring and trend analysis capabilities of SELMON. JPL is expected to provide development support for three different applications to be integrated with SELMON: the SSF thermal control system automation project, the EECOM expert system,

and the SSF environmental control and life support system (ECLSS) advanced automation project.

Stripchart Pattern Recognition

The stripchart pattern recognition project plans to explore the applicability of neural network theories to the recognition of standard stripchart signatures that are seen in a variety of disciplines. The most distinctive signatures are provided by the alternating current (AC) powered equipment's motor start-up currents. Most AC-powered Shuttle hardware have individual characteristic signatures that flight controllers can identify, with practice, as nominal or off-nominal start-up currents. This analysis of paper plotted data is the ground's best insight to the anomalous operations of this equipment. This means of analysis has been critical in diagnosing frequent problems with the waste containment system urine fan separators on several recent Shuttle missions. The approach this project will take is to use distinctive electrical signatures to determine the applicability of neural network technology to real-time telemetry monitoring and then to expand the scope of the project to other disciplines that require stripchart recorders to monitor high sample rate data (> 1 sample/sec).

Neural networks have been applied very successfully in the medical field to monitor electrocardiograms and other biomedical monitoring equipment. It remains questionable, however, whether the high sample rate data processing of the workstation coupled with the detailed signature analysis done by artificial neural networks will allow for keeping up with all parameters in "real time."

Cooperative Expert Systems (COOPES)

The COOPES project will be a cooperative venture with the Information Systems Directorate McDonnell Douglas contractors. This project has been waiting to get started since it requires the completion of the BLSS G2 application mentioned previously. The McDonnell Douglas COOPES team has spent significant time doing prototype demonstrations of cooperating expert systems, however, and has not had the opportunity to demonstrate an approach in the control center environment. RTDS intends to give the team that opportunity this year, however, because the work will need some customization for operating in the real-time environment of the MCC. The BLSS application will be used as the initiator application for communicating bus failure information to the other flight control positions via the networked RTDS workstations. Currently, bus loss information must be communicated verbally over the communication loops, which often results in misunderstood information or in operators not hearing the information at all. Other areas that will be explored as time permits are communication of multiplexer/demultiplexer and dedicated signal conditioner failures. It is an instrument and communication officer's responsibility to communicate

this information to the rest of the flight control room and is also currently done verbally.

CCC Development Support

The RTDS project was approached in August 1992 to provide assistance to the operations support contractor, Loral, to apply lessons learned from past RTDS experience to the development of the CCC being done by Loral. Three areas were targeted for planned support from RTDS during FY93; they are:

- Common Data Interface - Applying RTDS experience for data distribution, acquisition, and application programming interface.
- Expert System Server Study - Making use of RTDS expert system development experience and hardware to determine efficient placement of licenses in the CCC. We also are assisting in the selection of the CCC standard expert system development tool (COTS), and we have done research on several products.
- Global versus Local Limit Sensing - Making use of RTDS application development experience and hardware to prototype an appropriate transition of centralized MOC limit sensing to the distributed, networked environment of the CCC. RTDS has the resources (people and hardware) to provide this support.

Work is ongoing in the first two areas, and work in the third area will be started shortly.

CCC/JIN Gateway Project

This project was originated at the request of MOD management to build a bridge between the Mission Control Center upgrade (MCCU) networks and the RTDS network in the MCC. The purpose was to move development off of the operational flight support workstations and onto a less secure, more open development platform that RTDS provided. With this past year's change of plans for the future of control center development, the MCCU platform quickly became the wrong platform on which to expend our development efforts. We negotiated with MOD management to rethink this plan and instead build a gateway for the future that would not only allow development to occur off of the CCC operational workstations, but also allow development to occur outside the control center facility. This became the CCC/JIN gateway, and we are currently in full-scale development of this capability. Phase 1 of this project, which is targeted for completion this summer, will install a DEC workstation in the old transitional flight control room along with a network router that will force communications between the level 3 CCC networks and the level 1 JIN to be one-way only. This will provide the long-term capability that RTDS has provided in the past of distributing real-time telemetry to office buildings around site as well as to other locations, such as Ames Research Center. Phase 2 of the project will require more

detailed requirements and design to allow limited authorized access from the JIN into the CCC networks. We will not be able to accomplish Phase 2 during FY93 and will need to look to MOD for continued funding of the project next year to accomplish the path into the CCC.

Conclusions

In addition to RTDS, there are many efforts ongoing at JSC to upgrade old facilities to today's technologies. Most, if not all of these technologies, are necessary to enable manned spaceflight operations to move into the next century and to pursue a "better, faster, and cheaper" approach. Often these words are placed in reverse order when confronted with the realities that NASA's budget presents today. Perhaps what really needs change is the mind-set within NASA of sacrificing the move to new technologies as a means of saving money. In the long run, this will turn out to be the more expensive route to our goals. To quote our Administrator from a speech he made to the Association of Space Explorers: "The technology generated from space exploration is one of the highest yielding investments in our future this country can make." This statement must apply to our control center technology development with the same priority it applies to the vehicles we will monitor from these facilities.

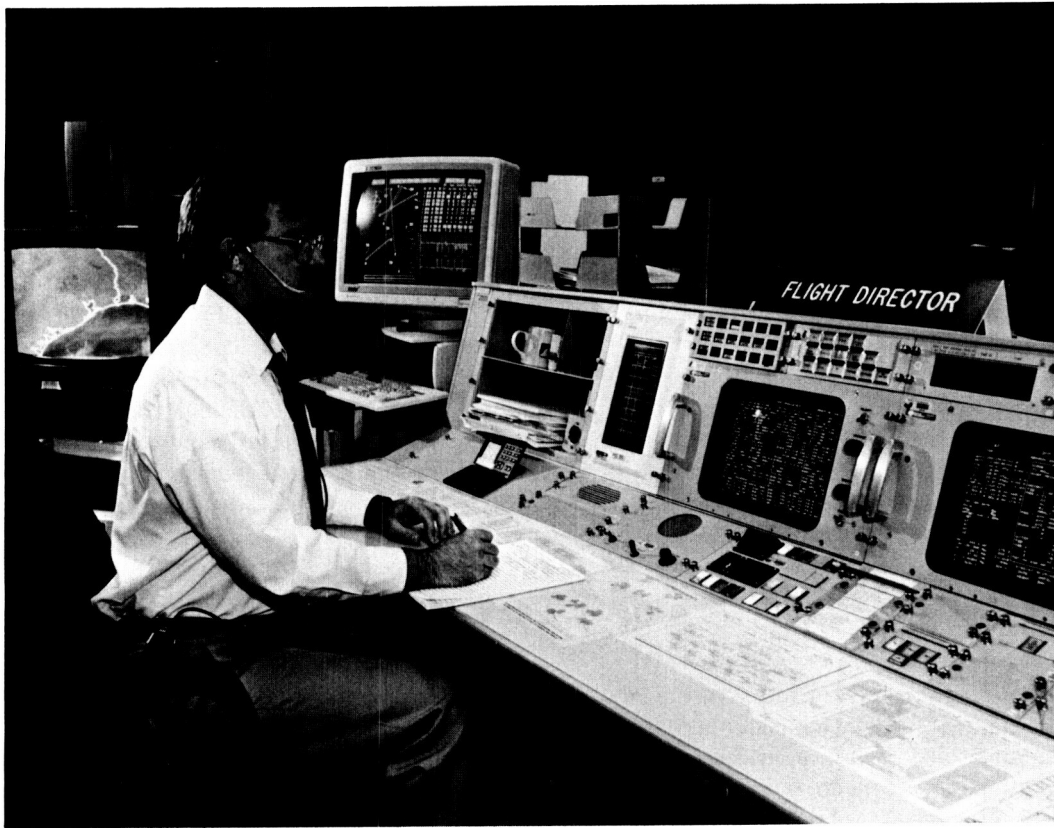
The RTDS project has succeeded in its original endeavor to demonstrate that new technologies can be used to meet the demanding requirements of manned space flight control center training and operations. RTDS—and the people who have been associated with the project over its 7-year life span—is arguably the key factor in showing a new direction for the future of control centers at JSC. The \$9M investment that RTDS

represents should appear to be money well spent and a positive reflection on the RTOP process that must continue into NASA's future.

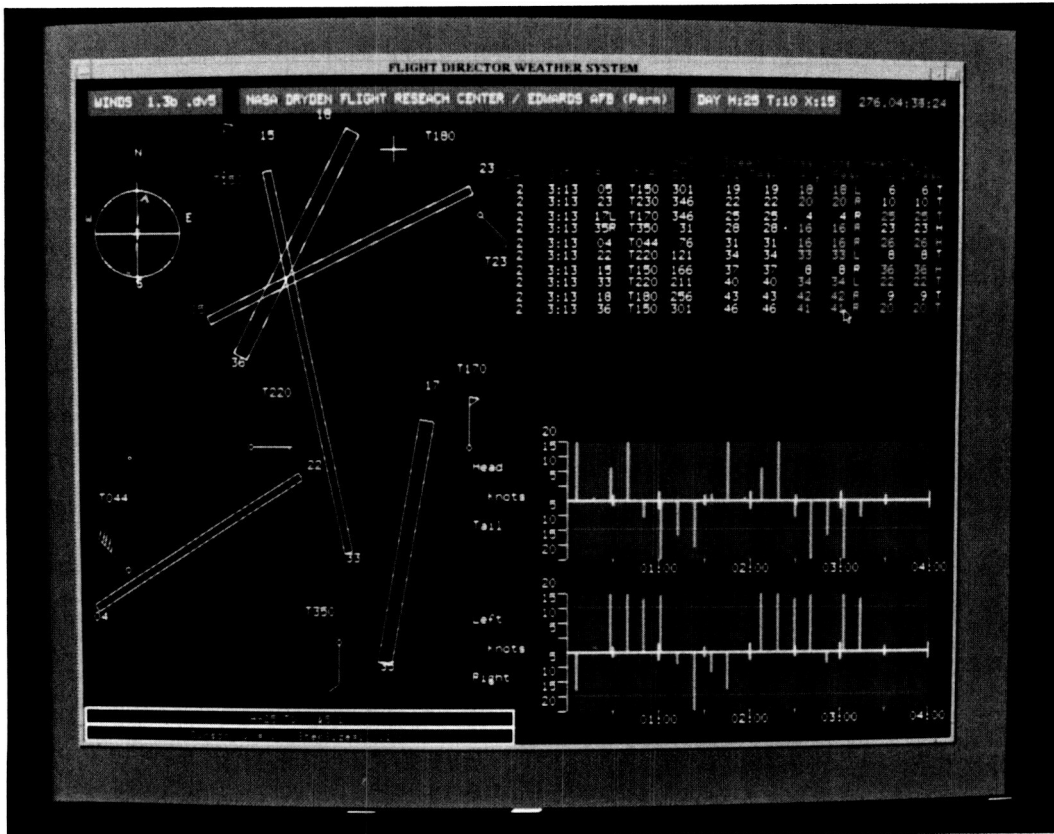
In FY94, under the new project title of ACCT, MOD plans to continue the successful efforts begun in the RTDS project. The new project will concentrate on keeping abreast of industry advances in technologies that have the potential for applicability in the control center environment. As stated earlier, MOD budget does not allow for the luxury of looking at new possible technologies, of determining how to integrate them, and of at the same time managing Space Shuttle and SSF day-to-day operations. Therefore, if NASA and MOD intend to keep pace with new technologies and to explore them as inexpensively as possible, a project such as ACCT will be a necessary and an integral part of MOD activities for many years to come.

Acknowledgments

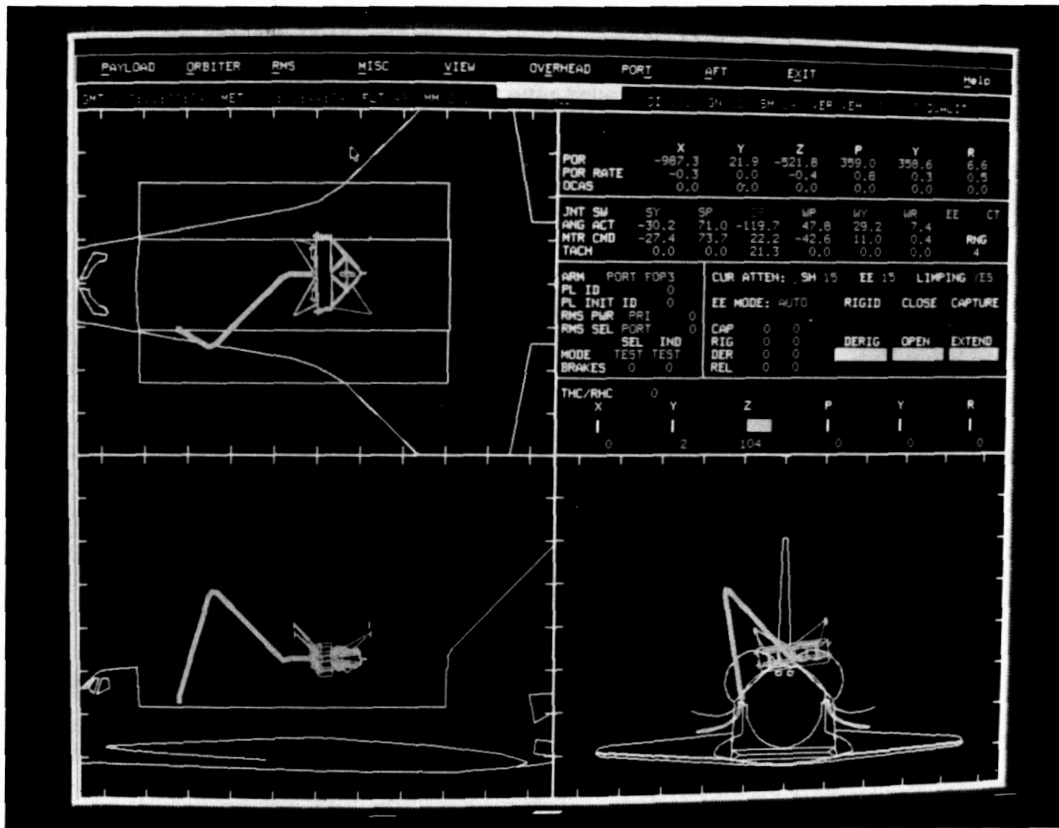
We would like to acknowledge the following individuals and companies: Arthur N. Rasmussen, MITRE Corporation; Ron Kerr, Rockwell Shuttle Operations Contract (RSOC); Mark Gnabasic, MITRE Corporation; Jim Ruszkowski, NASA/JSC; Al Mercier, Paramax Corp.; Mike Dinger, RSOC; Rami Al-Ayoubi, RSOC; Charlie Robertson and Jerry Snieder, McDonnell Douglas Corp.; Matt Barry, RSOC; SRI International; Daryl Brown, NASA/JSC; Debra Borski, RSOC; Linda Perrine, NASA/JSC; Dave Simon, RSOC; Jane Guyse, MITRE Corporation; Steve Koerner, NASA/JSC; Giau Ho, Paramax Corp.; Dave Hammen, MITRE Corporation; Collin Clark, McDonnell Douglas Corp.; Terry Murphy, NASA/JSC; and Hayes Moore, Computer Sciences Corp.



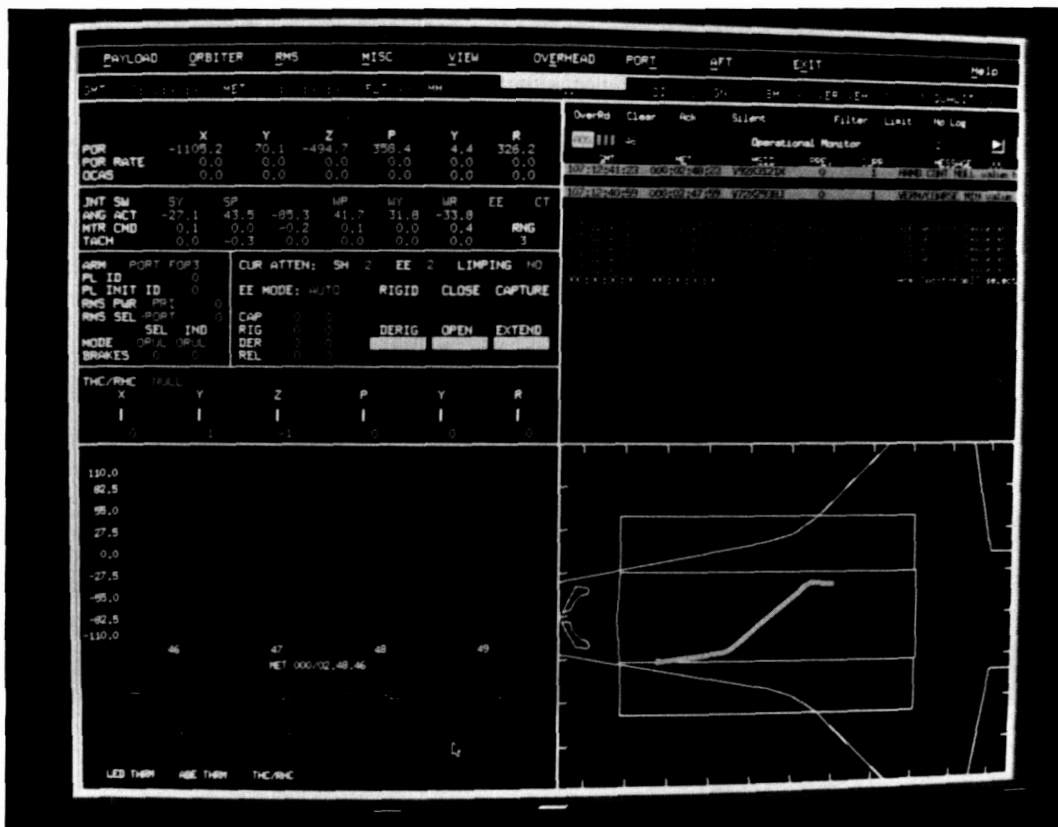
S92-47203 Flight Director Weather System



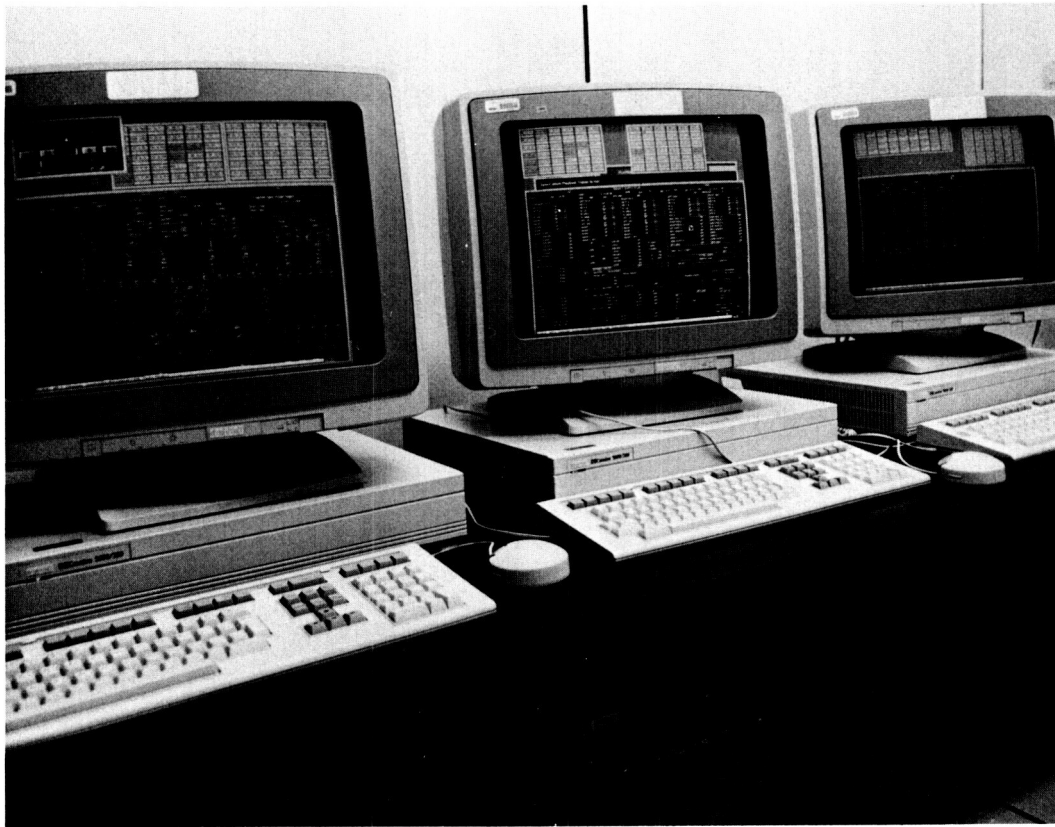
S92-47200 Flight Director Weather System



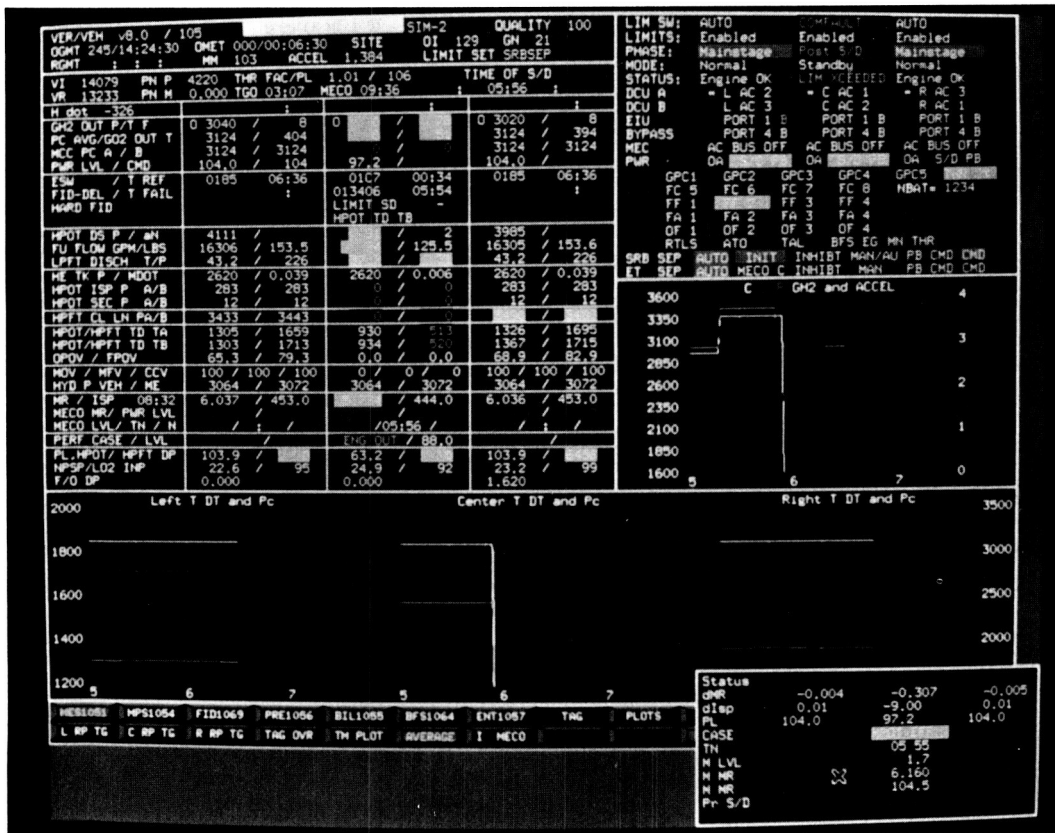
S92-47198 Remote Manipulator System (RMS) Position Monitor



S92-47197 Remote Manipulator System (RMS) Position Monitor



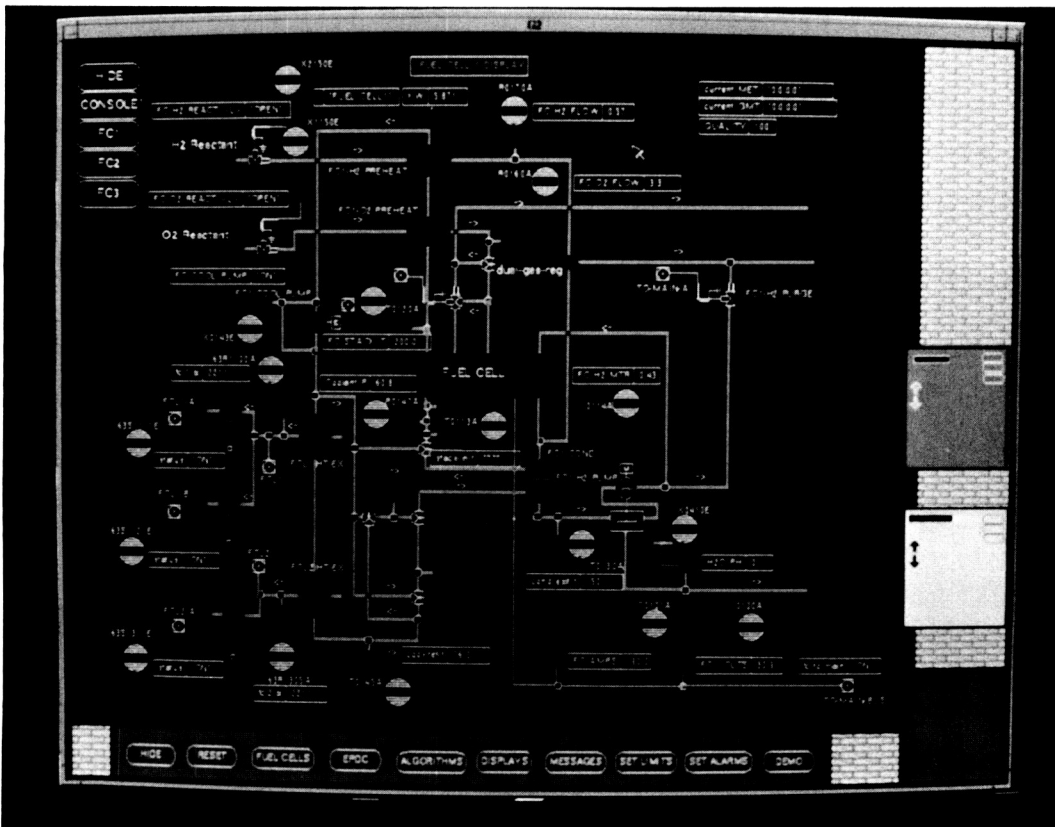
S92-47180 Playback Trainer (PBT)



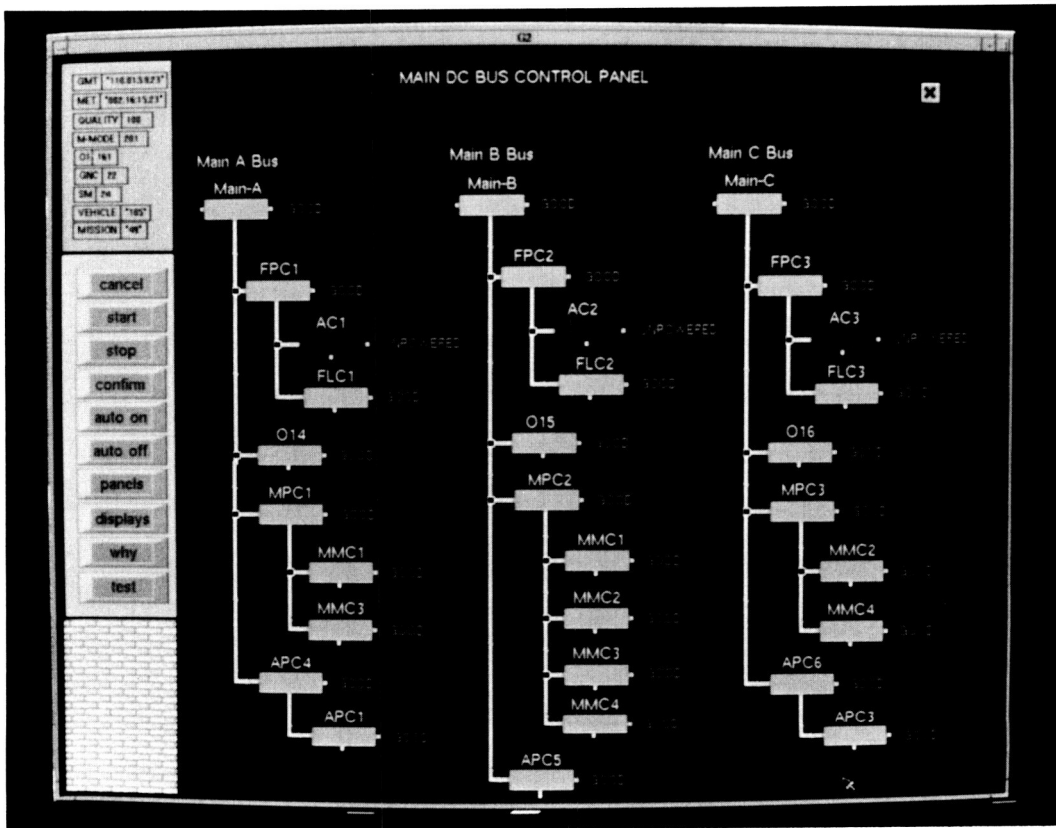
S92-47190 Booster Expert System



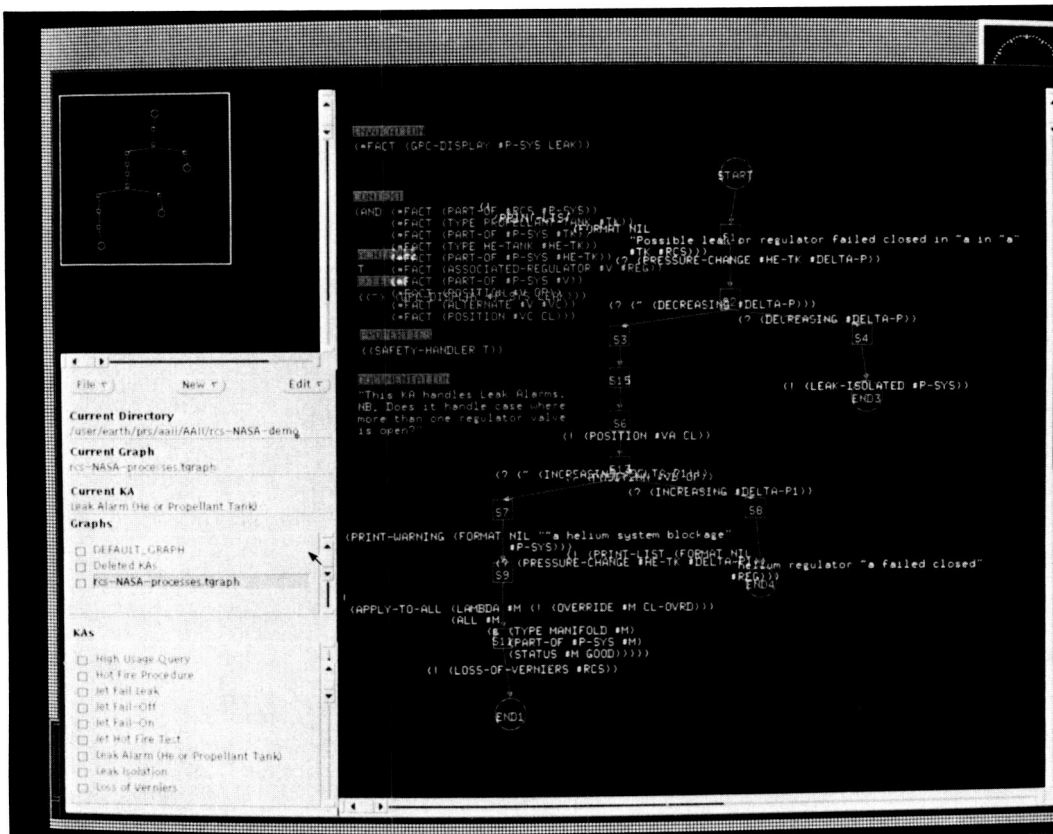
S92-47202 Booster Expert System



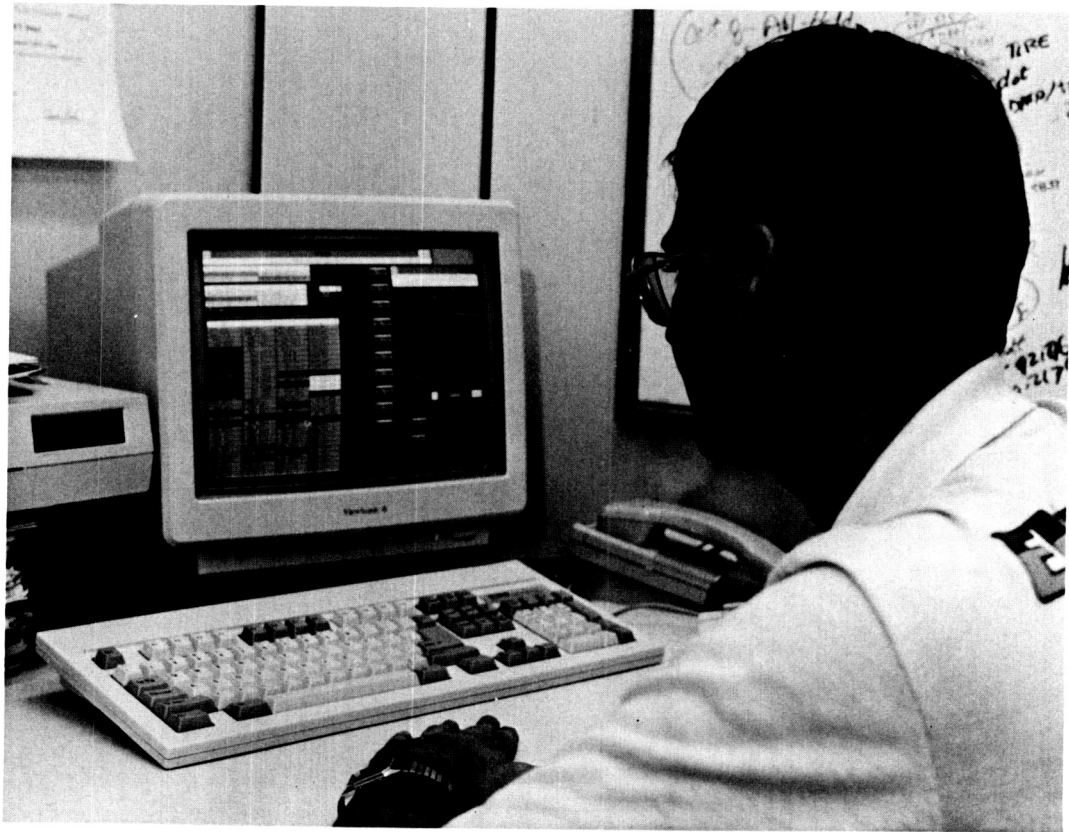
S92-47192 Fuel Cell Monitoring System (FCMS) and Bus Loss Smart System (BLSS)



S92-47193 Fuel Cell Monitoring System (FCMS) and Bus Loss Smart System (BLSS)



S92-47186 Procedural Reasoning System (PRS)



S92-47181 Office MPSR

Extended Real-Time FEAT: A Tool for Real-Time Automated Failure Identification in the Control Center Complex

Sarah Kirby, Janet Lauritsen, Ginger Pack, Anhhoang Ha,* Steven Jowers,*
Robert McNenny,* The Truong,* and James Dell**
Johnson Space Center/DJ

*McDonnell Douglas Space Systems Company

**Loral Space Information Systems

Abstract

A system that will provide real-time failure management to Space Station Freedom and Shuttle orbital operations is described in this paper. The system's use of a simplified form of model-based reasoning qualifies it as an advanced automation system. Our system differs from most such systems, however, in that it has been designed from the outset to meet two sets of requirements.

The first requirement is that the system must provide a useful increment to the fault management capabilities of the JSC Control Center Complex (CCC) fault detection management system. The second requirement is that the system must satisfy CCC operational environment constraints such as cost, computer resource requirements, and verification and validation. The need to meet both requirement sets presents a much greater design challenge than would be the case had functionality been the sole design consideration. In this paper, we will present an overview of the choice of technology by discussing aspects of our choice and the process for migrating the technology into the CCC.

Introduction

In this paper, we will provide an overview of the underlying technology and design of extended real-time [failure environment analysis tool] FEAT (ERF) within the context of its migration to the CCC. The fault detection and identification (FDI) problem will be described together with constraints imposed upon the developers—both those imposed because of good software engineering and those imposed by the nature of the environment. The approach we took will be addressed next; and the choice of technology, the algorithms developed, and the possible extensions and adjuncts to those algorithms are also examined. The solution settled on will be presented as well as its current status and general comments. We will end the paper with some concluding remarks.

Problem Description

Fault detection and management (FDM), which is a major mission controller area of responsibility, may be divided into two phases: FDI and recovery of some part of the lost capability. Immediate action that is required to safe

the system from further failure propagation is included, when appropriate, in the FDI phase.

The FDI Task

An analysis of the FDM process¹ showed that the FDI phase primarily consists of drawing logical conclusions about the cause of an observed problem from facts about the monitored system and telemetry data. The recovery process proved to be much more complex, however.

Although, in principle, FDI is a straightforward logical task, several factors can combine to make it very challenging. First, space vehicle systems have become extremely complex. Such systems consist of a very large number of component elements, which may interact in a variety of ways depending on the current system state. Furthermore, some interactions may be obscure and rare. Second, a very large number of parameters must be monitored. Third, the controller is usually under some degree of time pressure; thus, in many cases it is not practical to run traces through functional schematics and look up data in handbooks or other reference material.

The challenge of the FDI task gives rise to several concerns. For example, the controller may not remember the complete set of relevant facts, consider all applicable data, or identify the correct procedure to apply.

It was seen that some form of "controller's associate" could materially assist controllers working an FDM problem. Such an associate should not attempt to automate the controller. As a minimum, a controller's associate should assume the chores of storing and recalling facts about the failure behavior of the monitored system and of accessing real-time data to draw conclusions about possible system failures from those facts. ERF meets these requirements.

Constraints

Flight-critical software applications lie outside the scope of a research lab. Real-world constraints must be considered, among which are: robust interfaces to real-time data must be provided, missing and noisy sensor data must be dealt with, multiple problems must be queued, and analyses must be interrupted and resumed. Real-world applications also need to be considered, such as end-user constraints and implementation requirements.

Controller concerns imposed a number of constraints on the design of ERF. ERF's user requirements are either an explicit subset of the broad user requirement² or are derived therefrom. These include requirements for

- Compatibility with proven real-time mission support operations
- Prompt solution response
- Positive operator control at all times
- Generic FDI capability

Any automated system designed for real-time mission operations must support the process currently used by human controllers. Shifting part of a controller's responsibility to a computer means that the computer must play its part in a human/computer team; it cannot be a solo player.³

Accurate identification of the failure at hand is a prerequisite for dealing with critical situations. This means that, to be useful when it is really needed, a controller support system must take no longer to provide a solution than the time taken by an experienced controller. ERF is required to identify failures and to assess their impacts within 5 minutes on average, 6 minutes in the worst case.

Just as a human team player must take orders, ERF must always be directly controllable by the operator. This means that ERF must keep the controller informed of its intentions and allow the controller to redirect it, or to halt it if necessary, at any time.

Because failure identification is in principle a generic process, ERF is required to support FDI for all Space Station onboard systems for which its basic knowledge representation scheme is appropriate. Similarly, ERF must be able to support Shuttle on-orbit operations for systems that have been modeled in ERF-compatible form.

Any development of an application whose target is within the real, operational world needs to satisfy such real-world constraints as cost ceilings, resource allocation limits, and fast algorithm performance. Sometimes data will be noisy and/or missing. Interfaces must exist with other CCC systems (status and control, data base functions, the data streams, etc.). Choice of platform, development methodology, and language will be made by the control center developers, not by the technologists. The application and the models that an application uses must be susceptible to verification, validation, and maintenance.

In the case of the CCC, the constraints included the use of Ada for all new code, minimal cost, working within the constraints of the development environment for the CCC, following methodological guidelines for formal software development, and formal reviews.

Approach

Technology Description

ERF is fundamentally built on a bi-valued model representation. The models are causal networks of failure that are represented as directed graphs and are automatically configured, via telemetry and knowledge of system

degradation, to represent the system's observable state. These models are then operated to infer information about commonality among annunciated out-of-limit or alarm conditions, about what could have been the cause(s) of these annunciations, and about where these effects might propagate.

The FEAT, which is built by the JSC Intelligent Systems Branch, computes transitive closure for the given model and displays the results of queries graphically.^{4,5,6} ERF is a layer of software on top of FEAT that extends ERF capabilities. Specifically, ERF sequences queries to FEAT in a manner that is similar to the way in which a controller might use FEAT to analyze either real-time data or hypothetical data. The results are displayed on FEAT displays and/or on displays that are external to FEAT.

Currently, FEAT runs on both Macintosh and Unix platforms.^{4,5} A companion product, the Digraph Editor,⁴ provides an environment that aids in constructing failure models for FEAT, although other tools that adhere to the PICT standard can produce working digraphs for FEAT. Both products are written in C and are available for the Macintosh through COSMIC. The Unix version has just been submitted to the Space Station Freedom Program's Technical and Management Information System and is now available to the Space Station Program. Eventually, this version will be available to all users through COSMIC as well.

Rationale

ERF technology was selected because it provides the required functionality and satisfies the following constraints:

- It uses relational failure models of the systems being analyzed.
- The digraph failure models, which are documented via a graphical representation, are more easily maintainable than are equivalent text representations.
- It uses a standard mathematical technique for computing reachability (connectivity) analyses; i.e., transitive closure.
- In addition, it uses heuristic knowledge about how to diagnose failures in physical systems.

ERF allows FDI applications to be developed without the system operational failure experience heretofore thought essential for developing such systems. On the basis of design-derived knowledge, the digraph failure model describes how a system must fail. ERF algorithms provide a methodology for interpreting the model based on sensor data. Because the sensor interpretation algorithms are model independent, ERF will work for any system for which a FEAT-compatible failure model is provided.

Results

In this section we will summarize only at a conceptual level the analysis algorithms that ERF implements. At the highest level, these algorithms are commonality assessment,

failure identification, and impact assessment. We will also describe the results obtained during 1992.

ERF Core Analysis Algorithms

The commonality assessment algorithm uses a digraph to determine if there are paths between components that have failure indications. If paths exist and there are no dependencies that could impede failure propagation, we can assert that one of the sensors is "primary" and that the other sensors downstream of it are "secondary."

Failure identification takes the announced conditions, retrieves additional state information, and categorizes the observables in the model into one of three states: good, bad, or unknown. From this, ERF builds an initial set of possible causes. This set is pruned using knowledge about the known good components and digraph modeling artifacts to narrow the space of possible causes. Any remaining unknown observables in the model are then presented to the controller. If additional information can be obtained, the analysis is refined. An early version of this algorithm is detailed in Ref. 7.

The impact assessment function takes these possible causes and predicts their respective effects on the system. ERF will announce lost redundancies, where a failure may propagate if the other leg in the redundancy is lost, and new susceptibilities for critical functions (i.e., new single- and dual-failure sources).

Status

ERF is a subsystem of the CCC fault detection and management system. We held a preliminary design review in March 1992.⁸ Preliminary design inspection is scheduled for February 1993 to align the design with the new CCC architecture. The analysis algorithms will be available in the CCC advanced automation test-bed in June 1993.

An informal prototype for algorithm development and detail design activities currently exists. At the end of 1992, this prototype consisted of two separately running processes—the graphical user interface and the analysis routines. While far from being the system that will be delivered to the CCC, the current informal prototype demonstrates:

- Basic analysis functions (commonality, failure assessment, and impact assessment)
- Use of FEAT displays for analysis presentation
- Use of additional displays built outside of FEAT for results presentation

Conclusions

ERF is an application that will aid a mission controller in identifying the cause(s) and subsequent effect(s) of observed failure symptoms in a monitored system. It is a layer of software built upon the FEAT provided by the Intelligent Systems Branch at JSC. This additional layer provides: (1) automated fault identification and effects

analysis algorithms that are model independent, (2) hooks for alternate model representations and alternate analysis engines, (3) interfaces to real-time data, and (4) automated problem management functions.

ERF uses advanced automation techniques and provides automated FDI analysis for any system that can be modeled as a causal network of failure modes. As the controllers identify additional candidate functions for automation, there will be opportunities for ERF capabilities to expand and/or for ERF to work with other applications. ERF has been designed to provide hooks for swap-ping underlying representations and analysis engines, for incorporating more advanced analysis algorithms, and for communicating with other applications.

We intend to explore alternate analysis engines and representations, communication with other applications, the development of more sophisticated FDI algorithms, and the recovery problem. Some of these efforts have already started, while other efforts are still on the horizon.

References

- ¹Functional Description," (Internal Document) April 2, 1991.
- ²Space Station Control Center User Detailed Functional Requirements," JSC-13192, April 1991.
- ³Malin, J. T., and Schreckenghost, D. L., "Making Intelligent Systems Team Players: Overview for Designers," NASA TM 104751, 1992.
- ⁴Macintosh FEAT 3.4 User's Guide," JSC's Intelligent Systems Branch, August 24, 1992 (includes the Digraph Editor User's Guide).
- ⁵Unix FEAT 3.4 User's Guide," JSC's Intelligent Systems Branch, August 24, 1992.
- ⁶Stevenson, R., et al., "Failure Environment Analysis (FEAT) Tool Development Status," Presented at AIAA Computing And Aerospace VIII Conference, AIAA 91-3803, Baltimore, MD, 1991.
- ⁷Clark, Colin, et al., "Fault Management For The Space Station Freedom Control Center," Presented at AIAA 30th Aerospace Sciences Meeting & Exhibit, AIAA 92-0870, Reno, NV, 1992.
- ⁸Space Station Control Center Extended Real-Time FEAT Subsystem Specification," (Preliminary Draft) JSC-13416, March 1992.

Acknowledgments

Extended real-time FEAT (ERF) was developed by McDonnell Douglas Space Systems Company (MDSSC) under subcontract to Loral Space Information Systems for the Control Center Systems Division. We wish to acknowledge the efforts of two MDSSC engineers, Robert McNenny and Steven Jowers, who have provided outstanding support throughout the development of this project.

Consolidated Communications Facility

Linda Uljon, John Muratore, Carol Evans, Victor Lucas,
Brian Boland, Jim Allen and Steve Ngo
Johnson Space Center/DJ

Abstract

In the beginning of FY92, the development organizations of the Mission Operations Directorate (MOD) at JSC were poised to begin two major projects: the Space Station Control Center (SSCC) and the refurbishment of the telemetry processing area of the Space Shuttle Mission Control Center (MCC). A study team established that a common front-end concept could be used and that it could reduce development costs for both projects. A standard processor was defined to support most of the front-end functions of both control centers and to support a consolidation of control positions that effectively reduces operations cost. In this paper, we will define that common concept and describe the progress that has been made in the development of the Consolidated Communications Facility (CCF) during the past year.

Introduction

In preparation for ground support of the upcoming Space Station, the MOD had begun to plan to construct a Space Station Control Center. A building adjacent to the MCC was under construction and requirements had been written. At the same time, development efforts in the MCC had been refocused to replace the oldest and least reliable machines, those with front-end functions. A study team was established to determine whether there was a joint effort to develop a common design. It was hoped that such an effort would reduce both development and recurring costs.

Approach

We began the study by defining a model of the front-end functions. Once the functions were defined, the requirements were mapped against our model. A market survey was done to determine whether the needed equipment to accomplish the front-end functions was available in the marketplace.

Results

A three-layer view of the processing was produced and is shown in figure 1 below.

Layer 1 is the processing that terminated the ground-to-ground protocol and interfaced with the external world. The Goddard Space Flight Center communications network protocol is handled in this layer, thereby isolating

the remainder of the control center from any changes in ground network.

Layer 2 provides source-specific processing for the front end. This format manipulation layer does the specific format manipulation based on variations in spacecraft communications. It, in turn, isolates any changes in spacecraft telemetry from any other areas of the control center.

The final layer, layer 3, formats the data so that the data can be distributed to the remainder of the control center. Ideally, despite the spacecraft, the format is identical. This allows common applications, such as display building programs, to use and understand the data independent of source.

Each processing layer removes data formatting variation such that the entire front end produces a set of data that is identical despite its source (fig. 2). An application can use the data from any spacecraft without modifying the data to its processing code. This provides an excellent opportunity for duplication of several applications downstream of the front-end processing. Additionally, future support for additional spacecraft becomes easier.

This model provided an excellent framework against which to map the requirements of the Shuttle and Space Station Programs. In mapping these functions, layer 1 was designated the institutional layer. It contained the demultiplexers and modems that receive the data from the external world. Layer 1 included recording, switching, and routing functions. It also included processing to handle the ground network data that included data from other NASA sites, network scheduling, and network status data processing. Requirements for Space Station and Shuttle data processing revealed that the layer 1 functions were identical for both programs.

Layer 2 isolated most of the differences between the spacecraft telemetry. Space Station telemetry consists of consultative committee for space data systems (CCSDS) packets that use Reed-Solomon encoding. Its telemetry object lists are nonperiodic. Shuttle telemetry, which could require decryption, uses Interrange Instrumentation Group standards. The periodic nature of the Shuttle telemetry is key to validating and decommutating the data. It became clear in mapping the requirements for this layer that the two programs completely differed. If the unique processing could be isolated, however, it appeared that a synergistic approach to the front end could be achieved. Spacecraft-unique processing of data could be performed on a single type of machine. The use of a

single platform, even with a different configuration of boards, would allow a synergistic approach to the maintenance and operations of the machines.

Once the data have been extracted from their downlink format, layer 3 provides distribution of these data to other areas of the control center. Development of a common data format provides the potential that the data acquisition functions used to receive data throughout the control center can be identical and that additional synergistic savings can thus be created. The code to perform layer 3 functions for Shuttle telemetry differs somewhat from that of the Space Station Program, but both sets of code can be easily run on the same platform.

The allocation of control center requirements to the three-layer model is illustrated in figure 3.

Correspondingly, the uplink function was mapped in reverse—the building outbound commands were in a layered fashion. The basic elements of these layers are given in figure 3. Once again, it is apparent that the functions are parallel and that the programs could benefit from synergism.

The study team evaluated the requirements and did an initial survey of the marketplace. A straw-man architecture was proposed in which the front-end processor was a VME-based machine. Specialized boards to do spacecraft-unique processing were available that would run on such a platform.

Results

An estimate for a common front end for both control centers at JSC determined that NASA could save 15% of the estimated development costs and could reduce the maintenance staff by 30. Some savings result from the use of a single piece of hardware for both programs. Some savings are owing to the single development effort on common platforms that are customized for each program. The results of this study were used to launch the CCF project. This occurred approximately 1 year ago.

Current Status

Since that time a year ago, the requirements for a consolidated system have been written and the project has been divided into five subsystems. These are: the consolidated data select switch (CDSS), the consolidated data recording subsystem (CDRS), the front-end processor subsystem (FEPS), the consolidated distribution subsystem (CDS), and the test and checkout subsystem (TCS). Each of these subsystems has been designed and procurements are in progress. A mapping of the subsystems to the layered concept is shown in figure 4 below.

The CDSS performs high-rate and low-rate data switching, accepts multiple data lines from external sites, and routes data to external sites. The low-rate data switch handles the majority of this work—it is currently specified as a 600x500 port switch. Responses to the request for proposal for this switch are expected soon.

The high-rate data switch has few lines and might be patched rather than switched. It will not be developed until late in the project.

The planned CDRS technology is borrowed from the television industry, which keeps commercials on cassettes. A robot queues the tapes automatically and plays them as scripted. The control center taping system is envisioned as two sets of robotically operated tape silos. Because recorders do not operate efficiently at the slow data rates of the control center, data will be buffered and sent to the recorders in bursts. The recording system is expected to be run with minimal operator intervention. The operator will be needed only to remove any tapes for permanent storage or to arbitrate playback capability. This approach will reduce operations costs—a strong theme in the development of the CCF.

The FEPS contains the bulk of the processing in the CCF. The current design of the MCC contains several specialized hardware devices designed in the 1960s and 1970s. Over the years, other systems based on more modern commercial off-the-shelf technologies have partially replaced the front-end processing capabilities, but these systems were never able to do so completely. The result is that the MCC now has hardware supporting four different design approaches to the telemetry processing. These variant hardware will be replaced with the CCF.

The design of the CCF FEPS is based on a single VME-based machine. The machines will be tailored to suit the specifics of the spacecraft data for which they are used with special processing boards and software. The FEPS does all of the layer 2 processing. This isolation of layer 2 to a single processor means that the CCF could be expanded to handle future vehicles by changing only FEP processing. Additionally, FEPS provides the processing platform with which to create the common data format discussed in layer 3. Procurement for the FEPS is currently in progress.

The TCS will run on the FEPS platform and will provide the ability to run test data streams through the system and to score the output to assure proper processing. The TCS will be run routinely to validate that the hardware and software are ready. It will also be used by maintenance personnel to locate problems. Development of TCS software is currently being done on a UNIX platform, and the code will be transferred to the FEP platform after FEP delivery.

The CDS provides distribution of data to the computation and display systems throughout the control center complex, including the older IBM mainframes and the newer UNIX workstations. The CDS consists of a packet-based switch or a local area network (LAN) and assorted interfaces. One interface provides configuration management and status and control. Other interfaces will emulate current interfaces, thereby minimizing the changes required to the older MCC machines (to reduce risk). Interfaces that are not standard LAN products are hosted on FEP platforms to reduce hardware maintenance costs.

Conclusions

By looking at ground support for a joint Space Station and Shuttle project, MOD has found a better and a cheaper way of providing a telemetry processing area. The definition of a front-end concept and the mapping of functions required by both the Shuttle and Space Station Programs clarified the needs of each program. From this, MOD was able to determine what common hardware and software could support both programs. Subsystems were defined and designs done to accommodate the needs of both programs, as well as to expand for future needs. The procurement of much of the CCF is currently in progress, and the entire project is expected to be complete in 1996.

Because the format of the data output by the front end is common in nature for both programs, a single

display processor can be used for either Shuttle or Space Station data. This common basis for front-end output greatly simplified consolidation of the remainder of the control centers for each program. From this grew the Control Center Complex, which is currently being developed. The Control Center Complex contains the functionality of both the Space State Control Center (SSCC) and the MCC, but it costs less to build and to maintain than each center separately.

Acknowledgments

I would like to acknowledge the support of Stephen G. Bales, the Assistant Director for Program Support in MOD, for encouraging the creation and development of this project.

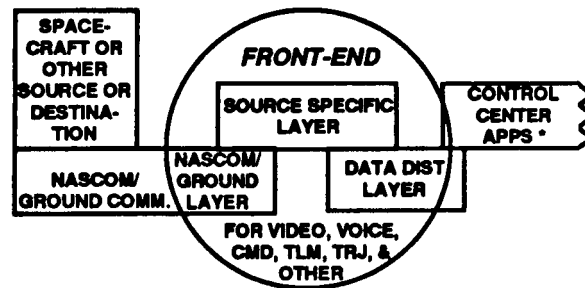


Figure 1. Three Layer View of the Front End.

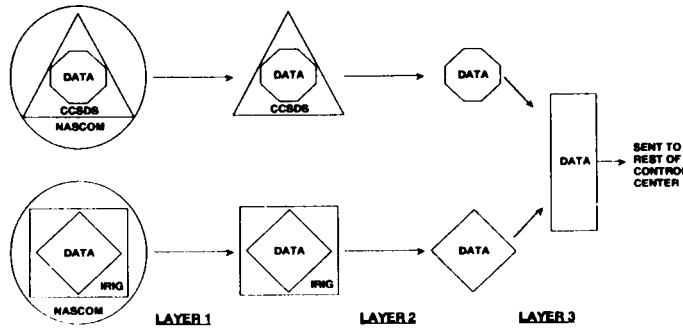


Figure 2. Removing the Layers of Protocol and Reformatting the Data to Provide a Common Output.

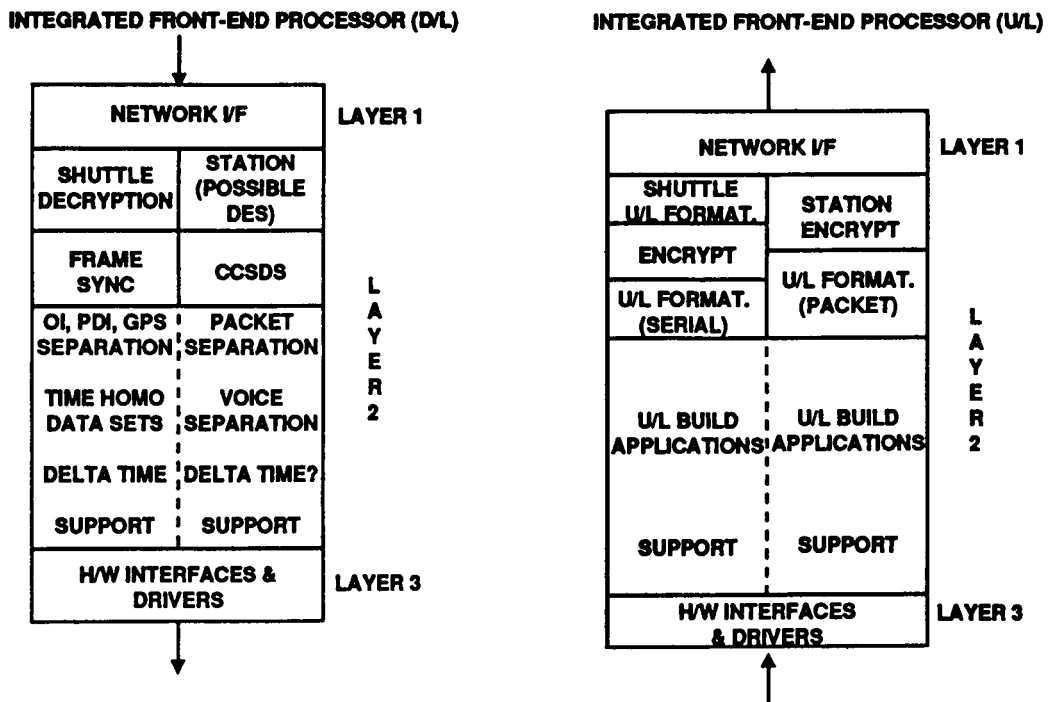


Figure 3. Mappings of Downlink and Uplink Front-End Processing.

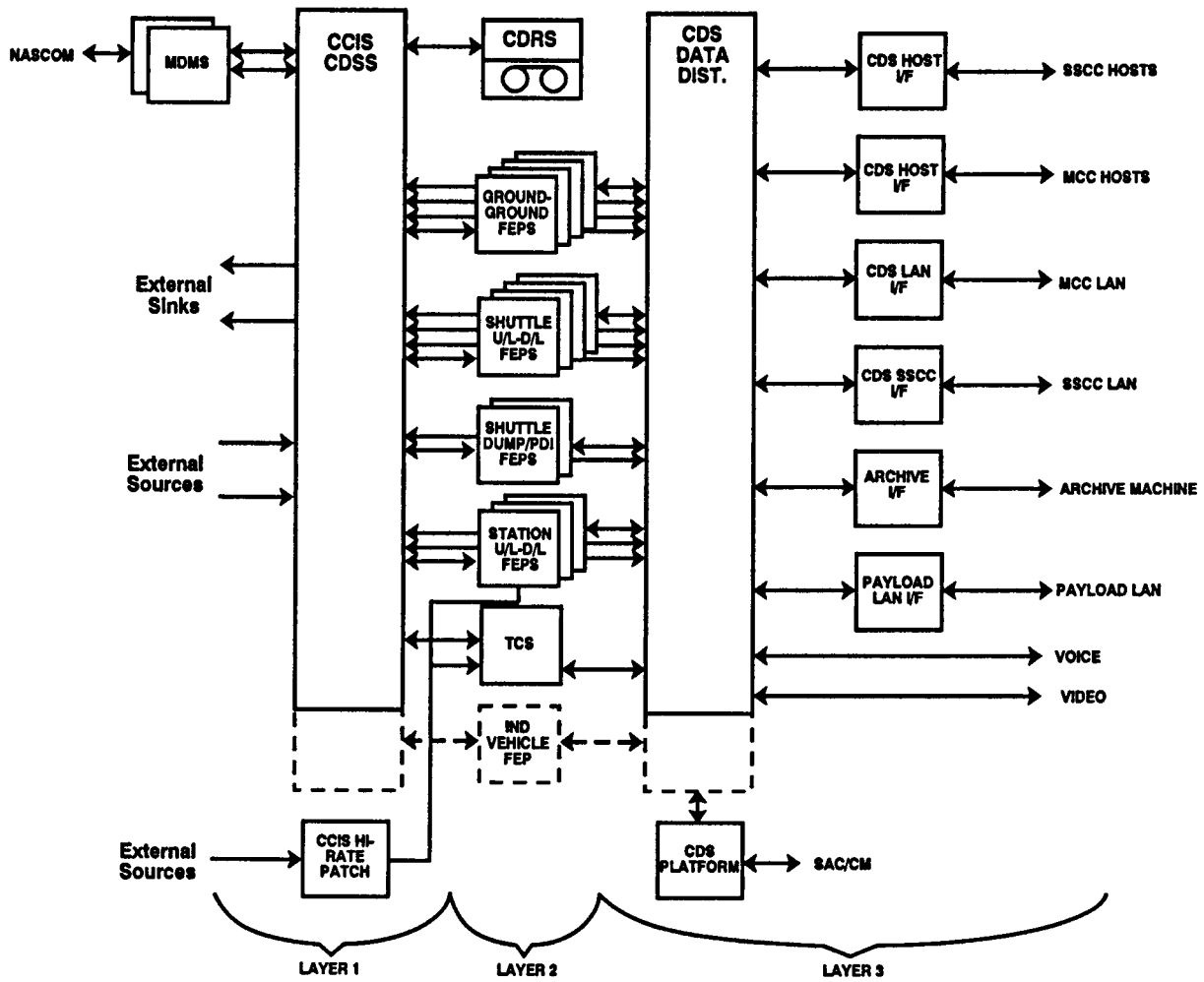


Figure 4. A Mapping of the CCF Components to the Three-Layer Model.

Improved FEAT Computation Times

Dennis Lawler, David B. Wadsworth,* and Steven Schnurer*

Johnson Space Center/ER

*Lockheed Engineering and Sciences Company

Abstract

The failure environment analysis tool (FEAT) application requires a fast algorithm to compute transitive closure of directed graphs with more than 70,000 nodes. The current algorithm will require days or weeks to perform this calculation. This report documents the initial evaluation of the speed and complexity of several alternative algorithms. Also, this report recommends areas for further study.

Introduction/Background

FEAT uses a directed graph (digraph) to represent system failure cause-and-effect relationships. Complex systems may be modeled using simple formalisms. A digraph used with FEAT consists of nodes representing failure events, edges representing causal relations between adjacent failures (nodes), and logical conjunctions between nodes. These conjunctions consist of logical OR connections and two-input logical AND connections. These digraphs may be cyclic. Reference 1 provides a detailed description of FEAT and the digraph representation of system failures.

FEAT processes system digraphs and computes transitive closure for the complete graph. This allows FEAT to provide information concerning the ultimate causes and effects starting at any node. Most transitive closure algorithms support only direct connections (such as OR connections in FEAT).² The current FEAT transitive closure algorithm is based on Warren's modifications to Warshall's algorithm,³ which allows computation of transitive closure on a matrix of boolean relations. These algorithms are $O(N^3)$, where N is the number of nodes.

FEAT models of more than 7,000 nodes have already been created. It is anticipated that models approaching 100,000 nodes will be generated for the Space Station Freedom (SSF) Program. Since the existing FEAT algorithm takes more than 388,800 sec to compute transitive closure for a 7300-node model on a Sun Sparc 2 workstation, it is clear that the computation time must be reduced for FEAT to be able to analyze large SSF models.

Several approaches have been taken to develop a more efficient method of computing transitive closure for FEAT digraphs. The Z1 algorithm was developed at JSC as a sequential approach to computing transitive closure for these models by taking advantage of the AND gate

structure in FEAT digraphs. This algorithm correctly solves acyclic digraphs only. A parallel computer version of this algorithm was developed for the multiple instruction, multiple data Intel hypercube and is called ZP. A third variant of the Z, called ZR, was developed to allow processing of cyclic digraphs; this variant takes advantage of experience acquired during the parallel computer development effort. A separate effort by Dave Iverson at Ames Research Center produced an object-oriented algorithm (called AMES), which computes transitive closure of cyclic as well as acyclic digraphs.

The Z1 algorithm starts by performing a topological sort of the digraph and then processes each node in order from roots (nodes with no inputs) to leaves (nodes with no outputs). Each node is evaluated based on whether it is an AND node or an OR node. At each AND node, the inputs are computed to determine the singletons (single-point failures) and doubletons (pairs of failures) that affect this node and that are to be passed on to the downstream nodes. An OR node simply inherits singleton and doubleton lists for all nodes that reach it. The process continues in order until all nodes have been processed. A final pass is conducted to update upstream nodes with downstream data. Each node contains all nodes that reach this node and all nodes that this node reaches.

Example

This example illustrates how the Z1 algorithm computes the transitive closure of a directed graph. The process will be examined using the digraph in figure 1.

Table 1 shows the adjacency for the graph in figure 1.

Step 1: Topological Sort

For the example digraph, the topological order for the nodes is A,B,C,D,E.

Step 2: Singleton and Doubleton List Propagation

Using the ordering from Step 1: If a node has AND inputs, the singleton and doubleton lists from its two inputs are used to compute this node's doubletons and any additional singletons.

The current node will then propagate its singleton and doubleton lists to each node on its output OR list.

In the example, node A will be processed first. Since it has no AND inputs, it will concatenate its singleton list to the singleton list of node B. Node A will then concatenate its doubleton list to the doubleton list of node B (uniqueness checks are made for each singleton and doubleton added to each list, so that multiple listings of

the same node are avoided). Once node A has completed, node B is processed. Since node B has no AND inputs, its singletons and doubletons are sent to node C.

Node C then begins processing. Since it has no output ORs, however, node C is complete; so control is passed to node D, which is also complete.

Finally node E is processed. Node E has AND inputs, so it must compute its singletons and doubletons before propagating its information to its outputs. Using the singleton lists of its two inputs—nodes C and D—node E creates the following doubletons, which are added to its input OR list: (A,D), (B,D), (C,D). This computation is simply a cross product of the singleton sets of node C and node D. Again, a uniqueness check is performed to eliminate any repetitive information.

Once this check is complete, the output lists are updated to indicate the forward reachability. For instance, since node A is a singleton to node C, node C is added to the output OR list of node A. In addition, since node A is a member of a doubleton pair to node E, then node E is added to the output AND list of node A.

Table 2 reflects the final results for the digraph in figure 1.

The ZP algorithm is designed to operate on parallel machines with message passing constructs and several powerful processors. The graph is subdivided using a depth first search, and each processor is assigned a subgraph from the digraph. Each processor then applies the Z1 algorithm to its subgraph. The algorithm does not conduct a topological sort but, rather, keeps track of whether the inputs to a node have been computed. A node is not processed until all inputs are computed. This effectively orders the digraph without the computational overhead of a separate topological sort. Messages are passed from a processor containing a node connected to a node on another processor for each edge that leaves the processor. The message contains all upstream information for the node. Each processor analyzes its subgraph as completely as possible and then waits for messages necessary to continue processing. After all processors complete, a final pass is made through the digraph that consolidates the results and updates upstream nodes with downstream data. The final result is the same as the Z1 algorithm, but it is obtained much more quickly.

The ZR algorithm is essentially a sequential adaptation of the ZP algorithm. The algorithm proceeds until all nodes have been completed. This algorithm does not keep copies of all upstream doubletons at each node; rather, pointers to upstream AND nodes are maintained. AND nodes contain all upstream data. This algorithm is also more suitable for processing cyclic digraphs.

The AMES algorithm takes an object-oriented approach to the computation of transitive closure. It does not use a formal sort to order data but uses an approach similar to that of the ZR algorithm.

Problem Statement

Which algorithm should be incorporated into FEAT? To determine the answer to this question, the performance of the Z1, ZP, ZR, and AMES algorithms was analyzed on a number of large digraph models. The results of these runs will be studied to determine the fastest algorithm and to estimate the computational complexity of the algorithm. This will allow a rough extrapolation of computation times to much larger models.

Approach

A collection of directed graphs was obtained for validation, verification, and testing of each of the algorithms. These graphs ranged in size from 8 to 14,000 nodes. Most were taken directly from actual system models, while others were developed to include special digraph configurations that would rigorously exercise the resiliency of each of the algorithms.

A 40 MHz Sun Sparc 2, with 24 MB of memory and 100 MB of swap space, was used in the testing of each of the sequential algorithms. An Intel IPSC860 hypercube, with 32 processors, was used in the testing of the parallel algorithm. Each of the sequential programs was compiled on this platform, using the same gcc compiler with -O optimization.

The Z1, ZR, and ZP algorithms were initially found to solve only acyclic digraphs, while the FEAT algorithm (FEAT3.3) and the AMES algorithm were designed to handle both cyclic and acyclic graphs. Cyclical digraphs are commonly found in models of actual systems because of feedback loops hydraulic and electrical systems, and other standard system designs. These loops could be manually or automatically found and broken to provide a quicker, but less satisfactory, answer because of the artificial nodes placed in the models to break the loops. Code to solve cyclic digraphs is currently being developed and tested in the ZR algorithm. To accurately compare each of the five algorithms, it was necessary to work with a set of acyclic graphs. A depth first search was used to determine those graphs that were acyclic.

A set of the smaller digraphs was used to verify and validate each of the algorithms by hand. Solutions for larger digraphs from each of the algorithms were compared by sorting the final solution and performing a "diff" Unix command. Each algorithm was run on very small test models, which contained models known potentially to cause incorrect answers, and the results were manually validated as being correct. Once we were certain that each of the algorithms computed the same solution, the analysis of each of the algorithms began.

The get-time-of-day function was installed in each algorithm to obtain the wall clock time of each run. Two times were recorded: preprocessing, which indicates the time spent to convert the input file into adjacency information; and transitive closure, which indicates the time spent to compute the reachability of the digraph.

In an attempt to estimate the order of complexity of each algorithm, the time versus node data were analyzed by linear regression techniques to determine the coefficients to the following equation:

$$t = a \cdot N^b \quad (1)$$

where

- t is the time in sec
- a is a multiplicative constant
- N is the number of nodes
- and b is the power constant.

The power constant, b, provides an estimate of the order of the complexity of the computational algorithm.

Results

The following table shows the actual wall clock time for each of the algorithms for each of the acyclic digraphs listed below. The times listed in table 3 below are in seconds. The ZP results are prefaced by "8" in the following tables and figures to indicate that the parallel algorithm was run on an eight processor hypercube.

The b value shown in table 4 represents the estimate of the exponent of the function, b in equation 1, for the curves describing the time versus nodes data shown in table 3 and in figure 2. The 95% confidence intervals shown in table 4 indicate that the AMES algorithm has a significantly higher exponent than the Z family of algorithms. It also indicates that the ZP algorithm has a significantly lower exponent than the other algorithms. The FEAT3.3 data have too few data points to determine the exponent with sufficient precision to make any comparisons. The coefficient of determination, also called R2, is shown for each set of data.

Conclusions

The results indicate that the ZR and ZP algorithms appear to be faster than the other algorithms for acyclic graphs. However, many of the digraphs being developed for SSF contain cycles. Modification and testing of the ZR and ZP algorithms are currently under way.

Two areas of study need to be pursued. First, the Z family algorithms require modification to allow correct processing of cyclic graphs. A follow-up set of timing runs needs to be completed to finally determine the appropriate algorithm(s) for incorporation into FEAT. Second, further analysis of the ZP algorithm with much larger model sizes is needed to verify the low b value observed during these tests.

References

- ¹Pack, G. and Wadsworth, D, "Failure Environment Analysis Tool Applications," Technology 2002 Proceedings, Baltimore, MD, December 1992.
- ²Cormen, T., Leiserson, C., and Rivest, R., *Introduction to Algorithms*; The MIT Press, Cambridge, MA, 1991.
- ³Warren, H. S., "A Modification of Warshall's Algorithm for the Transitive Closure of Binary Relations", Communications of the ACM, Vol. 18, No. 4, April 1975.

Acknowledgments

This project is funded by NASA through the Intelligent Systems Branch of the Johnson Space Center.

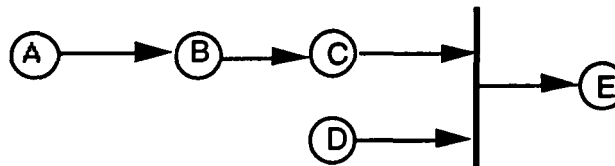


Figure 1. Graph Illustrating Z1 Algorithm Computation.

Table 1. Adjacency for Graph in Figure 1

NODE	INPUTS		OUTPUTS	
	OR (Singletons)	AND (Doubletons)	OR	AND
A	A		B	
B	A,B		C	
C	A,B,C			E
D	D			E
E	E	(C,D)		

Table 2. Final Results for Diagram in Figure 1

NODE	INPUTS		OUTPUTS	
	OR (Singletons)	AND (Doubletons)	OR	AND
A	A		B,C	E
B	A,B		C	E
C	A,B,C			E
D	D			E
E	E	(A,D),(B,D),(C,D)		

Table 3. Actual Wall Clock Time for Algorithms

GRAPH NODES	AMES (secs)	Z1 (secs)	ZR (secs)	FEAT3.3 (secs)	8ZP (secs)
210	0.9	2.8	4.3	4.1	79.5
554	6.1	134.1	142.3	211.9	291.3
871	8.0	31.2	9.3	264.3	126.0
1429	34.4	143.7	58.5	1951.0	169.6
3073	247.1	140.4	133.2	26952.0	233.9
3936	430.0	468.0	847.9		548.0
5305	830.0	574.0	489.0		544.0
5718	992.0	768.0	628.0		621.0
7272	1827.0	968.0	748.0		750.0
14504	12415.0	5365.0	2805.0		

Figure 2 graphically displays the data shown in table 3.

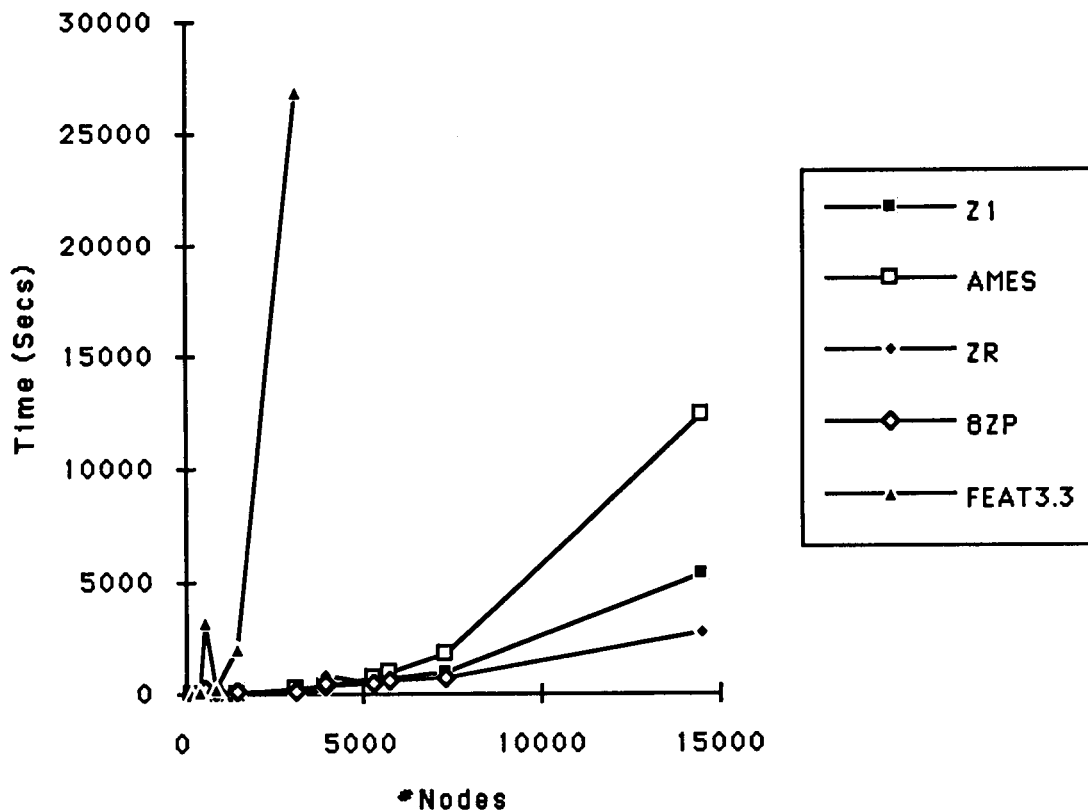


Figure 2. Graphical Display of Data in Table 2.

Table 4 shows the estimated complexity for each of the algorithms.

Table 4. Estimated Complexity of Algorithms

	AMES	Z1	ZR	FEAT3.3	8ZP
b	2.32	1.78	1.72	2.77	0.59
95% Confidence Interval	(2.20,2.44)	(1.43,2.14)	(1.31,2.12)	(1.32,4.22)	(0.43,0.76)
Coefficient of Determination (R²)	0.993	0.902	0.876	0.784	0.853

Failure Environment Analysis Tool Applications

Ginger L. Pack and David B. Wadsworth*

Johnson Space Center/ER

*Lockheed Engineering and Sciences Company

Abstract

Understanding risks and avoiding failure are daily concerns for the women and men of NASA. Although NASA's mission propels us to push the limits of technology, and though the risks are considerable, the NASA community has, instilled within it, the determination to preserve the integrity of the systems upon which our mission and our employees' lives and well-being depend. One of the ways this is being done is by expanding and improving the tools used to perform risk assessment. The failure environment analysis tool (FEAT) was developed to help engineers and analysts conduct risk assessment and failure analysis more thoroughly and reliably. The FEAT accomplishes this by providing answers to questions regarding what might have caused a particular failure, or, conversely, what effect the occurrence of a failure might have on an entire system. Additionally, FEAT can determine what common causes could have resulted in other combinations of failures. FEAT will even help determine the vulnerability of a system to failures, in light of reduced capability. Also, FEAT is useful in training personnel who must develop an understanding of particular systems. FEAT facilitates training on system behavior by providing an automated environment in which to conduct "what-if" evaluation. These types of analyses make FEAT a valuable tool for engineers and operations personnel in the design, analysis, and operation of NASA space systems.

Introduction and Problem Statement

FEAT was developed as part of an effort to find ways to identify and understand potential failures better that threaten the integrity of NASA systems. Past and current methods of failure assessment consist of developing often enormous amounts of documentation in the form of failure mode effect analysis (FMEA) worksheets. Engineers create these worksheets by exhaustively attempting to enumerate potential system failures and consequences. Hazards analysis is performed in a similar manner; experts are gathered together and are asked to brainstorm about the hazardous manifestations of various failures. System knowledge and experience are necessary for ensuring the comprehensiveness of this approach. There are, however, troubling drawbacks to this technique. First, the difficulty exists of anticipating every scenario. Analysis is also inherently constrained by the limits of actual experience. Further, such methods lack

consistency and do not enforce a standard level of coverage. Although there is certainly much to be credited to knowledge acquired through experience, it is not sufficient to avoid unanticipated interactions that may lead unexpectedly to undesirable consequences. As many industries have learned, sometimes experience comes at too high a cost. Those at NASA have been looking for better ways to anticipate failure and for tools to assist in "designing out" potential problems. FEAT was developed to address this problem.

Technical Approach

FEAT is a software application that uses directed graphs, or digraphs, to analyze failure paths and failure event propagation. The behavior of the systems to be analyzed is represented as a digraph. Then, the digraph model of the system is used by FEAT to answer questions concerning the cause and effect of events that are captured in the model. The first step, therefore, in using FEAT is to create the digraph model of the system in which one is interested. Once FEAT has analyzed the digraph, it has the information it needs to perform cause-and-effect analysis.

What are digraphs? Directed graphs are graphs that consist of a set of vertices and a set of edges, where there is an edge from one vertex a to another vertex b . The vertices are drawn as circles, and the edges are drawn as arrows. The direction of the arrows indicates a causal relationship between the vertices (fig. 1). The vertex from which the edge begins is called its source, and the vertex at which the edge terminates is called its target. Direct graph theory is an accepted and established area of mathematical study. We will, therefore, only introduce it in this paper to the extent necessary for an understanding of how it is used in FEAT. The interested reader may find further information by consulting the literature.

The structure of the digraph can be represented by a matrix and, consequently, can be easily implemented in a computer. The conversion from digraph to matrix is straightforward and is illustrated below in figure 2. This matrix is called the *adjacency* matrix (ref. 1) and is the basis from which other information about the graph can be derived. The matrix of the graph is obtained by entering either zero or one, depending on whether or not an edge connects two vertices. The presence of an edge from a to b in figure 1 indicates an entry of one (1) into the corresponding matrix entry. However, since there is no edge from a to c , a zero (0) would be entered in the corresponding matrix entry.

Additional information can be added to the digraph by applying logical operators to express conditional statements. FEAT uses AND and OR operators to accomplish its analysis. The AND operator is represented on the graph as a vertical bar with a horizontally placed arrow at its center. An OR operator is simply two or more edges whose target is the same vertex. These operators (fig. 3) and their use in FEAT (figs. 4 and 5) are described below.

The "AND" gate is shown in figure 5. The AND gate is used when both Event A and Event B must occur for Event C to occur. Conversely, if only Event A occurs or if only Event B occurs, Event C does not occur.

Analytical Capabilities The *reachability* of an event refers to whether there is a path by which other events in the digraph can be reached. A given event is said to reach another, if the first event can cause the second through some path of the graph. Using the adjacency information derived from the digraph, reachability can be computed for every event and pair of events in the digraph. Analysis can be conducted upstream or downstream from an event node. (References 2, 3, and 4 provide a much more detailed discussion of digraphs and reachability.)

Reachability information allows FEAT to answer the following questions about a modeled system:

- What happens to the system if "Event A (and Event B and Event C and ...)" occurs?
- What are the possible causes of "Event A"?
- What common cause could account for the simultaneous indication of numerous events?
- What is the susceptibility of the system to new events, given that one or more events have already occurred or the system has been reconfigured because of, for example, maintenance?

Digraph Example The following example demonstrates how a digraph might be implemented for a light and switch. The digraph provides a methodical way in which to express the topology and behavior of a system. It is worth noting that the digraph itself may have various constructions for the same information contained in it, depending on who created it. Different modelers may lay out the digraph differently. However, for a properly constructed digraph, the same information will be captured. In the following example (figs. 6 and 7), power source A provides current to switch A, which connects to the bulb. Similarly, power source B can energize the bulb.

- If "Power Source A Fails" or "Switch A Fails Open," then "Switch A Output Fails." This is an example of OR logic and is shown in the digraph by the arrows leading into "Switch A Output Fails."
- If output from both switches A and B fails, they will cause the "Power at Light to Fail." This logic appears as an AND gate on the digraph (the vertical line). In this case, the AND gate reflects redundancy designed into a system.

Why digraphs?

Directed graphs are useful because they visually depict the logical topology and dependency relationships of physical and conceptual systems and processes. Because they capture causal effects between events, they can be used to describe system behavior. Directed graphs are also easily converted into a matrix and, because of this, can be readily analyzed in a computer. Creating and laying out the digraph of a system also formalizes the method of evaluation during the analytical process and provides a standard representation convention. Finally, digraph analysis is mathematically sound, since methods for determining connectivity paths of the digraph vertices can be mathematically proved.

Method: Directed Graphs and FEAT

Digraph construction is facilitated by use of an editor specifically designed for the task. Such an editor is included in the FEAT package, which consists of two programs: Digraph Editor and FEAT.

Digraph Editor

The Digraph Editor facilitates construction of the digraph model by allowing the user to create event nodes, edges, and the logic operators, and to connect and arrange them into a digraph. Event nodes and edges are laid out and connected using the logic operators. The pieces that make up a digraph are supplied in a digraph toolbox from which items may be selected. These items are placed on the screen and arranged to produce the system digraph.

Other information is needed to complete the digraph and to make it usable by FEAT. Event nodes have an associated text block, which includes information that will identify the event node to FEAT, describe the event for the user, and relate the event to a drawing that contains the component to which the event pertains. This information is extracted from tables that the user creates. Digraph Editor uses the tables to generate automatically a mnemonic reference that FEAT will use to identify the event.

Digraph Editor also provides a number of tools for validating and verifying the model as it is being developed. Digraph Editor will check tables for duplicate entries, check nodes for incorrect form, and determine whether a selected node has a duplicate in the digraph. Digraph Editor also contains an algorithm that allows the user to analyze small or incomplete digraphs while still in the editor. Once the digraph is completed and the paths in it are analyzed, FEAT can return answers to questions regarding the behavior of the modeled system.

Currently, digraph models are created manually by selecting and arranging digraph components; the modeler must interpret drawings and other sources of information to generate the digraphs. This is a laborious task. Consequently, efforts are under way to develop methods

to translate schematics and drawings automatically into corresponding digraph models.

Digraph Editor is currently only available for the Macintosh II class of computer.

FEAT

FEAT is the portion of the package that analyzes single or multiple digraphs and graphically displays causes and effects of events. Propagation results are shown both on the digraphs and on another associated graphical representation, such as a schematic or block diagram. FEAT uses a multi-step algorithm, described in Reference 2, to compute reachability for each event and pair of events in the digraphs. Events are identified to FEAT through the mnemonic that is generated by Digraph Editor. Queries about the behavior of the system are made by selecting events and telling FEAT to return all of the causes of that event (targeting), or by telling FEAT to return all of the effects of that event (sourcing). FEAT displays all of the single events, and all pairs of events, that may cause a selected event. Multiple events may also be selected and analyzed. FEAT allows some events to be temporarily removed from the analysis so answers can be obtained about a reconfigured system.

FEAT also contains a feature that allows users to attach to a schematic, formatted data base information and graphics. In this way, component descriptions, parts lists, drawings, etc., may be displayed in conjunction with a schematic.

One of the major advantages of FEAT, as discussed in Reference 2, is that it allows the analysis of very large systems. Large systems can be digraphed by creating and connecting a series of smaller digraphs. FEAT understands when propagation occurs across the digraphs.

Planned enhancements to FEAT include the following: increasing the speed with which reachability is computed by improving the FEAT computational algorithm; providing a method for computing and displaying probabilities of events occurring; and computing and displaying the time it takes for an event to propagate through the graph.

FEAT is currently available for the Macintosh II class computer and for UNIX/X-Windows/OSF-Motif systems. No programming skill is required to use FEAT. A course, however, in digraph modeling is quite helpful in learning how to construct system models.

Results: Digraphs at NASA

Why NASA chose digraphs?

NASA's interest in digraphs began as part of the Shuttle Integrated Risk Assessment Project (SIRA). SIRA was initiated in the wake of the Challenger accident in an effort to find better ways of assessing risk and preventing failure. Digraphs support such analysis by providing end-to-end cause-and-effect analysis of

modeled systems. Digraphs also provide a standard and methodical approach for conducting safety analysis and risk assessment. Digraphs capture information in an easily retrievable format and facilitate the transfer of design information. FEAT takes advantage of these characteristics in a way that aids engineers and analysts with design, assists safety engineers with risk assessment, and promotes understanding of system behavior, thereby making FEAT a good tool for training inexperienced persons.

What has been done at NASA?

The first system to which digraph analysis was applied was the Space Shuttle Main Engine System. Since then, acceptance of digraphs and the use of FEAT have extended in several directions. Most recently, FEAT has been formally released to the Space Station Freedom Program (SSFP) Technical Management Information System (TMIS), as Digraph Data System (DDS) release 1.0. DDS will, through TMIS, be available to Space Station Freedom (SSF) Engineering and Integration, SSF Combined Control Center, and the various work packages and their contractors. A Macintosh Powerbook version of FEAT will be deployed as a development test objective (DTO) on the STS-52 flight scheduled for October 1992. Reliability and maintainability personnel at JSC are using FEAT to construct a model of the simplified aid for extravehicular activity rescue. FEAT is also being used to model the redesigned servo power amplifier for the remote manipulator system.

Proponents have used FEAT for a variety of analytical tasks, such as fault tolerance analysis and redundancy management (FT/RM), fault detection, isolation, and recovery (FDIR), and "What-If" analysis. Within the SSFP, FEAT is being used in the performance of integrated risk assessment for the Station, which includes FMEA, hazards analysis, and FT/RM. FEAT has also been established as a baselined tool in the Mission Operations Combined Control Center, where flight controllers will use FEAT models to assist with real-time monitoring tasks. The FEAT role is expanding in both Space Station and in Space Shuttle.

Space Station The Space Station Engineering Integration Contractor (SSEIC) is using FEAT to perform integrated risk assessment. This task consists of performing the analysis to assure that the Station design is safe, reliable, and has an acceptable level of risk (ref. 5). The Space Station design consists of modules designed and built by the United States and of modules that will be designed and built by NASA's international partners. The work to be performed by NASA is divided into four work packages distributed among different centers. Additionally, a variety of contractors are working in support of the work packages. Consequently, system integration is a paramount concern of the program. SSEIC is tasked with ensuring the integration of these various factions and is using digraph-based FEAT to work

the integration problem. Specifically, FEAT supports the following areas of the integrated risk assessment process:

- Reliability Analysis
- Safety Analysis
- Integrated Risk Analysis
- Integrated Risk Assessment

The models being developed for the Station integrated risk assessment will eventually be provided to Mission Operations personnel for use in FDIR of the on-orbit Station.

Space Shuttle FEAT is scheduled to fly on STS-52 as a DTO. A FEAT model of the S-band communications system has been installed on an Apple™ Powerbook,™ which will be flown aboard the Shuttle. Astronauts will use the model to perform onboard fault isolation for the S-band communication system. They will be able to configure the model to match the actual S-band system configuration and then will use FEAT to identify possible causes of failures of the S-band system.

Conclusions: Future Applications of Digraphs

Digraphs are gaining acceptance, within the NASA community, as a viable method for conducting many kinds of analyses. SSFP and Operations has mandated the use of digraph analysis for the Space Station Level II Integration effort and many others are beginning to take up the banner. Some of the potential areas of application include the following:

Fault Isolation/Testability

FEAT's ability to model and analyze system failures make it a natural candidate for fault isolation efforts. If a failure event occurs, FEAT can display all of the possible single and paired causes for that event. However, in a large system, potential causes can be enormous in number. A method of pruning the list of possible causes is then necessary. Sensor information associated with the system can be used to remove candidate causes that occur downstream of a known nominal condition. Incorporation of sensor data into the analysis can help reduce the number of candidate failures to a manageable sum. Then, using traditional techniques, further isolation can be accomplished. Figure 8 shows an example of such a case.

Sensor data may also be combined with FEAT to identify the potential for cascading alarms. For instance, if a fault occurs downstream from a sensor, the sensors upstream will eventually alarm as a result of the fault. FEAT can show the effects of a fault on the downstream sensors.

This solution is being implemented by NASA in an extension of FEAT, called extended real-time FEAT (ERF). ERF automatically prunes the list of possible faults according to sensor information. ERF is being developed as a part of the FDIR system for the On-orbit Control Center Complex. Mission controllers will use

ERF to resolve off-nominal system behavior by reducing the potential number of failure causes.

FEAT developers are pursuing the possibility of incorporating, or interfacing with, a testability analysis tool that will help to evaluate sensor coverage in systems and make recommendations regarding appropriate sensor locations. ERF is dependent upon adequate sensor information and proper placement of the sensors. Properly placed sensors provide information to locate faults quickly and accurately. The combination of FEAT, ERF, and testability tools will make a very powerful fault-isolation system.

Temporal Analysis

Not every event immediately affects the next downstream event. There may be appreciable delays within an event and between events. For example, an inappropriately shut valve may not, for some time, cause the pressure in the system to rise to an unacceptable level. In such a situation, time delay is an important aspect of calculating the potential failure space.

This issue will be addressed in FEAT when a modification is made to Digraph Editor to allow modelers to include time delays within events and delays between events. FEAT will then compute the maximum and minimum time delay between selected events. This capability will be supplied in a future version of FEAT.

Software Modeling

Physical systems are not the only candidates for digraph analysis. Software functions and data flow can be modeled as well. Particularly, the flow and effect of invalid/improper data can be modeled. This can provide insight to the designer in determining mission-critical software functions. Additionally, the effect of invalid data on other system functions (both software and hardware) may be shown. For instance, a software functional component that generates invalid data as an event may then provide those data to other software and hardware as an invalid data input event. FEAT can be used to model these behaviors, too.

Design Evaluation and Redundancy Management

Digraph models can be used to determine whether or not a system design provides sufficient redundancy. Maintenance and configuration effects on the system can be evaluated by selectively removing (setting) components from the system. The reconfigured system can then be evaluated for induced single and paired events. This can be particularly useful in determining new vulnerabilities after a system has encountered failures and/or has portions of the system secured for maintenance.

FEAT contributes to design evaluation by rapidly displaying all single events caused by the event of interest

as well as all pairs of events that will result in that event. Unexpected single-point, common-cause events are also quickly identified. As the design is modified to provide additional redundancy, the digraph model can be updated to reflect the changes, and the new set of single events and pairs of events can be evaluated.

Logistics Analysis

Logistics analysis addresses corrective and preventive maintenance tasks and determines the kinds and numbers of repair parts needed for a system. This type of analysis is associated with the reliability and availability (ref. 6) of systems. Reliability is defined as the measure of the mean time between failure and concerns the probability that a system will operate over a specified period of time. No provision is made for repair when calculating reliability. Availability varies from reliability, in that it is a measure of the mean time to repair or the probability that the system will operate over a period of time, considering that something can be done to restore functionality lost as a result of a failure. How system repairs can be supported, or supportability, is important to determining availability. If repairs can be made instantaneously, availability is increased. However, long delays between failure and repairs make the system proportionally less available.

FEAT models can help to identify critical components and the effect of their failure upon the system. Digraph models of the system can, along with specific part reliability, help to determine priorities for inventory stocks and schedules for maintenance. Spare parts inventories are a major factor in determining supportability. For example, spares for parts that cause single-point, common-cause events should have higher priority for stocking than parts that contribute to pairs of events.

Maintainability concerns the time it takes to remove and replace a component. Digraph models can identify components prone to low reliability and single common-cause failure. Designers can then either improve the reliability of the component or ensure that such items are accessible and easily replaced.

Summary

As NASA continues to search for better and innovative approaches to new and old problems, directed graph analysis has emerged as a viable addition to the methods applied to risk assessment. Directed graphs are a well-established area of mathematical study and analysis and provide an easily comprehensible visual representation of cause-and-effect relationships.

Conversion of the digraph to an equivalent matrix is straightforward and allows analysis of digraphs to be mathematically calculated and verified. The nature of matrices also makes them ideally suited for computerized calculations, which in turn provide a vehicle for automating the task of risk assessment and failure analysis.

FEAT uses directed graph theory to provide engineers and analysts with a powerful and flexible automated analytic helper. FEAT can provide end-to-end analysis of cause-and-effect events. Very large systems can be modeled in modules, then connected to form the entire system. This feature also allows digraphs to be arranged in mix and match fashion. FEAT can detect and return information about single-point failure vulnerability, failure-event pairs, common-cause events, and reduced capability analysis. FEAT shows the results of event propagation on system schematics and on the associated digraph. Digraph Editor provides a helpful way for the analyst to create digraphs.

References and Bibliography

- ¹Levy, L., "Discrete Structures of Computer Science," John Wiley & Sons, 1980.
- ²Stevenson, R., Miller, J., and Austin, M., "Failure Environment Analysis Tool (FEAT) Development Status," *AIAA Computing in Aerospace VIII*, AIAA-91-3803, Oct. 1991.
- ³Sacks, I., "Digraph Matrix Analysis," *IEEE Transactions on Reliability*, Vol. R-34, No. 5, Dec. 1985.
- ⁴Sacks, I., Keller, G., and Rauch, R., "Application of Digraph Matrix Analysis to the Space Station," RDA, Logicon, R & D Associates, RDS-TR-148400-001, Sept. 1987.
- ⁵Schier, J., "Integrated Risk Assessment (IRA): Defining the Level II Safety and Reliability Job and Implementation Plan Using Digraphs," Unpublished Grumman presentation, Sept. 1992.
- ⁶Blanchard, B., *Logistics Engineering and Management, 4th Edition*, Prentice-Hall, Inc., Englewood Cliff, NJ, 1992.
- ⁷Haasl, D., Roberts, N., Vesely, W., Goldberg, F., *Fault Tree Handbook*, GPO Sales Program, U.S. Nuclear Regulatory Commission, Washington, D.C., 1981.
- ⁸Pearl, J., "Probabilistic Reasoning in Intelligent Systems," Morgan and Kaufman, 1988.

Acknowledgments

The FEAT Project is funded by the NASA SSF Advanced Programs Development Office (Code MT) and the SSF Program Office (Code MS).

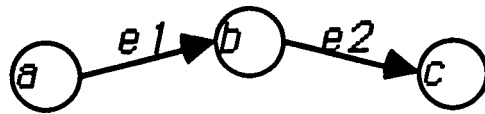


Figure 1. A Digraph.

	a	b	c
a	0	1	0
b	0	0	1
c	0	0	0

Figure 2. Conversion from Digraph to Matrix.

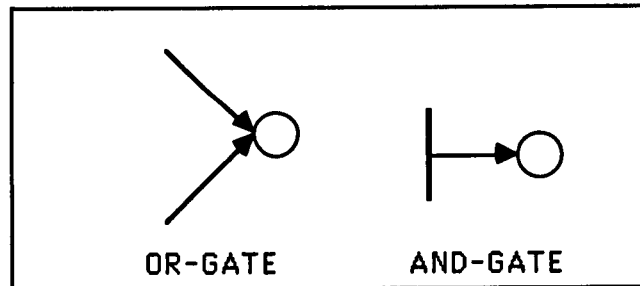


Figure 3. The AND and OR Operators.

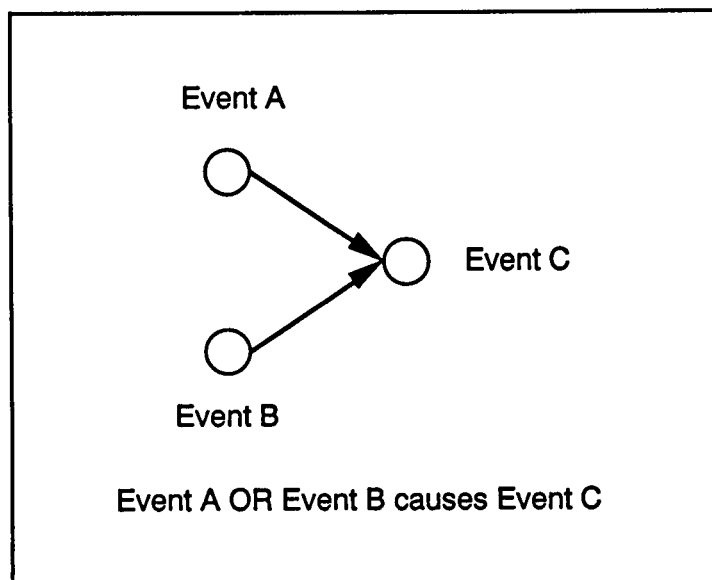


Figure 4. The OR Operator as Used in FEAT.

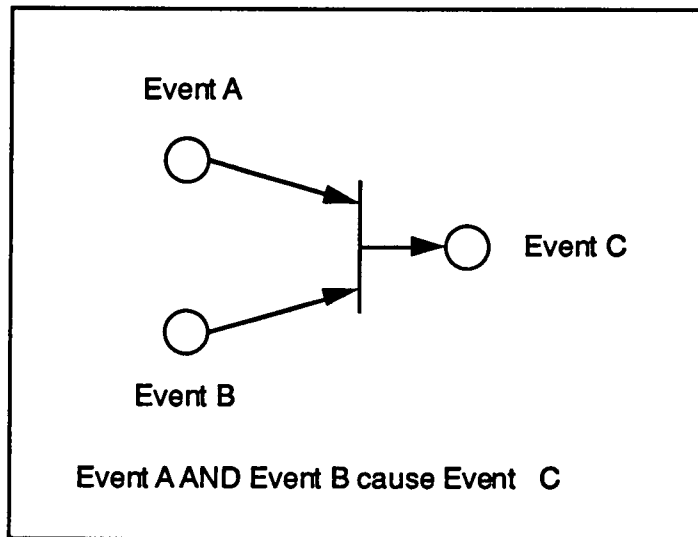


Figure 5. The AND Operator as Used in FEAT.

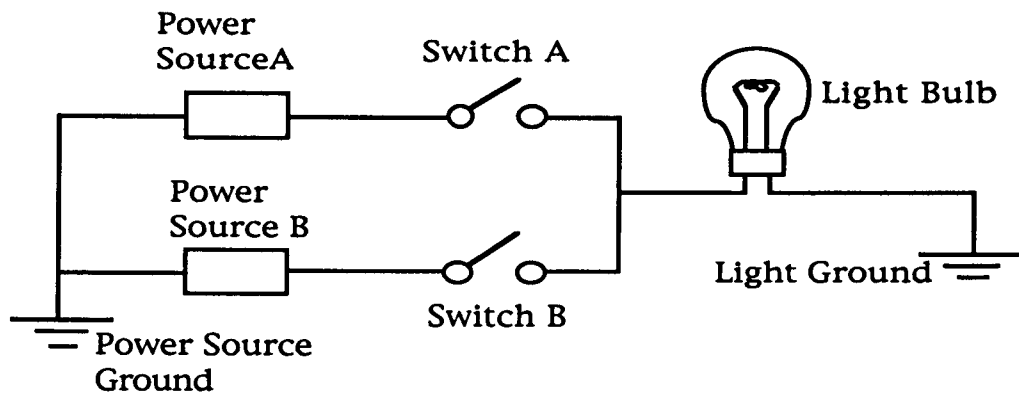


Figure 6. Light Bulb and Power Source Schematic.

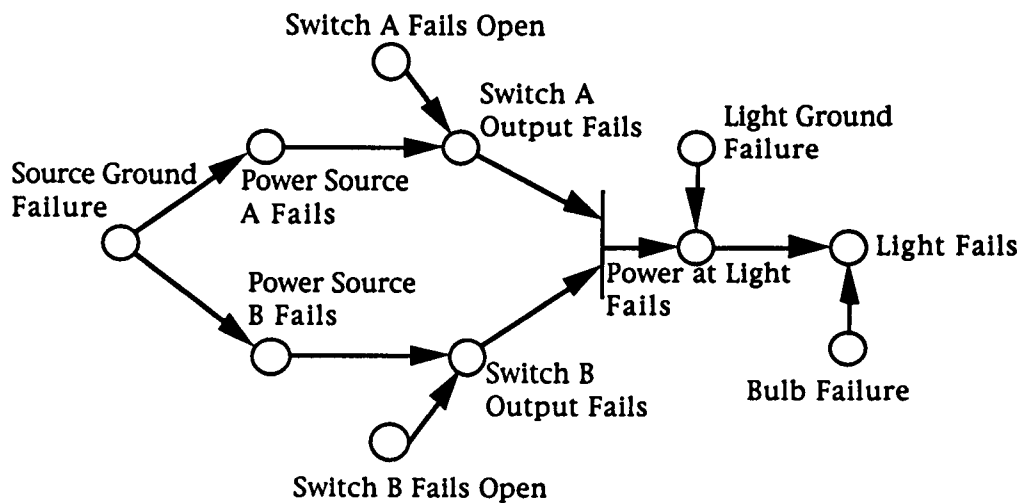


Figure 7. Digraph of Light Bulb Schematic.

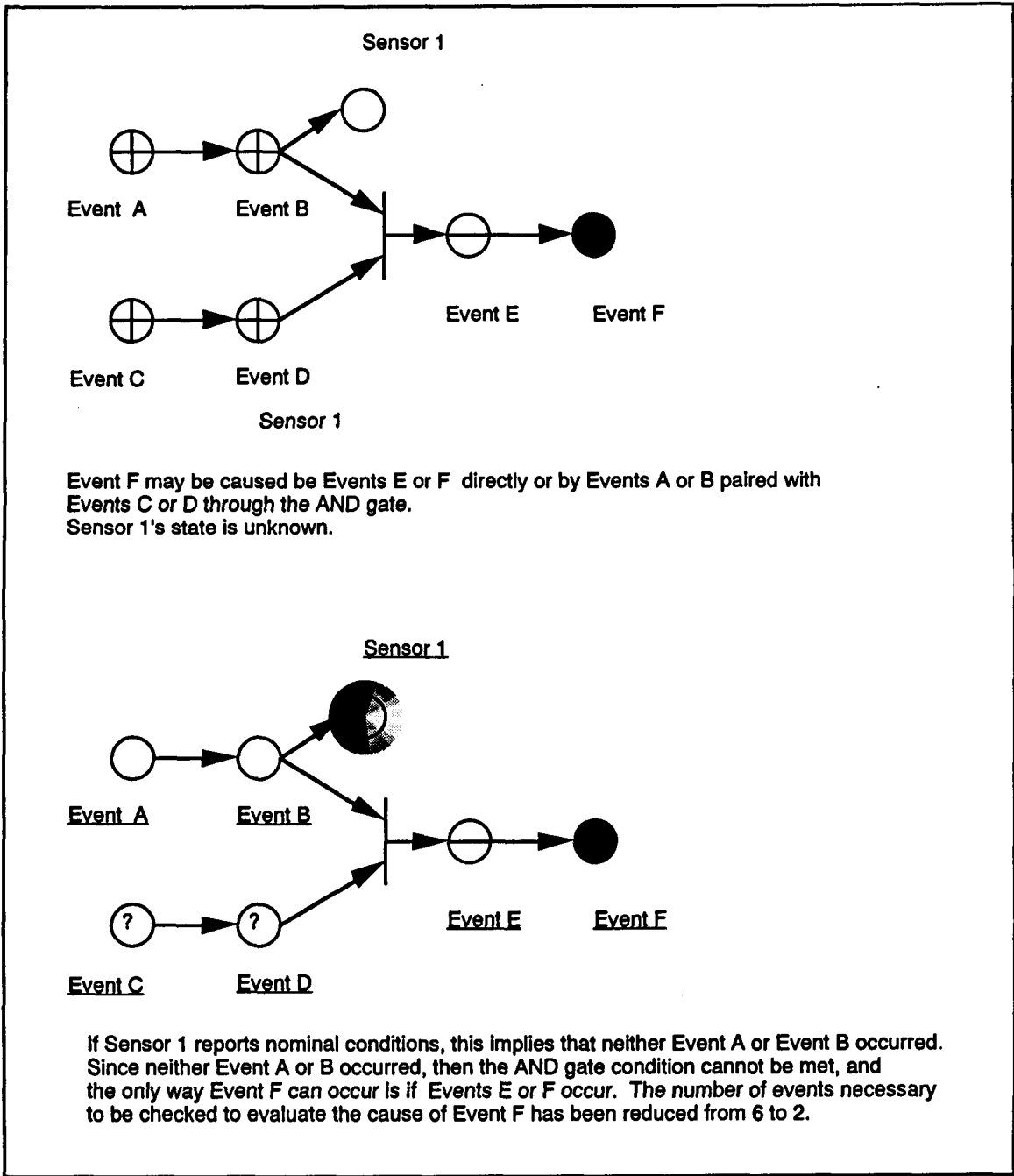


Figure 8. FEAT Failure Analysis.

Application of Automation and Intelligent Software to Analysis of Engineering Space Shuttle Systems

Ginger L. Pack
Johnson Space Center/ER

Abstract

The role of mission evaluation room (MER) engineers is to provide engineering support for Space Shuttle systems. These engineers are concerned with ensuring that the systems for which they are responsible function reliably and as intended. The MER is a central facility from which engineers may work to fulfill this obligation. Engineers participate in real-time monitoring of Shuttle telemetry data and provide a variety of analyses associated with the operation of the Shuttle.

Currently, the tasks involved with filling this role require excessive expenditure of human resources, which translates into unnecessarily high costs for Shuttle mission ground support. Prudent and judicious application of computer technology can reduce the cost of gathering and analyzing the data needed by engineers to fulfill Engineering's MER responsibilities.

The goal of the MER Intelligent Diagnostic and Analysis System (MIDAS) task is to streamline the engineering activity by applying advanced automation to eliminate some of the tasks humans are required to do, tasks which are better accomplished by computers, thereby reducing the computational burden placed upon humans and allowing engineers to quickly and accurately determine the health and status of their systems.

This can be done by off-loading to computers and software the tasks of data gathering, filtering, and analysis. Incorporation of these tasks into software provides the engineers with information that is in a more concise and usable form needed to support decision making and engineering evaluation. Engineers are then able to concentrate on more difficult problems as they arise.

Introduction

The technology used to support MER engineering analysis activity has changed little since the days of NASA's Apollo Program, which placed men on the Moon. Yet the reusable Space Shuttle is decidedly more complicated than the craft flown during the Apollo days. Engineers now must worry about long-term trends and effects of system behavior and performance. Data concerning past flights may be directly relevant to current operations. Also, flights are now commonly as long as 8 to 10 days duration and occur at more frequent intervals. This places a great deal more burden on humans to process and analyze system information.

These factors contribute to the complexity of analysis tasks and result in ever increasing amounts of data that engineers must collect and interpret.

Advances in computer technology have provided the means to relieve humans of the burdensome aspects of some analysis. JSC's Automation and Robotics Division is working to transfer advances in technology to the operational environment. Specifically, the MIDAS project provides MER engineers with software to assist them with monitoring, filtering, and analyzing Shuttle telemetry data during and after Shuttle missions.

Problem Statement/Description

Historically, engineers have had to rely strictly upon numerical values, displayed as ASCII text, to understand the state and operating condition of their system. Information in this form is crammed onto displays that engineers must monitor and interpret (fig. 1). Several of these displays exist for each subsystem. Engineers visually monitor these displays during missions to obtain an understanding of the behavior of their systems. Only one display at a time may be shown. This arrangement precludes the engineers noticing changes in information that is not contained on the display being viewed. The selection of screens available for viewing is controlled by Mission Operations personnel. During missions, engineers must often "chase around" the displays that contain the information in which they are interested. This further complicates the duties that engineers must perform to maintain the health of the systems for which they are responsible.

There are several aspects to the work that engineers must do to monitor and analyze the behavior of Shuttle systems. Specific methods and approaches used depend upon the nature of the system. Some systems are analyzed by looking for the occurrence of known, expected behaviors and events. Others are better analyzed by looking for behaviors and events that do not fit known patterns. Still others may be understood in terms of past system behavior by comparing current behavior with historical information.

Whatever view is taken of the system, the most basic-level task associated with accomplishing this work is that of monitoring the data as they are downlinked from the Orbiter. The data values found in the downlink consist of discrete valued parameters, which can be considered as on/off, or of set/un-set bits, and of analog parameters whose values are continuously increasing or decreasing.

The configuration and/or behavior of these data values are used by engineers to infer the health and performance of Orbiter systems.

The next level of tasks consists of identifying and collecting relevant data needed to support analysis and evaluation. Training and experience educate engineers to convert numerical information mentally into models of system behavior and performance. This in turn allows them to identify data that appear to be inconsistent with the expected model and its states. When appropriate sets of data have been defined and collected, various levels of detailed analysis can be performed.

There are major drawbacks to using humans, as is now done, to perform all of these tasks. People must stare at screens full of data, and assimilate this information into a cohesive mental model of the system. Also, it is incumbent upon the engineer to notice that data have changed and to recognize the significance of a change. Even after the engineer has noticed something of interest and written it down on paper, it remains for the engineer to determine where, in the vast collection of mission data, relevant information is located. Often only a general idea of which data are needed is known by the engineer. A request for the actual data values is then submitted. If the range is off, another request must be generated and submitted for processing. Engineers may be required to submit several requests for data before actually obtaining the information that is relevant to their analysis. Often, engineers order up large numbers of plots, then pore over them to ascertain system behavior.

Consequently, a great deal of effort goes into finding the data to be plotted, creating the plots, and refining the set of plots to reflect pertinent information prior to any analysis of the results. For some systems, plots of associated data are generated over a sequence of intervals, and the collection is reviewed in an effort to detect significant changes in the system. Working from the plots, engineers sift through data in an attempt to locate inconsistencies, confirm events, and gather supporting information for trend analysis. The engineer must be able to recognize and note any inconsistencies in the plotted data. Additional plots may be requested to confirm or dispel anomalies or "funnies" detected in the data and to support diagnosis of failed conditions.

This mode of operation is plagued with inherent inefficiency. Humans are a poor choice for performing tedious and boring tasks such as continuous eyes-on monitoring. Distraction, boredom, and errors in translation from screen to paper are some of the pitfalls of this approach. Much time is also wasted in looking for and obtaining data for analysis. Further, system knowledge often remains locked up in the years of experience it takes to become proficient in these methods. Loss of such an employee, due to attrition and retirement, equals loss of the knowledge.

Because engineers have few tools to assist them in gathering, filtering, and refining these large amounts of data, a significant amount of their efforts is dedicated to

this process. This in turn translates into unnecessarily high costs for supporting Shuttle and, eventually, Station operations. Automation and intelligent software can be used to off-load the routine and tedious tasks, which comprise a large part of the MER engineer's efforts, and to filter and refine data sets to contain pertinent information. Engineers will spend less time accumulating and sifting through data and more time performing analysis. Discussions with Orbiter subsystem managers reveal a real need for assistance in this area as flight rates increase, and as the prospects for increased amounts of continuously supplied data from Space Station Freedom systems become reality.

Approach/Method

The MIDAS project addresses these issues by providing software that selectively monitors data, filters data, and interprets and graphically displays results.

Areas that have been identified as candidates for automation within the scope of this project include the following:

- status monitoring and "smart" logging of system data to verify configuration and provide notification of incorrect or unexpected states
- event detection and explanation to identify events that cannot be explained by known states and conditions
- trend monitoring and recognition to assist in detecting wear and degradation of components
- comparisons between current and historical data to enable detection of changes and inconsistencies in behavior
- automated verification of in-flight checkout and associated fault diagnosis
- calculation/prediction of consumption rates to enable management of resources
- comparison of actual usage rates to predicted usage rates to detect leakage

Automation requirements are developed through close interaction with Shuttle subsystem engineers. User feedback is solicited and incorporated into the architectural design, and the implementation of the design. Product reviews are also conducted with the user to ensure appropriateness and accuracy of results, and to train the user in operation of the application. Finally, products are iteratively revised after being used in the operational environment. This approach involves users continuously throughout the product development and implementation and gives them a stake in the final product. It also ensures user "buy in" to the technology, since they help to define the implementation of the technological solution.

MIDAS applications are written in the "C" language using X-windows version 11, release 5 (X11R5), which is standard with most UNIX operating systems. Also used is the commercial off-the-shelf Motif widget set and an extensively modified public domain plot widget, from which some data displays are created. The applications

currently run on the SUN (OS 4.1.3 version of UNIX) Sparc1+ and Sparc2 machines, Masscomp workstations, and DEC stations.

Results

Several products have been generated under the MIDAS project. Applications have been developed for the tracking and communications system, the remote manipulator system (RMS), and the propulsion and power system.

Fiscal year (FY) 1992 activity began by converting previously developed applications to XWindows. Tracking and communication was the first system for which applications were constructed. During FY 1992, an existing application, the S-band automated monitor and logging application, was cloned and applied to the payload communications systems and the text and graphics system (TAGS). The S-band, payload, and TAGS logging functions automatically monitor and log discrete parameters for each of these systems. Results are displayed on a screen and are also written to a file. Information included in the log consists of the previous value of the changed parameter, the new value of the parameter, the Greenwich mean time (GMT), and the mission elapsed time (MET). Users may also attach a comment to any entry in the log, either by entering the comment through an edit function or by selecting a previously defined "canned" comment (fig. 2).

Another S-band Comm System application was constructed to monitor the S-band analog parameters. This application continuously monitors and plots the value of the S-band analog parameters. The plots are organized into pages, with three plots to a page and up to four curves per page. Curves may reflect a specific parameter value over time or may be calculated using some combination of parameters or other logic. Pages may be viewed singly or two at a time. Pages may be combined in any order.

The forward link status application automatically collects statistical data on the availability of the S-band antenna system. Logic in the software monitors, identifies, and records the occurrence and duration of drops in the forward communications link. Statistics on the usage and performance of the antenna are collected and displayed. Similar information is displayed on an application that tracks the position of the Shuttle and orbital trace over a world map (fig. 3).

The Tracking and Communications applications have been used by engineers during each mission since the launch of STS-32.

In April 1992, an application for the RMS was completed and deployed. The direct drive test (DDT)

monitor (fig. 4) was constructed to monitor the DDT of the RMS joint motors. The six joints of the Shuttle robotic arm are moved by six motors, which are tested before the arm is deployed. The motors are tested by driving each of them in the forward (positive) and reverse (negative) positions. The DDT monitor automatically detects the initiation of the direct drive test and plots the results on a screen as the test occurs. The plotted data can be overlaid upon a historical template of DDT data for comparison of current behavior to past behavior. This software is used whenever a flight includes use of the Shuttle robotic arm.

During 1992, MIDAS was also extended to include the fuel cells and power reactant storage and distribution (PRSD) systems. Applications were defined that assist engineers in determining leak rates and consumption rates for the Orbiter fuel tanks. This analysis will become increasingly important when the long-duration Orbiter is in use.

Conclusions

Past MIDAS efforts have provided the groundwork for more sophisticated automated analysis. Plans for FY 1993 include an Intelligent Ku-band self-test monitor. This application will detect the occurrence of the Ku-band self-test, monitor its progress, and analyze the results of the test. Deployment of the first version of this software is scheduled for the fall of 1993.

Other efforts will be dedicated to completion of the fuel cells and PRSD applications, and to extending the MIDAS work to another area, the crew and thermal systems.

References

- ¹MIDAS Applications Description Sheet.
- ²MIDAS FY 93 Project Schedule.
- ³MIDAS Software Requirements Document.

Acknowledgments

The MIDAS project is sponsored by the Automation and Robotics Division, Intelligent Systems Branch, with funding from the Orbiter Projects Office at JSC. The NASA project manager for this task is Ginger L. Pack/ER2. Programming support is performed by the NASA engineering support contractor, Lockheed Engineering and Sciences Corporation (LESC). The programmers for this task are Jane Falgout, Joe Barcio, Leroy Gay, and Charles Smith, all of LESCE.



Figure 2. Display of a Comment Attached to a Log Entry.

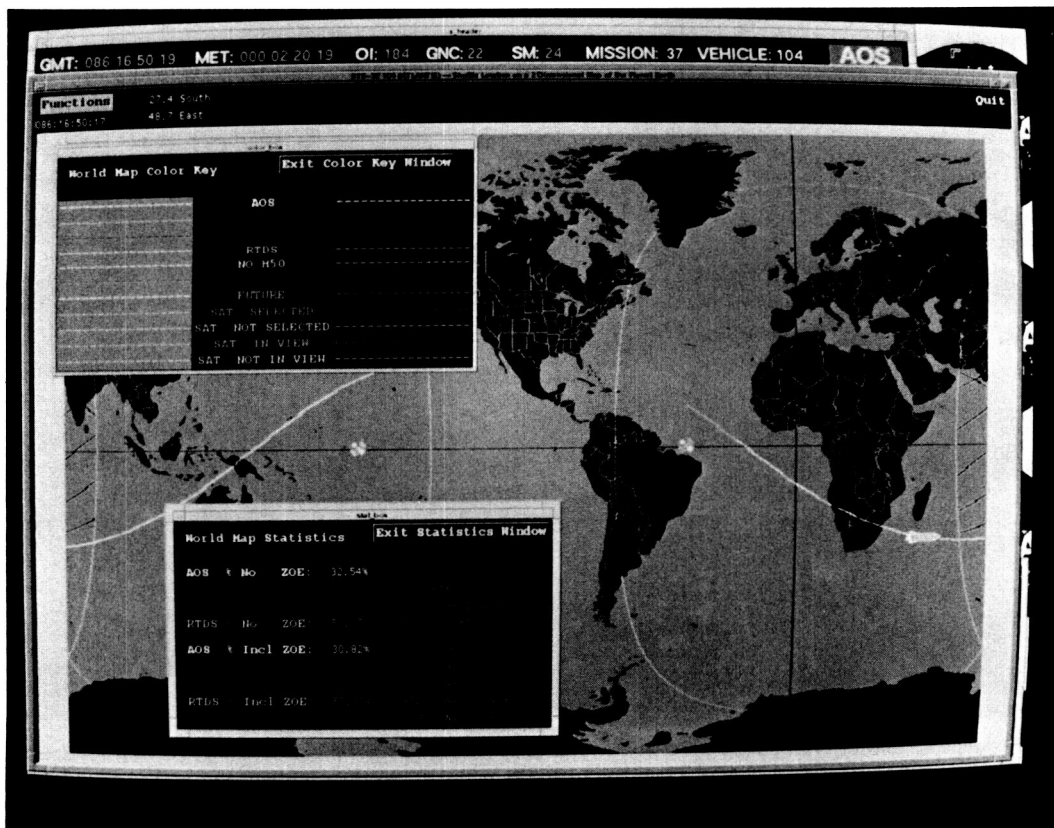


Figure 3. Display of a Tracking and Communications Application Which Tracks the Position of the Shuttle and Orbital Trace Over a World Map.

A Monitoring System with Tolerance for Real-Time Data Problems

Sherry A. Land and Jane T. Malin
Johnson Space Center/ER22

Abstract

Expert systems for monitoring and diagnosing real-time space operations must address the challenges of incorrect, noisy, and missing real-time data. Conventional approaches to solving such problems are not adequate to achieve the tolerance for bad data exhibited by human experts monitoring dynamic systems. We propose a set of methods to handle data problems, including rule disabling, use of context, and expectations to make assessments that tolerate some bad data, and graceful recovery through system correction when reliable data return. These methods have been used in a prototype called DESSY, or Decision Support System, a rule-based system that monitors the operational state and status of the manipulator positioning mechanism and manipulator retention latches (MPM/MRL) systems of the Space Shuttle payload deployment and retrieval system (PDRS). This robust monitoring system is capable of lengthy periods of uninterrupted use in real-time operations and has been successfully demonstrated in the Mission Control Center during Shuttle missions.

Introduction

Intelligent systems for computer-assisted support during aerospace operations usually provide real-time data monitoring and failure diagnosis. A major challenge for these systems is robustness in handling unreliable data. The principal real-time telemetry data problems encountered in space operations include (1) missing data, (2) erratic or noisy data, and (3) data lags and irregularities during state transitions, commanding, and other operational events. We describe a combination of methods to handle these types of data problems, including rule disabling, use of context and expectations to make assessments that tolerate some bad data, and graceful recovery through system correction when reliable data returns. Although all telemetry data monitored by this application are binary, these problems could occur with any data format.

Conventional approaches, such as data filtering or data validation, may not be sufficient to eliminate all bad data, and the use of unfiltered data gives the flight controller a better understanding of the telemetry. Statistical approaches^{2,6,8} use sampling and statistical testing or probability estimates; however, these approaches may require sample sizes or sensor redundancy that is not available. Another approach,

sensor failure diagnosis,⁷ requires sensor redundancy or testing to identify the failures and to shift the focus from process monitoring to sensor diagnosis. An approach we use is to handle some bad data while relying on diagnostic expectations and the preponderance of the data.¹ Other similar approaches provide graceful degradation in the face of bad data,⁴ permitting reasonable interim assessments while eliminating most false conclusions. However, since bad data will inevitably enter the system, a recovery approach is needed. A system should be able to recover by incrementally reinterpreting data as the data are gathered.³ Our recovery implementation, graceful recovery involves both the reevaluation of new data as the data enter the system and adjustments of expert system conclusions based on those data.

Problem Statement/Description

A real-time expert system must address three major types of data problems. They are (1) missing data, (2) erratic or noisy data, and (3) data lags and irregularities during operational events. Each has its own distinguishing characteristics and each can affect the monitoring system in a different way. Thus, to build a robust system, all data problems must be addressed both stand alone and together.

Loss of Data

The most common data problem is loss. Data loss usually takes the form of a complete loss of signal (LOS) and may be unexpected or expected; i.e., when the Shuttle enters the zone of exclusion (ZOE) where there is no telemetry downlink. Unexpected data loss may occur due to ground processing or computer hardware problems. Although LOS seems a simple phenomenon to account for, hardware implementation of telemetry processors can complicate the situation. Depending upon how the telemetry processor handles LOS, the monitoring system may receive an inactive state for all data, no data, or a static frame of the last data. The first step in dealing with loss of data due to LOS is to find out the form of data that will be received during this time. To detect LOS in DESSY, we used a data quality measurement directly from the telemetry processor called OI-Quality. However, OI-Quality does not always reflect true data quality, and, inevitably, bad data periodically enters the system.

Erratic Data

Erratic data are unstable and do not meet expected behavior for a given operational context. Such data are most likely seen immediately before or after LOS or at the time of state transitions. Erratic data are characterized by frequent flipping of bits (in the binary case) in a data set. Bit flipping occurs when a data value toggles between values of 0 and 1. This signature may also result from intermittent sensor failures, and that possibility should not be ruled out. For large sets of data, however, it is more likely that bit flipping is due to bad data rather than bad sensors. For DESSY, periods surrounding an LOS are a common time for erratic data to appear. As the Space Shuttle moves in or out of a satellite range, the telemetry link has a period of degradation, during which the OI-Quality has not yet dropped. The result is a significant amount of bad data entering DESSY. Because there has been no previous low quality indication, DESSY has no indication of the degraded data and is thus susceptible to errors.

Data Lags and Irregularities During Operational Events

The final type of data problem results from unexpected data activity when data are expected to change because of an operational event such as a state transition or command. Data that are expected to change may "flicker" or "lag" before reaching a new stable state. Given a set of data that is expected to change at transition time T , subsets may flicker or lag, causing the data transition to occur over some delta time t . Typically delta t is 1-3 seconds. Figure 1 depicts five examples of data transitions from low to high values, including a normal data transition and four anomalous cases. The delta time for this data set, 2 sec, is the time it took for every piece of data in the set to change to its new expected value. Data lags and irregularities during operational events may occur because of telemetry noise or may be owing to the physical properties of the hardware being monitored. Failure to include this behavior in the system monitoring rules will often lead to erroneous conclusions.

Approach/Method

Our approach to dealing with unreliable telemetry data attempts to achieve human-like tolerance to bad data. We tolerate data problems by monitoring data quality, using diagnostic expectations, and correcting wrong conclusions when good data returns. Table I lists each of the data problems with their applicable solutions. These methods include rule disabling to ignore data when data quality is low or uncertain, context-sensitive pattern recognition for minimizing incorrect conclusions based on bad data that has entered the system, and graceful recovery through system correction when reliable data

returns. Each method works independently to prevent or correct erroneous expert system conclusions resulting from bad or missing data. It is their combination, however, that assures a robust program capable of lengthy periods of uninterrupted use in operations.

Rule Disabling

The most straightforward method of handling data of uncertain quality is not to respond to changes in those data. There may be times when data quality is so low that the data should not be used at all. The expert system should, therefore, be capable of ignoring data when the data are unreliable by a method such as disabling rule sets. Although this tactic seems simple, the quality indicator and its data are in the same timeframe, making immediate disablement impossible. Also, as the Shuttle enters or leaves the ZOE, the telemetry link deteriorates, and OI-Quality itself is unreliable at that time. However, although erroneous data may have already entered the system, it is still desirable to disable rules to minimize the number of faulty conclusions.

To supplement automatic rule disabling, the DESSY user may also "turn off" the expert system portion of DESSY at any time, leaving DESSY to act as only a data monitor. Actually, this turning off merely grays out parts of the DESSY display that present expert system conclusions, allowing DESSY to continue to work in the background. Even if DESSY has made incorrect conclusions and the user has grayed out the expert system part of the DESSY screen, the built-in self-corrective rules should eventually lead to recovery. The intent is that even if DESSY has been turned off because of erroneous expert system conclusions, it will recover by itself, and the user will once again be able to use the expert system part of DESSY. Nonetheless, this feature gives the user the opportunity to override the expert system at the level of user interface.⁵

Context-Sensitive Pattern Recognition

The second technique we have implemented to assure DESSY robustness deals with characteristics of the sets of data that DESSY uses to detect events and identify failures. Because of problems with data lags and irregularities, the expert system often has insufficient or even erroneous evidence from the data set, upon which it can determine the occurrence of an event or failure. In DESSY we require that all rules except recovery rules tolerate a single data failure in any set of data we consider. If the data set is insufficient, context and expected events are included as a supplement of additional information. This inclusion of context and expected events eliminates many problems associated with insufficient or incorrect data. This includes both false conclusions and failure of the system to make an expected conclusion.

Graceful Recovery Through System Correction

Although some expert systems attempt graceful degradation in the face of trouble, DESSY has extended this concept to one of graceful recovery. If the system makes faulty conclusions because of bad data, a set of corrective rules acts to restore the expert system once good data return. This includes correction of individual data, state, and status. The system does not have to be restarted by the user, because the corrections automatically restore offending parts of the knowledge base. Corrective rules are similar to other system monitoring rules, except that they do not allow for any inconsistencies in the data sets they observe when making conclusions; i.e., every piece of data in the set must be exactly correct. Additionally, corrective rules are written only for the cases where the system can be determined with certainty to be in a particular configuration. These rules, therefore, can be thought of as the axioms of the expert system. They can be as simple as determining that a single piece of data is reliable again because it returned to a legitimate value after it had previously been deemed unreliable. A more sophisticated example is the reevaluation of system state when all data for a new state become active.

We have found the correction features not only to be very useful, but to have good side effects. Complementing the correction rules, initialization rules allow DESSY to be started during any stable MPM/MRL configuration and to be initialized to the proper states and statuses. In addition, if DESSY is started during transition periods, once the transition is complete, DESSY can initialize itself. This has been an important and even necessary feature of our real-time expert system.

Results

DESSY is implemented in a commercial real-time expert system development environment. The system currently monitors approximately 80 pieces of MPM/MRL telemetry, receiving its data once each second. DESSY has been demonstrated successfully in Mission Control during the STS-46 and STS-49 missions and has been used in Mission Control integrated training simulations. Benefits of our data handling methods, especially graceful recovery, have been demonstrated regularly in Space Shuttle missions, showing the robustness of the software. A scenario observed during STS-49 depicts a typical case. Because of ground hardware problems, a significant amount of data frames were being lost, so DESSY did not receive data for seconds at a time. Unfortunately, those were crucial seconds in which an MRL state transition was taking place. DESSY was unable to monitor the transition procedure, because it never received the data. When DESSY did receive a data frame again, although the procedure was over, it was able to evaluate the current data and reflect the new MRL state. A similar example

occurred during MRL operations during STS-46. Seconds after an MRL release began, an LOS occurred, and the telemetry downlink was lost. This LOS lasted several minutes, and when data returned, the operation was complete. At this time, DESSY evaluated the new data and reconfigured itself to reflect the new MRL state. In both cases, it was unfortunate that we were not able to monitor the operations, but the fact that DESSY was able to keep up once data returned prevented a situation where the wrong state would be reflected, certainly causing a loss of user confidence.

Conclusions

The data handling techniques implemented in DESSY have repeatedly proved to be effective in maintaining robust expert system operation while tolerating bad data. Disabling rules when data are unreliable reflect the human process of ignoring bad data at this time. The pattern recognition approach allows tolerance in conclusions by considering context and expectations. Finally, if the expert system makes a mistake based on bad data, we provide a mechanism for graceful recovery. Although each of the techniques we use has merit by itself, it is their combination that most reflects the human monitoring process and allows us to build a system with a human-like level of tolerance to data problems.

The future DESSY goal is to complete all modules of the PDRS, and currently the end effector system is being implemented. This will add a new level of complexity to DESSY, particularly in module integration. Also, a developer's guide for real-time automation software for Mission Control is to be a product of the DESSY project. We hope to document our own lessons learned to provide others in the space industry with development guidelines. The content will include the design and development process and issues concerning robustness and usability. We believe that the guidelines we are developing provide a good set of ground rules from which a robust and useful system can be built for real-time monitoring.

References

- ¹Chandrasekaran, B. and Punch, W. F. III, "Data Validation During Diagnosis, a Step Beyond Traditional Sensor Validation," Proc. AAAI-87, Seattle, WA, 778-782.
- ²Cooper, G. F., "The Computational Complexity of Probabilistic Inference Using Bayesian Belief Networks," *Artificial Intelligence*, Vol. 42, 1990, pp. 393-405.
- ³DeCoste, D., "Dynamic Across-Time Measurement Interpretation," *Artificial Intelligence*, Vol. 51, 1991, pp. 273-341.
- ⁴Hayes-Roth, F., Waterman, and Lenat, *Building Expert Systems*, Addison-Wesley, 1983, p. 46.
- ⁵Malin, Jane and Schreckenghost, Debra, et al., "Making

Intelligent Systems Team Players: Case Studies and Design Issues," NASA Technical Memorandum 104738, NASA Johnson Space Center, Houston, Texas, September 1991, pp. 530-538.

⁶Paasch, R. K. and Agogino, A. M., "Automated Diagnosis for the Time of Flight Scintillation Array: Development of a Structural and Behavioral Reasoning System," Proc. 8th CAIA, 1992, pp. 74-80.

⁷Scarl, E. A., Jamieson, J. R. and Delaune, C. I., "Diagnosis and Sensor Validation Through Knowledge of Structure and Function," IEEE Trans. Syst. Man Cybern, Vol. 17, No. 3, 1987, pp. 360-368.

⁸Wellman, M.P., "Fundamental Concept of Qualitative Probabilistic Networks," *Artificial Intelligence*, Vol. 44, 1990, pp. 257-303.

Acknowledgments

The authors would like to thank the PDRS Section/DF44 for their participation in this effort, and particularly Don Culp, who acted as the MPM/MRL expert.

Table 1. Data Problems and Solutions

Data Problem	Solution Methods
loss of data	rule disabling, graceful recovery
erratic data graceful recovery	pattern recognition,
data lags and irregularities during operational events	pattern recognition, graceful recovery

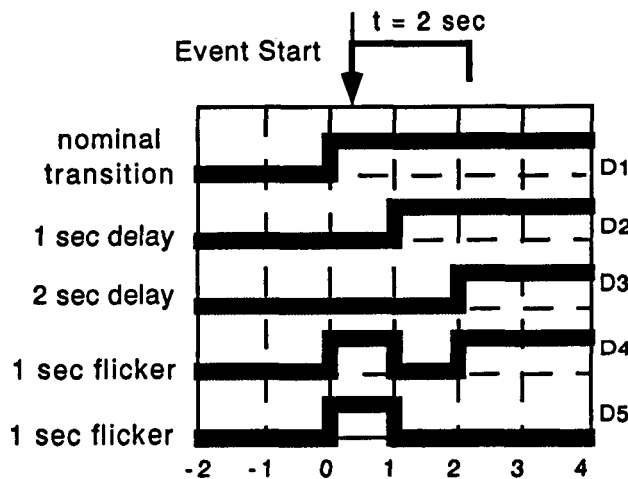


Figure 1. Examples of Data Lags and Irregularities.

Integration of Advanced Teleoperation Technologies for Control of Space Robots

Michael J. Stagnaro
Johnson Space Center/ER

Abstract

Teleoperated robots require one or more humans to control actuators, mechanisms, and other robot equipment given feedback from onboard sensors. To accomplish this task, the human requires some form of control station. Desirable features of such a control station include operation by a single human, comfort, and natural human interfaces (visual, audio, motion, tactile, etc.). These interfaces should work to maximize performance of the human/robot system by streamlining the link between the human brain and the robot equipment.

This paper describes development of a control station test-bed with the characteristics described above. Initially, this test-bed will be used to control two teleoperated robots. Features of the robots include anthropomorphic mechanisms, slaving to the test-bed, and delivery of sensory feedback to the test-bed. The test-bed will make use of technologies such as helmet-mounted displays, voice recognition, and exoskeleton masters. It will allow for integration and testing of emerging telepresence technologies along with techniques for coping with control link time delays.

Systems developed from this test-bed could be applied to ground control of space-based robots. During man-tended operations, Space Station Freedom may benefit from ground control of intravehicular activity (IVA) or extravehicular activity (EVA) robots with science or maintenance tasks. Planetary exploration may also find advanced teleoperation systems to be very useful.

Introduction

Remotely controlled robots may be successfully applied in hazardous environments such as high-radiation zones, deep-sea locations, Earth orbit, and extraterrestrial sites. Three dominant control modes are teleoperation, supervised autonomy, and shared control.¹ Teleoperation is characterized by direct human-in-the-loop manual control and small time delays (< 1 sec). In supervised autonomy, commands are generated by the operator and sent to the robot control system for execution. Shared control makes use of both teleoperation inputs and an autonomous robot control system. In each of these modes, a human operator is involved who must interact with some form of computer-based control station.

Figure 1 illustrates a spectrum of technologies that may be used in a remote robot-control station. At one end are conventional technologies such as hand controllers, 2-D video, keyboards, and computer monitors. The other end is

labeled as telepresence technologies and includes force reflective exoskeletons, stereo (3-D) video, voice recognition, and synthetic speech.

Telepresence can be defined as the sense of being physically present with an object(s) at a remote site.³ Telepresence technologies attempt to immerse a human operator in the remote environment with actuator control and sensory feedback devices that closely interface to the human central nervous system. Robots at the remote site are designed with anthropomorphic actuators and sensory devices, such as stereo camera pairs and tactile sensors.

Telepresence technologies offer interfaces to the human sensory system, which are more direct than those of the conventional technologies defined. This frees the brain from many unnatural input/output conversion tasks, allowing more concentration on higher level control and process-oriented tasks. The result is a more intuitive way of controlling remote robots.

Major challenges facing telepresence technologies include working with time delays, increasing video resolution and field of view, and providing adequate force/torque and haptic feedback.

Project Overview

Objectives

The primary project objective is to develop a teleoperator control station test-bed that makes use of telepresence technologies. This test-bed is referred to as the teleoperated robot interface platform (TRIP) and should provide teleoperation capabilities for two JSC development robots. One robot is the dexterous anthropomorphic robotic test-bed (DART).⁴ DART is a dual-arm, dual-hand robot with a camera platform that provides stereo video. It will be able to operate under human control augmented by onboard intelligence for use in development of IVA and EVA robotic systems. The second, AERCAM, is a prototype mobile camera platform capable of teleoperation. Initially, this prototype will be flown on an air-bearing floor at JSC.

In a more general sense, TRIP will be used as a test-bed for emerging telepresence technologies, such as head-mounted displays, exoskeletons, and programming systems. In addition, TRIP will allow testing of proposed solutions to the problems induced by control link time delays. Systems developed with the TRIP test-bed should support future operations on board the Space Station Freedom, including the possibility of ground control using shared control techniques.

Goals and Constraints

TRIP development goals include flexibility, ease of use, and growth paths. A flexible system will support the test-bed objectives through maximum use of standard hardware and software interfaces, a modular approach to system design, and the use of software for most calibration tasks. The system should also allow for ease of development and use by minimizing and simplifying the software learning curves. Ease of use will support tight schedules and minimal manpower. A system designed with growth paths will foster an evolutionary development by protecting both hardware and software investments. Design for growth seeks to avoid obsolescence by choosing established software tools with supported growth paths and by avoiding hardware with closed or unsupported architectures.

Development constraints consist of cost and system performance. Design must be sensitive to costs by maximizing system capability, given current year funding. Basic system-level results should not depend on large amounts of future funding. Basic performance requirements, such as data rates and connectivity, must also be satisfied. Optimization of performance variables at the expense of system flexibility will be avoided unless required.

Facilities and Support

TRIP is under development in the Dexterous Robotics Lab of the Automation and Robotics Division at JSC. The two target robots are also under development in division labs. To date, all primary design and development work has been conducted in-house by JSC civil service staff members. Only a limited amount of contractor support has been available or used.

System Description

Organization

TRIP is the integration of assorted telepresence technologies as illustrated in figure 2. These include exoskeletons for the operator's hand, wrist, and arm joints, a head-mounted display for viewing stereo video and graphics, speech synthesis and voice recognition systems, and a network interface for passing data to/from a remote robot. These systems should work in concert to provide intuitive control of a remote robot by one human operator. TRIP is organized into five subsystems, each consisting of hardware and associated software.

Hardware Architecture

The hardware architecture is shown in figure 3. Selections were driven primarily by the flexibility goal along with the availability and cost of both software and special-purpose boards (video, audio, etc.). Hardware cost

and growth-path trends were also considered.

The hardware architecture consists of exoskeletons, a head-mounted display, a chair platform with control pedals, i486 & i386 microprocessors in ISA and VME buses, and assorted I/O, audio, and video boards. A single family of processors was selected to minimize software learning curves and keep costs relatively low. The ISA bus offers reasonable performance and a myriad of low-cost, special-purpose I/O boards from which to choose. The VMEbus offers an industry standard with high bandwidth performance, extreme flexibility, and a large number of I/O and processor boards. Selections of boards for both buses were based on a balance of cost, flexibility, and performance. Software driver libraries were also considered in the board selections, as this represents a potentially labor-intensive set of development tasks.

Exoskeletons are attached to a body harness and gloves, which the operator wears. An analog signal conditioning box provides power to the exoskeletons and filters the signals produced by potentiometers and hall-effect sensors. These signals are then read by an analog-to-digital (A/D) converter board in the VMEbus. An embedded i386 computer processes raw data from the A/D board and makes the results available on the VMEbus.

The head-mounted display (HMD) consists of monitors, optics, a position sensor, headphones, and a microphone. The position sensor reports roll, pitch, and yaw to an embedded i386 computer via an RS-232 link from its own processor-based control box. Two i486-based computers deliver video with text or graphics overlay to the monitors. The headphones are driven by a third i486 computer that handles speech synthesis and other audio feedback functions. This computer also handles voice recognition tasks, making use of the microphone. All three computers use ISA to VME bus adapters to communicate with the VMEbus. Video and audio signals from a remote robot are currently transmitted through dedicated channels.

A chair platform includes control pedals and a transmitter for the HMD position sensor. Potentiometers in the pedals are powered and read by the same hardware used with the exoskeletons. Signals are also processed by the embedded i386 computer, and results are available on the VMEbus. The HMD position sensor transmitter has its own power supply and processor-based control box.

An i486 embedded in the VMEbus serves as the command and control computer of TRIP. Through the VMEbus, this computer can communicate with all subsystems and coordinate their interactions. In addition, this computer handles all data communications with remote robots through an ethernet network board and a single dedicated cable.

Software Architecture

Figure 4 displays the current high-level software architecture. Software modules are shown in round-edge rectangles, and hardware is represented in square-edge rectangles.

The software architecture consists of control and configuration tasks, command routers, command handlers, bus data exchange drivers, RS-232 interface drivers, and TCP/IP network interface drivers.

The control and configuration tasks reside on an embedded i486 computer in the VMEbus. These allow the operator to calibrate subsystems and define subsystem interaction rules. Control tasks coordinate the interactions between various subsystems.

Command routers serve two functions. First, data are processed from input devices to produce specific subsystem commands. Second, these commands are routed to the appropriate subsystem message areas. Command routers are used with the voice recognition system and all motion input devices.

Command handlers accept commands or messages from command routers and execute the commands or answer messages. Command handlers are used with output systems such as video and graphic overlays, speech synthesis, and environmental audio.

Bus data exchange drivers allow commands and messages to be physically exchanged between the ISA buses and the VMEbus. Both embedded and external computers use these drivers

Drivers for the RS-232 ports are used by the embedded i386 computer to communicate with the HMD position sensor controller. Commands can be sent to the controller, and raw orientation data are read. These raw data are also parsed and made available to bus data exchange drivers.

Network access is provided by interface drivers using the TCP/IP protocols. These are used by the communication subsystem to transmit commands to or receive messages from a remote robot. They are also used to handle commands from TRIP subsystems and to route commands from the robot to the appropriate handlers.

Software Tools

Current software tools comprise two operating systems and three compilers. Windows 3.1 and iRMX are the operating systems, and they support development with Visual Basic (VB), Borland C++, and iRMX C.

Windows 3.1 provides cooperative, event-driven multitasking with an easy-to-use graphical human interface. A large number of board-level drivers directly support this operating system and development through the system's standard user interface. Windows 3.1 also provides a growth path to a 32-bit preemptive multitasking/multiprocessing environment with Windows NT. Windows NT is backward compatible with 3.1 and uses the same graphical interface standards.

iRMX provides 32-bit mode operation of the Intel microprocessors and real-time task scheduling for low-level, time-critical tasks. A unique feature of this operating system is its ability to run Windows as a task and communicate between the two operating systems. This enables the best of two worlds: 32-bit hard, real-time tasking and an easy-to-use standard interface.

VB is an object oriented-visual development environment for the Windows operating system. Objects can send or receive messages, and events can be used to trigger user-developed code or operating system calls. The syntax is similar to that of Basic, but the code structure and object orientation endow it with many features found in C++. The visual development environment lends itself to very rapid prototyping of code and almost effortless user interface development. VB does not support some of the low-level capabilities found in C or C++, but Dynamic Link Library (DLL) functions written in C or C++ may be easily called. Operating system functions also may be called directly from VB. Dynamic Data Exchange (DDE), a client/server intertask communication protocol, is also supported and is easy to use.

Borland C++ is an object-oriented C development environment that supports development for the Windows operating system. Specific to this project, it allows the development of low-level DLL functions, which may be called from VB code. Borland supplies an efficient code development environment with extensive debugging support. The object orientation promotes development of complete code modules, which are easy to reuse and build upon.

iRMX C is a compiler and assorted tools for developing C-code task modules, which run in the iRMX real time operating system. These modules will accommodate time-critical, low-level functions as required by the TRIP. These functions may communicate with Windows-hosted code to report system status, alarms, or data needs.

Floor Layout

A planform view of TRIP hardware is displayed in figure 5. Shown are the chair platform, a 19-in. equipment rack, and two development work sites. An adjustable chair is mounted to the platform and serves as the operator worksite. Pedals, exoskeletons, and the HMD are all connected from the chair platform to equipment in the 19-in. rack. The rack contains all TRIP computers along with audio and video ancillary equipment. Two development worksites each incorporate a keyboard, mouse, and two SVGA monitors. One worksite supports development on VMEbus subsystems, which include command and control, communication, and motion. The other worksite supports development on the audio and video subsystems.

Subsystem Details

Motion Subsystem

The motion subsystem generates commands to control position or rate of all articulated members on a remote robot. Robot members include arms, hands, torsos, camera platforms, and mobile bases. The operator controls these using a combination of exoskeletons, foot pedals, and

position sensors. Force reflection and tactile feedback for the operator are planned as growth paths in the arm and hand exoskeletons of this subsystem.

Current components of this subsystem are detailed in figure 6. It consists of an embedded i386 computer, an HMD position sensor, an A/D board with a signal conditioning box, exoskeleton arm and hand masters, and foot pedals.

An embedded i386 based computer from the Radisys Corporation is used for subsystem processing and control. It runs at a clock speed of 25 MHz, contains 8 MB of DRAM, a keyboard controller, serial ports, and an ISA-compatible private bus that supports a 40 MB hard disk and a super VGA controller board. It boots with a PC/AT-compatible BIOS ROM and supports a number of operating systems. Radisys also supplies low-level functions that allow direct access to all VMEbus memory spaces. These functions are compatible with TRIP software tools.

A Logitech 6D mouse is used to sense the HMD position and orientation. It makes use of an ultrasonic transmitter and receiver triangles to determine location in Cartesian space (x, y, z) and orientation (roll, pitch, yaw) as euler angles or quaternions. Also included is a dedicated control processor that communicates with the host processor via RS-232. Advantages of ultrasonics over magnetic sensors include reduced lag times and no interference from metal structures. A disadvantage is that the full range (0-360 deg) of euler angles is not supported, although TRIP does not require the full range for HMD tracking.

A VMIVME 3118 scanning A/D board is used in conjunction with a signal conditioning board developed in-house to support 64 differential channels. The A/D board interfaces to the VMEbus via control registers and a dual-ported RAM data buffer. The signal conditioning board is housed in a separate box with a dedicated power supply. The board low pass filters (10 Hz) each channel and buffers the signal lines to the A/D board. It also supplies power to sensors on the exoskeletons and foot pedals.

Two exoskeleton arm masters (EAMs) and two dexterous hand masters (DHMs) from Exos, Inc., are utilized in TRIP. The EAM provides precise measurements of human shoulder and elbow joint angles. Potentiometers are currently used to sense the angles. The DHM uses hall effect sensors to measure joint angles of the human hand. A GripMaster is integrated into each DHM to measure wrist motion. Development continues to be funded by NASA, with future objectives including the addition of sensory feedback in all areas. The current TRIP design will be capable of integrating these planned improvements.

Foot pedals can be used to control robot torso and/or mobile base motion. In both cases, potentiometers are used to sense ankle joint angles that provide rate and directional control of robot motors. These pedals are attached to the chair platform.

Software tasks running on the i386 read and process raw data from each of the input devices. One task reads a data buffer on the A/D board and processes for joint angle

or rate commands. Processing includes some simple (i.e., boxcar) noise filtering and any required coordinate transforms. The A/D board continuously scans all active channels and updates the entire data buffer at about 800 Hz. A second task on the i386 reads and parses data from an RS-232 port to determine roll, pitch, and yaw of the HMD. This port communicates with the position sensor controller, which continuously updates position readings at about 50 Hz. A third task on i386 accepts processed data from the other tasks and routes it to the appropriate command handlers (i.e., communication, graphic overlay, etc.) using bus data exchange drivers.

Video Subsystem

A video subsystem handles all live video signals along with any computer-generated graphics. Video is supplied by camera pairs on the remote robot, which are designed to provide stereo video to the human eyes. Computer-generated graphics and/or text may be calibrated to the video and overlaid to provide visual feedback, simulation results, or task tools to the operator.

Figure 7 is a diagram showing half of the video subsystem. Each half feeds one of the operator's eyes, and both halves are identical. Components include a helmet with HMDs, a video scan converter, a frame grabber and video compression board, an SVGA graphics board, an i486-based ISA bus computer, and ISA to VMEbus adapter boards.

An HMD helmet from Virtual Research is currently in house. It incorporates headphones, the Logitech 6-D mouse receiver triangle, two color LCD displays (360 x 240 pixels), and wide-angle optics from Leep Systems. The helmet, designed for comfort, is extremely easy to don and doff. The Leep Systems optics have become an industry standard and can provide a field-of-view in excess of 100 deg. Currently available LCD displays do not have the resolution required to support the detailed video or graphics ultimately desired in TRIP. In response, work is progressing in house to develop higher resolution black-and-white HMDs that make use of wide-angle optics and flat panel CRTs. Other concepts for increased resolution and color are under consideration.

The Genie scan converter from Jovian will accept 60 Hz non-interlaced RGB signals (i.e., VGA at 640 x 480) as input and produce a 30 Hz interlaced NTSC signal as output. Monitors in most HMDs currently require an NTSC signal. In addition, the scan converter provides a gain adjustment and flicker filtering. Without the flicker filtering, certain horizontal lines appear to flicker and may contribute excessively to operator fatigue.

The frame grabber and video compression boards are supplied by New Media Graphics, and both include low-level software drivers that are compatible with TRIP software tools. The frame grabber digitizes and scan converts live video from external cameras, allowing software manipulation of the images. In addition, this board will genlock and overlay (via graphics color keying) VGA

signals using a dedicated video (VESA) bus. The video compression board enables compression and decompression of full motion (30 Hz) video using a C-Cube CL550 JPEG chip. It supports storage, playback, and network transmission of video signals using a private video bus with the frame grabber.

An Orchid Fahrenheit 1280° graphics accelerator was selected as the VGA board. It provides complete Super VGA functionality and makes use of a dedicated onboard processor to support graphics-intensive applications. Low-level drivers are included for the Windows operating system.

Two i486-based computers are used for subsystem control functions and as graphics engines. Each runs at a clock speed of 33 MHz, contains 8 MB of DRAM, a keyboard controller, serial ports, and an ISA bus that supports a 210 MB hard disk and subsystem video boards. They boot with a PC/AT compatible BIOS ROM and support all TRIP operating systems.

Bus adapters are supplied by Bit3 Corporation and provide a high bandwidth link between the VMEbus and ISA bus. Boards in each bus are linked with a shielded, multiconductor cable. The VMEbus board contains 2 MB of dual-ported RAM, which maps into the memory space of both buses.

This subsystem accepts commands and messages from the VMEbus through the bus adapters. Software tasks running on the i486 computers are used to control the display of live video and to generate desired graphics or text overlays. Graphics can include wire frame models driven by simulations, and text may include voice menu selections or data from the remote robot. The video, graphics, and/or text are merged in the frame grabber and fed to the scan converter. This converter produces a filtered 30 Hz interlaced NTSC signal, which the HMD directly accepts and displays to the operator. Future HMDs with higher resolutions may directly accept the 60 Hz non-interlaced RGB signals, allowing scan converters to be bypassed.

Audio Subsystem

Speech synthesis, environmental audio, and voice recognition are all part of the audio subsystem. Speech synthesis provides TRIP an additional path for relaying data or messages to the operator. Environmental audio can be used to supply cues or feedback on the remote environment. This can take the form of actual environmental sounds (where possible) and/or computer-generated sounds that cue the operator. Voice recognition essentially replaces the keyboard as an operator input device and is required when the operator is wearing exoskeletons.

Figure 8 diagrams the audio subsystem. Components include helmet-mounted headphones and microphone, a voice recognition system board, a speech synthesis board, an audio mixing system with an interface board, an i486-based ISA bus computer, and ISA to VMEbus adapter boards.

The headphones and a microphone are part of the helmet assembly. Headphones are driven by an audio mixing system, and the microphone supplies audio signals to a voice recognition system.

The voice recognition system was developed by Speech Systems, Inc. It provides continuous speech recognition, which is speaker independent, and includes a large vocabulary dictionary (about 40,000 words) that can be amended by the developer. A unique combination of speech encoding, acoustic frame compression, and linguistic decoding is used to support large, variable duration segments.

Speech synthesis is provided by the DoubleTalk PC board and drivers from RC Systems. The board uses its own 10 MHz, 16-bit microprocessor and supports multiple speech technologies such as text-to-speech, LPC, PCM, ADPCM, and CVSD. The analog output can directly drive headphones or be directed through a mixing system.

Audio switching, mixing, and signal processing are accommodated with a CDPC multimedia system by Media Vision. The system is based on the electronics of their Pro Audio Spectrum 16 and includes multiple audio input and output signal options. Signal processing includes digital filtering, tone control, bass enhancement, and signal equalization. The analog mixer supports volume control of each source, fade in/out, and audio panning. The system includes an ISA bus interface board and low-level drivers that are compatible with TRIP software tools.

An i486-based computer is used for subsystem processing and control. It runs at a clock speed of 33 MHz and contains 8 MB of DRAM, a keyboard controller, serial ports, and an ISA bus that supports a 210 MB hard disk and subsystem audio boards. It boots with a PC/AT compatible BIOS ROM and supports all TRIP operating systems.

A Bit3 bus adapter provides a high bandwidth link between the VMEbus and this subsystem. Boards in each bus are linked with a shielded, multiconductor cable. The VMEbus board contains 2 MB of dual-ported RAM, which maps into the memory space of both buses.

The audio subsystem exchanges commands and messages with the VMEbus through its bus adapter. Software tasks running on the i486 computer handle commands for speech synthesis and environmental audio functions. Synthetic speech and environmental audio signals are processed and mixed by the CDPC system and then fed to headphones in the helmet. The operator's voice is picked up by the microphone and fed to the voice recognition system for interpretation. Resulting commands are routed to the message areas of appropriate subsystems.

Communication Subsystem

The communication subsystem provides full duplex data transfers between TRIP and the remote robot using an ethernet-based network. Data can represent commands, sensory information, event messages, or requests for information.

Hardware for this subsystem is shown in figure 9. It basically consists of an embedded i486 computer from Radisys and an ethernet communications board.

The i486 runs at a clock speed of 33 MHz and contains 8 MB of DRAM, a keyboard controller, serial ports, and an ISA compatible private bus that supports a 210 MB hard disk and a super VGA controller board. It is operationally similar to the i386 controller of the motion subsystem and uses the same low-level drivers for VMEbus memory accesses.

The ethernet board is Western Digital (8003EB) compatible and uses commonly available packet drivers. It also supports both thin and thick ethernet cables along with TCP/IP socket libraries.

Software tasks running on the i486 computer serve three functions: (1) transfer data packets to and from the remote robot, (2) parse data packets and route information to other TRIP subsystems, and (3) handle commands from TRIP subsystems and build data packets. The data packets consist of structures that organize messages, commands, and information into a form that TRIP and the remote robot can both understand and easily parse. Future plans include incorporation of TelRIP software developed at Rice University. TelRIP (TeleRobotic Interconnection Protocol) is a layer built on top of TCP/IP with characteristics specific to teleoperation of robots. Other software tasks running on the i486 route messages to other TRIP subsystems.

Command and Control Subsystem

The command and control subsystem coordinates interactions of all subsystems with one another. It also serves as the focal point for system configuration and subsystem calibration efforts.

This subsystem consists primarily of software but shares the embedded i486 used by the communication subsystem shown in figure 9.

Software running on the i486 computer provides system-level arbitration of subsystem task and data interactions. These interactions may be defined in terms of the active communication paths between subsystems and the messages or commands understood on those paths. In addition, each of the other subsystems may be calibrated or adjusted from here to correspond to systems on the remote robot. Examples of this include mapping of exoskeleton joints to robot joints, definition of joint limits, activation of video targeting functions, and selection of environmental audio convolution methods.

Closure

The project described in this paper is primarily a system-integration effort. Architectures and approaches discussed are driven by a combination of operational needs, available technologies, and flexibility to incorporate projected technologies. Design goals included ease of use, configurational flexibility, and the inclusion of growth

paths. These goals were constrained by cost and performance limits.

Current Status

All the basic hardware elements of TRIP are currently being integrated. Software tasks are either in the detailed design or implementation phase of development. The DART anthropomorphic target robot is currently in the implementation phase and will be interfaced to TRIP by the end of this year. The AERCAM free-flying target robot is in the detailed design phase of development.

Future Work

Future work will address the implementation and testing of newly developed subsystem and programming technologies. Examples in the video area include higher resolution black-and-white monitors, direct VGA interfaces with wide-angle optics, and computational graphics models as in reference 14. Motion control examples include the addition of force/torque reflection, haptic feedback, and teleprogramming concepts as described in reference 25. TRIP will also make use of 3-D acoustics research and signal processing techniques, such as those of reference 19. Robot communications will be enhanced through updated versions of TelRIP^{20,21} software. Finally, an icon or block-diagram-based visual environment will be used for system configuration and subsystem calibrations.

References

TRIP System Level

- ¹Backes, P. G., "Ground Remote Control for Space Station Telerobotics with Time Delay," 15th Annual AAS Guidance and Control Conference, Keystone, CO, Feb. 1992.
- ²Schenker, P. S., Bejczy, A. K., Kim, W. S., and Lee, S., "Advanced Man-Machine Interfaces and Control Architecture for Dexterous Teleoperations," IEEE Oceans '91, Underwater Robotics Session, Honolulu, HI, Oct. 1-3, 1991.
- ³Sheridan, T. B., "Musings on Telepresence and Virtual Presence," *Presence - Teleoperators and Virtual Environments*, Vol. 1, No. 1, MIT Press, Cambridge, MA, 1992, pp. 120-125.
- ⁴Li, L. C., Nguyen, H., and Sauer, E. "A Integrated Dexterous Robotic Testbed For Space Applications," Fifth Annual Workshop on Space Operations Applications Research, Vol. 1, Telerobotics and Mechanisms Session, Houston, TX, July 1991, pp. 238-245.
- ⁵Korane, K. J., "Sending a Robot to do a Man's Job," reprint from *Machine Design*, Vol. 63, No. 22, Nov. 7, 1991.
- ⁶Anon, video entitled "TOPS System Demonstration," Naval Ocean Systems Center, San Diego, CA, June 1991.

⁷Anon, video entitled "Introduction to Technology and Application," Kraft Telerobotics, Inc., Overland Park, KS, Dec. 1991.

Motion Subsystem

⁶Marcus, B. A., and Eberman, B., "Exos Research on Master Controllers for Robotic Devices," Fifth Annual Workshop on Space Operations Applications Research, Vol. 1, Sensing and Display Session, Houston, TX, July 1991, pp. 238-245.

⁹Anon, "2D/6D Mouse Technical Reference Manual," Logitech, Inc., Fremont, CA, 1991.

Video Subsystem

¹⁰Anderson, P., "Virtual Reality: Is it for Real? and What's in it for Imaging?," reprint from *Advanced Imaging*, June 1991.

¹¹Howlett, E., "Wide Angle Orthostereo," LEEP Systems/Pop-Optix Labs, Waltham, MA, Feb. 1990.

¹²Howlett, E., "Wide Angle Color Photography Method and System," U. S. Patent 4406532, Sept. 27, 1983.

¹³Carollo, J. T., "Helmet Mounted Displays," Proceedings of the International Society for Optical Engineering, SPIE Publication No. 1116, Bellingham, WA, March 1989.

¹⁴Robinett, W., and Rolland, J. P., "A Computational Model for the Stereoscopic Optics of a Head Mounted Display," *Presence - Teleoperators and Virtual Environments*, Vol. 1, No. 1, MIT Press, Cambridge, MA, 1992, pp. 45-62.

¹⁵Anon, "Flight Helmet Operating Instructions and Owners Manual," Virtual Research, Sunnyvale, CA, 1992.

¹⁶Anon, "Super Video Windows Programmers Guide," New Media Graphics Corp., Billerica, MA, 1991.

Audio Subsystem

¹⁷Meisel, W. S., Anikst, M. T., Pirzadeh, S. S., Schumacher, J. E., Soares, M. C., and Trawick, D. J., "The SSI Large-Vocabulary Speaker-Independent Continuous Speech Recognition System," IEEE International Conference on Acoustics, Speech, and Signal Processing, Vol. 1, Toronto, Ontario, Canada, May 1991, pp. 337-340.

¹⁸Meisel, W. S., and Anikst, M. T., "Efficient Representation of Speech for Recognition," reprint from *Speech Technology*, Feb./March 1991.

¹⁹Wenzel, E. M., "Localization in Virtual Acoustic Displays," *Presence - Teleoperators and Virtual Environments*, Vol. 1, No. 1, MIT Press, Cambridge, MA, 1992, pp. 80-103.

Communication Subsystem

²⁰Wise, J. D., and Ciscon, L., "TeleRobotics Interconnection Protocol, Version 1.5," Universities Space Automation / Robotics Consortium, Technical Report #9103, Dept. of Electrical and Computer Engineering, Rice University, Houston, TX, May 1991.

²¹Wise, J. D., Ciscon, L., presentation notes from the "First Annual TelRIP Workshop," Johnson Space Center, Houston, TX, April 1992.

²²Kochcan, S. G., and Wood, P. H., "Unix Networking," Hayden Books, Howard Sams & Co., First Edition, Carmel, IN, 1990.

²³Anon, "Distinct TCP/IP for Microsoft Windows - Software Development Kit," Distinct Corp., Saratoga, CA, 1992.

Command and Control Subsystem

²⁴Small, C. H., "Real-Time Operating Systems," EDN, Jan. 7 issue, Denver, CO, 1988, pp. 115-138.

²⁵Funda, J., Lindsay, T. S., and Paul, R. P., "Teleprogramming: Toward Delay Invariant Remote Manipulation," *Presence - Teleoperators and Virtual Environments*, Vol. 1, No. 1, MIT Press, Cambridge, MA, 1992, pp. 29-44.

²⁶Petzold, C., "The Visual Development Environment - More Than Just a Pretty Face?," *PC Magazine*, June 16, Vol. II, No. 11, Boulder, CO, 1992, pp. 195-237.

²⁷Anon, "Microsoft Windows NT Operating System," Data Sheet, Microsoft Corp., Redmond, WA, 1992.

²⁸Anon, "Microsoft Windows Operating System Version 3.1 - An Overview of New Features," Corporate Backgrounder, Microsoft Corp., Redmond, WA, 1992.

²⁹Small, C. H., "Windows and Engineering Software," EDN, April 9 issue, Denver, CO, 1992, pp. 123-132.

³⁰Peterson, W. D., "The VMEbus Handbook," Second Edition, VFEA International Trade Association, Scottsdale, AZ, 1991.

³¹Anon, "EPCConnect Software Manuals," Radisys Corp., Beaverton, OR, 1990.

³²Anon, "Real Time Operating System Runs Windows," reprint from *Microcomputer Solutions*, May/June 1991.

³³Carvallio, C., "Adding DOS Software to Real-Time Systems: New Strategies for Real World Control," Intel Corp., Industrial Computer Div., Hillsboro, OR, 1991.

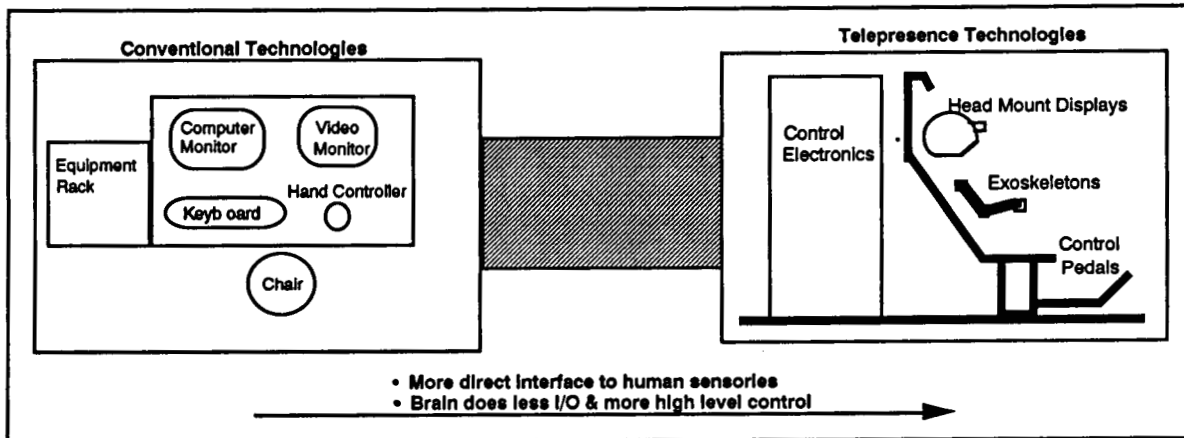


Figure 1. Remote Robot Control Technology Spectrum.

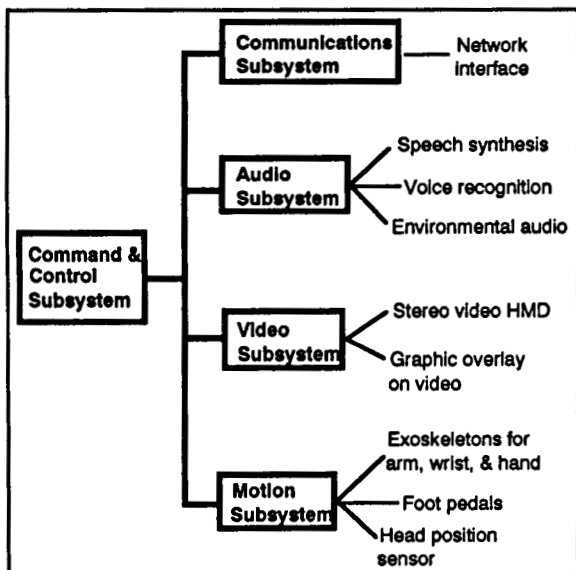


Figure 2. TRIP Subsystems and Technologies.

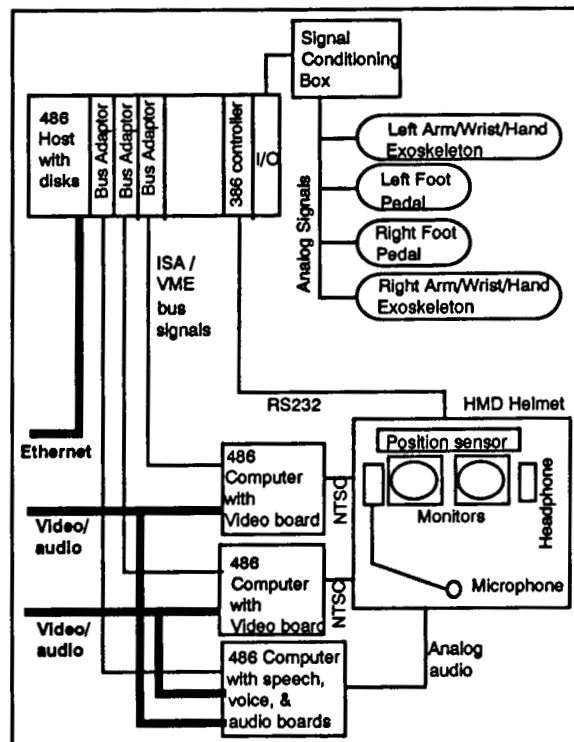


Figure 3. Hardware Architecture.

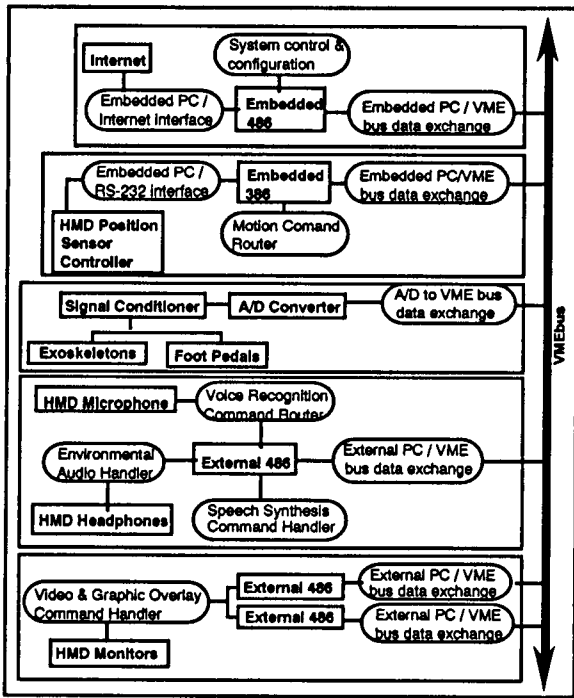


Figure 4. Software Architecture.

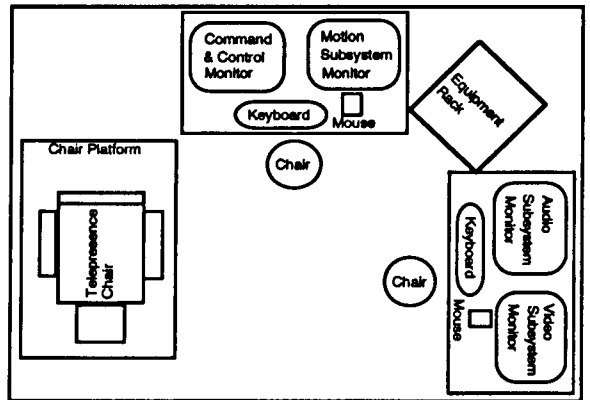


Figure 5. Floor Layout.

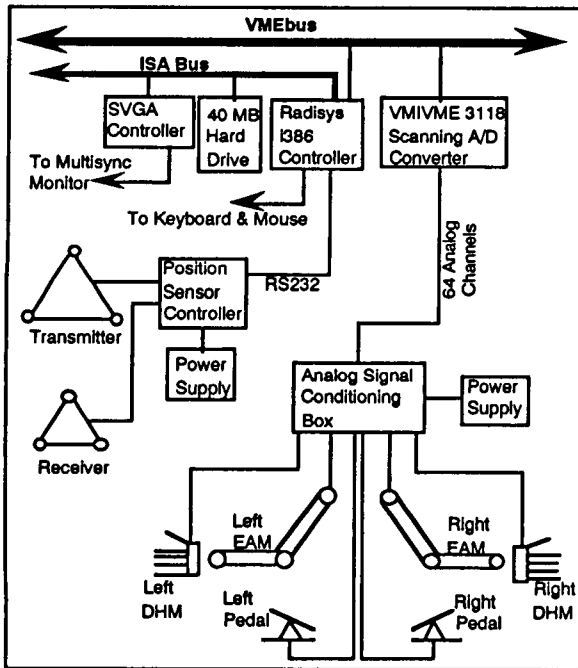


Figure 6. Motion Subsystem Block Diagram.

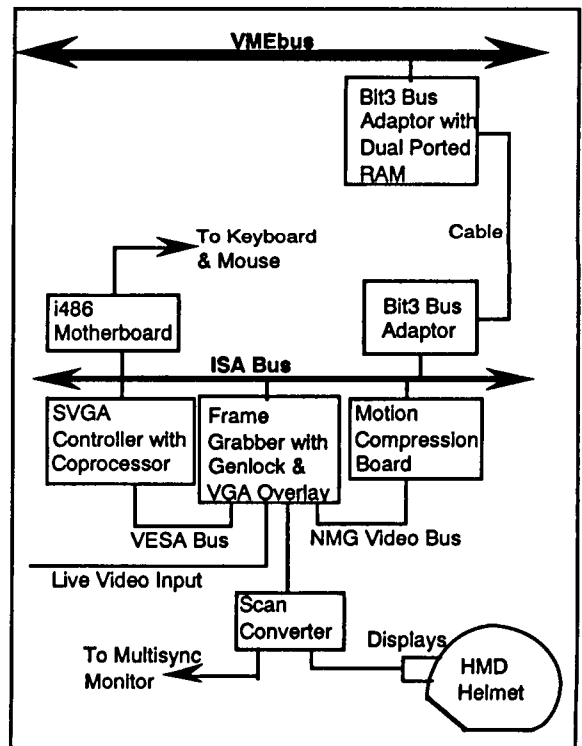


Figure 7. Video Subsystem Block Diagram.

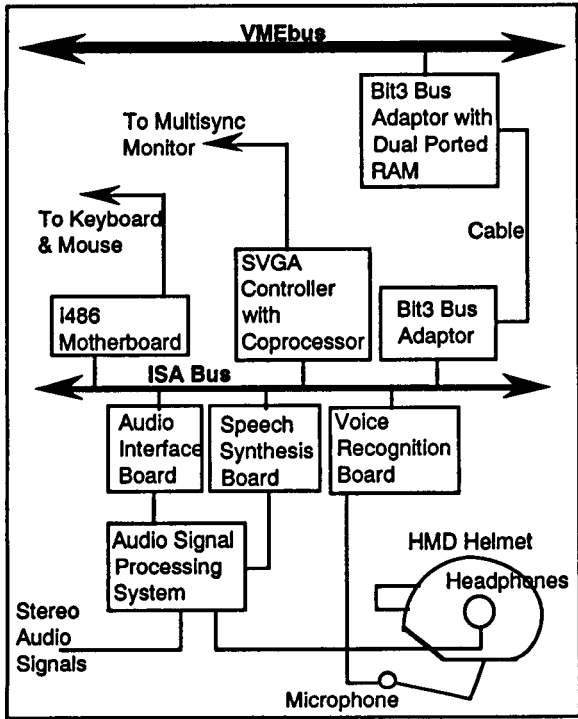


Figure 8. Audio Subsystem Block Diagram.

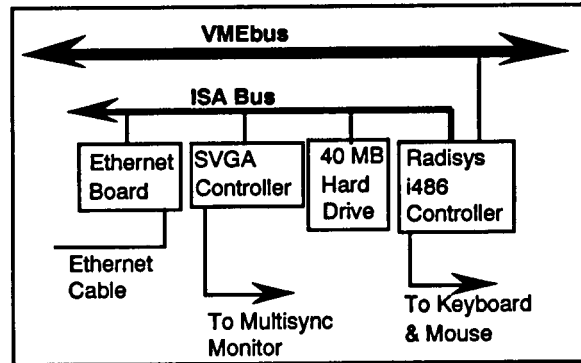


Figure 9. Communication and Command/Control Subsystem Block Diagram.

An Intelligent, Free-Flying Robot for Crew Help and Crew or Equipment Retrieval in Space

Jon D. Erickson
Johnson Space Center/ER

Abstract

The ground-based demonstrations of extravehicular activity (EVA) retriever, a voice-supervised, intelligent, free-flying robot, are designed to evaluate the capability to retrieve objects (astronauts, equipment, and tools) which have accidentally separated from the Space Station. The EVA retriever software is required to autonomously plan and execute target rendezvous, grapple, and return to base (while avoiding stationary and moving obstacles), with subsequent object handover. The software architecture incorporates a hierarchical decomposition of the control system that is horizontally partitioned into five major functional subsystems: sensing, perception, world model, reasoning, and acting. The design provides for supervised autonomy as the primary mode of operation. It is intended to be an evolutionary system, improving in capability over time and earning crew trust through reliable and safe operation.

Presented here are an overview of the hardware, a focus on software, and a summary of results achieved recently from both computer simulations and air bearing floor demonstrations. Limitations of the technology used are evaluated. Plans for the next phase, in which moving targets and obstacles drive real-time behavior requirements, are discussed.

Introduction

EVA crew rescue and equipment retrieval is a Space Station Freedom requirement. During the lifetime of the Space Station, there is a high probability that a number of objects will accidentally become untethered. Members of the crew, replacement modules, and key tools are frequently cited examples. The retrieval of these objects from space within a few minutes is essential.

The Space Station cannot chase separated crew or equipment, even though crew safety is top priority. Other vehicles such as the Space Shuttle Orbiter or orbital plane-change vehicle will not usually be available. Real-time simulation of manned maneuvering unit (MMU) retrievals indicated that short response time was critical and that major risk to a second astronaut was involved, which was not acceptable. Equipment that might be used in retrieval may be too valuable to lose because it is required in operations and replacement is not available on the station. There is also collision potential on later orbits; though the potential is small, collisions have occurred previously.

A potential solution is a supervised, intelligent, free-flying space robot. Supervised means here that the

human chooses at the time and in the place of the operation how the robot will perform as a team player. This adjustable autonomy depends on machine intelligence, which is the ability to achieve goals in the face of variabilities, difficulties, and complexities imposed by the environment.

The free-flying space robot would operate near a spacecraft such as the Space Station in a primarily voice-supervised, autonomous mode for mobility and manipulation. The concept of supervised, intelligent, autonomous robotics provides for autonomous behavior of an intelligent type, normally controlled by humans at a high level of goal-setting and in mixed-initiative communication. By contrast, telerobotics provides a partially automated remote extension of human task performance with occasional control delegation for specific parts of tasks given to the telerobot for efficiency reasons.

Requirements call for an unassisted deployment from a mounting on the external part of the airlock, with propulsion capabilities provided by a more powerful version of the existing MMU. Performance guidelines include target retrieval within 120 minutes of subsystem deployment. Reliability considerations mandate the use of fault-tolerant and fail-safe designs with embedded fault detection and isolation capabilities. EVA retriever and crew would often cooperate in the same work envelopes. Safety, reliability, robustness, and maintainability in space are key attributes.

The EVA retriever ground-based technology demonstration¹⁻³ was established to design, develop, and demonstrate in three phases an integrated robotic hardware/software system which supports design studies of a spaceborne crew rescue and equipment retrieval capability. Goals for 3 phases were established.⁴ Phase I goals were to design, build, and test a retriever system test-bed by demonstrating supervised retrieval of a fixed target. Phase II goals were to enhance the test-bed subsystems with significant intelligent capability by demonstrating target retrieval with avoiding of fixed, arbitrarily oriented obstacles. Phase III goals are to more fully achieve supervised, intelligent, autonomous behavior by demonstrating retrieval of a moving target while avoiding moving obstacles.

There have been recent developments in artificial intelligence (AI) planning and control techniques⁵⁻⁹ that make safe and reliable operations of supervised autonomous robots possible. These techniques, known collectively as situated reasoning, tightly couple planning and execution through rapid and continuous sensing of the environment. These advances, as well as those in real-time perception,¹⁰ show promise of achieving supervised

autonomous robotics that are safe and reliable enough for use in space.

Presented here are an overview of the hardware and a summary of the Phase II results from both an orbital simulation and an air bearing floor demonstration.

Problem Statement

Space Station scenarios¹¹ were examined in some detail to aid in the definition of a set of design reference missions. A number of systems engineering studies were conducted in support of the software design. Level A requirements for a projected Space Station version were developed in a conceptual design study.¹² Level B software requirements were derived in greater detail for this possible future Space Station application.¹³

The EVA retriever software is required to autonomously plan and execute a target rendezvous, grapple, and return to base while avoiding stationary and moving obstacles. The design provides for supervised autonomy as the primary mode of operation. It is intended to be an evolutionary system, improving in capability over time and earning crew trust through reliable operation.

The system is required to monitor plan execution, estimate probability of mission success, and dynamically replan when needed to achieve system goals. The mission profile requires appropriate actions for the following maneuvers:

- Activation - Perform system health status and data base initialization.
- Pop-up point rendezvous - Plan and execute a move with obstacle avoidance to one of a set of preselected pop-up points simulating movement away from the target obscuring environment near the Station.
- Target acquisition - Plan and execute a target search (moving as required), identification, and determination of location.
- Target rendezvous - Plan and execute a trajectory to near vicinity of one selected target object which avoids obstacles.
- Grapple analysis - Plan and execute a grapple approach which allows vision based analysis of a grasp strategy.
- Grapple - Plan and execute a one- or two-hand or arm (depending on target class) grasp using closed-loop vision control and force feedback sensors. Plan and execute maneuver of combined retriever/object to stable state for return to Space Station.
- Handoff and deactivation - Plan and execute target handover at Space Station, retriever return to base unit, and deactivation.

Approach - Phase II Prototype

Phase II Hardware

The current EVA retriever prototype (fig. 1) is an anthropomorphic manipulator unit, with dexterous arms and

hands, seated in an MMU. Sensor data include accelerometers, gyroscopes, two independent vision systems, and force/proximity sensors on the hands and arms. The accelerometers and gyroscopes measure the instantaneous translational and rotational acceleration/rate of the EVA retriever. The primary vision system consists of a laser scanner imager (128 x 128 pixels of both range and gray-scale intensity) and a camera mounted on a controllable turntable. The turntable provides for ± 180 deg. rotation at 5 deg/s. The secondary vision system is a multicamera video imaging system, with a 3 chest-camera array.

The MMU has twenty-four thrusters, four on each rectangular side. These thrusters provide a fixed force in three perpendicular translational directions and a fixed torque in each of the three perpendicular rotational directions. The MMU accepts simple translation and rotation on/off command to fire thrusters to provide fixed acceleration in any of the three translational or three rotational directions. The EVA retriever weighs approximately 1100 lbs with each thruster providing approximately 1.75 lbs force. A translation command to the MMU results in approximately 2.6 in/s/s acceleration in the commanded direction. A corresponding rotation command results in a rotational acceleration of roughly 3 deg/s/s.

The current technology demonstrations are being conducted on the JSC Precision Air Bearing Floor (PABF). The retriever/MMU unit is mounted on a test stand with compressed air supplied through an umbilical. Thus, the test unit is constrained to x, y, and yaw motion. The prototype has dual 6-degree-of-freedom arms with roll and pitch at the shoulder, elbow, and wrist. One of the arms has a compliant grasping hand and the other has a 3-fingered dexterous hand. The right hand incorporates proximity sensors in order to support compliant grasping of an object with force limiting.

The processor configuration contains two 15-MHz T414 transputers, twelve 20-MHz T800 transputers (five of which are dedicated to vision processing), a 16-MHz 80386, and six 68020 controllers. The transputers and 68020s are programmed in C and the 80386 is programmed largely in LISP.

Phase II Software

Based on the previously mentioned analysis of Level A and B software requirements projected for Space Station, a set of Phase II Level B software requirements was developed¹⁴ as were Phase II PABF scenarios.

The software architecture incorporates a hierarchical decomposition of the control system that is horizontally partitioned into five major functional subsystems: perception, world model, reasoning, sensing, and acting (fig. 2). In traditional hierarchical software architectures, the flow of messages and data through the command tree is strictly enforced with no horizontal flow. A disadvantage of this architecture is that bottlenecks may develop

due to lack of horizontal communications between components at the same level. The design presented here utilizes hierarchical flow of command and status messages but allows horizontal flow of data between components at the same level. Computation is performed at the lowest possible level and, in general, knowledge-based systems are utilized only when algorithmic solutions are lacking in power or flexibility. This approach handles multiple levels of abstraction well and permits the incorporation of special data paths between time-critical components.

The state perception module estimates the dynamic state of the EVA retriever (translational and rotational position and velocity). State estimation is based on measurements from the accelerometers, the gyroscopes, and a camera. These measurements provide information on translational acceleration and rotational velocity at 100 Hz, and updated relative position vectors to objects of known position at approximately 0.5 Hz.

The world model provides a representation of the external environment and internal status that is three-dimensional in space and dynamic in time. It contains a variety of general world knowledge as well as specific mission-related facts and constraints. The world model maintains over time the identity of the objects instantaneously sensed by the vision subsystem and provides notice when new obstacles or targets are detected, supplying a consistent model of the environment for the purposes of navigation.

The reasoning functions of the system are partitioned among the mission control and assessment, the action arbitrator, and the planning modules.

The mission control and assessment component directs the development and execution of a mission plan with supervisory direction from a human controller. Commands are received from the operator through a voice recognition processor with confirmation via voice synthesis. The module acts primarily as a plan execution monitor and as a meta-planner, delegating the creation and execution of detailed plans. Cue action modules, which look for specific events to occur in the world, initiate a wide range of monitoring, planning, and control actions. An internal assessment module initiates replanning whenever an expected cue fails to appear within a reasonable period of time. Also, replanning is initiated when a cue is triggered reflecting a change in the environment (e.g., a new obstacle) in the planned path.

The planning module consists of five functional components: vision, speech, motion, manipulator, and reconfiguration. For the current technology demonstration, the speech and reconfiguration planning components were not implemented.

In general, the planning module responds to requests from the mission control and assessment component, issues data requests to the world model, and sends plans and status information to the world model. The total set of action primitives available to the planning module is

based on the action requests recognized by the hand/arm, MMU, and the camera turntable subsystems.

The motion planner calculates a grid-based transition cost field based on safety zone and world model estimates of target/obstacle (fixed) location and size. The transition cost field is dynamically updated in response to changes in obstacle location or number. The path is constructed of straight line segments with node location determined by a change in direction or the need to maintain the target/body orientation required by the vision system.

The vision planner constructs motion plans which support vision processing such as a search for an obscured target or positioning of the retriever for an analysis of a target grapple. The module maintains internal models of the vision sensor's field of view given obstacles and plans a move to see the most probable part of a target region which has not been previously observed.

The manipulator planner handles gross hand/arm positioning for grappling based on target type. Small targets are grasped with one hand, medium size targets with two hands, and targets the size of an astronaut are grappled in a bearhug using both of the retriever's arms.

The action arbitrator is the primary interface between the reasoning and action subsystems. Under the supervision of the mission control and assessment module, plan fragments are retrieved from the world model and transmitted to the appropriate action subsystem interface. Depending on the subsystem, actions may be occurring in both a serial and a parallel manner.

The motion control module accepts motion commands generated by the planning module and/or the mission control and assessment module. Commanded motions basically include a translation to a desired position and/or a rotation to a desired orientation. The motion controller uses the state estimation provided by the state perception module as control feedback. The motion controller uses the MMU propulsion system to control the position and attitude of the body.

Approach - Phase II Environments

Precision Air Bearing Floor (PABF)

PABF was used in Phase II for integrated testing and demonstration. This 24 x 32 ft floor is composed of metal plates which are laser-levelled to approximate a perfectly smooth surface with error of < .005 inches. The retriever hardware is levitated off this surface by supporting pads releasing pressurized nitrogen. The lights on the ceiling above the PABF eventually played a critical role: A camera facing the ceiling was mounted on the retriever to track the lights and compute a correction for the retriever's position and attitude estimate in analogy to using the global positioning satellites in space.

Before integration and testing on the PABF, the software, with the exception of the one-handed tool grasp, was integrated and tested in a simulated PABF

environment. The following elements were simulated: (1) acceleration of the retriever due to minute slopes on the PABF, (2) idealized output of the vision system for a given set of objects on the PABF (position, radius for navigation, orientation for grasping), (3) turntable rotating the laser range imager, and (4) manipulator kinematics and motion assuming constant joint angular velocities.

The unsensed changes in location due to the imperfections in the PABF were significant because the onboard accelerometers do not measure gravitational acceleration. A simulated corrective measurement of retriever position was developed to test motion control alternatives with various assumptions about how this correction would be implemented.

This simulation was used primarily to integrate our distributed software modules and preliminary test execution of the various mission phases under a variety of conditions while the hardware itself was being assembled.

Orbital Simulation

An integrated dynamics simulation of the current EVA retriever hardware in an orbital, Space Station Freedom-based environment has been developed.¹⁵ This simulation includes models of the 6-degrees-of-freedom dynamics of orbiting bodies, the Odetics laser scanner range imager, the MMU dynamics and plume impingement, scanner turntable, and trivial manipulator/target capture logic. Failure modes in the manipulator/target capture logic have been implemented, as has the ability to freeze the simulation and alter the positions/velocities in both translation and rotation for all the bodies in the simulation.

This simulation provides a capability to allow development and evaluation of various software technologies such as situated reasoning and those which will be needed to deal with moving objects and a dynamic, unpredictable environment.

Phase II Results - PABF

The system capabilities described earlier have all been demonstrated. These include retrieval of 2 types of targets: (1) a small "wrench" which will fit inside the Jameson dexterous hand, and (2) a large astronaut-sized cylinder which can be enclosed by the EVA retriever body/arms. The targets may be initially obscured and arbitrarily oriented, given the degrees of freedom available to the retriever and the constraints of the target supporting stands. An operator provides (1) direction to target, (2) target identification based on image display, and (3) notification if the target is obscured. Retrievals may be accomplished in 7 to 15 minutes, depending on degree of difficulty. Fuel is available for 200 ft of travel. Unique and special aspects of the retriever are summarized in table 4.

Self-Location

One aspect of PABF simulation-based testing in Phase II bears discussion: the failure to detect a software design flaw because of low fidelity in the simulation. The undetectable accelerations due to minute slopes on the PABF and the need to correct this via some other measurement source have been mentioned. The initial approach was to infer the retriever's position from objects' positions determined through laser-scanner-based vision. The vision algorithm used was a simple one: after the image has been segmented, each object's position would be computed as the average of all its range pixels; i.e., centroids. These positions would be passed to a tracking algorithm which would match them, if possible, to objects already seen. The difference in their positions would represent movement of the retriever itself because the objects were stationary. The simulated system was not tested with noise in the centroids, and the system worked fine. Once we began integrated testing with the hardware, we found this method to be unworkable. Ultimately, a correction method based on a camera tracking overhead light was adopted.

Target Acquisition/Tracking

Objects' size and location are perceived dynamically—only the retriever's position is known initially. An operator is used to identify the target, although testing of model-based recognition showed promise (it was limited by sensor noise). Finally, the laser scanner limits the targets to those with high reflectivity.

Navigation

Navigation, rendezvous, and stationkeeping are completely autonomous. Paths are executed at speeds of 0.375 ft/s in translation and 8 deg/s in rotation. Translation is limited by PABF size (24 ft x 32 ft) and MMU acceleration (< 7 lb/s). While following paths, the position deviates by < 3 to 4 in (combination of position est. error + pos. control) and the attitude deviates by < 3 deg. Path generation is based on minimum distance. Objects are assumed to be stationary and symmetrically shaped (they must occupy or not grid cells). If target is not visible to the retriever, it plans a path to the largest obscured space in target direction. The scanner faces the direction of motion continuously.

Target Grasping

Target grasping is completely autonomous as well. The target is assumed to be stationary. Computer vision algorithms were tested against oddly shaped objects, but weren't robust in target orientation due to sensor noise. Because the target is stationary, the manipulator(s) path could be followed at any speed—Remotec arms took

roughly 5 seconds for reach. "Trajectory" planning wasn't necessary, and the control was not closed loop relative to the target, for the same reasons. Finally, the size of the target for single-handed grasping was limited to those that fit within the size of the Jameson hand (largest opening is 5 in). Error in positioning the arms is estimated at 1 to 4 in, limited by Remotec joints accuracy. The dexterous hand is commanded to close when the target trips a proximity sensor in the hand and stops closing when a fixed level of force on the target is measured. The two-armed grasp is terminated by pressure sensors in arms and chest.

Phase II Results - Orbital Simulation

This simulation has been used to develop software for MMU orbital control, model-based object pose and motion estimation, and situated reasoning and reactive planning. The reactive planner, developed by Advanced Decision Systems (ADS),⁷ provides logic for continuing the retrieval mission despite the occurrence (at any appropriate point in the mission) of one of the failure modes mentioned in section 4. These include losing track of the target, having the EVA retriever or target moved prior to capture, "accidentally" dropping the target after capture, etc. This enables the retriever to react in real time to dynamics of its environment, act to acquire knowledge, act on beliefs, react to failed expectations, and act predictively by reasoning about dynamics. A demonstration video of the retriever reactive planner in this 6-degrees-of-freedom simulation has been produced.

Conclusions

Robotic technology has been evaluated for practical application to retrieval of detached crew and equipment in space. The completed phase described here comprises an initial attempt to build and understand a limited version of a supervised autonomous robot for use in space. Supervised intelligent systems, including supervised autonomous robots, also need to be developed for Earth applications.¹⁶⁻¹⁸

Phase III, during which moving targets and obstacles drive real-time behavior requirements, will also explore crew helper tasks. Table 2 lists tasks and possible capability improvements. Evaluation of real-time vision and moving object grasp with new, faster equipment is planned for the KC-135 reduced gravity aircraft in 1993. Recent work^{19,20} offers promise that safe and reliable space robotic systems can be achieved. Recent studies²¹ show that such systems will be useful on planet surfaces as well as being needed in orbital applications.

References

¹Reuter, G. J., et al., "An Intelligent, Free-Flying Robot," SPIE Symposium on Advances in Intelligent Robotic

Systems, Space Station Automation IV, Cambridge, MA, Nov. 6-11, 1988.

²Erickson, J. D., et al., "A Prototype Autonomous Agent for Crew and Equipment Retrieval in Space," *Proc. 2nd Intl. Conf. on Ind. and Engineering Appl. of AI and ES* Tullahoma, TN, June 1989.

³Erickson, J. D., et al., "Technology for an Intelligent, Free-Flying Robot for Crew and Equipment Retrieval in Space," *Proc. Space Operations Automation and Robotics Workshop*, NASA Johnson Space Center, Houston, TX, July 1989.

⁴EVA Retriever Program Plan," Johnson Space Center, JSC-22144, Houston, TX, May 1987.

⁵Kaelbling, L. P., and Rosenschein, S. J., "Action and Planning in Embedded Agents," *Robotics and Autonomous Systems*, Vol. 6, No. 1, 1990, pp. 35-48.

⁶Schoppers, M. J., "Representation and Automatic Synthesis of Reaction Plans," Ph.D. Thesis, University of Illinois at Urbana-Champaign, Urbana, IL, 1989.

⁷Shapiro, D., "Architectures for Semi-Autonomous Planning," ADS TM 3249-08, Advanced Decision Systems, Mountain View, CA, July 1991.

⁸Agre, P., and Chapman, D., "Pengi: An Implementation of a Theory of Activity," *Proc. AAAI*, 1987, pp. 268-272.

⁹Dean, Thomas, and Boddy, Mark, "An Analysis of Time-Dependent Planning," *Proc. of 7th National Conference on AI*, Minneapolis, MN, 1988.

¹⁰Ballard, D. H., "Animate Vision," *Artificial Intelligence*, Vol. 48, 1991 pp. 57-86.

¹¹Shapiro, D., "An EVAR Scenario," Advanced Decision Systems, Mountain View, CA, June 1988.

¹²Freeman, J., "Autonomous Robot Control System Design Study," Johnson Space Center, Houston, TX, internal report JSC-12421, May 1988.

¹³Taylor, D., et al., "Level B Post-PMC Space Station EVAR Functional Requirements," Internal JSC project report (draft), Houston, TX, March 1988.

¹⁴Taylor, D., et al., "EVA Retriever Phase II Derived Software Requirements," Internal JSC project report (draft), Houston, TX, June 1988.

¹⁵EVA Retriever Hardware and On-Orbit Environment Simulation Requirements and Design, Johnson Space Center, Houston, TX, internal report JSC-24653, Nov. 1990.

¹⁶Bureau of Export Administration, "National Security Assessment of the U.S. Robotics Industry," Department of Commerce, Washington, D.C., April 1991.

¹⁷Engelberger, J. F., "Robotics in Service," MIT Press, Cambridge, MA, January 1991.

¹⁸Office of Technology Assessment, "Exploring the Moon and Mars: Choices for the Nation," Congress of the U.S., Washington, D.C., August 1991.

¹⁹*IEEE Trans. on Sys., Man, and Cybernetics: Special Issue on Unmanned Vehicle and Intelligent Robotic Systems*, Vol. 20, No. 6, November/December 1990.

²⁰*ACM SIGART Bulletin: Special Section on Integrated Cognitive Architectures*, Vol. 2, No. 4, July 1991.

²¹Erickson, J. D., et al., "Future Needs for Space Robots for SEI," Proc. of SPIE Symposium on Cooperative Intelligent Robotic Systems in Space, Boston, MA, November 1991.

Space Center and R. Norsworthy, G. Anderson, L. Merkel, and D. Phinney from Lockheed Engineering and Sciences Company. The EVA retriever is a project of the Automation and Robotics Division of the Engineering Directorate at JSC, under funding from the JSC Director's Discretionary Fund. The contributions of the project team encompassing civil servants and contractors are gratefully acknowledged. Partial funding of the orbital simulation was provided by NASA Headquarters, code MT.

Acknowledgments

The principals in the work presented are J. Erickson, R. Goode, K. Grimm, and C. Hess from the Johnson

Table 1. Unique and Special Aspects of EVA Retriever

<ul style="list-style-type: none"> • Is a prototype supervised, intelligent, autonomous robot • Responds to voice commands providing goals and directions • Clips into spaceworthy MMU which has flown from Shuttle • Flies by propelling pressurized gas from MMU thrusters it controls • Can determine its own location with camera, gyroscopes, and accelerometers, in analogy to space use of global positioning satellites • Builds its own internal dynamic knowledge of its environment based on continuous sensory perception (no preprogrammed environmental model to which the environment must conform) • Plans/replans based on goals and internal dynamic knowledge of its environment and constraints such as flight rules - Path planner for obstacle avoidance and rendezvous can reason in advance about the success of the mission 	<ul style="list-style-type: none"> - Actions are synchronized to events in the world through sensing of preconditions of planned actions • Location of range image obstacles and target tracking, orientation, and grasp location • Acts to acquire knowledge about obscured target • Maneuvers to optimize grasp success relative to target orientation • Chooses between one- and two-handed grasp or two-armed grapple, depending on target size • Dexterous grasping uses proximity sensors, compliant grasp, and force-limited grasp <ul style="list-style-type: none"> - Right hand has five proximity sensors - Left hand has three proximity sensors and nine tactile sensors (three per finger) • Pressure sensors on chest used in two-armed grapple of large targets • Uses fourteen 10 million instructions per second (MIPS) transputers, six 68020 controllers, and one 80386 processor in a hierarchical, distributed architecture
--	--

Table 2. Phase III Plans

Tasks and Environments	Improved Capabilities
<ul style="list-style-type: none"> • Crew helper tasks <ul style="list-style-type: none"> - Moving obstacle avoidance and moving target rendezvous - Grasping translating and rotating objects - Retrieving objects from storage or current location - Returning objects to storage - Inspection - Assistance in holding objects - Maintenance site preparation - Orbital replacement unit exchange • Environments <ul style="list-style-type: none"> - Vicinity of Space Station via computer simulation - PABF with spacecraft mockup - Laboratory testing 	<ul style="list-style-type: none"> • Model-based object recognition and motion description • Situated reasoning/reactive planning to dynamics of environment • Speech recognition and limited natural language understanding • Guarded, compliant, and fine motion manipulation • Knowledge representation of objects, event, processes, and states of affairs • Internal knowledge of competencies • Fast 7-DOF manipulator • Faster frame rate laser range imager • 200 MIP/25 Mflop transputers enable computer hardware and software to all be packaged on board • Self-contained hand design • More effective use of tactile sensors

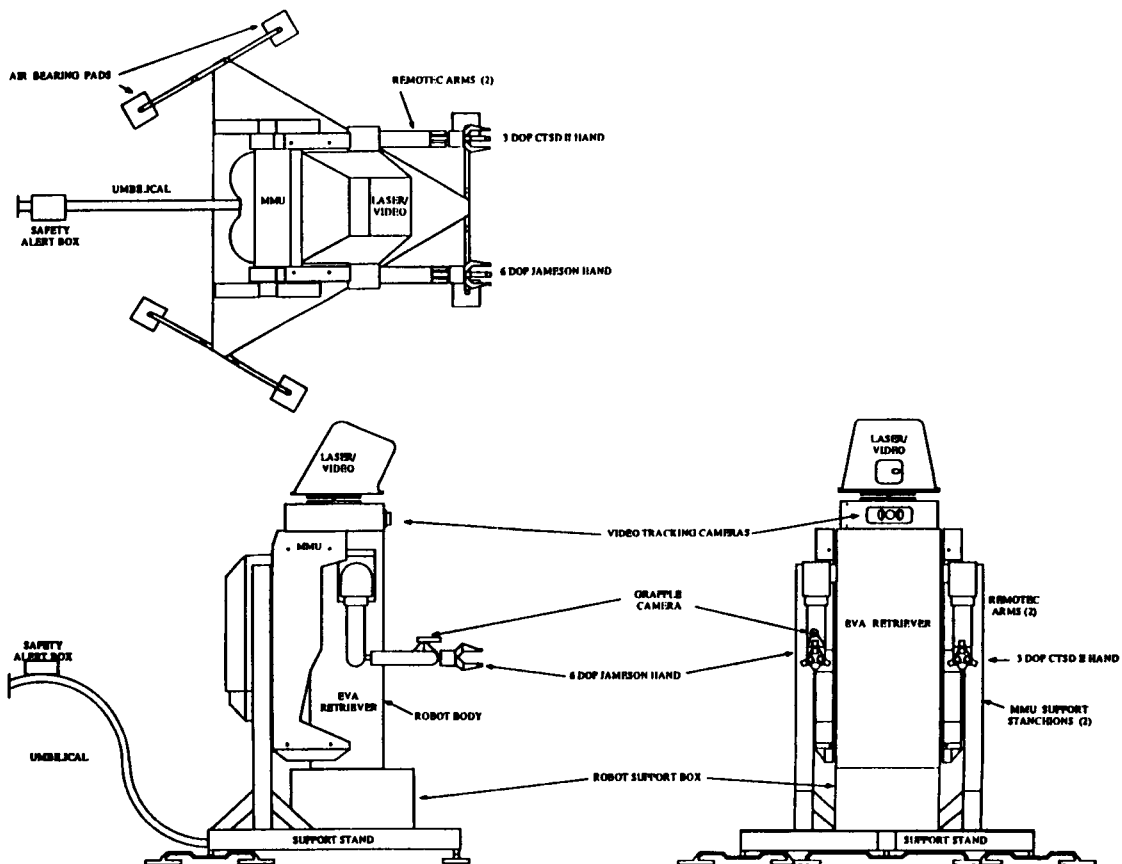


Figure 1. Retriever Test Article.

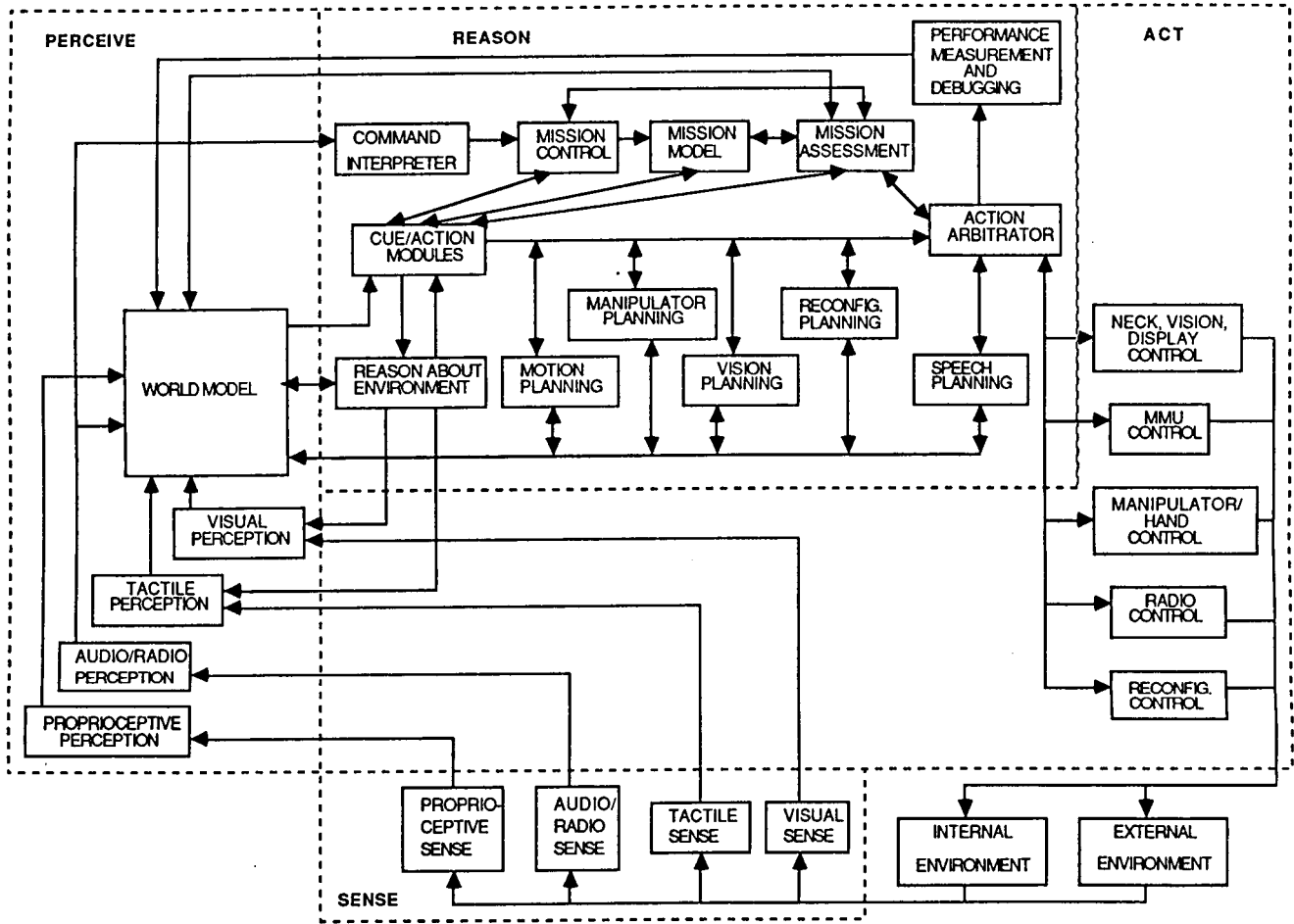


Figure 2. EVA Retriever Software Components.

The Space Station Freedom Reliability and Maintainability Assessment Tool and Its Use for Prediction of Maintenance Demand

Will Blumentritt
LORAL

Abstract

This paper describes a computer simulation program that has been developed to analyze the reliability and maintainability of the Space Station Freedom (SSF). The program is a stochastic, event-oriented simulation process written in FORTRAN and implemented on a personal computer. The program which simulates hardware failures as well as preventative maintenance tasks, uses user-specified maintenance resources to perform maintenance. The program has the capability to interface dynamically with Space Station function minimal cut sets in order to determine queuing priorities and to assess the status of Space Station functions. This model, the Reliability and Maintainability Assessment Tool (RMAT), is being used as a program-wide resource for predicting maintenance levels for the Space Station. It is also being used by the Reliability and Maintainability Division to assess the functional capability of Space Station.

Introduction

NASA's SSF is a complex, long-term project containing numerous components which may require maintenance one or more times over the expected life of the Station. NASA must be able to accurately assess the maintenance needs of the Station in order to determine the feasibility of the current design and to monitor the results of design changes and Station restructuring. The SSF RMAT is a stochastic, event-based simulation program designed to predict the maintenance needs of the Space Station and to assess the availability of Space Station functions. Development of the RMAT began in the summer of 1990, and it was first used for Space Station analysis later that summer. Additional analysis capability has been added to the RMAT as additional Station data have become available.

Description

The RMAT is a stochastic simulation program written in FORTRAN and implemented on a personal computer. Figure 1 shows the general flow of the program. Input to the program includes component reliability and maintainability (R&M) data, function reliability block diagrams or a functional criticality level for each component, and maintenance resource levels. The reliability data are used to simulate maintenance action demands such as equipment failures, preventive maintenance tasks, and induced failures. The reliability

block diagrams or the criticality levels are used to evaluate the impact of the failures and determine the queuing priorities. The maintainability data and the maintenance resources are used to simulate the performance of maintenance. Program output includes predictions for the number of maintenance actions and hours by time period, the availability of Space Station functions, maintenance demand by location, and maintenance demand by type of component.

RMAT can use two methods to assess the impact of the failure to determine queuing priorities. When available, cut sets generated from reliability block diagrams of the functions can be used to determine queuing based on functional criticality and the current level of redundancy. This allows assessment of the availability of the functions. When reliability block diagrams are not available, functional criticality levels are used to queue components.

The program is large enough to handle the entire station (up to 16,000 components) so that the competition for crew resources can be accurately modeled. The program gives the user the ability to perform trade studies on the maintenance resource levels and the configuration of the functions to optimize the availability of the Station.

Methods

Failure Generation

Failure modeling is done using a Monte Carlo simulation approach. To simulate each time to failure, a uniformly distributed random number between 0 and 1 is drawn and is set equal to the reliability function for that component. Time to failure is calculated by solving this equation. This is done individually for each modeled component.

The failure rate is assumed to be three components: random failures, early failures, and life-limit failures. The random failure rate is assumed to be constant and is modeled as an exponential time to failure function. The duty cycle (operating ratio) of each component is factored into the random failure reliability equation. This equation also includes failures while the equipment is off or dormant. Component input data include a cold failure rate factor which is the ratio of the cold failure rate to the hot failure rate.

The early failure rate is considered as a time-varying modification of the random failure rate. This modification causes the failure rate to begin at a higher level than the constant, random failure rate, and then to

decrease fairly rapidly over time as the infant mortality rate decreases and reliability growth occurs. Use of this early failure/reliability growth modification curve is optional.

The third component of the failure rate is the life-limit, or wearout, component. This is modeled with a two-parameter Weibull distribution.

Failure rate multipliers, called K-factors, are used to account for maintenance actions which occur for reasons other than the inherent component failure. K-factor values are assigned to components by category and have default values which are currently determined by a NASA working group. Components are categorized for K-factor purposes as being electrical, electronic, mechanical, electromechanical, structural, or structure-mechanical. Separate K-factors are also assigned for internal and external hardware. A K-factor is composed of four terms: K_1 , human-induced; K_2 , environment-induced; K_3 , equipment-induced; and K_4 , no defect or false alarm.

The RMAT also allows for three types of preventative maintenance: preventative remove and replace, servicing, and inspection. The times between preventative maintenance are not randomly distributed by the RMAT but are scheduled to occur at fixed intervals of time as supplied in the component data file. The failure of a component will cause all preventative maintenance for that component to be removed from the event calendar or queues. A preventative remove and replace being performed or placed in the queue will also clear other types of preventative maintenance from the event calendar or queues.

Evaluation of Failure Impact

When a component failure occurs, a decision must be made regarding prioritization of the repair of the component. There are eight priority level queues available for use in the program. Within a single queue, tasks are time-ordered with the longest jobs having the highest priority.

When functional reliability block diagrams are available, minimal cut sets which are generated from the reliability blocks diagram via an off-line software package can be used to dynamically monitor Space Station functions. In this case, queuing of components is based on functional priorities and the redundancy remaining in that function at the time of the failure.

When reliability block diagrams are not available, components are queued according to a predefined input criticality level. The user assigns queuing priorities separately for corrective and preventative maintenance through file input. Queuing by functional criticality level rather than by reliability block diagrams, however, does not account for redundancy. Both the maintenance performed and the maintenance backlog are reported by queue.

Performing Maintenance

Maintenance task time consists of two parts: the worksite time and the maintenance task overhead time. The worksite task time includes only the actual time to perform the maintenance action itself. The overhead time includes the time necessary to obtain the spare part and necessary tools, to travel to the worksite, and to set up the worksite.

A lognormal distribution with a 95th percentile equal to three times the given mean is used to simulate the variability in maintenance task times. Both the worksite time and the overhead time are randomly distributed according to this lognormal distribution. The mean time to repair (MTTR) and the overhead category for each component are supplied in the component input file. The time values for each overhead category are supplied by user input. Because of the modular construction of the program, other distributions can be easily substituted.

Both internal and external maintenance is packaged into shifts of work. A certain amount of overhead is associated with performing maintenance, particularly external maintenance. This overhead, which is called sortie overhead, is charged once per maintenance shift. Packaging the maintenance into shifts reduces the impact of sortie overhead.

No task will be started by the program unless its predicted maintenance time is less than the time remaining in the shift. Therefore, some shifts may end early because no maintenance actions are in the queue which would fit into the time remaining in a shift. Due to the lognormal distribution of maintenance task times, some tasks may run beyond the planned end of a shift. According to current NASA flight rules, external maintenance may only run fifteen minutes over the scheduled time. A job not completed during this time must be redone later.

To allow maintenance to be packaged into shifts, a maintenance threshold is used. The maintenance threshold is a minimum backlog of crew maintenance hours which must accumulate before maintenance is triggered. Separate thresholds exist for EVA and IVA maintenance. Both thresholds may be set by the user. When crew maintenance resources become available, maintenance is performed based on the queue priorities and the maintenance threshold for as long as maintenance resources still exist.

Maintenance resources are specified in two phases, the assembly phase and the postassembly phase. During the assembly phase, the resources can change with each Shuttle flight. Once assembly is complete, however, the resource levels are assumed to be constant throughout the life of the Station. Resources can be from the Station crew, from the Shuttle crew, or from Station or ground-controlled robots. Separate resource levels are specified for internal, external, and robotic maintenance.

Results

The RMAT program is currently used by the Space Station analysis community for maintenance prediction. Users include the external maintenance solutions team, the in-flight maintenance working group, and the internal maintenance task team. The RMAT is also used to generate crew worksite time predictions included in the NASA Level II Resource Margin Summary Document. These users have utilized the RMAT, without cut sets, to assess predicted levels of maintenance demand for the SSF and to assess levels of maintenance backlog due to constrained resource levels. The SSF Program has now identified functional criticality levels for almost all of the components. By assigning different criticality levels to different queues and by examining the maintenance backlog by queue, the user can assess the impact of the backlog by functional criticality level.

An example of the extravehicular activity (EVA) maintenance demand for Work Package 2 during the assembly phase is shown in figure 2. These results were generated with some preliminary SSFP R&M data and should not be considered as actual or approved predictions of SSF maintenance needs. Early failures were not considered for this run. The figure shows a distinction between those items on the minimum equipment list (MEL) and those items not on the MEL. Because flights during the assembly phase are not equally spaced in time, the figure has a sawtooth look.

Analysis Capability

It is necessary to develop the capability of assessing the availability of SSF functions resulting from the maintenance backlog. RMAT may be used to determine availability if all the Station functions are modeled with reliability block diagrams. However, to date, only a few Station functions have been modeled with reliability block diagrams.

Extendibility

The program is modular in nature and can be extended and modified as the need arises. One of the next planned extensions is the addition of overhead calculations for robotic maintenance. Data to support such calculations have not existed in the past, but are expected to become available during the Spring of 1993. The RMAT will be modified to accept this data. Other examples of model components that can be modified include the early failure mechanism and the maintenance time lognormal distribution. In-house tests have been done using other distributions or algorithms in the RMAT which have proven quite easy to implement.

Summary

The RMAT is a viable analysis tool for the Space Station. Its success has depended on keeping the level of modeling detail consistent with the availability of the SSF data.

A number of significant factors are not included in the RMAT program, for example spares and mission operations, but at this point in the development of the SSF, the RMAT tool appears to be the best available predictor for Station maintenance. It is essential that the SSF Program be adequately prepared to handle this expected level of maintenance. Recognizing the levels of maintenance that will be required will help the logistics and mission operations areas plan for the provision of adequate levels of SSF support.

Acknowledgment

This program is funded by JSC and is controlled by the Safety, Reliability, and Quality Assurance Office's Reliability and Maintainability Division.

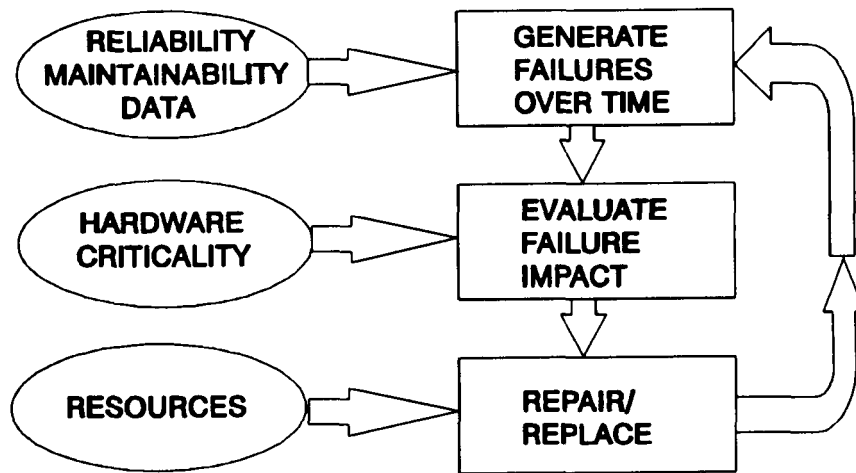


Figure 1. RMAT Program Flow.

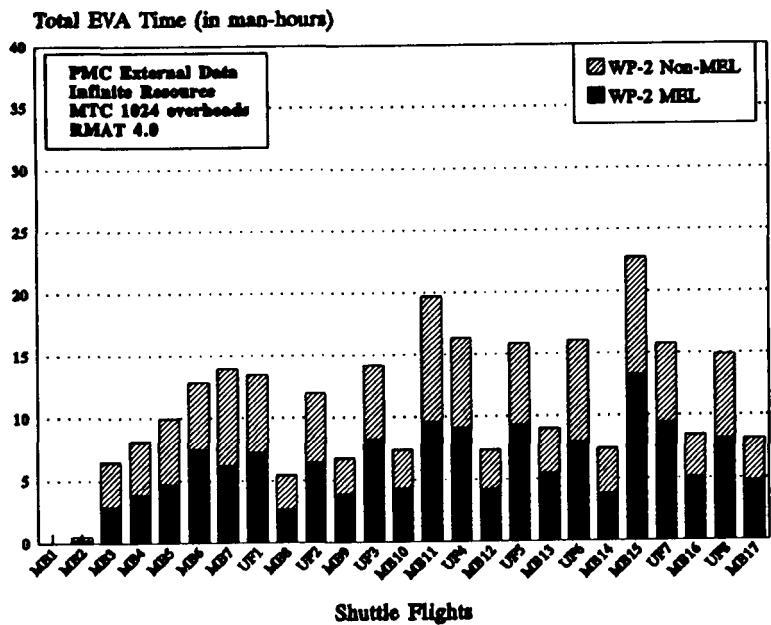


Figure 2. Work Package 2 External Maintenance Demand During the Assembly Phase.

A Dynamic RMAT Model: A Method for Assessing the Space Station Freedom Program Functional Capability During Assembly Phase

Keith P. Sample
LORAL

Abstract

The Reliability and Maintainability Division within the Safety, Reliability and Quality Assurance Office at JSC uses the reliability and maintainability assessment tool (RMAT) to simulate future failures and repairs of the Space Station Freedom (SSF) components and to assess possible maintenance scenarios associated with the SSF Program (SSFP). The RMAT is also used to generate measures of the projected availability of critical functions of the SSF during and after assembly. It must, therefore, be capable of simulating the assignment of repair priorities for items requiring repair, and of evaluating the impact of the nonrepaired items as a function of time. This capability exists, in part, in a RMAT version that uses cut sets (equipment/component failure combinations that will fail critical SSF functions). During the permanently manned configuration (PMC) phase, the probability of the failure of these functions can then be estimated. Reliability and availability assessments during the assembly phase, however, are more difficult because they require the use of system and functional hardware configurations that change with time (i.e., time dependent cut sets). A new version of RMAT was developed to address this situation. This paper discusses the overall RMAT analysis approach and describes the version of RMAT that was developed to better assess the SSFP safety, reliability, and maintainability characteristics during the assembly phase of the Program.

Introduction

The previous standard RMAT version 3.2 was created so that the reliability and availability of a SSFP function, such as attitude control, could be evaluated based on the reliability block diagram configuration of the function. The RMAT 3.2 performs this task by using cut sets of the function as input. These cut sets are generated from reliability block diagram analyses (RBDA) efforts and represent equipment/component failure combinations that will cause the associated SSFP function to fail. When a component fails, the program reviews the cut sets to determine the status of the function after the component failure. The function status is dependent on the redundancy level remaining after the failure. If the failure causes the function to fail, then the function status becomes red (not available). The item which caused this condition is put in the highest priority queue, with its repair becoming the most urgent. If this failure results in one level of redundancy remaining, the function status

becomes orange; two levels of redundancy, the status becomes yellow; and three or more levels of redundancy, the status becomes green. The orange, yellow, and green statuses result in successively lower priorities of repair queues. When a component is repaired, the function status is reevaluated and reset, again, depending on the redundancy level of the function. All those items in the red queue are repaired prior to those in the lower priority queues.

The RMAT 3.2 keeps track of the amount of time a function spends in each of the four possible states (colors) and at the completion of a run will print these as percentages of the total simulated mission time. For example, the program could be run for a simulated mission period of 10 years with an input attitude control function (ACF) hardware configuration reflecting the expected configuration of the SSF after mission build (MB) six. In this case, the results could show that the ACF was in the red for 6 months out of the total 120 month period, and the RMAT summary report would indicate a red ACF condition (not available) 5% of the total mission period. The RMAT 3.2 also tracks the number of times that the function was in the red, or how many times the function went down. This counter is necessary for calculating the probability of success for the function.

Problem

In an initial study, the RMAT 3.2 was used to determine the reliability and availability for different MB configurations of the SSFP ACF. The elapsed time between the completion of a specific mission build flight and the following Shuttle flight was varied from 30 days to 180 days. Figure 1 depicts how the ACF reliability decays as the delay between Shuttle flights is increased after the completion of four MB configurations (MB 2, 4, 5 and 6). The decreasing availability function for the same conditions is depicted in figure 2. The only conclusions that could be drawn from this analysis were relative to the maximum Shuttle flight intervals between the MBs and the associated ACF availability. One of the restrictions of this analysis was that the RMAT 3.2 made the assumption that all SSFP components were operating properly at the start of each of the MB phases under consideration. Thus, no carryover (backlog) of unrepaired failures from a previous assembly phase was possible. In order to eliminate this restriction and to produce a realistic availability analysis, a modification of the RMAT was completed.

Approach

A dynamic RMAT was developed (version 4.2) with the capability to track failures from MB to MB and to update the system hardware configuration at any time. That is, at the start of a new assembly mission, those components from the previous build which had failed are carried forward and are used to produce system status from the effects of the component failures on the next assembly flight. The components from the previous failures which caused the function status to be red will have the highest priority for repair purposes and will remain red until the appropriate components are repaired. This analysis tool yields more appropriate assessments of the risks and survival probabilities of the SSFP during the assembly phase.

The RMAT 4.2 yields the same output as the RMAT 3.2 but with additional results on a assembly-flight-by-assembly flight basis. That is, the summary report gives the percentage of time and the number of times the functions, such as the attitude control function, were in the four states (colors) while the SSFP was in a specific hardware configuration. The RMAT 3.2 assumption that all components are up and running at the start of a run is no longer necessary.

The RMAT 4.2 is able to perform multiple runs with up to 170 different Space Station configurations (a maximum of 10 different functions and up to 17 assembly flights for each function). As the program executes, it constantly updates the configuration of each function and then determines the status of each function based on those

components which have failed. Hence, as the assembly phase progresses and the configuration changes, the cut set information that the RMAT uses to determine the reliability effects is modified accordingly.

Results

Modifications reflecting the RMAT version 4.2 are complete. Testing and verification are presently underway with the utilization and reporting of RMAT 4.2 analyses planned before SSFP Critical Design Review in April of 1993. The critical functions of attitude control, reboost, and mating as a function of assembly through MB-6 were completed in April 1993. The RMAT 4.2 analysis of the SSF availability of these functions was completed in April 1993.

Conclusions

The RMAT version 4.2 provides a more accurate assessment of the survival and risk probabilities of the SSFP during the assembly phase. Analyses and results were addressed during the SSFP Critical Design Review.

References

- Johnson Space Center Space Station Freedom Reliability and Maintainability Assessment Tool (RMAT), Version 3.2, Users Guide, June 1992.
- Reliability Block Diagram Analysis (RBDA) Users Manual, SAIC, February 1992.

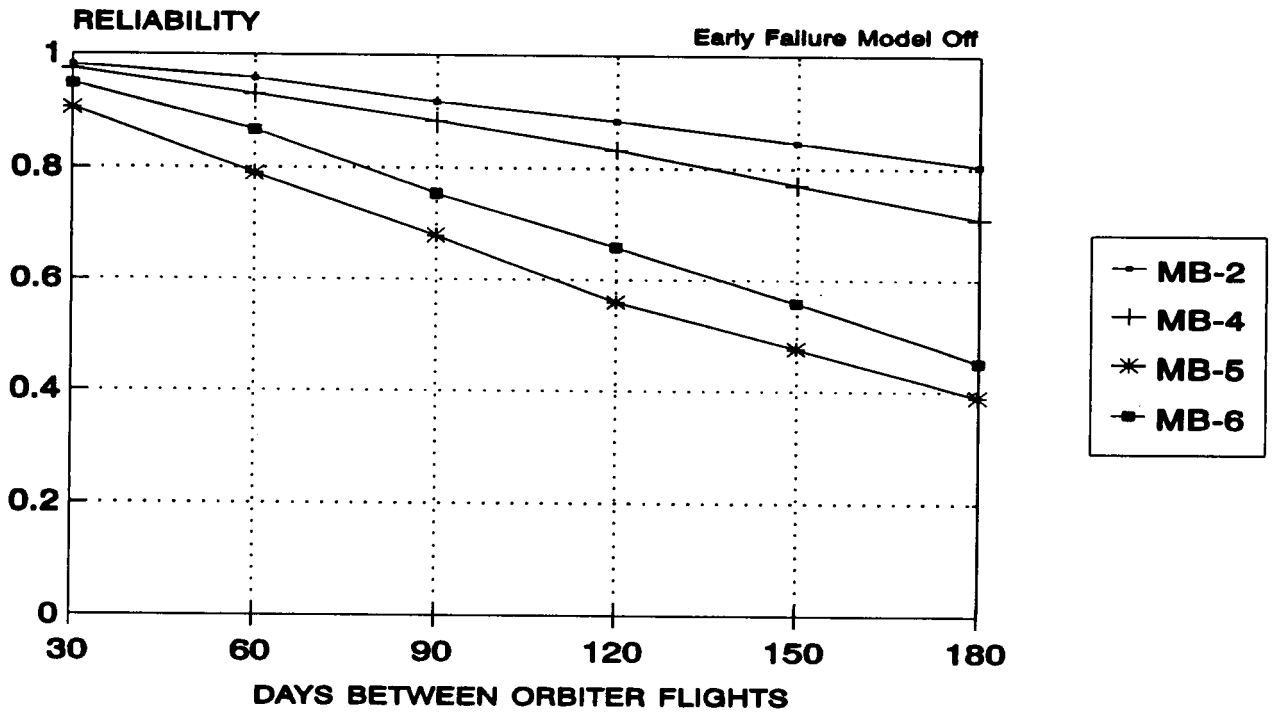


Figure 1. MB2, MB4, MB5 and MB6 ACF Reliability.

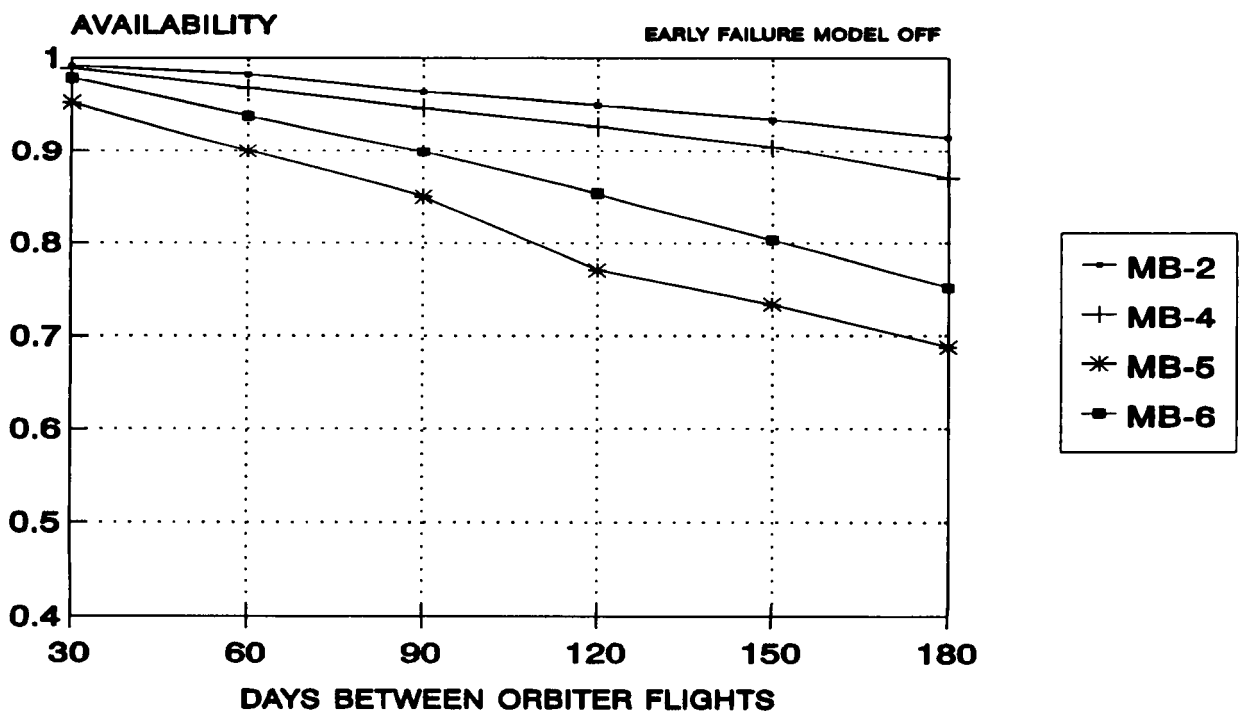


Figure 2. MB2, MB4, MB5 and MB6 ACF Availability.

Verification and Validation (V&V) of Knowledge Based Systems

Chris Culbert, Huyen-Anh Ly, David Hamilton,* and Scott French*
Johnson Space Center/PT4
*IBM-Federal Sector

Abstract

Expert systems (ESs) technologies have demonstrated the capability of solving a diverse range of problems. However, in operational or mission-critical environments, they have achieved only limited acceptance. Because software engineering methods were not used in their development, ESs have met with limited acceptance and an overall lack of confidence in their technologies. More specifically, the need for verification and validation (V&V) during ESs development was identified as a major factor. Attempting to improve the state of the practice in verifying and validating ESs, the Software Technology Branch has developed a workshop to

- Convince ESs developers that verifying and validating their software is important and should be done
- Teach some basic techniques that help in verifying and validating Expert Systems
- Provide some guidelines that Expert Systems developers can follow when applying these verification and validation techniques.

This paper reports the accomplishments of the workshop and the future works on verification and validation of knowledge-based systems (KBSs).

Introduction

Since 1987, V&V of KBS has been one of the major tasks of the Software Technology Branch (STB). The more significant efforts in this task (through September 1991) include

- Building a verification tool
- Attending the American Association of Artificial Intelligence (AAAI) tutorial on V&V of ESs
- Participating in the workshops on verification, validation and testing (VV&T) of KBSs held by the AAAI
- Surveying the state of practice in V&V of ESs
- Sponsoring a workshop that gathers all the experts in the V&V of the KBSs field so they can come up with the standard methodology and guidelines for verifying, validating and testing of KBS

As a direct result of the state of practice in V&V of ESs survey, a workshop on V&V of ESs was developed to assist developers in doing a better job of building high-quality ESs. The focus of the workshop was to encourage the application of more systematic V&V approaches to ESs development and provide hands-on experience in using proven V&V techniques.

Problem Statement

The survey used responses (in paper form and from interviews) of roughly 60 different ESs projects within both IBM and NASA. The survey questioned both developers and users of ESs. The goal was to generate some hard facts from which to draw conclusions rather than relying upon more theoretical speculation.

The survey sought to answer the following questions:

- What kinds of V&V techniques are used
- What kinds of problems are most often encountered
- To what extent is V&V practiced
- What is the level of satisfaction regarding ESs quality

One significant recommendation from the survey was that developers needed help in verifying and validating their projects. Many of the developers questioned had no background in computer science (i.e., they were engineers, flight controllers, etc.) and, as a result, had limited experience in the systematic application of V&V approaches. The ESs V&V workshop described in this paper would help developers by teaching the "why" and "how" of software V&V.

Approach/Method

Purpose

The ESs V&V workshop addressed two major obstacles in the application of V&V techniques to ESs projects. The first obstacle concerned lack of experience in applying V&V techniques. This affected the understanding of how to use the techniques and when to apply them. The workshop addressed this obstacle by

- Increasing awareness about V&V
- Providing information and hands-on practice for specific techniques
- Providing a set of guidelines for applying V&V

Another obstacle was that many developers did not believe in V&V. The developers felt the additional "up-front" costs typically associated with V&V are too high. They were convinced that applying V&V can lower development cost and have a positive impact on other aspects of the system other than just correctness (e.g., reduced maintenance costs).

Workshop Outline

The ESs V&V workshop was divided into three parts: Part 1, basic concepts, reviewed the concepts that

- Defined V&V

- Dispelled some common myths about artificial intelligence (AI) and software development
- Examined the differences between ES and conventional software
- Assessed the impact of these differences on the basic concepts of V&V

Part 2, techniques, examined a wide range of techniques developers could use to build more reliable systems. Most of these techniques were drawn from the study of conventional software development. For each technique, the method was described and an example shown. During the first part of each class, an example problem was discussed. Technique examples were drawn from solutions to this example problem. Part 3, guidelines, prescribed a complete set of "things to think about" when performing V&V on an ESs.

Basic Concepts

Part 1 of the ESs V&V workshop encouraged V&V for ESs by helping developers understand the underlying principles behind V&V. "Correctness" in software was examined and discussed within the framework of a puzzle. Demonstrating correctness involved examining many different facets of a system behind functionality. Facets (or pieces) were explored in order to gain a complete view of system correctness.

With a clear understanding of the many types of software correctness, focus shifted to the kinds of activities that must be performed to demonstrate correctness. These activities were called test phases. Three test phases were presented:

- Static testing
- Unit/integration testing
- System testing

Characteristics, inputs, and implications of each phase were discussed beginning with system testing.

After discussing software correctness and test phases, focus shifted toward understanding application of these concepts to ESs. This shift was where the obstacles in the application of V&V to ESs had occurred. These obstacles existed, to a great extent, because of many misconceptions regarding software in general and AI in particular. The workshop addressed many of the most common misconceptions that negatively influence developers concerning V&V. For example, some consider ESs to be fundamentally unreliable due to their heuristic nature. Even though reliability may be more difficult to prove given the heuristics, the ESs should still be

- Predictable
- At least as accurate as the heuristic
- Safe

Specific techniques were presented to support these notions.

Dispelling some common misconceptions regarding software development, the workshop focused on differences between ESs and a procedural program.

Developers learned about the differences in how systems are built (implementation differences) and the kinds of problems they solve (problem differences).

At this point, developers understood important V&V concepts. They also recognized differences between ESs and procedural systems and how those differences impacted V&V. This foundation allowed them to begin learning techniques, although they still needed to learn V&V planning. Survey results indicated the need for planning. For example, the fact that so many projects were either operational prototypes or did not follow a life-cycle model indicated that planning was a problem. If a project was poorly planned, then knowledge about V&V techniques and the theory behind V&V was of little value. For this reason, developers learned the importance planning, along with a specific planning approach, play in successful V&V.

Techniques

Part 1 established the basic building blocks necessary to understand and use V&V techniques. Part 2 taught the developer 47 different V&V techniques. Some of these 47 techniques were very specific (i.e., the technique implied a specific method), while others were more general (i.e., the technique implied a class of errors for which many different methods applied). For example, path coverage was a very specific technique that implied a specific approach and error detection capability. Stress testing, on the other hand, pointed to many possible methods demonstrating the system worked correctly under stress.

Guidelines

Part 3 examined implications to V&V resulting from key points from the previous parts. Developers learned an approach to V&V along with ways they could tailor the approach to fit the specific V&V needs of their project. Guidelines were high-level suggestions. One reason for this approach was that all projects were different. Dictating a specific approach with no allowable deviations was not only controversial, but extremely difficult to carry out. The guidelines provided a step-by-step approach addressing the following key activities:

- Project Management
- Problem Analysis
- Requirements Definition
- Design
- Technique Selection

Developers learned to use guidelines to find errors early and to perform "smarter" testing by matching the right technique to the right situation and system representation.

Key Points of the ESs V&V Workshop

The workshop provided a new, positive mindset which convinced the students to learn and to use the V&V techniques. To sell the need for ESs V&V, the workshop focused on several key points:

- V&V is part of the development process
- ESs are software
- ESs are different
- Find and correct errors as early as possible
- Requirements are needed for validation
- Good design helps verification

Results (What Was Achieved)

We have found that there is still significant outside demand for the workshop and have received many positive comments about the value of the material. However, it is still too early to detect the long-term impact of the class on current V&V practice. Activities are underway, however, to begin assessing this impact.

As with any successful job, however, there is always room for improvement. The remainder of this report will focus primarily on areas where the workshop can be improved. These areas of improvement have been derived from informal discussions with the students, student evaluations, and instructor observations. However, before discussing specific recommendations, we feel it is important to discuss the profile of students that attended the workshop. Their jobs and perspectives on software testing certainly impacted the success of the workshop.

Conclusion and Future Directions

In summary, a lot of work needs to be done if the state of the practice in ESs V&V is to be improved. The ESs V&V Workshop is just one small step in that direction. Right now, it is still too early to tell what the impact on the state of the practice within the NASA environment will be. Clearly there have been some positive results (many projects leads that attended the

class indicated they would be applying the workshop concepts immediately), however, there is still room for more success.

Based on the instructors' observations and comments from students, future work in improving the state of the practice in V&V of ESs will include the following: First, we will be identifying specific projects within NASA that we can work with directly (as consultants) to apply V&V to the project. One drawback to just teaching a workshop is that the student alone bears the responsibility for applying what they have learned. We feel this leaves too much to chance. Working directly with students on their project removes this uncertainty and can yield a more positive impact. Next, we will be expanding the workshop to include other topics that are a little less understood but that are starting to get some attention. In particular, we will begin to focus on V&V of object-oriented systems and V&V of ESs that use techniques such as fuzzy logic, probabilistic reasoning, etc. Finally, we will modify the workshop to teach an entire development methodology (e.g., clean room) and focus on learning fewer techniques in greater detail. This should help students close the loop on the V&V overview they received in the first workshop.

References

French, S., Hamilton, D., and Culbert, C., "An Approach to Improve the State of Practice in Verification and Validation of Expert Systems." Presented at the Knowledge-Based System Verification, Validation and Testing Workshop at the 10th National Conference of Artificial Intelligence of the American Association of Artificial Intelligence (AAA1-92).

Acknowledgments

The workshop is the result of the efforts of Chris Culbert and Bebe Ly of the Software Technology Branch at JSC, and David Hamilton and Scott French of the Federal Sector Corporation of IBM in Houston.

NETS: A Tool for the Development and Delivery of Neural Networks

Robert Shelton
Johnson Space Center/PT4

Abstract

The network execution and training simulator (NETS) is a software tool that provides an environment for the development and evaluation of neural networks. NETS was written by the Software Technology Branch at JSC. With NETS you can create and execute arbitrary configurations of neural networks which use the "back propagation" learning technique. NETS is portable and will run on a variety of machines from desktop hardware to supercomputers. NETS, version 3.0, is currently available and is free to NASA and its contractors for use on NASA projects. NETS can be obtained by calling the Software Technology Branch help desk between the hours of 9:00 a.m. and 4:00 p.m. (CST) Monday through Friday at (713) 280-2233. NASA contractors should have their contract monitor call the help desk to obtain NETS. Others may purchase NETS, including all documentation, from COSMIC at a nominal fee for unlimited copies with no royalties. A brief introduction to neural networks along with a description of the history, purpose, applications, and features of the NETS software package are included.

Introduction

The concept of a neural network was originally conceived as an attempt to capture aspects of the behavior of a biological nervous system with electronic circuits. Early work beginning in the 1940s¹ identified the critical concept of the artificial neuron. Establishing such a concept essentially amounts to making the crucial decisions that determine which of the multitude of features of a biological nerve cell will be retained in the artificial neuron.

With the advent of high-speed digital computers in the 1960s, the emphasis shifted from electronic implementations to computer models. At this time, research interest focused on a special neural network model known as the single-layer perceptron.² Apparently researchers of that era failed to note the similarities between simple perceptron models and standard fitting techniques such as linear regression. These oversights were noted by a pioneering researcher in artificial intelligence, Marvin Minsky, in his book *Perceptrons*.³ Minsky's argument showed that a single-layer perceptron was theoretically equivalent to a linear separation scheme, i.e., could solve only those classification problems for which the class boundaries are hyperplanes. A simple and now famous example of a problem which cannot be

solved by a single-layer perceptron is the exclusive or XOR problem where the desired output is the exclusive or ORE, or the modulo 2 sum of the inputs. Since there were well known techniques for determining optimal hyperplane separation boundaries, Minsky's book relegated neural networks of the time, i.e. the single-layer perceptron, to a historical footnote. It was only with the rediscovery of the gradient learning rule for multilayer perceptrons⁴ that interest returned to the field. The NETS software is an implementation of the Rummelhart-Werbos gradient descent learning algorithm for multilayer perceptrons.

Unlike their single-layer counterparts, a multilayer perceptron of the type shown in figure 1 can approximate almost any continuous function. It is this task of approximation of nonlinear functions or curve fitting that is the crucial capability offered by multilayer perceptrons, also known as back-propagation neural networks.

Given the many classical methods for curve fitting with well known properties and efficient computer implementations, it is natural to wonder why back-propagation networks of the type implemented by the NETS software are needed. The answer to this question lies in the well known limitations of the classical methods. Standard statistical methods for function estimation require sufficient data to adequately sample the domain space of the function which is to be approximated. If the domain space is low-dimensional, e.g., 1-dimensional, as in the case of a simple plane curve, then a sample of the input or domain space sufficient enough to ensure an accurate estimate of the distribution can easily be taken. Methods such as cubic splines can readily provide high-fidelity approximations of a function of a single scalar variable given a table of sample values for the function which is to be approximated. If, on the other hand, the desired function depends on even a modest number of parameters—say 10—it would never be possible to provide enough samples to accurately estimate the function by means of traditional statistical techniques.

Every known approach to the problem of estimating functions of several variables rely on variants of a single strategy, namely to represent the function or its input space, or both, in a simple form. The feature that distinguishes neural networks from other methods is that no fixed, simplified representation is assumed. Rather, the internal representation is allowed to evolve from the data. It is this key adaptive property of the back-propagation neural network which provides the capability to learn to approximate a function rather than requiring a

programmer to anticipate all models needed to perform the desired mapping.

Problem Statement/Description

The problem that NETS solves can be simply stated as follows. Suppose that there is some process which produces an output based on an input, and that both the input and output of this process can be described numerically, i.e., as an input vector

$X = \langle x_1, \dots, x_m \rangle$ and an output vector,
 $Y = \langle y_1, \dots, y_n \rangle$, where x_i and y_j are real numbers.

As an example, think of the components of the vector X as being rainfall totals and spillway flow rates at various locations in a river-lake system, and the components of the vector Y as being water levels at locations of interest. A hydrologist might well be able to predict the vector Y corresponding to an input vector X , provided that the characteristics of the terrain were known and that enough locations were monitored for the input vector X to have predictive value for Y . Even so, experienced hydrologists faced with this prediction problem would most certainly look at historical records, at least as a verification of their theoretical estimate of Y . Now suppose that we do not have a hydrologist, but do have a wealth of historical data for the watershed. We could then assemble a table of input/output pairs of the form X_i, Y_i where X_i and Y_i are samples of input vectors X and output vectors Y of the process. The problem is to find an approximation $Y(X)$ based on the historical examples. If such an approximation could be found, then given a new set of data X^{new} corresponding to an observed weather event, a resulting set of river levels Y^{new} could be predicted.

As valuable as such a prediction tool might be in its own right, consider the implications of the neural network approximation $Y(X)$ that is given in terms of equations which are themselves amenable to manipulation by numerical methods. In particular, suppose that the portion of the X vector corresponding to rainfall totals is known, as is an acceptable set of river levels, Y . The equations in the approximation $Y(X)$ could then be solved to fill in optimal spill rates which would produce the desired vector Y . The above scenarios correspond to the companion tasks of system identification and control which are central to applications of great interest.

Another important use of neural networks is as trainable classifiers. Classification applications are usually implemented by passing raw sensor data through various transformations designed to suppress variation within a given class and enhance class discrimination. Such transformations would also normally extract a vector X corresponding to an observation of an object. This vector, sometimes known as a feature vector, would be the input to the neural network. The output Y would then be some vector indicating the class corresponding to

the input X . A standard way of producing such a vector for a problem having n possible classes is to set the vector

$$Y = \langle y_1, \dots, y_n \rangle = \langle 0, 0, \dots, 1, 0, \dots, 0 \rangle$$

where the position of the 1 in the Y vector corresponds to the class of the object which is observed.

Applications of the kind described here have driven research in neural networks for years, but until recently, neural network exploration was impeded by the requirement for special hardware and/or software to implement the network algorithm. One of the main selling points for neural networks over conventional solutions was that the same algorithm is applicable to many different applications. A need was thus perceived to produce a generic package to implement the back-propagation neural network algorithm. The requirements for the package can be summarized as

- **Portability:** The software should run on the widest possible range of computer systems. There should be no special hardware required, but the code should be capable of taking advantage of any commonly available resource such as math coprocessors.
- **Simplicity:** The software should be easy to install and use. It should not be assumed that users will have any initial knowledge of neural networks. The code should facilitate entry, exploration, and application.
- **Examples:** Since most users would be unfamiliar with neural networks, the package should include examples and tutorial material.
- **Delivery:** In order to close out the cycle of research, development, and application, it is necessary to support the delivery of a trained network module which could easily be imbedded in the user's application.

The NETS Software

The network execution and training simulator (NETS) is a software tool that provides an environment for the development and evaluation of neural networks. NETS was written by the Software Technology Branch at JSC. With NETS you can create and execute arbitrary configurations of neural networks which use the back propagation learning technique. NETS is portable and will run on a variety of machines from desktop hardware to supercomputers. Some of the features of NETS are

- **Learning Method:** NETS uses the back propagation learning method for all of the networks which it creates.
- **Macintosh Graphical User Interface (GUI):** NETS 3.0 now offers a Macintosh GUI option along with the original Command Line Interface (CLI) version.
- **Example Networks:** NETS 3.0 comes with three sample network specification files and three I/O files containing training data. One of these is the original XOR problem. The other two are more advanced applications which are accompanied with tutorial material in the new user's guide. There are also executable programs for generating virtually unlimited

amounts of additional training or test data for the two advanced applications.

- **Delivery Capability:** Once a network has been debugged to your satisfaction, NETS can produce portable C source code which implements the network. This code can then be incorporated into other software systems.
- **Portability:** NETS is written in the C programming language and can be executed on a variety of machines with no code changes. To date, NETS has been implemented on a variety of machines including IBM personal computers, Apple Macintosh, VAX, Sun, HP 9000, and CRAY.
- **Scaling Option:** NETS 3.0 allows you to scale training and/or test data. You may scale inputs, outputs or both.
- **Quick Test Capability:** You can now perform a quick check of your network's performance on a test set from the main menu.
- **Dribble Facility:** NETS provides features for saving weight values, errors, and test cases of a network to files at any time before, during, or after the training of the network. This feature is extremely useful for debugging network structures.
- **Memory:** The memory requirements for NETS are only 4 bytes per node and 4 bytes per connection.
- **Multiple Formats:** NETS contains facilities for operating in either floating point or scaled integer format. The floating point format provides greater accuracy, while the scaled integer format allows for greater execution speeds on platforms without floating point coprocessors.
- **Multiple Executable Versions:** The Macintosh version of NETS is distributed with four compiled NETS applications—scaled integer (CLI and GUI) and 68020-6881 (CLI and GUI). The MS DOS version is distributed with executables compiled for floating point and scaled integer operation.
- **Source Code:** NETS comes complete with all source code.
- **Documentation:** A full description of the features of NETS is provided by the NETS User's Guide. There is a supplement describing the new Macintosh GUI.
- **Availability:** NETS version 3.0 is currently available and is free to NASA and its contractors for use on NASA projects. It can be obtained by calling the Software Technology Branch help desk between the hours of 9:00 a.m. and 4:00 p.m. (CST) Monday through Friday at (713) 280-2233. NASA contractors should have their contract monitor call the help desk to obtain NETS. Others may purchase NETS, including all documentation, from COSMIC at a nominal fee for unlimited copies with no royalties. An electronic bulletin board containing information regarding NETS can be reached 24 hours a day at (713) 280-3896 or (713) 280-3892. Communications information is 300, 1200, or 2400 baud, no parity, 8 data bits, and 1 stop bit.

Applications

The NETS software has been extremely popular with a total user community numbering over 1,000. NETS is in use at all the NASA centers, all branches of the military, at many universities and throughout the private sector. The most popular applications generally involve pattern matching, system identification, and signal processing. The following are a few examples of those applications which have come to the attention of STB through our help line.

- **Pattern Identification** - The Army (Rock Island Arsenal) is using NETS to examine radiograms of munitions to scan for defects.
- **Signal Processing** - Research at the Colorado School of Mines uses NETS to determine the arrival time of special wave forms in seismic data.
- **System Identification** - In work at NASA Lewis Research Center, NETS is used to predict optimal parameters for Space Station design.

Current and Proposed Research

The research agenda can be described in terms of two prime objectives:

- to find applications of the new function estimation capabilities offered by neural networks
- to gain an understanding of how neural networks build internal representations so that other methods can benefit from such a capability

The best examples of the first objective are the research initiatives in neural control. The STB has been acknowledged as a leader in this critical area as evidenced by the recognition of D. G. Roger's paper, "SPLINES: A Hybrid of Friedman's Multivariate Adaptive Regression Splines (MARS) Algorithm with Holland's Genetic Algorithm," as best paper at the Auburn workshop on neural networks (February 92). This paper describes the implementation of an intelligent adaptive controller which learns how to back a two-wheeled trailer along a trajectory generated by a simple, rule-based system. The integration of the neural network into a rule-based system results in a hybrid system displaying the most desirable aspects of both methods. The hybrid system, uses networks and rule bases which are orders of magnitude simpler than those which would be required if the problem were to be solved with only a network or with only a rule-based controller.

The second objective is being addressed with research such as that being carried out at Ames Research Center by R. O. Shelton and J. K. Peterson, and with ongoing research in the STB which integrates local linear discriminant-based decision trees with back-propagation neural networks. Again, the objective is to understand the factors which provide the adaptive capability offered by the neural network so that other methods can be made to learn.

References

- ¹McCulloch, W. S., and Pitts, W., "A Logical Calculus of the Ideas Immanent in Nervous Activity," *Bulletin of Mathematical Biophysics*, Vol. 5, 1948, pp. 115-133.
- ²Rosenblatt, F., *Principles of Neurodynamics*, New York, Spartan, 1962.
- ³Minsky, M., and Papert, S., *Perceptrons*, Cambridge, MA, MIT Press, 1969.
- ⁴Rumellart, McClelland, and the PDP Research Group, "Parallel Distributed Process," *Learning Internal Representations by Error Propagation*, Vol. 1, Chapter 8.
- ⁵Rogers, D. G., "SPLINES: A Hybrid of Friedman's Multivariate Adaptive Regression Splines (MARS) Algorithm with Holland's Genetic Algorithm." To appear in the Proceedings of Neural Information Processing Society (NIPS) 92, Research Institute for Advanced Computer Science, 1992.

⁶Shelton, R. O., and Peterson, J. K., "Controlling a Truck with an Adaptive Critic CMAC Design," *Proceedings from the Workshop on Neural Networks*, 1992.

Acknowledgments

The NETS software was originally written by Paul T. Baffes while he was working for the Artificial Intelligence Section at JSC. Baffes is now pursuing a doctoral degree in Computer Science at the University of Texas in Austin, Texas. Following his original work, NETS has benefited from the talents of many authors, most notably Mr. Todd Phillips, Systems Development Branch, JSC, who authored the MacIntosh graphical user interface.

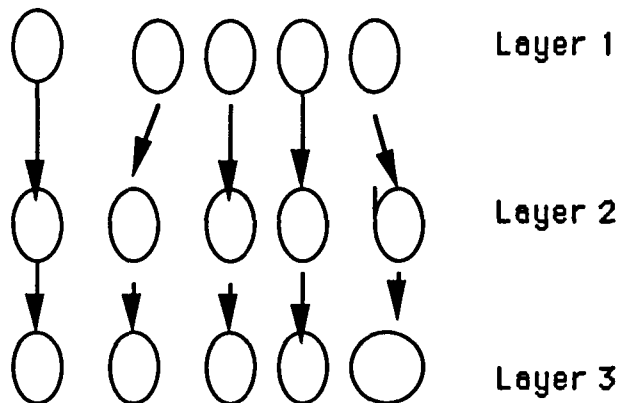


Figure 1. Multilayer Perceptron.

NASA Electronic Library System

NELS 2.0

Mark E. Rorvig
John on Space Center/PT4

Abstract

This paper discusses NASA Electronic Library System (NELS) 2.0, a general system for enterprise-wide information management. The present main features of this system are

- the ability to search, retrieve, print, and copy text, image, or sound objects,
- the provision of a natural language search interface that ranks retrieved objects by their relevance to a query,
- the support for communications between libraries on other computer systems through the Wide Area Information Server (WAIS) using the Z39.50 Protocol for information retrieval,
- loads structured data about objects (metadata) and source files of full text objects for searching,
- a layered architecture for quick replacement of graphical user front ends and data base schemas, and
- interface links for X Windows, Microsoft Windows, ASCII and Macintosh.

Introduction and Problem Statement

The general assumption since the mid 1970s is that information retrieval (I-R) is about the problem of specialists attempting to keep abreast of or review specialty literature. Indeed, since the classic studies of Project INTREX, this assumption has tended to dominate the practice of I-R and has resulted in an ever greater number of publicly available data bases in an ever greater number of specialties, each in turn awash with its own terminology, special features, and idiosyncrasies. The counter notion, that I-R might be about the problem of nonspecialists, attempting to answer cross-disciplinary, multidomain questions is far less frequently considered in the construction and use of commercial systems.

But this state of affairs has not always been the case. Indeed, the images of potentiality set forth early in the development of I-R presumed a system for general users which included documents, sounds, and images in basic system design and never assumed that specialist assistance would be required for information access. Instead, over time, the commercial world focused on retrieval methods, in particular retrieval by Boolean intersection, that precluded general user access. Of interest on this point is a historical note by Cyril Cleverdon published in 1987. In his note, Cleverdon asserts that Boolean searching of documents became the focus of the field by unplanned accident and characterizes present systems as "user hostile." Additionally, these

systems were constructed on mainframe devices, requiring high maintenance costs and high marginal costs for system expansion.

Approach/Method

One of the primary objectives of the NELS project is to allow a user to retrieve personal, corporate, and wide area information through one easy-to-use interface. For example, instead of using Lotus Magellan™ for personal information, Verity Topic™ for corporate data, and Mead Data Dialog™ for published text, one application can access all three categories of information. The user is not required to become familiar with several entirely different systems. In addition, since the interface consolidates data from many different sources, they can be manipulated effortlessly, virtually without regard to their origins. In NELS 2.0, therefore, Wide Area Information Server (WAIS), as supported by a consortium of companies and the National Science Foundation, is used as a replacement for Oracle, a costly commercial product.

The prototype WAIS system as incorporated into NELS 2.0 takes advantage of current state-of-the-art technology, and presents solutions to all of the above problems. The system is composed of three separate parts: clients, servers, and the protocol which connects them. The client is the user interface; the server does the indexing and retrieval of documents; and the protocol is used to transmit the queries and responses. The client and server are isolated from each other through the protocol. Any client capable of translating a user's request into the standard protocol can be used in the system. Likewise, any server capable of answering a request encoded in the protocol can be used. To promote the development of both clients and servers, the protocol specification is public, as is its initial implementation.

On the client side, questions are formulated as English language questions. The client application then translates the query into the WAIS protocol and transmits it over a network to a server. The server receives the transmission, translates the received packet into its own query language, and searches for documents satisfying the query. The list of relevant documents are then encoded in the protocol and transmitted back to the client. The client decodes the response and displays the results. The documents can then be retrieved from the server. Figure 1 displays these concepts.

WAIS alone, however, is merely one of the building blocks for the total NELS 2.0 system. The complete system is composed of two interfaces, a session manager

to manage the transfer of information from WAIS to the interface, a data manager to provide an SQL access protocol to WAIS, WAIS itself, the protocol, Z39.50 for communication among servers and networks, and, finally, the UNIX operating system resting on physical network protocols. Figure 2 displays these system layers.

Results

This task will improve the operational capabilities of JSC through cost savings in the printing, distribution, filing, and storage of paper documents. GM savings alone would be approximately \$350K annually, which is estimated simply by dividing the total number of pages (4.5 million) of documents by \$25 per 100 printed pages (\$1.125 million) and multiplying that figure by 30%. Actual savings might be higher. Assuming that other directorates and offices could save only \$100K per year, cost savings centerwide of \$1,000,000 annually are likely. These estimates are conservative.

Additionally, considerable interest has been expressed by other NASA and defense agencies in WAIS technology. For example, on December 21, 1992, a video teleconference of the Space Technology Interdependency Group (STIG) was held to investigate the use of WAIS technology to provide access to electronic data on space technology. STIG participants include NASA centers, Air Force, Defense Advanced Research Projects, Defense Technical Information Center (DTIC), Jet Propulsion Laboratory (JPL), and various contractors.

The meeting at JSC was attended by Terry Spencer, Tamara Bosque and James Whittington from the New Initiatives Office, Capt. Terrell Scroggins from the Armstrong Lab at Brooks AFB in San Antonio, and Dick Ramsell, who attended part of the afternoon session. Video link attendees included participants from Lewis, Ames, Jet Propulsion Laboratory, Marshall, Kennedy Space Center, Goddard, and NASA Headquarters. Among the D.C. participants were representatives from NASA, DTIC, and the Army Space and Technology Research Office. The meeting was chaired by Stan Sadin, the technical manager of the Office of Advanced Concepts and Technology (OACT) at Headquarters.

The meeting was offered as a proof-of-concept demonstration and the objectives listed were to

- demonstrate WAIS technology
- spark interest in suppliers and users
- make the best use of current work
- develop system users

At this time, only JSC and Goddard Space Flight Center have integrated this technology into information management activities.

Conclusion and Future Directions

NELS exists in two versions. Version 1.2 was released in August 1992 and was specifically developed

for software reuse. It is the retrieval engine presently in use by MountainNet to support the ADANet software reuse program. Version 2.0 is a generalized version that will eventually replace the ADANet software and will also be used to support documentation efforts at JSC and other Centers as required. Version 2.0 is structured into three layers: GUI/AUI, a session manager, and a retrieval engine. The retrieval engine used in this version will be WAIS. The session manager will modify WAIS references to permit extensive browsing of collections. Internal field and element structures will conform to those of NASA's Center for Aerospace Information. Internal data representations will conform to Library of Congress MARC specifications.

Future plans emphasize the development of graphic objects, surface mapped to selections of drawings, documents, images, and voice recordings.

References

- ¹Rorvig, M. E., "Psychometric Measurement and Information Retrieval," *Annual Review of Information Science and Technology*, Vol. 23, 1988, pp. 157-189.
- ²Rorvig, M. E., "The Simple Scalability of Documents," *Journal of the American Society for Information Science*, Vol. 41, No. 8, 1990, pp. 590-598.
- ³Rorvig, M. E., "Intellectual Access to Graphic Records," (Issue Editor and Forward), *Library Trends*, Spring, Vol. 38, No. 4, 1990, pp. 639-836.
- ⁴Lincoln, B., "Wide Area Information Servers (WAIS) Bibliography," Thinking Machines Corp., 1010 El Camino Real, Suite 310, Menlo Park, CA, 94025.
- ⁵Z39.50-1992: Information Retrieval Service Definition and Protocol Specification for Library Applications," National Information Standards Organization (Z39), P.O. Box 1056, Bethesda, MD, 20817. Available from Document Center, Belmont, CA.

Acknowledgments

The author wishes to acknowledge the contributions of Mr. Kenneth Jenks of the Shuttle Programs Office for his interface design of NELS 2.0, Mr. Brewster Kahle of WAIS, Inc., for his helpful suggestions regarding WAIS itself and the philosophy of its use, and Mr. Gary Riley of the Software Technology Branch for his architectural design contributions to NELS 2.0. Finally, no work of this type could be completed without the outstanding engineering efforts of the contractor staff of the Software Technology Branch, which included Mr. L. D. Donnell, Mr. Dann Danley, Mr. Mark Hutchison, Mr. Terry McGregor, Ms. Stephanie Smith, Mr. Wesley White, and Mr. Marwan Yazbeck.

WAIS OVERVIEW

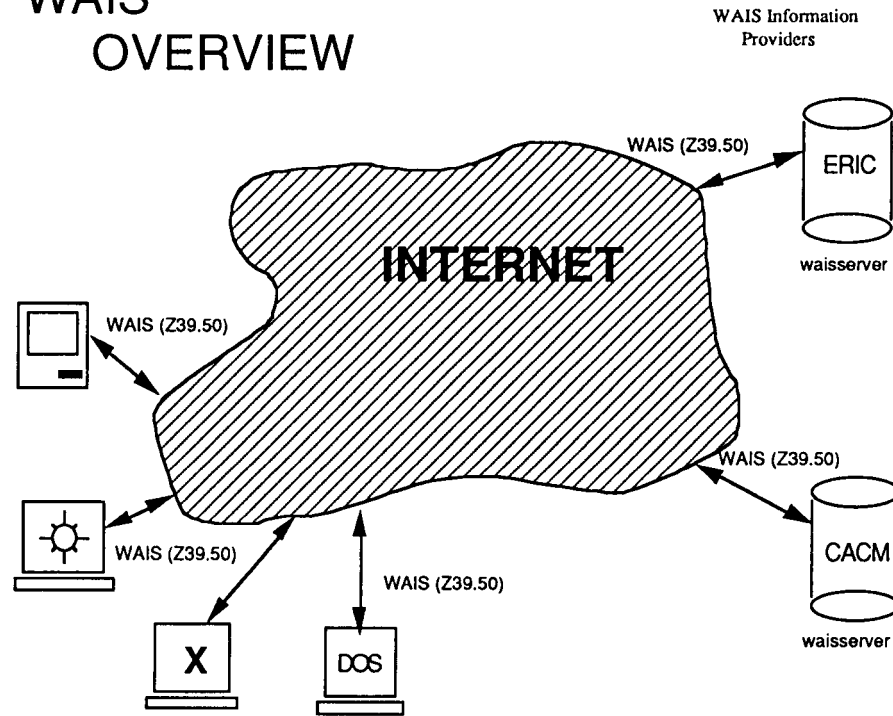
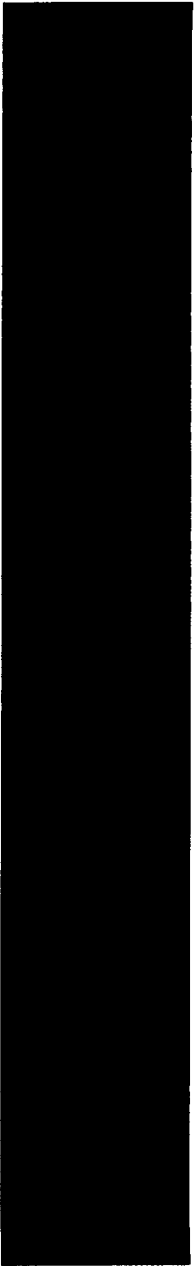


Figure 1. NASA Electronic Library System (NELS 2.0) WAIS Overview.

NELS 2.0 with ASCII Interface	NELS 2.0 with Motif Interface
ASCII Interface Library	Motif Interface Library
Session Manager	
Data Manager	
Structured Data System (Wide Area Information Server)	
Z39.50 Protocol	
Operating System (UNIX)	
NFS	N e t w o r k
XDR	
RPC	
TCP/UDP	
IP (Internetwork)	

Figure 2. NASA Electronic Library System (NELS 2.0) Architecture.



Mission
Operations



Optical and Photo Equipment Bracket for the Shuttle Starboard Overhead Window

Thomas Rathjen
Johnson Space Center/SP43

Abstract

Observing payloads, the Earth, and celestial objects through the windows of the Shuttle is an important part of every mission. Occasionally, steady and precise positioning of optical or photographic equipment is required. Therefore, Flight Crew Support Division (FCSD) developed a system which secures a variety of hardware to the structure at the Shuttle's starboard overhead window and that provides both coarse and fine two-axis pointing.

Introduction

In the past, equipment that needed to be secured at the overhead windows was clamped into existing provisions normally used for window shades. These clamps were not designed for this application and NASA became concerned that continuing to do this could damage the window glass. Therefore, Rockwell International was tasked to add interface provisions specifically designed for supporting observation hardware to the Shuttle fleet. However, hardware to attach optical and photographic equipment to these interface points was left for NASA to provide.

In the fall of 1991, Flight Crew Support Division was approached by the crew for STS-46. They planned to view the Tethered Satellite System (TSS) with a Celestron telescope as it was deployed 12.5 miles from the Shuttle; however, they needed hardware to mount the telescope in the window. In order that the device could be used for other applications on additional Shuttle missions, it had to be designed to accommodate several different telescopic lenses as well as the telescope.

Problem Statement

The hardware not only had to rigidly mount the telescope at the overhead window, it also needed to provide two-axis adjustment so the crew could track the TSS as the Orbiter "dead banded" (as the Shuttle orientation varied by +/- 5 deg about the x and y axes). Since viewing the TSS was the first application to require attaching hardware to the new Shuttle interfaces, a unique design was required. Funds for developing the hardware were limited, and designing a custom pointing system could be expensive. Therefore, a means of meeting the requirements at minimal costs had to be found. The hardware also had to be stowed for launch and landing.

The new interface points consisted of two threaded fasteners and two holes for pins. This design

accommodates dimensional tolerance differences between Shuttles; however, it presented problems in securing a bracket to these points rigidly. An undersized pin could potentially rattle in the holes, ruining observations.

A survey of the various telescope lenses optionally flown on Shuttle missions revealed a wide variety of sizes and mounting footprints. Accommodating the different lens lengths, while still allowing all lenses to be positioned close to the window surface, could not be accomplished with a single piece, static bracket. Furthermore, none of the equipment included positioning holes which could be used to firmly secure them to the bracket. Therefore, a clamping mechanism that could be used with all mounting footprints had to be designed.

Isolating the observation equipment from cabin light was also important. Fabric shrouds, which tie around lenses, are available for Shuttle missions, but they would not accommodate the large diameter telescope. Therefore, a new shroud had to be designed. Because the shroud would likely be the last thing installed during equipment setup, it had to be possible to install and remove it without disconnecting the interface attachments.

Approach

The FCSD's resulting hardware consisted of two major components: an interface frame and an adjustable bracket. The frame, which includes the light shroud, rigidly connects to the new Shuttle attach points. It is stowed in the Shuttle window shade bag for launch and landing. The bracket, which includes the pan and tilt features, is locker stowed for launch and landing. The bracket is easily attached to the frame via three captive thumb screws (fig. 1).

To provide fine, two axis adjustment, an off-the-shelf pan-and-tilt head was identified. If used as is, there would have been too much slop for the STS-46 application. It was easily modified, however, by machining parts to tighter tolerances. Although it provided more than the required +/- five degree range for the dead banding, it did not adjust enough to account for all planned positions of the TSS relative to the Orbiter. Therefore, coarse adjustment about the y-axis up to +/- 90 degrees was built into the bracket.

To eliminate the potential rattling of the pins in the loose interface holes, O-rings were added to the base of the interface pins. Upon installation in the window, as the pins are pushed into the holes, the O-rings are compressed between the interface frame and the Shuttle structure, ensuring a tight fit.

A coarse adjustment in the z-axis was added to allow for an adjustment to account for short and long lenses. Because of the significant length differences and the size limit on the bracket due to stowage requirements, two attach points for lenses were included. Figure 2 shows the resulting minimum and maximum lengths for the lens attach points to the window.

Clamping the telescope and lenses tightly to the bracket became a challenging design problem. Because none of the lenses included positioning holes, sliding clamps were designed that provide torsional support. These clamps slide against the sides of the mounting bases on the lenses, preventing them from rotating. High-friction surfaces between the clamps and the bracket prevent them from being forced aside if a rotational load were applied to a lens.

To solve the problem of providing a shroud that completely blocks cabin light, yet can be installed and removed without removing the interface frame, black Nomex fabric material with strategically placed stiffeners was used. While most of the shroud is flexible, the forward and aft end shade provisions, which are clamped in the Shuttle window, included aluminum bars. The inboard and outboard sides include Armelon stiffeners to provide some rigidity so the shroud will not float in front of the lenses or telescope. The open end of the shroud includes a Velcro pattern which matches the existing shrouds.

Results

The overhead window bracket system was used successfully on STS-46 during TSS activities. Since the

TSS could not be deployed to the desired 12.5 miles from the Shuttle, the telescope was not used for observation as planned. However, the crew did set the system up and verified that it performed as required. Figure 3 shows astronaut Jeff Hoffman installing the Celestron telescope in the bracket on STS-46. Two flight units were fabricated and will be available for future flights as the need arises.

Conclusions

The Flight Crew Support Division met the STS-46 crew's needs with the overhead window bracket system, and the design is versatile enough to support future missions as needs are defined. The experience on STS-46 confirmed that it does provide steady and precise positioning of optical or photographic equipment while secured to the new Shuttle interfaces. The next planned flight of the overhead window bracket system is STS-51.

References

¹Flight Equipment Configuration Control Board (CCB), Directive G2771.

Acknowledgments

The overhead window bracket hardware development was managed by Thomas Rathjen in the Flight Crew Support Division. Engineering and technical support were provided by Lockheed Engineering and Sciences Company.



Figure 1. Interface Frame With Bracket Attached.

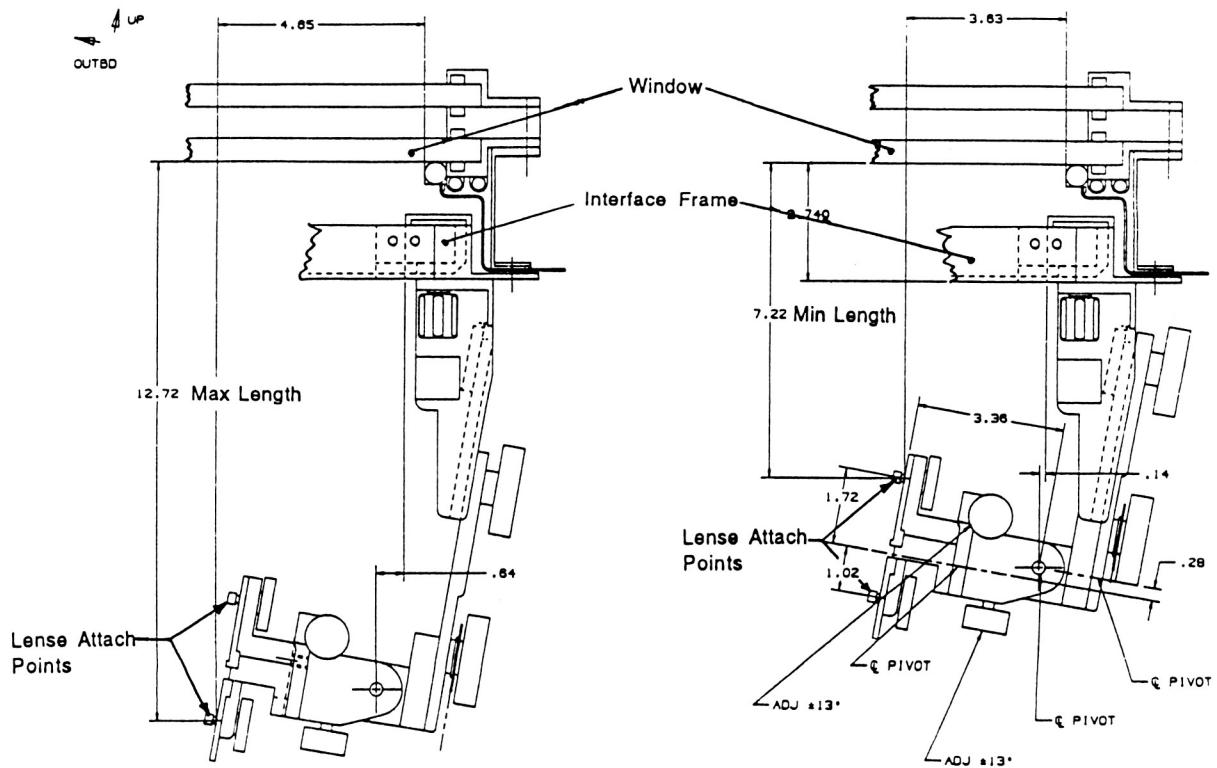


Figure 2. Maximum and Minimum Lengths for Lens Attach Points to Window.

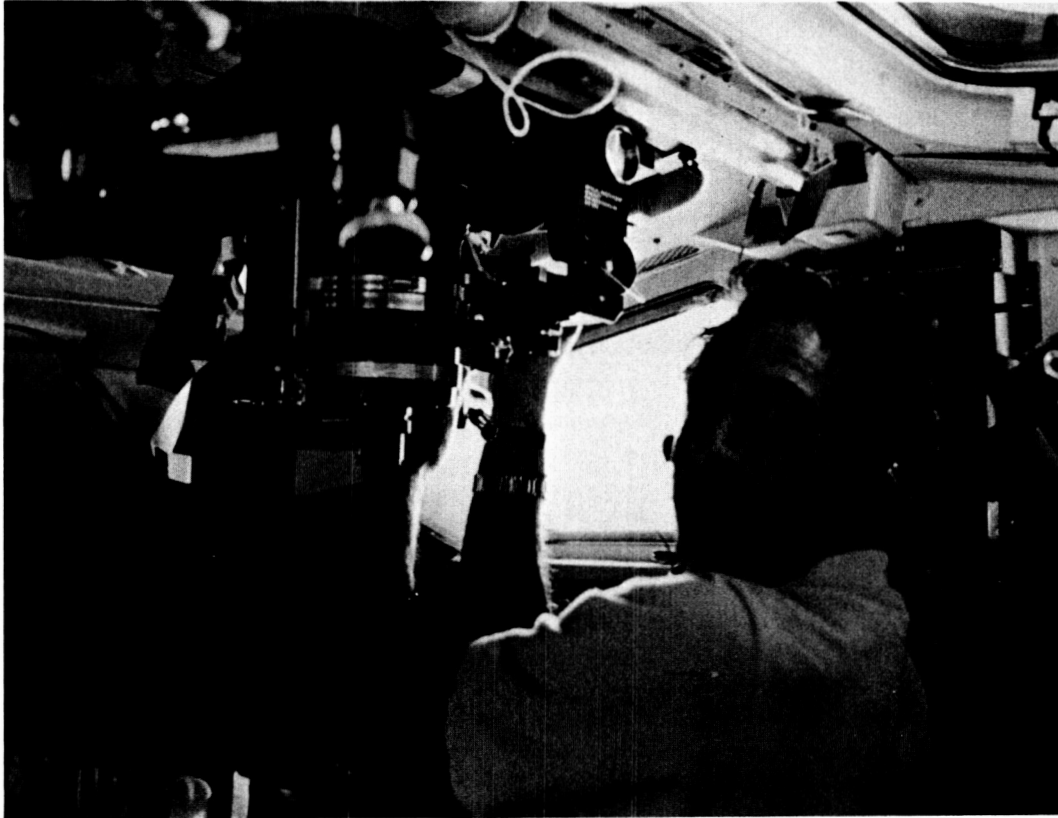


Figure 3. Overhead Window Bracket System Being Set Up on STS-46.

Shuttle Orbiter Repackaged Galley (SORG)

Thomas Rathjen
Johnson Space Center/SP43

Abstract

The new Shuttle Orbiter repackaged galley (SORG) developed by the Flight Crew Support Division (FCSD) at JSC began flying on all Space Transportation System (STS) missions in 1992. Although the weight and volume of the SORG were substantially reduced with respect to its predecessor, it provides the same food preparation capabilities for Shuttle crews. Several design deficiencies were also eliminated with the SORG, and the maintainability was improved.

Introduction

In late 1986, the backlog of experiments resulting from the STS-51L accident prompted plans to add additional payload carrying provisions to the Shuttle middeck. Because the existing galley utilized middeck volume inefficiently, and future Extended Duration Orbiter (EDO) missions would require optimized use of crew compartment space, it was a prime candidate to be replaced by these new payload provisions. The alternate food preparation hardware available required locker stowage volume and more crew time for meal preparation. Therefore, JSC's Space and Life Sciences Directorate and the Astronaut Office recommended developing a new, smaller galley which could be located in previously unused areas of the crew compartment. The resulting SORG Program was approved by the Shuttle Program Office in January 1989 as an in-house JSC project to be managed by the Flight Crew Support Division.

In addition to producing a smaller galley without sacrificing food preparation capabilities, several other goals became part of the SORG Program. In-flight anomalies and ground-test failures identified several design deficiencies with the existing galley. Solving these problems and improving the maintainability were important. Despite the problems, however, NASA had gained significant experience with the old galley and its interfaces with the food system and crew. Therefore, the SORG was to utilize existing components and designs where practical.

Description

The SORG had to provide a method to dispense both hot and cold water into all rehydratable food and beverage packages. An oven for heating rehydrated and shelf-stable foods was also required, and it had to accommodate

up to seven meals at a time. The Shuttle provides ambient and cold water only for the galley, so the SORG had to heat water and store it in a tank maintained at a temperature sufficient to provide hot dispenses on demand.

One of the more troublesome problems with the old galley was the inaccuracy of the dispensed water quantities. During several of the missions after return to flight, crews reported significant overdispenses. Although they could compensate for this by selecting lower quantities, it was difficult to predict the amount of overdispense. During later missions, several crews reported erratic and unpredictable dispensing. Eliminating this problem was a SORG Program priority.

The SORG design also had to solve the two electromagnetic interference (EMI) problems of the old galley. Radiated EMI did not meet Shuttle requirements, and a waiver was required for all flights of the old galley. Self-induced EMI transients also caused functional problems with the galley itself: operating the oven fans in certain modes could cause unwanted dispenses, and the cycling of the pumps and valves occasionally caused microprocessor lockup. Both situations required special crew procedures as workarounds.

Finally, a potential hazard with the hot water tank was left for the SORG Program to solve. Nominally, the galley or SORG is connected to the Shuttle's water system, which can accommodate the thermal expansion when water is heated. However, if a valve or quick disconnect failed closed, isolating the galley from the Shuttle's water system, then thermal expansion could have caused the galley tank to rupture. Again, this required special crew procedures to avoid the hazard, and the SORG Program had to eliminate it.

Approach

Several potential locations for the SORG in the middeck were identified and evaluated, and the area just forward of the old galley location (forward, port corner of the middeck) was chosen. Based on the volume available in that area, the functional requirements, and the desire to preserve experience with food and crew interfaces, the following parts were identified to be reused: the hot water tank, water heater coil, rehydration station, and electronic control box. All these components would require extensive modifications, however, to eliminate the problems discussed above.

All hardware requiring easy access during meal preparation (oven, rehydration station, controls, etc.) were

located in the main SORG package, just aft of the lockers on the port wall. The hot water tank was located just forward of that, in the previously unused volume between the lockers and the port wall (fig. 1). The weight and envelope of this packaging was calculated early in the Program based on preliminary designs. That information was communicated to Rockwell International, who could then make the necessary structural changes to the Shuttle fleet.

The FCSD discovered the primary reason for the dispense quantity problems for the old galley was differences between the actual water system of the Shuttle and the ground support equipment (GSE) water system used to calibrate the dispense times for the old galley. Dispense quantities were controlled by these times, assuming constant pressures. Although the static water pressure could be simulated by the GSE, the pressure drop during water flow was much greater than in the Shuttle. This resulted in longer dispense times than needed and overdispenses in flight. To resolve this, the GSE was changed so that it more closely approximated the Shuttle. However, because modifications to the Shuttle could change the performance of the water system, some of the adjustment capability was added to the SORG; pressure-compensating flow regulators were designed and fabricated in house at JSC and added to the SORG's ambient and cold water inlet lines (fig. 1). The pressure compensating feature helps keep quantities constant as the Shuttle's water pressure varies between 15.5 and 20 PSIG.

The erratic dispense quantities of the old galley were related to the EMI problems, as were the microprocessor lockups. To eliminate all EMI-related problems, the sources of the EMI noise were identified to be primarily the pumps and the microprocessor. These components were then completely enclosed in EMI sealed containers, and EMI filtered connectors were used. EMI sealed backshells were then used on all interconnecting cables inside and outside the SORG.

The improved electrical packaging also resulted in improved maintainability for the SORG. Because all electrical subassemblies are interconnected via cables and connectors, they can be removed and replaced without cutting wires or soldering. Many components can be removed and replaced without removing the SORG from the Shuttle.

To eliminate the potential hazard from the thermal expansion of water in the tank, a spring-loaded expansion cylinder was developed. An off-the-shelf accumulator could not be used because of the requirement to have no dead spaces in the potable water system where microorganisms could develop. The head of the piston in the cylinder has a machined groove through which water

flows during each hot water dispense. The piston remains at the top of the cylinder unless thermal expansion actually causes an over-pressure condition. In such a case, the piston would then move against a spring, opening a volume large enough to accommodate thermal expansion of the entire SORG hot water loop.

Results

The final SORG design occupies about half the volume of and weighs about 45 lb less than the old galley. EMI certification testing verified that EMI levels are within requirements, and none of the EMI-related erratic behavior of the old galley could be duplicated on the SORG. All food preparation capabilities were maintained, and by reusing key components from the old galley, crew training has been kept to a minimum.

To date, three flight SORG systems have been delivered and have flown on five Shuttle missions, including the longest mission ever, with no major in-flight problems. Samples taken on STS-50, as well as qualitative crew comments, indicate dispense quantities are within the allowed tolerance of +/- 10%. Crews have also commented favorably on the performance of the hot water tank and oven and on the performance of the water recirculation, which assures that the cold dispenses are cold and the hot dispenses are hot immediately on demand.

Conclusions

The FCSD must still provide a SORG for the Space Shuttle Atlantis in late 1993, as well as two spare flight units and a fourth trainer. Crew comments and the SORG's in-flight performance will continue to be monitored, and design improvements will be recommended and implemented if required.

References

- ¹Flight Equipment Configuration Control Board (CCB), Directive G2149.
- ²Program Requirements Document for the SORG, JSC-23595.

Acknowledgments

The SORG hardware development was managed by Thomas Rathjen in the Flight Crew Support Division. Engineering support was provided by Lockheed Engineering and Sciences Company. Fabrication was performed by the JSC Technical Services Division.

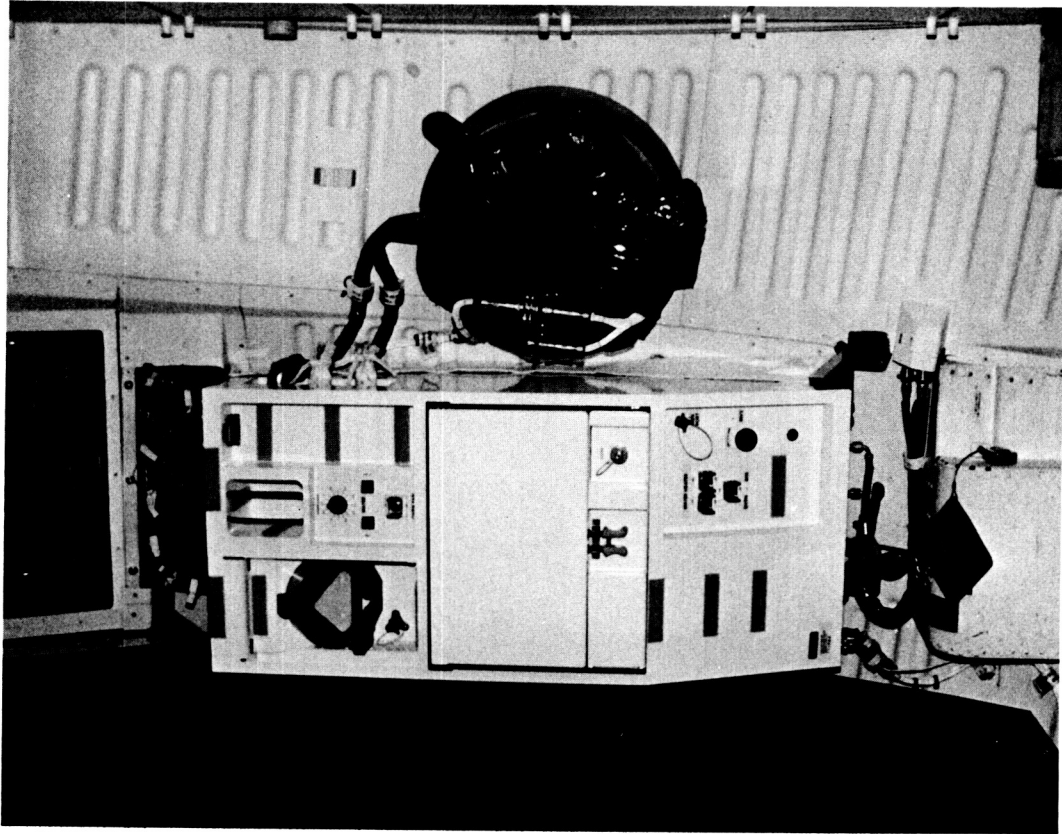


Figure 1. SORG Installed On Shuttle Middeck (Lockers Removed).

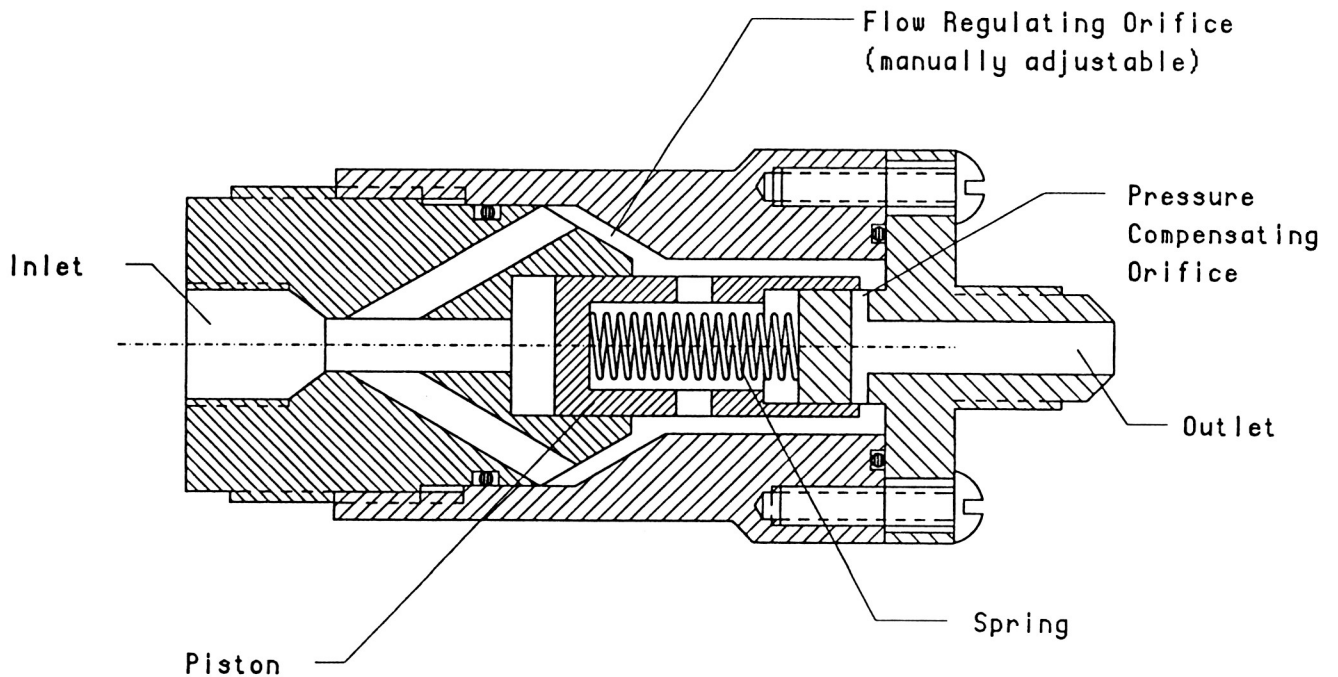


Figure 2. Cross Section of In-House-Designed Pressure-Compensating Flow Regulator.

Space Station Maintenance Studies Using Plaid Graphics

Mary Helm
Lockheed Engineering and Sciences Company

Abstract

The Graphics Analysis Facility (GRAF) has been used frequently to study extravehicular activity (EVA) maintenance scenarios on Space Station Freedom. The ability to use 3-dimensional visualization gives a more accurate estimate of the Space Station environment. Moreover, human EVA and robotic kinematics can be accurately simulated for volumetric reach and collision detection analysis. An animation was developed to study and discover problem areas involved with doing external Space Station maintenance tasks. It was discovered that items such as handholds and temporary restraint mechanisms should more effectively facilitate EVA movement about the Space Station structure for the suited personnel. Issues concerning the crew and equipment translation aid (CETA) cart configuration, portable work platform (PWP) stowage location, and locations of the EVA stowage of equipment and tools (ESE&T) boxes were also identified by use of the animation. There is also a strong desire to make EVA and robotics interfaces compatible on items such as replacement units and unpressurized logistics carriers. Graphics animation provides a mechanism to simultaneously analyze several mission parameters, and this has proved to be an effective method for mission evaluation.

Introduction

This animation was developed at the request of JSC personnel to provide an end-to-end scenario of Space Station EVA maintenance tasks. The mission timeline, along with the design for much of the EVA support equipment, was developed by McDonnell Douglas Work Package 2 (WP-2). The on-orbit retrievable units (ORUs) chosen for replacement were believed to represent worst cases for EVA worksite tasks and thus would identify the most issues.

Problem Statement

Maintenance tasks on the Space Station can be very complex because they involve several different worksites and the integration of numerous pieces of equipment. With this complexity, it is difficult to pinpoint the problems in the mission procedures or those in the hardware designs. Animating the maintenance procedures from end to end gives a visual of what is happening in the timeline and of how well all the components of the Space Station work together. In this

way, developing an animation for a complex task can aid in bringing out the problems in a task timeline and the inadequacies of hardware design.

Approach

The first step of the analysis involved refining the mission timeline to an acceptable level of detail that would best identify the issues of EVA maintenance without bogging down the animation with procedures common to all EVA tasks, primarily tethering and untethering.

Before the animation could be generated, many of the models had to be updated to the latest design to give an acceptable representation of the Space Station environment. Most of the EVA hardware and support equipment designs were new and had to be completely modeled. With the mission timeline and the Space Station models all updated, the animation could then be generated.

Results

The issues identified in this analysis were based both on the development phase of the animation and on the results of the end product.

It was found that many of the EVA support structures such as handholds and temporary restraint mechanisms were not effective in facilitating the EVA personnel about the Space Station structure. Many of the handholds were too far apart, and in some cases there were no handholds in the crewmember's vicinity.

The CETA cart configuration did not allow easy movement about the cart, and the top of it could not be reached while the crewmember was in the adjustable portable foot restraint (APFR). Handholds were added to the cart to facilitate the crewmember's tasks (fig. 1).

The stowage locations for the unpressurized logistics carrier (ULC), PWP, and ESE&T were not easily accessible, which caused very lengthy and sometimes difficult translations on the part of the EVA crewmember (fig. 2). The amount of time for worksite setup was nearly 50% of the total time of the animation, and much of that was spent acquiring EVA equipment from stowage and spare ORUs from the ULC.

In the area of EVA versus robotics, many of the worksite setup tasks such as acquiring the PWP from the mobile based servicer (MBS) could probably have been done via robotics before the EVA crew egressed from the airlock (fig. 3). This would make better use of the crew's

time on EVA by giving them more time to perform the tasks that can only be accomplished by a human.

Conclusions

In this analysis, several important issues were brought out. All of these issues had a negative effect on the efficiency with which an EVA crewmember can perform maintenance tasks. Many of the problems which involved EVA equipment design are now being targeted by various Space Station groups at JSC.

The CETA handrail and other handholds are being evaluated for EVA reach, and new requirements are being set to assure that all handholds are properly placed for EVA reach and safety.

The CETA cart configuration is now undergoing changes, and the GRAF lab is directly involved in this analysis. Several different configurations have been analyzed to see which design best integrates the EVA crewmember with the EVA equipment on board the CETA cart.

The GRAF lab is currently analyzing different locations and configurations for placement of the ULC during EVA maintenance missions. This analysis has the ULC placed on the MBS rather than at the port end of the Space Station structure.

Graphics animation provides a mechanism to analyze several mission parameters simultaneously (i.e., EVA reach, volumetric analysis, and task procedures and timelines) and thus has proven to be an effective method for mission evaluation. By utilizing this type of lab, designers and integrators can find hardware design problems as well as problems in the configuration of complex pieces of equipment.

References

Helm, M., "Space Station Maintenance Studies Using PLAID Graphics," *Proceedings of the 1992 Space Operations Application and Research Workshop*, August 1992.

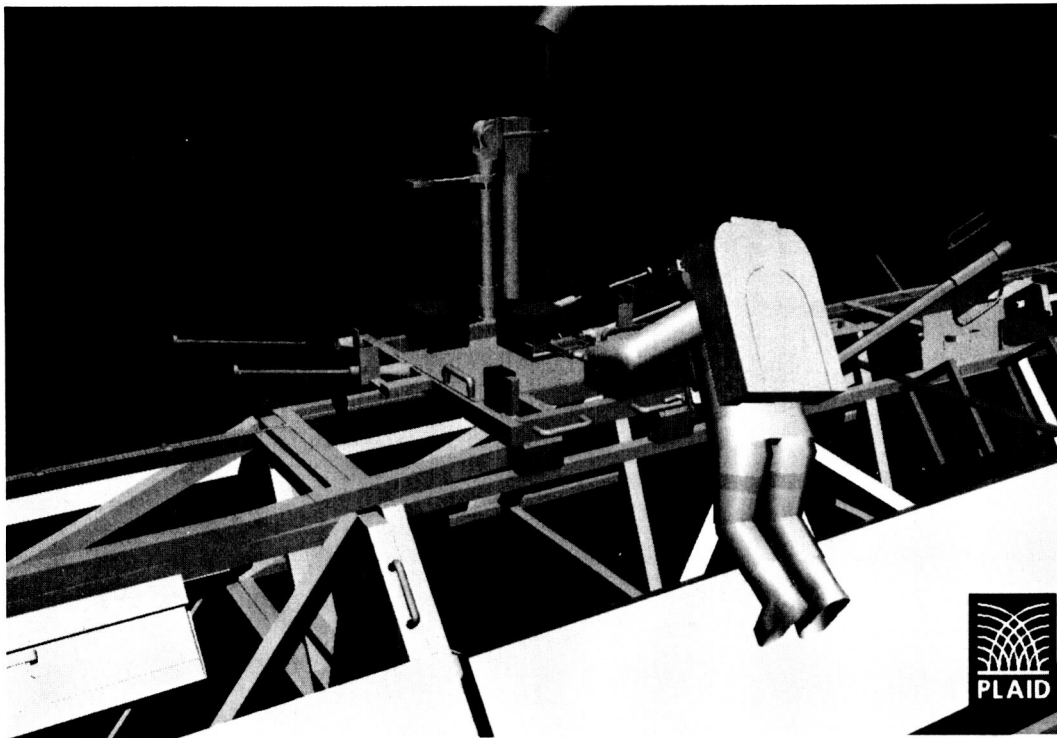


Figure 1. CETA Cart Configuration.

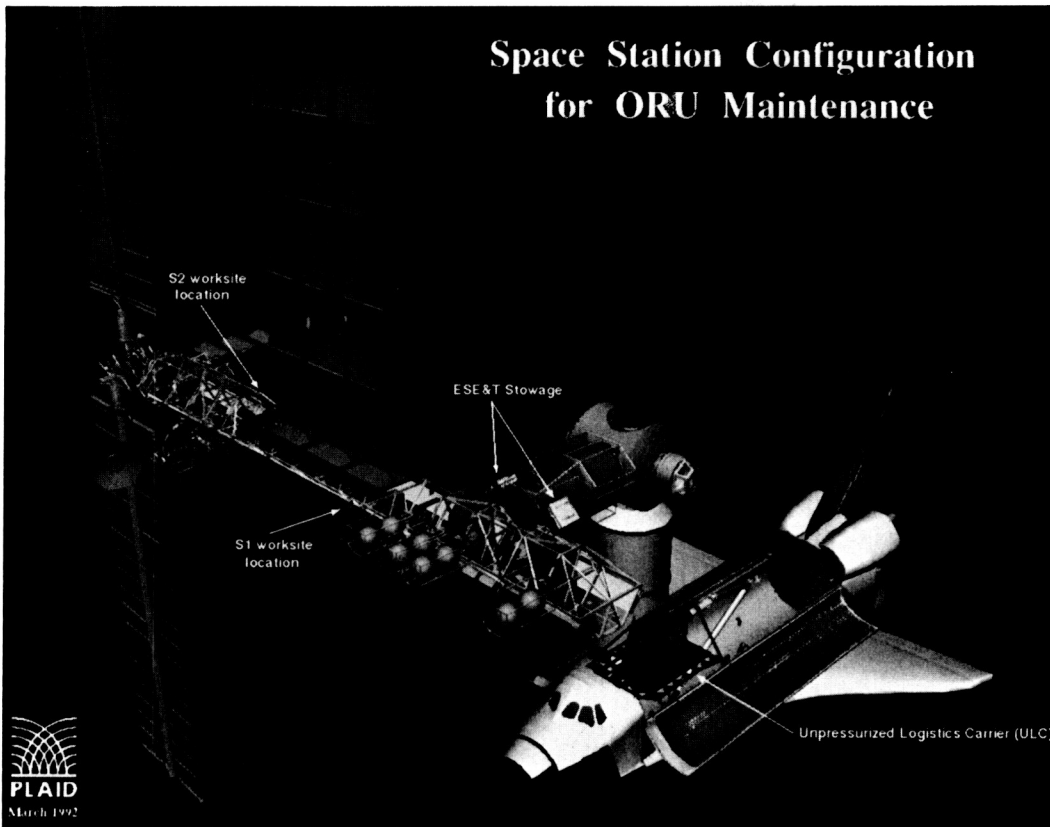


Figure 2. Locations of Stowage and Worksite Areas.

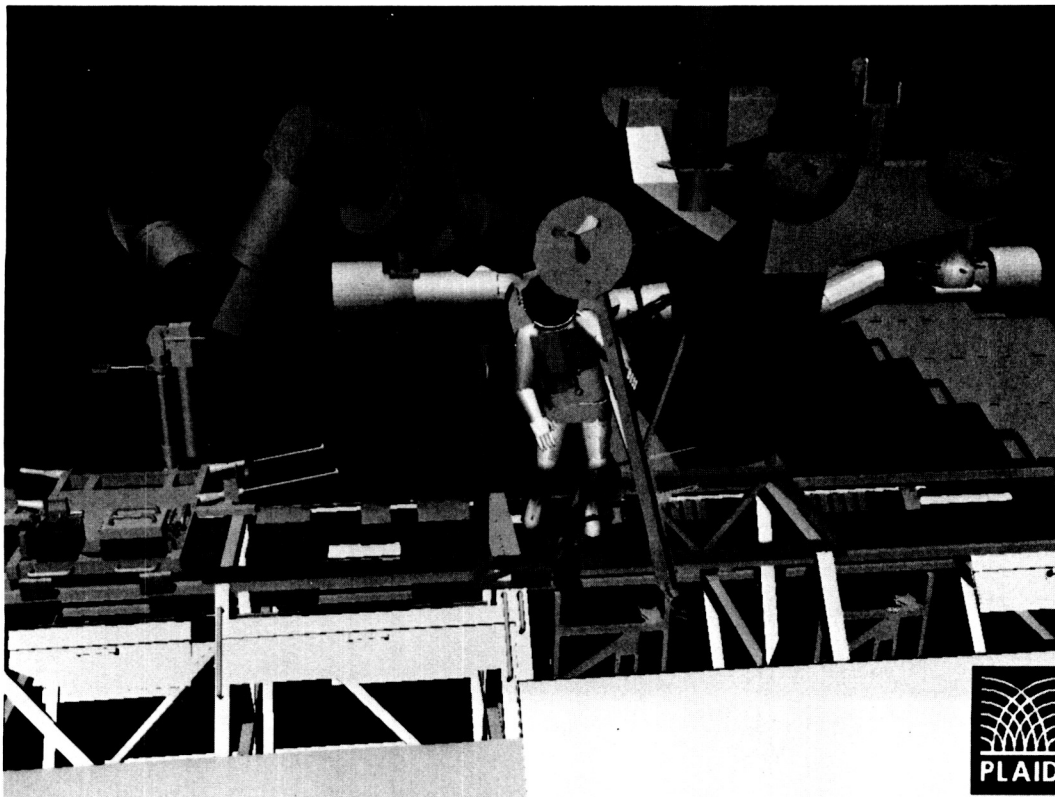
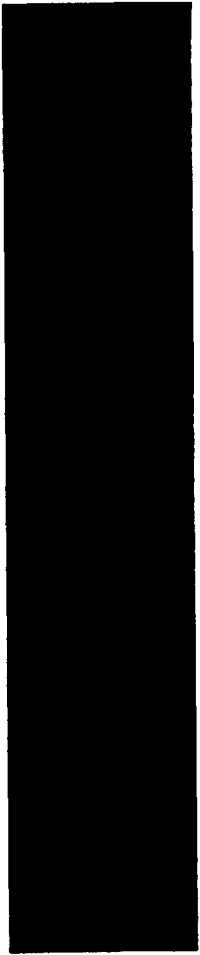


Figure 3. EVA Acquisition of the Portable Work Platform.



*Medical
and
Life
Sciences*



Image Analysis and Flow Cytometric Measurements of Urokinase In Metastatic Cancer Cells

Dennis R. Morrison, Howard Gratzner, Ph.D.,* Ruth L. Katz,** and M. Zouhair Atassi†
Johnson Space Center/SD5

*DNA Sciences, Inc.

**M.D. Anderson Cancer Center

†Baylor College of Medicine

Abstract

Tumor cells are characterized by abnormally high amounts of DNA within the nucleus, rapid proliferation, loss of attachment dependence and the lack of contact inhibition which is manifested as uncontrolled growth. At some point in the development of many cancers, certain tumor cells (metastatic cells) are directed to leave the primary tumor, invading adjacent tissues and migrating to a new metastatic site. These metastatic cells secrete proteolytic enzymes as a mechanism to dissolve the extracellular matrix between cells, enabling the tumor cell to migrate through normal tissues. Urokinase (uPA) is a key enzyme related to metastasis in cancers of the lung, colon, gastric, uterine, breast, brain, and malignant melanoma. Currently, urokinase is extracted from the tumor biopsies and measured as the ng/mg of total protein. The Johnson Space Center has developed microassays for urokinase produced by human cells in support of spaceflight experiments, including monoclonal antibodies that are specific for both active and inactive forms of the enzyme. This NASA technology has been combined with other cytological testing of tumor cells to identify aggressive tumor cells that are actively metastasizing. This technology utilization project has combined fluorescence microscopy, image analysis, and flow cytometry, using fluorescent dyes and urokinase-specific antibodies to measure uPA and abnormal DNA levels inside the cancer cells. Cytopathology and image analysis has shown that uPA is present in high levels in many breast cancer cells but not found in a normal breast. Significant amounts of uPA also have been measured in glioma cell lines cultured from human brain tumors. Comparisons of flow cytometry (FCM) and digital image cytometry (ICM) of fluorescent-labeled tumor cells have shown that ICM can provide measurements that have less variation than FCM and can measure uPA concentrations on the surface of the cells. Combining FCM and ICM has resulted in new analytical procedures that are suitable for rapid screening and more precise analytical measurements of cells that contain high levels of DNA and uPA. Commercial applications include new diagnostic tests for metastatic cells in different cancers, which are being developed with a company that provides a medical testing service which uses flow cytometry for DNA analysis and measurement of hormone receptors on tumor cells from

patient biopsies. If a significant number of tumor cells contains large amounts of uPA (especially membrane-bound), then the post-surgical chemotherapy or radiotherapy can be targeted for metastatic cells that have already left the primary tumor. A retrospective study of biopsy tissues from 500 node negative, stage I breast cancer patients is under way. This research also may provide the basis for developing a new therapeutic treatment against metastasis using chemotherapeutic drugs or radioisotopes conjugated to urokinase-specific monoclonal antibodies that only bind to metastatic cells.

Introduction

Malignant cells are characterized by abnormal levels of DNA, rapid proliferation, uncontrolled growth, and the ability to invade surrounding normal tissues. The measurement of biochemical markers on cancer cells can provide quantitative information about disease-free survival and time to relapse, thus providing the physician with valuable data for planning adjuvant therapy. Indirect immunoassays of markers extracted from biopsy tissues are important, but more precise measurements can be made by analytical cytometry. The current trend is toward microscopic analysis of the immunochemically stained tumor sections or dissociated cells, coupled with quantitation by image analysis. Specific markers can be directly associated with the cancer cells, as opposed to biochemical extraction procedures. Tumor markers currently assessed include those that measure cellular proliferation, the presence of specific onco-genes, tumor-suppressor molecules, and cancer-related proteins.¹⁻⁵

The tumor-related proteins include marker proteins (p53, Ki 67, etc.) that are over-expressed in tumor cells and proteolytic enzymes that are correlated with recurrent disease and metastasis. These enzymes are involved in a cascade of proteolytic interactions with other enzymes and inhibitors that allow the cancer cells to dissolve the surrounding extracellular matrix, thereby enabling the cells to invade adjacent tissues rapidly and migrate to metastatic sites quite distant from the primary tumor. Among these proteases are the plasminogen activators (PA), collagenase IV, laminase, and in some cases cathepsin D, which together mediate key steps in invasion process of metastasis.

Measurement of Abnormal Tumor Cell Proliferation

The DNA content in normal cells is a precise amount depending on the phases of the cell cycle. DNA can be measured by labeling with DNA-specific fluorescent dyes or DNA precursors (BrdU, IdU). Then, fluorescent-labeled antibodies, specific for the DNA precursor, can be used to identify and localize which cells are synthesizing DNA.¹ Fluorescent labeled cells then can be analyzed in a laser flow cytometer or fluorescent microscope. A histogram of DNA content in normal cells shows a single diploid peak (at G₁ phase) and a tetraploid peak (at G₂+M phase). However, in most biopsies the abnormal DNA content of tumor cells is detected as a second G₁ peak or multiple peaks. Abnormal DNA (DNA aneuploidy) is considered an independent indicator of tumor aggressiveness and poor prognosis that is used to supplement cytopathology grading of the tumor.

Flow cytometric measurement of the percentage of proliferating tumor cells that are involved in synthesizing DNA (S-phase cells) is also an independent indicator of malignancy. High percentages (15 -20%) of S-phase tumor cells usually indicate an aggressive malignancy and usually correlate well with abnormally high DNA content. The labeling index (LI) obtained by pulse-labeling cells with DNA precursors represents the rate at which DNA is being synthesized in tumor cells. Usually, a LI > 4% is associated with a higher probability of recurrent malignancy.² Antibodies against PCNA have been used as a measure of tumor cell proliferation.³ In tumors, high levels of PCNA usually are expressed in all cell phases of the proliferating cells. Pulse labeling with BrdU is used to label cells specifically in S phase.⁴

Enzymatic Mechanisms of Metastasis

Cancer cells must secrete proteolytic enzymes to dissolve the basement membranes and intracellular matrix between the densely packed normal cells to leave the primary tumor and migrate to a new metastatic site via the blood or lymphatic circulatory systems. Proteolytic enzymes such as cathepsin D, collagenase IV, and plasminogen activator enzymes have been linked with the invasion of tumor cells into adjacent normal tissues and with metastasis. Urokinase is not produced in most normal cells except for low levels in certain types of normal kidney cells, colon, gastric mucosa, macrophages, and endothelial cells lining small arteries. However, high levels of urokinase is produced in many tumors such as breast,^{8,9} lung,¹⁰ colon,¹¹ gastric mucosa,¹² uterine,¹³ bladder,¹⁴ prostate,¹⁵ and malignant melanoma.¹⁶

High levels of urokinase (>3.49 ng/mg of total protein) extracted from breast tumor tissues have recently been shown to be a good prognostic indicator for high risk of recurrence and shorter patient survival times.¹⁷ Primary lung and colon tumor cells also produce more uPA than metastatic cells, but different extraction assays

often give widely variable results.¹³ Total uPA measured from tumor tissue or secreted by cultured explants is difficult to quantitate, especially if the measurements are made on a large group of cells. The data obtained are an average value of all normal and cancer cells rather than a measurement of each individual cell. Few direct measurements of intracellular and extracellular urokinase have been made.^{10,18} Urokinase (uPA) can be present in the tissues in several molecular forms. The inactive proenzyme is a single-chain protein (scuPA) that is cleaved at Lys.158 to form the double chain, high molecular weight active form (HMW-uPA) that is 54 kDaltons. A low molecular weight form (LMW-uPA) can also be formed by cleavage of the HMW-uPA at Lys.135 - Lys.136 giving a 35 kD active enzyme. The active urokinase enzyme converts plasminogen into plasmin, which in turn dissolves intracellular fibrin matrix components as well as activates collagenases, laminases, and other related protease enzymes which are important to the anchorage and growth regulation of cells (fig. 1). Recently, it has been shown that the HMW active form of urokinase, bound to the tumor cell membrane, is responsible for the local lysis of the extracellular matrix, hence the tissue invasion mechanism for metastasis.¹⁰ Receptor (membrane) bound uPA is twice as efficient (catalytically) as free fluid-phase uPA.¹⁹ The unbound uPA and the LMW form is not responsible for most of the local dissolution of extracellular matrix in the immediate vicinity of the metastatic tumor cell. The presence of plasminogen activator inhibitors (PAI-1, PAI-2) also is correlated with a better prognosis and is inversely related to high levels of uPA (poor prognosis). PAI-1 binds to the active HMW-uPA, but not to the inactive scuPA.²⁰ Also, after PAI-1 binds to the membrane-bound active uPA, the complex is internalized into the cell and degraded.²¹

The complexity of the many interrelationships within the cascade of proteolytic activations makes it difficult to use an average value for the level of uPA produced by all of the cells in the tumor, especially since most of the normal cells do not produce uPA, nor do many of the tumor cells unless they are actively metastasizing. The challenge is to quantitatively measure uPA inside and on the surface of the cancer cells and then correlate those uPA levels with other specific markers to characterize the metastatic scenario for each tissue type and stage of cancer. No previous method has been developed to accurately measure the intracellular urokinase content, membrane-bound urokinase and cellular secretion levels and then correlate those urokinase levels with DNA content, DNA synthesis, hormone receptors, and other markers of aggressive tumor growth to determine the metastatic potential. Figure 2 illustrates the difference between the current assays for extracted urokinase and the new NASA method for precise measurements of urokinase contained within the cell or bound to the cell surface. This project has developed a quantitative diagnostic test for urokinase to be used first with existing

panels of cytological evaluations of breast cancer and brain tumors cells. Later, it will be applied to other types of cancer.

Quantitative Analysis of Individual Cells

Correlations of uPA with other markers require more precise knowledge about uPA and the multiple biochemical interactions that affect its proteolytic action. Figure 2 illustrates the current methods of measuring average levels from all tumor cells versus our method for measuring uPA directly in the cells. Our technology utilization project has used flow cytometry and image analysis of fluorescent microscopic images to measure urokinase and DNA in histopathology tissue sections of breast tumors, in dissociated cells (prepared in single cell suspensions) taken from tumor biopsies, and in several cell lines of malignant brain tumors (gliomas). Fresh cells are isolated from tumor tissue or cytological samples and prepared for antibody incubation in the same manner. Histology sections are prepared from frozen tissues or deparaffinized sections cut from previously embedded biopsies. The antibodies specific for urokinase are incubated with the cells or tissues first, then the cells are incubated with a second antibody having a fluorescent marker detectable by analytical cytometry techniques. DNA content and synthesis rate (based on DNA stains or uptake of DNA precursors) is measured by flow cytometry or image analysis. The same cell sample can be measured for DNA content and urokinase by staining of the DNA and labeling the urokinase with a fluorescent marker that emits at a wavelength different from that of the DNA dye or marker. Thus, both the DNA and urokinase can be measured simultaneously, using two-color image analysis or flow cytometry. Image analysis can localize and quantitate uPA in the cytoplasm and cell membrane. An advantage of the use of cell lines is the ability to study uPA expression in relation to cell proliferation and DNA replication. We also are conducting a retrospective study on biopsies from 500 Stage I, node negative, breast cancer patients in collaboration with the Ontario Oncology Working Group made up of researchers from three Canadian and three U.S. cancer centers.

Methods

The expression of uPA was studied during exponential growth, as well as in cultures that were placed on serum-free medium. Quantitation of uPA levels involves immunofluorescent staining with anti-uPA monoclonal antibody (#394, obtained from American Diagnostica, Greenwich, Connecticut) as the primary antibody using the indirect technique. The second antibody consisted of fluorescein-conjugated goat antimouse IgG for flow and image cytometry studies or, in some cases, rhodamine-labeled goat antimouse IgG for image cytometry. DNA labeling was performed using

propidium iodide or antibodies against bromodeoxyuridine following incorporation into DNA.

Digital image analysis was conducted using both Nikon and Zeiss fluorescence microscopes equipped with a high resolution video camera connected to a QuickCapture board (Data Translation, Inc.) for the Macintosh II Fx. The fluorescent filters in the Zeiss microscope were matched closely with the bandpass filters of the EPICS flow cytometer so image cytometry and flow cytometry data on cells from the same sample could be compared. Images were stored as TIFF files and later analyzed using NIH Image Version 1.4. Individual cells were scanned for mean optical densities and normalized for area. Relative fluorescence was compared after subtracting any background or autofluorescence measured from control cells on the same slide. Areas of concentrated uPA, within the cell and bound to the cell membrane, were further analyzed by density slicing and thresholding followed by particulate analysis of those specific areas.

Analysis of fluorescence by FCM was conducted with the 488 nm line of an argon laser of a EPICS Profile flow cytometer (Coulter Corporation, Hialeah, Florida). Green light from fluorescein emission was passed through a narrow bandpass interference filter (520 +/- 10nm), while red light from PI or rhodamine was passed through a 630 long pass filter. Bivariate, 64 x 64 channel histograms were obtained for analysis of mean fluorescence intensity. Data also were normalized for area and fluorescence intensity after the background was subtracted. This allowed comparisons among cells from the same samples and comparisons between cell lines and different samples. Statistical analysis of the data was performed by multivariate analysis using Statview 512 (Abacus Concepts, Inc.)

Results

Image Analysis of uPA

Each cell can be scanned to obtain optical density levels that can be compared among cells after normalizing with area of each cell measured. It is possible to measure the membrane-bound uPA by differential analysis using the mean density level of the weaker cytoplasm subtracted from that of the whole cell containing the membrane-bound enzyme. The zone size is defined as a number of pixels to be counted; then the relative amount of uPA in that particular density slice of fluorescence can be measured automatically by particle analysis. This data is expressed as the number of particles, average particles per group, area, perimeter of the cells, and location of particle groups larger than a defined size. The particle analysis method is efficient for the quantitative measure of membrane-bound uPA.

Brain tumors

Glioma cells that have been labeled with rhodamine-conjugated antibodies for uPA are shown in figures 3a and 3b. These tumor cells (CS line) contain large amounts of urokinase per cell, and there is considerable variation in total uPA from cell to cell. It is clear that the uPA concentration also is quite varied throughout the cytoplasm. Some cells exhibit "hot spots" of concentrated uPA, especially on the membrane. Specific areas of uPA can be measured by selecting a density slice(s) that represents the major portion of concentrated uPA (fig. 4) and conducting particle analysis using the density threshold that corresponds with the concentrated zones of uPA.

Breast Tumors

Evaluations of anti-uPA-labeled breast cancer sections reveal that normal breast tissue does not contain uPA except for some endothelial cells lining the arterioles. Intraductal carcinomas, however, do express measurable quantities of uPA using immunoperoxidase detection methods.²² Measurements of uPA by absorption of immunologic stains as light passes through tumor cells usually is recorded by the image analysis system as the mean optical density of groups of cells in the field of view. This is more difficult to quantitate, especially for individual cells, since light absorbed by the histopathology counterstains adds to the absorption of the uPA antibody labels. Measurements of fluorescence is a better quantitative method since the light is emitted only from the uPA molecules and at a wavelength different from the incident light. Also fluorescent stains are used at lower concentrations than absorbing stains, and the net background from autofluorescence is less than the contribution of nonspecific staining by light absorbing stains.²³ Fluorescence emitted from whole cells in cytopreps can clearly show the concentrations of uPA on the cell membrane as well as "hot spots" within the cytoplasm. Figure 5a shows an example of a breast tumor section illustrating the areas of uPA found in foci of tumor cells. Distinct areas of concentrated uPA are shown (white lines). Clearly, many tumor cells are not producing significant quantities of uPA and neither are most of the normal cells. Thresholding and image enhancements can often give size distribution and more information on the cells producing the uPA. Figure 5b shows the same tissue section as figure 5a; however, this image (5b) has been digitally analyzed and pseudocolor added to the display to illustrate that considerable cellular detail remains obscured in the black and white image in 5a. These methods can be used in retrospective studies where the time to reoccurrence and the degree of metastasis and morbidity are known. Cumulative data can then be used to provide a prognostic indicator for the presence of active metastasis.

Flow Cytometric Studies of Urokinase in Cultured Glioma Cells

To establish the parameters for comparing immunofluorometric analysis of urokinase (uPA) using flow and image cytometry, studies were begun with normal kidney cells. Once the methods were standardized, the cytoprep studies were extended to measurement of uPA in U937 lymphoma and human glioma cell lines, which were found to produce high levels of the plasminogen activator. Several glioma cell lines employed in the studies were obtained from Dr. Marylou Ingram, Huntington Research Foundation, Pasadena, California. These cell lines, which were cultured from patient surgical biopsy material, have different morphological characteristics and growth rates. The first of these lines, CS, grows very rapidly as polygonal cells in monolayers and, in the absence of serum, tends to form spheroid structures. The second cell line, HBRO9, has a fibroblastoid morphology, although it has the characteristic immunological marker associated with gliomas, glial fibrillary acidic protein (GFAP).²⁴ This cell line grows at about 25% the rate of CS.

Initially, some problems arose with autofluorescence from the cells which interfered with uPA quantitation. Optimized methods allowed measurement of significant differences in the immunostaining with the anti-uPA Mab. Dual staining with propidium iodide (PI) following ribonuclease treatment and fluorescein-labeled anti-uPA antibodies enabled bivariate analysis of DNA and uPA content as shown in figure 6. The graph on the left is a plot of numbers of cells versus DNA content (abscissa), which reflects the distribution of cells in different stages of the cell cycle. The plot on the right shows the uPA content (ordinate) and the same relative DNA content (abscissa, different scale). It is clear that most of the cells in G₁ and all of the cells in S phase have very high levels of uPA.

We are comparing flow cytometric analysis of uPA levels in several glioma cell lines. Similar FCM graphs of DNA and uPA fluorescence in the CS cell line are shown in figure 7. In contrast to the HBRO9 cells (fig. 6) a majority of these cells in G₁ and in S phase have much lower levels of uPA (right-hand plots). Both glioma cell lines produce uPA during growth and also during stationary (G₁/G₀) phase, with HBRO9 producing significantly higher levels of intracellular uPA. The higher levels of uPA in the HBRO9 line indicate more active metastatic potential than cells with lower uPA levels. The relative levels of uPA as measured by immunofluorescence flow and image cytometry are tabulated in table 1. The HBRO9 cells have considerably more variability in the uPA (fluorescence) measurements than do the CS cells, and the HBRO9 cells also appear to produce more membrane-bound uPA (based on qualitative examinations of some 150 cells); however, quantitative measurements are still under way. Further studies are concentrating on image cytometry

measurements of uPA to better quantify the membrane-bound (receptor) versus cytoplasmic uPA since flow cytometry only measures fluorescence at "zero resolution."

DNA can also be quantified on a per-cell basis using image analysis. However, when using PI for DNA and fluorescein label for uPA, the amount of DNA fluorescence was often more predominant than the uPA-related fluorescence (green wavelength) since PI fluorescence overrides FITC emissions. This required adjustment of the incident light intensity to keep both fluorescence signals in the same range to avoid resetting the video camera sensitivity between measurements on the same field of view. DNA quantitation can be performed more effectively by staining a dye excited in the U.V. (Hoechst 33258) and analyzed in the blue region.

Discussion

The importance of urokinase as a key enzyme in the initial mechanisms leading to tumor cell invasion and metastasis has been underscored in the past three years. Previous methods of measuring extracted uPA /mg of protein or of measuring secretion levels in cultured explants have provided statistical correlation with disease-free and overall survival.²⁵ There also is a strong correlation between uPA production and lymph node status in breast cancers and multivariate analyses have shown that high levels of both uPA and PAI-1 mean a maximum risk of relapse. It is now time to develop more specific tests that can accurately determine the active uPA versus the inactive scuPA, the membrane-bound uPA and the PAIs that appear to have interlinked, critical roles in the migration and metastasis of breast and other cancers.

The first research step has been to compare the DNA measurements and the intracellular levels of urokinase in tumor cells and normal cells. The initial FCM analyses will determine the effect of cell cycle on those cells having elevated uPA and the general relationship between abnormal DNA and uPA in breast and brain tumors. Additional data is being collected on DNA synthesis rates and uPA levels using more specific flow cytometry and/or image analysis techniques. Urokinase levels can be determined in those subpopulations of tumor cells that have abnormal DNA (using two parameter flow cytometry). We currently are measuring the intracellular and membrane-bound levels of urokinase per cell using fluorescent anti-uPA antibodies and image analysis. Next, different forms of uPA and uPA receptor complexes will be measured using molecular-specific antibodies. Finally, measurements of PAI-1 or PAI-2 per cell are compared to the abnormal DNA and high uPA to determine the final relative metastatic potential. Correlations with hormone receptors and other proteolytic enzymes also can be made to provide additional prognostic information for custom design of adjuvant therapy following surgical removal of the primary tumor.

Commercial Applications

Many intricate biochemical interactions are involved in dissolution of the extracellular matrix, which enables metastatic cells to leave the primary tumor. Intracellular metabolism appears to have a major role in the initiation of cellular metastasis. The complexity of these interactions makes it too complicated for laboratory test kits to be effective in routinely measuring the DNA, uPA, PAIs, hormone receptors, etc., necessary to develop a comprehensive prognostic panel for a particular cancer patient. Such a task requires a specially equipped, expert medical testing service where pathologists, surgeons and oncologists can send patient biopsies for complete analysis. Several companies already offer this type of cancer testing as a commercial service; however, tests for uPA as a prognostic marker of metastatic potential are not yet offered. Once the metastatic relationships are characterized at the cellular level, clinical studies will be required to statistically correlate these biochemical tests with recurrent disease and survival. Quantitative measurements of uPAs, uPA receptors, and inhibitors can be added to the existing panel of breast cancer cytological tests. The first use of these tests will be in providing additional information that indicates active metastasis at the time of initial surgery. This information can help oncologists design better, more effective followup therapy for those patients who have high levels of multiple markers indicating metastasis is already under way even though clinical manifestations are still undetected.

This NASA-sponsored project is developing methods for a routine analytical test of intracellular and membrane-bound uPA that can be added to the existing panel of breast cancer markers. Each year more than 170,000 new breast cancers are discovered in the U.S. alone. Unfortunately, about 30% of these patients will die from their breast cancer.²⁴ The current tests for DNA content, DNA synthesis and hormone receptors cost about \$350. More complicated tests will likely cost \$450 each. A practical test for urokinase combined with other metastatic markers of breast cancer would create a significant new market for cancer testing laboratories. And of course, uPA is important in many other types of metastatic cancers. Better adjuvant therapy, used only when critical markers are known to indicate active metastasis, could make a significant impact on the survival of cancer patients and reduce medical costs required to treat recurrent disease.

Finally, antibodies specific against urokinase can be used for more than diagnosis of the beginning steps of metastasis. As the entire scenario is better understood, it may be possible to develop treatments targeted against just those metastatic cells that have large amounts of membrane-bound urokinase or large concentrations of inactive scuPA. Anti-uPA antibodies could be conjugated with antitumor drugs or radioisotopes to treat specific metastatic cells that are actively trying to invade adjacent tissues. This could be the basis for the first therapy

directed against metastatic cells that were not removed by cancer surgery or that had begun migration prior to removal of the primary tumor.

References

- ¹Gratzner, H. G., and Leif, R. C., "An Immunofluorescence Method for Monitoring DNA Synthesis by Flow Cytometry," *Cytometry*, Vol. 1, 1981, pp. 385-389.
- ²Merkel, D. E., Dressler, L. G., and McGuire, W. L., "Flow Cytometry, Cellular DNA Content and Prognosis in Human Malignancy," *Journal of Clinical Oncology*, Vol. 5, 1987, pp. 1690-1703.
- ³Celis, J. E., and Celis, A., "Cell Cycle-Dependent Variations in the Distribution of the Nuclear Protein Cyclin Proliferating Cell Nuclear Antigen in Cultured Cells: Subdivision of S Phase," *Proc. Natl. Acad. Sci.*, Vol. 82, 1985, pp. 3262-3266.
- ⁴Lee, J. S. et al., "Determination of Biomarkers for Intermediate End Points in Chemoprevention," *Cancer Research*, Vol. 52 (Suppl.), 1992, PP. 2707S-2710S.
- ⁵McQuire, W. L., "Prognostic Factors in Primary Breast Cancer," *Cancer Surveys*, Vol. 5, 1986, pp. 527-836.
- ⁶Raber, M. N. et al., "Ploidy, Proliferative Activity and Estrogen Receptor Activity in Human Breast Cancer," *Cytometry*, Vol. 3, 1982, pp. 36-41.
- ⁷Bacus, S. S. et al., "Tumor-Inhibitory Monoclonal Antibodies to the HER-2/Neu Receptor Induce Differentiation of Human Breast Cancer Cells," *Cancer Research*, Vol. 52, 1992, pp. 2580-2589.
- ⁸Duffy, M. J. et al., "Urokinase-Plasminogen Activator, A Marker for Aggressive Breast Carcinomas," *Cancer*, Vol. 62, 1991, pp. 533.
- ⁹Janicke, F. et al., "The Urokinase-Type Plasminogen Activator (u-PA) is a Potent Predictor of Early Relapse in Breast Cancer," *Fibrinolysis*, Vol. 4, 1990, pp. 69-78.
- ¹⁰Oka, T., Ishida, T., Nishino, O. T., and Sugimachi, K., "Immunohistochemical Evidence of Urokinase-type Plasminogen Activator in Primary and Metastatic Tumors of Pulmonary Adenocarcinoma," *Cancer Research*, Vol. 51, 1991, pp. 3522-25.
- ¹¹Hollas, W., Blasi, F., and Boyd, D., "Role of Urokinase Receptor in Facilitating Extracellular Matrix Invasion by Cultured Colon Cancer," *Cancer Research*, Vol. 51, 1991, pp. 3690-3695.
- ¹²Harvey, S. R. et al, "Secretion of Plasminogen Activators by Human Colorectal and Gastric Tumor Explants." *Clin. Expl. Metastasis*, Vol. 6, 1988, pp. 431-450.
- ¹³Camiolo, S. M., Markus, G., and Piver, M. S., "Plasminogen Activator Content of Gynecological Tumors and Their Metastases," *Gynecological Oncology*, Vol. 26, 1987, pp. 364-373.
- ¹⁴Hasui, Y. et al., "Comparative Study of Plasminogen Activators in Cancers and Normal Mucosa of Human Urinary Bladder." *Cancer Research*, Vol. 49, 1989, pp. 1067-1070.
- ¹⁵Camiolo, S. M. et al., "Plasminogen Activator Content and Secretion in Explants of Neoplastic and Benign Human Prostrate Tissues," *Cancer Research*, Vol. 44, 1984, pp. 311-318.
- ¹⁶Meissauer, A. et al., "Urokinase-Type and Tissue-Type Plasminogen Activators are Essential for in vitro Invasion of Human Melanoma Cells," *Experimental Cell Research*, VOL. 192, 1991, PP. 453-459.
- ¹⁷Schmidt, M. et al, "Tumour-Associated Fibrinolysis: The Prognostic Relevance of Plasminogen Activators uPA and tPA in Human Breast Cancer," *Blood Coagulation and Fibrinolysis*, Vol. 1, 1990, pp. 695-702.
- ¹⁸Gaylis, F. D. et al., "Plasminogen Activators in Human Prostate Cancer Cell Lines and Tumors: Correlations with the Aggressive Phenotype," *Journal of Urology*, Vol. 142, 1989, pp. 193-198.
- ¹⁹Kirchheimer, J. C. and Remold, H. G., "Functional Characteristics of Receptor-Bound Urokinase on Human Monocytes: Catalytic Efficiency and Susceptibility to Inactivation by Plasminogen Activator Inhibitors," *Blood*, Vol. 74, 1989, pp. 1396-1402.
- ²⁰Andreasen, P. A. et al., "Plasminogen Activator Inhibitor from Human Fibrosarcoma Cells Binds Urokinase-Type Plasminogen Activator, but not Its Proenzyme," *J. Biol. Chem.*, Vol. 261, 1986, pp. 7644-7651.
- ²¹Cubellis, M. V., Wun, T., and Blasi, F., "Receptor-Mediated Internalization and Degradation of Urokinase is Caused by Its Specific Inhibitor PAI-1," *EMBO Journal*, Vol. 9, 1990, pp. 1079-1085.
- ²²Katz, R. L., unpublished data.
- ²³Lockett, S. J. et al., "Automated Fluorescence Image Cytometry: DNA Quantification and Detection of Chlamydial Infection" *Anal. Quant. Cytology and Histology*, Vol. 13, 1991, pp. 27-44.
- ²⁴Patau, A., "Glial GFAP, Vimentin and Fibronectin in Primary Cultures of Human Glioma and Fetal Brain," *Acta Neuropathology*, Vol. 75, 1988, pp. 448-455.
- ²⁵Janicke, F., Schmitt, M., and Graeff, H., "Clinical Relevance of the Urokinase-Type and Tissue-Type Plasminogen Activators and of Their Type 1 Inhibitor in Breast Cancer," *Seminars in Thrombosis and Hemostasis*, Vol. 17, 1991, pp. 303-312.

Acknowledgments

The authors wish to express their gratitude to Dr. Mohammed Abaza of the Baylor College of Medicine, Dr. Thomas Brooks of the M.D. Anderson Cancer Center, Norwood Hunter of KRUG Life Sciences, and Heather Lawson of DNA Sciences for their laboratory assistance and technical contributions. This work was supported by the NASA Technology Utilization Program through contracts NAS9-18065 (Baylor) and NAS9-18189 (DNA Sciences).

Table 1. Urokinase Levels in Glioma Cell Lines Measured by Immunofluorescence Flow and Image Cytometry.

<u>CELL LINE</u>	MEAN FLUORESCENCE \pm S.D.	
	<u>FLOW CYTOMETRY</u>	<u>IMAGE ANALYSIS</u>
CS	6.13 \pm 0.10	11.3 \pm 0.86
HBRO9	32.25 \pm 11.3	74.1 \pm 6.34

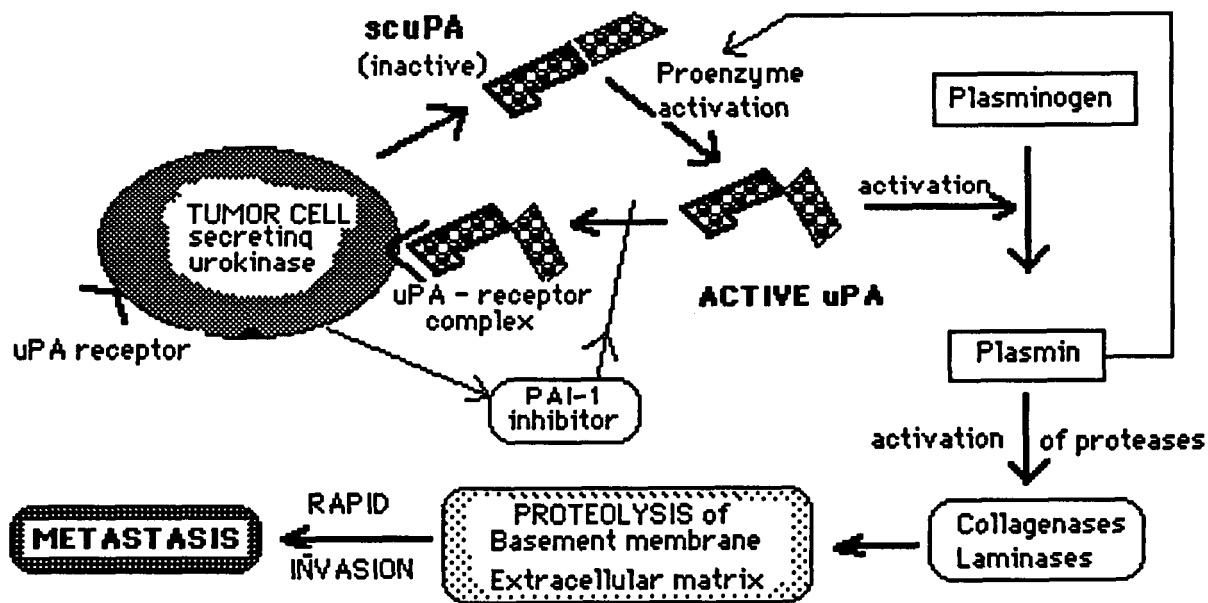


Figure 1. Schematic of Urokinase Secretion, Inhibitor (PAI-1), uPA Receptor, Activation of Plasmin and Subsequent Protease Steps That Enable Tumor Cell to Lyse the Extracellular Matrix, Invade Adjacent Tissues and Metastasize.

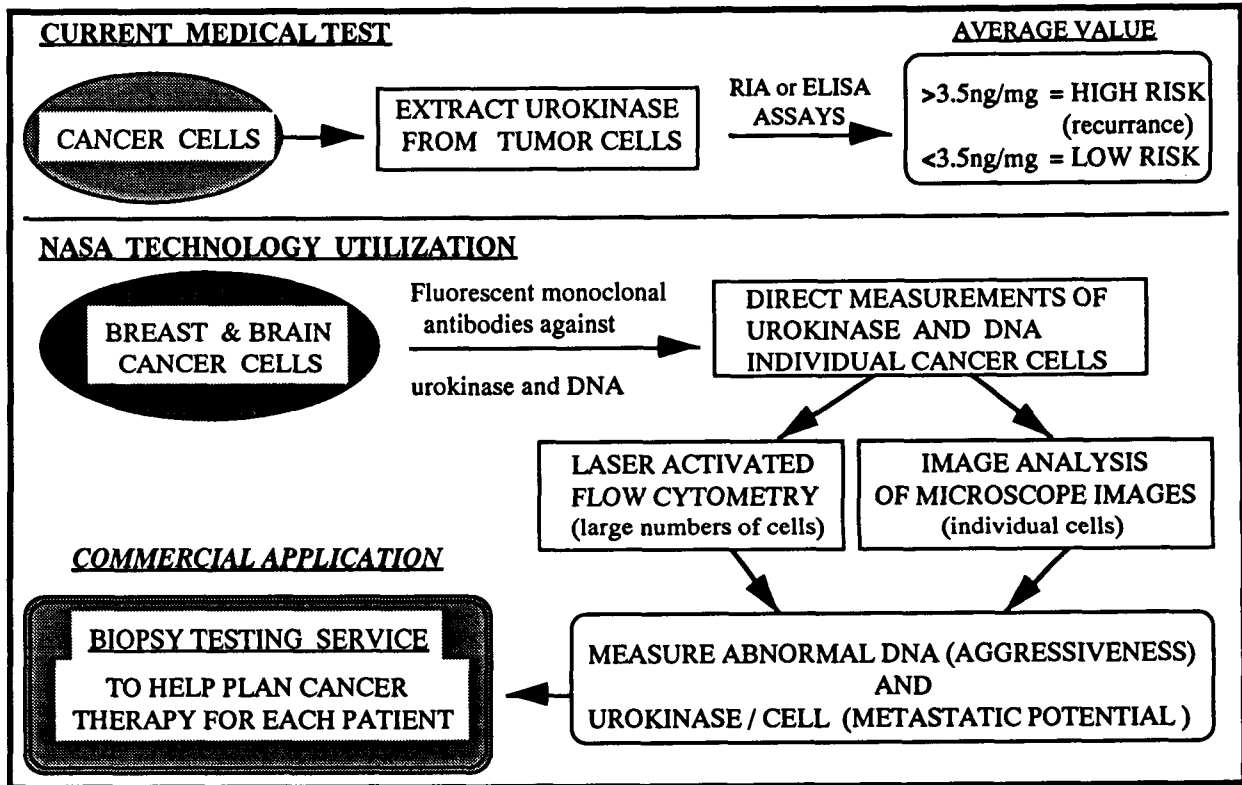
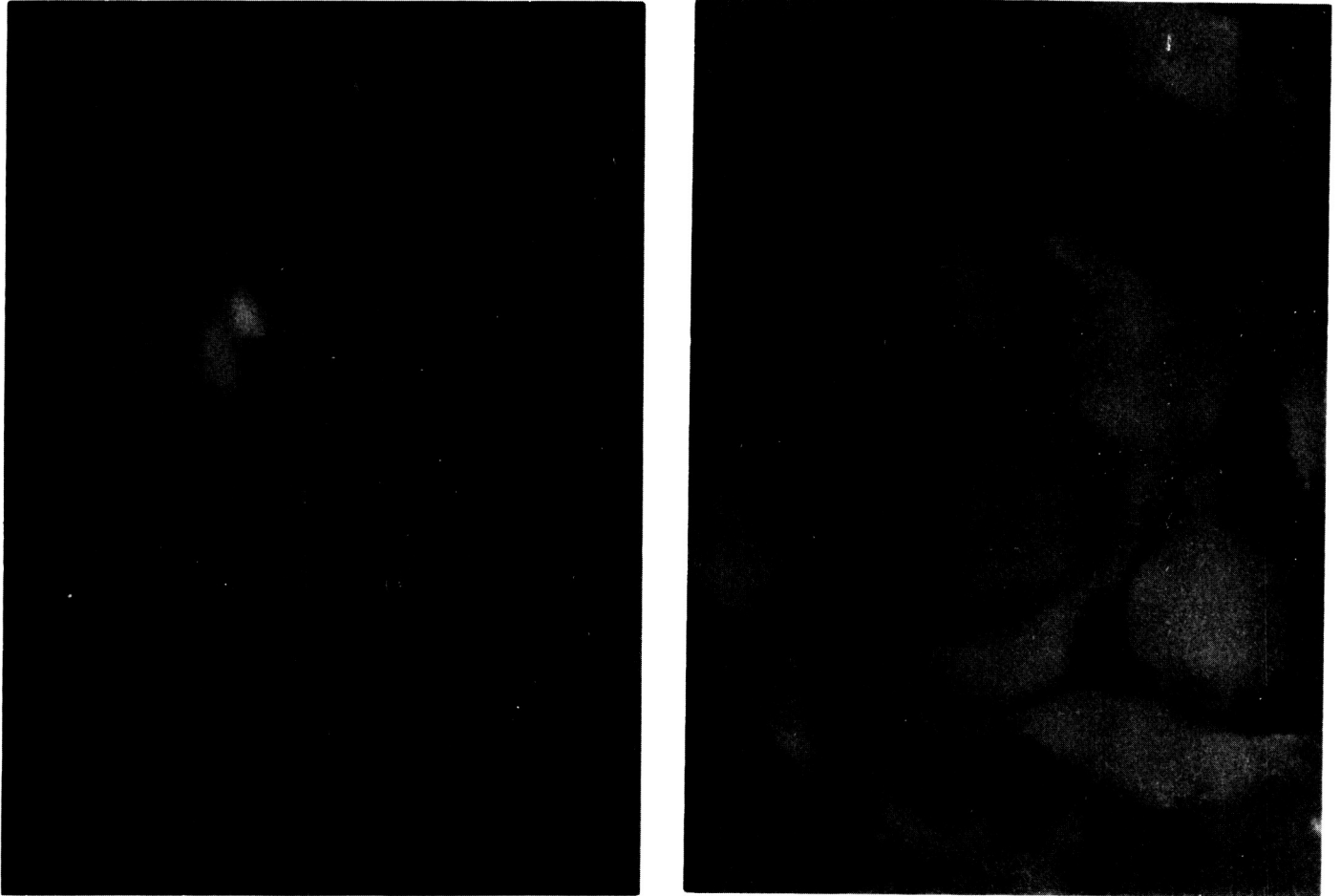


Figure 2. Conceptual Comparison of Current Method to Measure Extracted Urokinase and the NASA Flow and Image Cytometry Analyses That Are Being Developed into a New Metastatic Assay for Commercial Cancer Testing.



Figures 3a and 3b. Photomicrographs of Human Glioma Cells Stained for Urokinase (uPA) by Rhodamine Labeled Antibodies. Note the Intense Fluorescence in Localized Areas of Concentrated uPA.

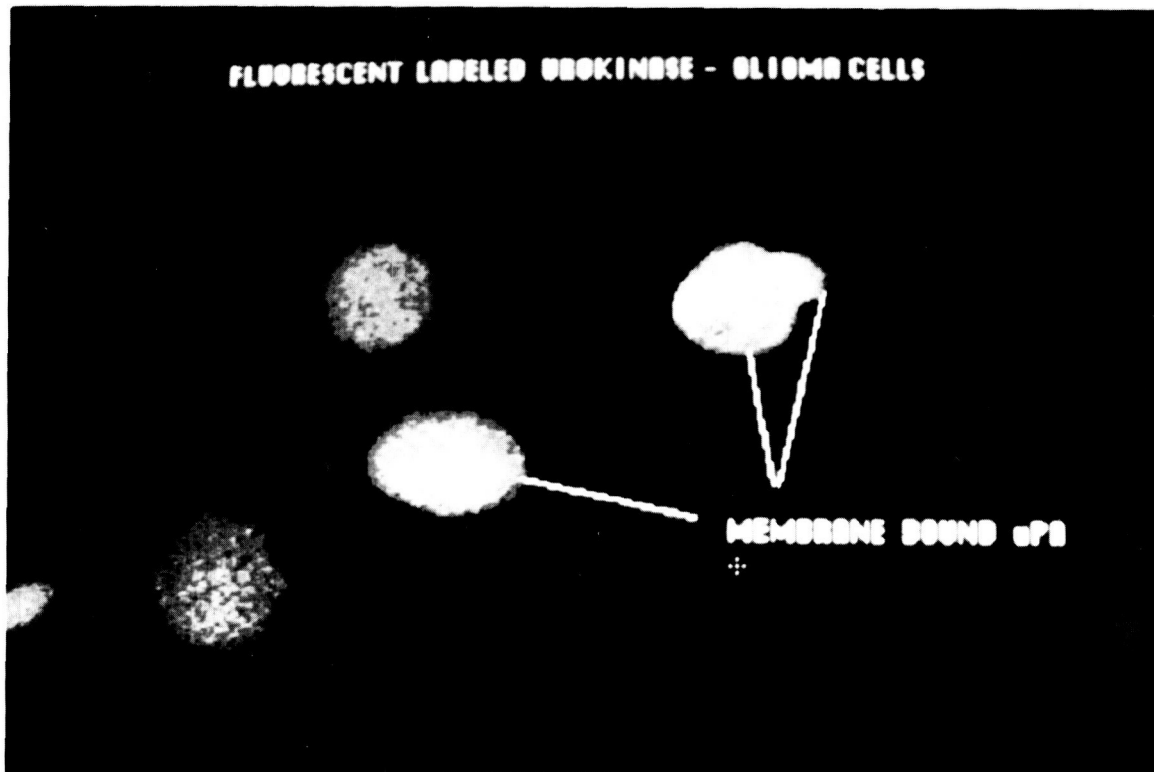


Figure 4. Digital Pseudocolor Image of Glioma Cells Labeled with Rhodamine-Conjugated Anti-Urokinase Antibodies. Concentrated uPA Bound to the Cell Membrane is Shown by Intense Fluorescence Along the Margin of Two Cells (White Lines) and Throughout Most of the Other Two Cells (Upper and Lower Left). Quantitative Measurements are Performed by Density Slicing Then Measuring Fluorescence Intensity and Relative Area for Statistical Comparisons Among Biopsied Cells.

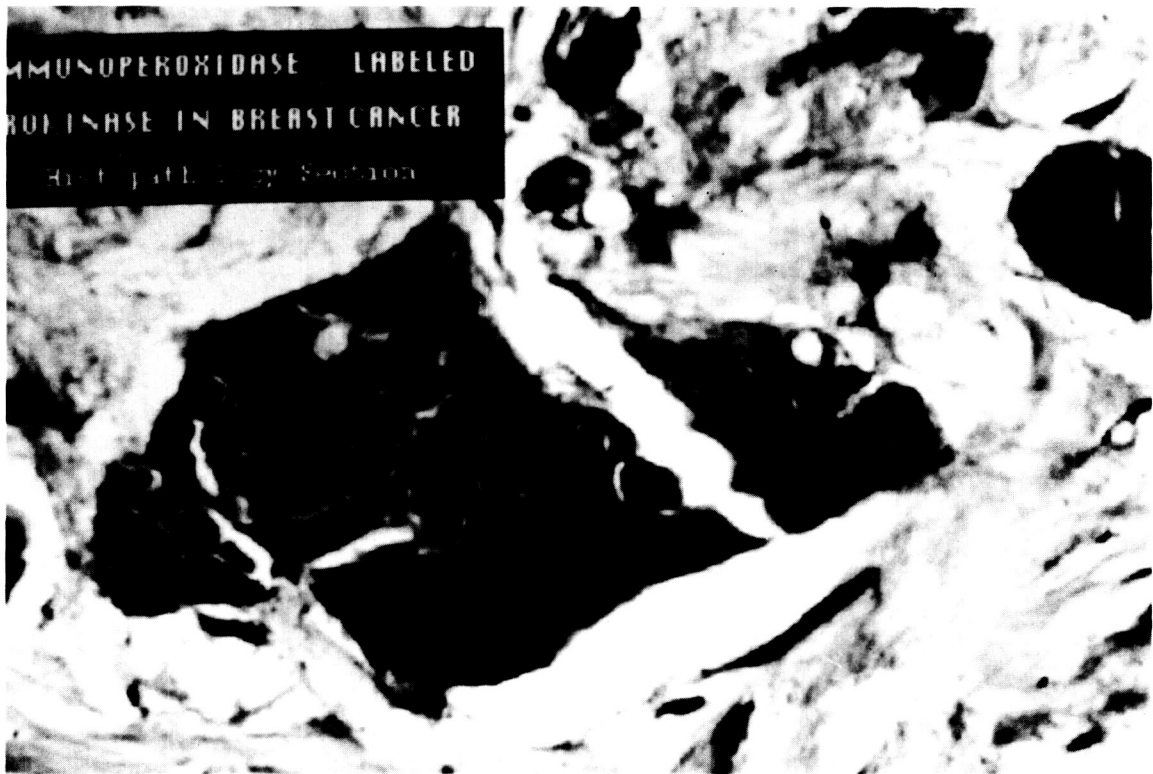


Figure 5a. Digital Image of Breast Histology Section Showing Tumor Cells and uPA Labeled with Antibodies. Mean Optical Densities are Measured and Normalized for Area to Measure the uPA (Fluorescence Intensity) in the Active Cells.

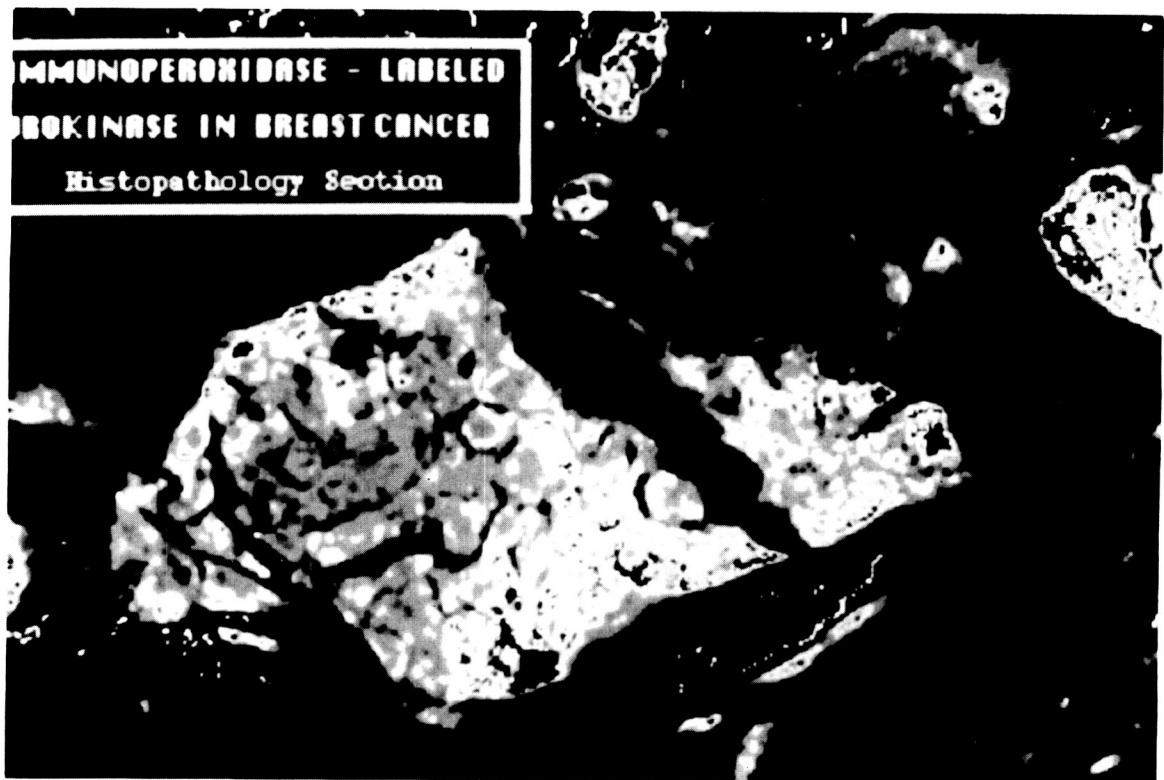
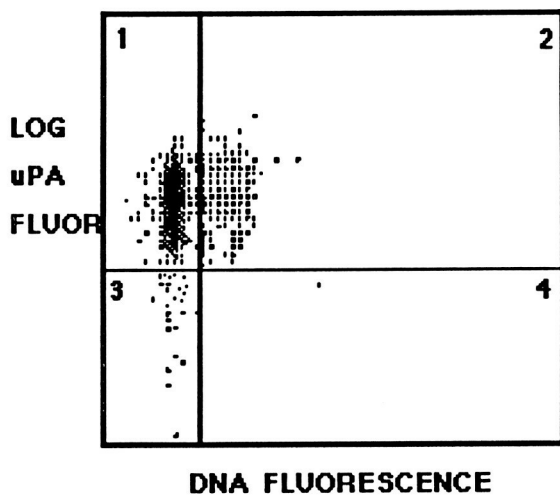
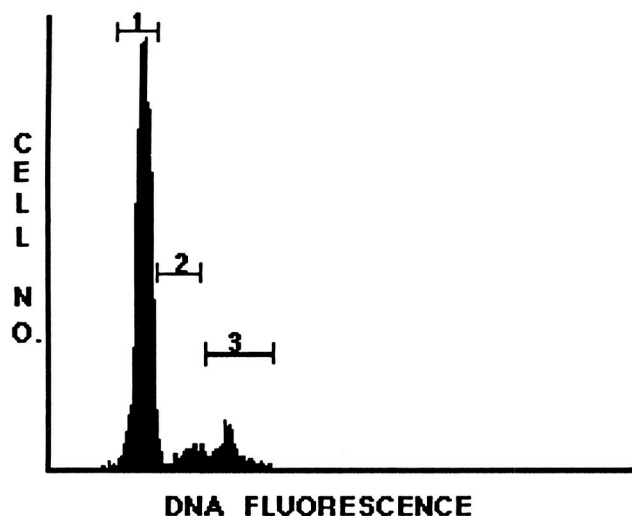
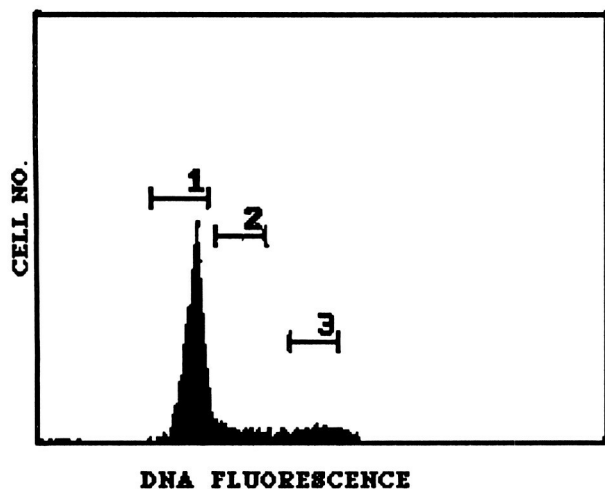


Figure 5b. Color Enhanced Image of 5a Showing the Additional Morphological Information That Is Recorded But Not Evident in the Black and White Image Above with Only One Density Slice Colored for Contrast.



	MIN.	MAX	PERCENT	MEAN FL.	SD	%HPCY
1 X	0	13	82.6	9.9	1.0	7.26
Y	3.24	1023		12.2	0.17	8.62
2 X	14	63	15.0	17.4	2.2	13.2
Y	3.24	1023		15.48	0.18	10.9
3 X	0	13	2.2	9.5	1.1	9.59
Y	0.102	3.24		12.16	0.26	4.08

Figure 6. Flow Cytometry Immunofluorescence of Glioma Cells (HBR09 Line) Labeled with Propidium Iodide (PI) for DNA and Fluorescein-Conjugated Antibodies for Urokinase (uPA). Panel A Shows the DNA Histogram of These Cells with G_1 , S and $G_2 + M$ Subpopulations. Panel B Compares the uPA and DNA Fluorescence for Cells in G_1 (82% of Total), in S Phase (15% of Total) and in $G_2 + M$ (22% of Total).



#1141
cs uPA

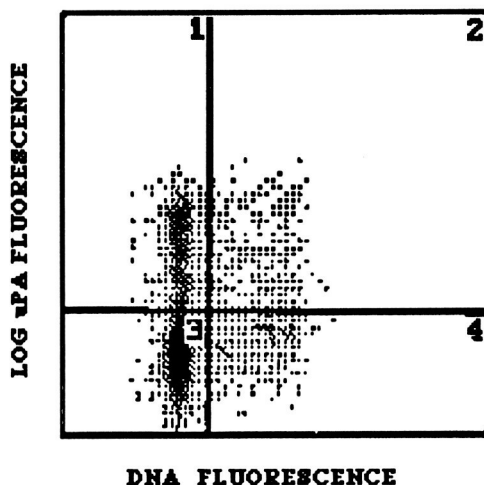


Figure 7. Flow Cytometry Analysis of CS Cell Line for Comparison with Figure 6. Panel A Shows the CS Cell Cycle Distribution of DNA Fluorescence (PI). Panel B Shows the Fluorescence Distribution of uPA versus DNA. Most of the Cells in G_1 Phase (22% of Total) and in S Phase (7% of Total) Contain Significant Levels of uPA.

Time to Detection of Circulating Microbubbles as a Risk Factor for Decompression Sickness

Michael R. Powell, James M. Waligora, K. Vasantha Kumar,*
Dick S. Calkins,* and John H. Gilbert*
Johnson Space Center/SD5
*KRUG Life Sciences

Abstract

Decompression Sickness (DCS) is due to the formation of a free gas phase in the form of microbubbles in tissues during decompression to reduce ambient pressure. The microbubbles so formed are frequently detectable in the precordial location using a Doppler ultrasound device. These circulating microbubbles (CMB) are frequently detected in individuals presenting with symptoms, but not all individuals with CMB develop symptoms. This study used survival analysis techniques to examine the association between time to detection of CMB and time to onset of symptoms. Survival analysis is commonly used in chronic disease (such as cancer) epidemiology.

Materials and Methods

The records were examined for 125 test subjects (100 men and 25 women) who participated in the NASA hypobaric chamber trials, which studied the risk of DCS during extravehicular activities (EVA). The subjects breathed 100% oxygen at site level for periods ranging from 0 to 6 h as a protective measure for DCS. Eighty percent of the subjects were exposed to an altitude of 9,144 m (30,000 ft) and the rest were exposed to an altitude of 6,400 m (21,000 ft). All subjects breathed 100% oxygen at altitude and exercised for 180 minutes, simulating EVA work at rates approximating 200 KCal/hr¹.

For comparison of individual characteristics, as well as of times to onset, we used non-parametric methods such as chi-square and Mann-Whitney's rank sum tests. To investigate the study question, we used survival analysis methods including Cox proportional hazards regression.¹

Since the prognosis under decompression changes with detectable microbubbles, CMB status was used as a "time-dependent" covariate.^{1,2} Individual CMB status was coded as 0 before and 1 after the detection of microbubbles. Age (≤ 32 and > 32 years), gender (male and female), body mass index (≤ 24 and > 24), activity levels (active and inactive), exposure altitude (6,400 m and 9,144 m) and duration of ground-level denitrogenation (nil, 3.5 h, 4.0 h, and 6.0 h) were used as covariates in the regression.

A subgroup regression analysis was also carried out on individuals with CMB (n=49) using time to detection of CMB (≤ 60 min=early and > 60 min=late) and other

variables discussed above. All p-values ≤ 0.05 were considered statistically significant.

Results and Discussion

Of 125 individuals, 18% presented with symptoms of DCS (all type I, bends pain) and 42% with symptoms of CMB. There were significant differences in the CMB status (present or absent) and in the time to detection of CMB between individuals with and without symptoms of DCS (table 1).

The Cox regression analysis showed heterogeneity in the risk of symptoms of those with and without CMB. Individuals who developed CMB were at higher risk (relative risk [RR]=29.56; 95% confidence interval [95% CI]=7.66-114.27) of developing symptoms than those without CMB.

In the subgroup of individuals with CMB, there was a reduction in the risk of symptoms with late onset of CMB (RR=0.92; 95% CI=0.89-0.95), compared to early onset (table 2).

Precordial Doppler ultra-sonography is frequently used to monitor the severity of decompression, but the temporal relationship between CMB and symptoms has not been examined in detail before. The analysis of the effect of time to onset of CMB on symptoms of DCS is confounded by several factors. The information on symptoms is usually incomplete or "censored" since not all subjects present with symptoms during an exposure. Further, the influence of one failure time (time to onset of CMB) on another failure time (time to symptoms) is not amenable to traditional methods of analysis.

Survival analysis uses both complete and censored information. Survival models account for the influence of failure due to CMB on the failure due to symptoms by using a time-dependent covariate in the analysis.² Using this approach, we found that individuals with CMB were at greater risk of symptoms. Delayed onset of CMB was associated with a reduced risk of symptoms. This reduction in risk may be due to the lesser amounts of dissolved gas available for growth of microbubbles after prolonged stay at altitude.

It appears that differences in time to detection of CMB are a measure of the individual's propensity to develop symptoms. The use of survival methods provides a way to examine the association between symptoms and microbubbles in the presence of censored information.

References

- ¹Cox, D. R., and Oakes, D., *Analysis of Survival Data*, Chapman and Hall, London, 1984.
- ²Prentice, R. L., and Kalbfleisch, J. D., "Hazard Rate Models with Covariates," *Biometrics*, Vol. 35, 1979, pp. 25-39.

Acknowledgment

This study was supported by NASA contract no. NAS9-18492.

Table 1. Comparison of Baseline Factors by Symptom Status

	Symptoms Present (n=22)	Symptoms Absent (n=103)	p-values
Age in years	34.4 (7.7)	31.4 (7.1)	0.09
Body mass index	23.9 (2.7)	23.9 (2.7)	0.83
Activity levels	4.5 (2.5)	4.5 (2.5)	0.99
Time to CMB in minutes	61.9 (33.2)	150.8 (50.5)	0.001
Gender			
Male	20 (91%)	80 (78%)	0.13
Female	2 (9%)	23 (22%)	
Final Altitude	18 (82%)	82 (80%)	0.81
9,144 m	4 (18%)	21 (20%)	
6,440 m			
Prebreathe	4 (18%)	21 (20%)	0.12
Nil	10 (45%)	24 (23%)	
3.5 h	5 (23%)	23 (22%)	
4.0 h	3 (14%)	35 (35%)	
6.0 h			
CMB	22 (100%)	30 (29%)	0.001
Present	0 -	73 (71%)	
Absent			

Table 2. Relative Risk of Symptoms in the Subgroup of Individuals with CMB

	Symptom Present (n=30)	Symptom Absent (n=19)	Relative Risk (95% CI)
Time to Onset of Microbubbles			
≤60 minutes	10	12	1.00
>60 minutes	9	18	0.92
			(0.89-0.95)

95% CI=95% Confidence Interval; * p<0.05

Verification of Methods to Permit Flying after Diving in Neutral Buoyancy Facilities

William T. Norfleet, Michael R. Powell, James M. Waligora, and K. Vasantha Kumar*
Johnson Space Center/SD5
*KRUG Life Sciences

Abstract

The findings of recent investigations in environmental physiology indicate a need for extensive changes in those sections of JSC Management Directive 1830.3, "Limitations Applicable to Personnel Exposed to Diving," which concern flying after diving. Because development of safe pressure/time exposure profiles is largely an empirical process, it would be highly desirable to verify the new tables calculated under laboratory conditions during the revision of this Management Directive. This study verifies the safety of profiles from a portion of these tables which is particularly relevant to operational concerns. Specifically, 19 human subjects were exposed to a pressure of 1.59 atmospheres absolute pressure (ata; 161 kPa, equivalent to a depth of 6.1 m) for 400 min, then to 1.0 ata (101 kPa) for 14 h, then to 0.69 ata (69 kPa, equivalent to an altitude of 3048 m) for 180 min. Air was breathed throughout. Precordial Doppler ultrasound monitoring for intravascular gas emboli (an indicator of the development of decompression sickness(DCS)) was performed at selected points during the exposures to 1.0 ata and 0.69 ata. Any signs or symptoms of DCS were noted. None of the subjects developed DCS, although four subjects exhibited high grade (grade III or IV) Spencer Doppler scores at some point during the hypobaric excursion. Through comparisons of these results with those of previous studies, we conclude that in this profile the risk of developing DCS, which would require hyperbaric therapy, is probably less than 1% per person-exposure.

Introduction

Relative to typical diving practices, neutral buoyancy training, involves a host of peculiar factors. For example, following training, the T-38 aircraft can be used as a means of transportation. This aircraft is often flown at high altitudes utilizing a differential cabin pressure, which is considerably less than that of aircraft operated by major air carriers (34 kPa versus 55 kPa differential pressure, respectively). Flight in a T-38 after a very long, shallow dive is a wholly unique scenario, and very little relevant data are available from any source. In the absence of such data, procedures could be formulated utilizing highly conservative assumptions. However, access to a T-38 offers obvious, substantial operational benefits, and unnecessary restrictions on such flying are to be avoided.

Rules regarding diving and flying after diving are stated in JSC Management Directive 1830.3, "Limitations

Applicable to Personnel Exposed to Diving." Results from recent investigations in environmental physiology indicate a need for extensive changes in the sections of this document which deal with flying after diving. Because development of safe pressure/time exposure profiles is largely an empirical process, it would be highly desirable to verify, under laboratory conditions, the new tables calculated during the revision of this Management Directive. This study investigated the risk of decompression sickness which is particularly relevant to current operational concerns.

Problem Statement/Description

Human subjects were exposed to a pressure of 1.59 ata (161 kPa) for 400 min, then to 1.0 ata (101 kPa) for 14 hours, and then to 0.69 ata (69 kPa) for 180 min. Air was breathed throughout. Precordial Doppler ultrasound monitoring for intravascular gas emboli (an indicator of the development of decompression sickness) was performed at selected points during the exposures to 1.0 ata and 0.69 ata. Any signs or symptoms of DCS were noted.

We hypothesized that an interval of 14 h at 1 ata, as described above, would result in a risk of DCS which would require hyperbaric therapy. This risk would not exceed 1% per person-exposure over the course of all phases of the pressure/time profile.

Methods

The essential elements of the experimental protocol are as follows:

- A hyperbaric exposure to a pressure of 1.59 ata (161 kPa) for 400 min while breathing air. This was followed by:
- An interval at 1 ata for 14 h while breathing air. This was followed by:
- A hypobaric exposure to a simulated altitude of 3,048 m (10,000 ft) for 3 h while breathing air.

During the hyperbaric portion of the experimental protocol, a series of exercises was performed that simulated the workloads involved in extravehicular activities. The subjects engaged in their daily activities during the surface interval between hyperbaric and hypobaric exposures, except that exercise training was prohibited. Air was breathed throughout the surface interval. While at simulated altitude, the subjects remained comfortably seated and performed no specific exercise.

Results were quantitated as follows: Any signs or symptoms of DCS were noted. Additionally, precordial Doppler ultrasound monitoring for circulating gaseous microemboli was performed in each subject for 5 min every 30 min for 1 h following the hyperbaric exposure and throughout the hypobaric excursion. Doppler signals were assigned a numerical grade.^{1,2,3} Further analysis of these signals was performed utilizing the "time-intensity" method⁴. Acquisition and processing of Doppler ultrasound data in this manner yielded far more data than arises from a simple "bends/no bends" scoring method, thereby permitting establishment of conclusions after a minimum of experimentation and expense.

Nineteen volunteers participated. They were healthy adult men and women in the age range of 25 to 55 yr. The subjects were selected to match the astronaut population as closely as possible in age, gender, height, weight, body surface area, percent body fat, and physical fitness level. Individuals having conditions or injuries that may have made them predisposed to DCS, as well as candidates with a history of neurologic DCS, were excluded. All subjects executed informed consent agreements and were free to withdraw from the project at any time.

Results

No subject exhibited signs or symptoms of DCS. Maximum precordial Spencer Doppler bubble grades achieved are as follows:

Maximum Grade	Number of Subjects
0	9
I	3
II	3
III	1

Conclusions

Interpretation of these data is difficult because the risk of DCS implied by a given Spencer Doppler bubble grade in a combined hyperbaric and hypobaric pressure/time profile is not known. In our study 4 of 19 subjects

demonstrated high bubble grades (grades III or IV). This incidence is similar to that observed by Eckenhoff et al.,⁵ following saturation exposure at a pressure of 1.48 ata (150 kPa), a profile which carries a risk of DCS below 1% per person-exposure. Based upon this comparison, we conclude that the risk of DCS requiring hyperbaric therapy in this profile is probably less than 1% per person-exposure. This conclusion must remain tentative until a larger data base is developed which permits correlation of bubble grades with risk of DCS in combined hyperbaric and hypobaric profiles.

References

- ¹Powell, Doppler Ultrasound Monitoring of Venous Gas Bubbles in Pigs Following Decompression From Helium, Neon, and Air. *Aerospace Med*, Vol. 45, 1974, p. 505.
- ²Spencer, M. P., and Johanson, D. C., *Investigations of New Principles for Decompression Schedules Using the Doppler Ultrasonic Blood Bubble Detector*, Institute of Applied Physiology and Medicine, Seattle, WA, 1974.
- ³Powell, M. R., Spencer, M. P., and von Ramm, O. T., "Ultrasound Surveillance of Decompression," *Physiology and Medicine of Diving*, edited by P. B. Bennett and D. H. Elliott, 3rd ed., Bailliere Tindall, London, 1982, pp. 404-434.
- ⁴Powell, M. R., "Doppler Indices of Gas Phase Formation in Hypobaric Environments: Time-Intensity Analysis," NASA TM 102176, 1991.
- ⁵Eckenhoff, R. G., Olstad, C. S., and Carrod, G., "Human Dose-Response Relationship for Decompression and Endogenous Bubble Formation," *J Appl Physiol*, Vol. 69, 1990, pp. 914-918.

Acknowledgments

The staff of Environmental Physiology Laboratory supported these studies with excellent technical assistance. The Manned Test Support Section of the Medical Operations Branch provided many hours of access to hyperbaric and hypobaric chambers.

The Effect of Gravitational Acceleration on Ventricular Filling: Diastolic Ventricular Function in Microgravity and 1g

John B. Charles, George M. Pantalos,* Thomas E. Bennett,**
Barbara S. Bennett,† and M. Keith Sharp*
Johnson Space Center/SD5
*University of Utah
**Bellarmine College
†KRUG Life Sciences

In-flight echocardiographic measurements of astronaut heart function on the Space Shuttle have documented a 15% to 20% reduction in stroke volume with a compensatory increase in heart rate to maintain cardiac output. To date, no mechanism for the reduced stroke volume has been elucidated. We propose that the reduction in stroke volume is biophysical in origin.

Many factors influence the filling of the heart during diastole (fig. 1). These factors include

- the atrial pressure,
- the kinetic energy of the blood as it enters the ventricle,
- the transmural pressure gradient,
- the passive, elastic recoil attributed to the "parallel elastic element" of the myofibrils, and
- the gravitational acceleration-dependent hydrostatic pressure gradient that exists in the ventricle due to its size and anatomic orientation.

This pressure gradient, which can be estimated to be 6660 dynes/cm² (~5 mm Hg) in an average adult, acts to augment the diastolic filling of the heart. It has been estimated that the effect of this pressure component contributes between 10% to 30% of the total ventricular filling. We hypothesize that the absence of this contribution to the ventricular filling process in the microgravity environment of spaceflight may account, in part, for the 15% to 20% reduction in stroke volume reported for astronauts while in orbit.

To test this hypothesis, ventricular function test were conducted using an artificial heart (AH) left ventricle with the longitudinal axis anatomically oriented (@45° to the horizontal) and horizontally oriented to null the hydrostatic pressure difference (ΔP) between the base and apex of the ventricle. Additional ventricular function test were conducted in the microgravity environment of the

NASA KC-135A aircraft. The experimental apparatus consisted of a pneumatically actuated, elliptical artificial ventricle (UTAH-100 human version left ventricle) connected to a closed-loop, hydraulic circuit (Penn State) with compliance and resistance elements to create physiologic pressure and flow conditions. The ventricle was instrumented with high-fidelity, acceleration-insensitive, catheter-tip pressure transducer (Millar Instruments) in the apex and base to determine the instantaneous ventricular pressures and ΔP across the left ventricular ($LVP_{\text{apex}} - LVP_{\text{base}}$). The ventricle was also instrumented with flow probes (Transonic Systems) and pressure transducer (Millar Instruments) immediately upstream of the inflow valve and downstream of the outflow valve. By varying the circulating fluid volume, ventricular function was determined for varying payload pressures with fixed afterload pressure and ventricular control parameters.

Elimination of the intraventricular hydrostatic ΔP between the ventricular apex and base by horizontally aligning the ventricle or ventricular operation in the microgravity environment resulting in the predicted rightward shift of the ventricular function curve (Fig. 2 and 3). This finding offers a biofluid mechanical explanation for changes in AH recipient cardiac output with changes in posture and suggests new AG automatic control parameters to maintain a consistent cardiac output with changes in AH recipient posture. Furthermore, these results indicate the need to document AH pumping performance in extremes of device orientation. Finally, this finding provides a biofluid mechanical explanation for the reduction in cardiac stroke volume experienced by Space Shuttle astronauts while in orbit as documented by echocardiography.

Validation of the Clavicle/Shoulder Kinematics of a Human Computer Reach Model

James C. Maida, Ann M. Aldridge,* and Abhilash K. Pandya*

Johnson Space Center/SP34

*Lockheed Engineering and Sciences Company

Abstract

An accurate human computer reach model capable of simulating complex 3-dimensional tasks would be a valuable tool in the evaluation of workspace volumes. This model could be used to design workstations, configure hand holds/foot restraints, and simulate realistic motions on Earth and in microgravity environments. The most kinematically complex interaction to model in the human arm is the shoulder girdle. The motion of the shoulder complex involves several joints moving simultaneously, with a complicated and dependent interaction. This shoulder motion was measured in all rotational planes using a magnetic tracking device. These measurements were used to validate and refine a clavicle/shoulder kinematic model. Accurate relaxed reach positions can now be computed in all planes of motions to within, on average, 1 cm of the measured data.

Introduction

Essential to accurate reaching with the arm is a comprehensive model of the shoulder girdle. The complexity of the shoulder motion and the interdependence of the joints affecting the shoulder complex have been studied for years.¹ Inman, Saunders, and Abbott measured and documented the complex motions of the shoulder girdle to include four different joints: the sternoclavicular, the acromioclavicular, the scapulothoracic, and the glenohumeral. The motion of the shoulder complex is due to the combined motion of all these joints. The model we use simplifies the shoulder motion into two joints, a clavicle joint and a humerus joint. Neither of the two joints in the model necessarily represents their corresponding anthropometrically correct position in the shoulder complex. Nevertheless, this simplification still allows the prediction of accurate motions.

Early computer models have had a clavicle joint with two degrees of freedom and a humerus joint with three degrees of freedom. These models did not have an automatic clavicle/humerus interaction. Often the clavicle joint motion was ignored because of the difficulty in moving both the upper arm and the clavicle independently. This has led to unrealistic reach volumes and motions. E. M. Otani developed equations relating the clavicle motion and humerus motion to the elevation and abduction of the shoulder complex.² Measurements of reach sweeps were compared with the Otani model's calculated reach sweeps in an attempt to validate his

model. There was an unacceptable 10-15 cm error in the computed reach sweeps. Modifications of model parameters were made to reduce these errors.

Methods and Measurements

Experimental Setup

Measurements of reach sweeps were obtained using a low-frequency magnetic tracking device (Polhemus Navigation Sciences, McDonnell Douglass Electronics Company). This device was integrated with a Silicon Graphics Workstation and an in-house software package to allow quick, accurate data flow from the tracker directly into the Graphics Analysis Facility's modeling programs. A magnetic sensor was secured to the upper arm near the elbow joint and provided positional information relative to a fixed coordinate system. A wooden frame was built to hold the magnetic source, reducing distortions in the magnetic field caused by metal in the environment. This frame was elevated to shoulder height to have maximum sensitivity over the range of the arm sweeps. A study of the limitations of the tracking system was done to determine the accuracy of the setup. Measurements taken showed an error of less than 1.5 cm in the range of our measurements (1 m). Beyond this range, the measurements were inconsistent. Attached to the wooden frame was a wooden rod used to stabilize the subjects. Each subject was positioned with this rod centered in his back and was directed to keep his back secured against this rod at all times during the sweep. This minimized the upper body motion during the sweeps and still allowed natural (unconstrained) motion. Repeated sweeps over the range of motion of the subject in three orthogonal planes were recorded: a forward sweep, a side sweep, and a horizontal sweep. In addition, horizontal and random stretched (extreme) sweeps were also collected.

Clavicle/Shoulder Model Development

Model Overview The motion of the shoulder complex can be described in spherical coordinates by determining the elevation angle (e) and the abduction angle (ab) of the end effector (elbow, or fingertip) (fig. 1). The model computes the clavicle angles of elevation (c_e) and abduction (c_{ab}) given the shoulder angles. The humerus angles of elevation and abduction are calculated from the geometry to position the arm at the determined shoulder complex elevation and abduction.

Determining Joint Center of Rotations A

major concern in the accurate characterization of the shoulder complex is the location of the joint centers of rotation of the clavicle and the humerus joints. The previous computer model placed the rotation points of the clavicle joint and humerus joint at the physical locations of both ends of the clavicle bone in the human figure. However, allowing the shoulder clavicle complex to rotate at these points generated reach envelopes which were much larger than measured. Figure 2 shows side sweeps generated with and without joint center lowering. The lower portions of the computed sweeps fit the measured data. However, the horizontal and the vertical regions have unacceptably large errors. To resolve this discrepancy, the joint centers needed to be adjusted. In order to determine the optimal joint center location for each individual, we used an iterative process. Figure 3 shows the maximum and average errors resulting from lowering the clavicle and humerus joint centers for a particular individual. Optimal values were selected for each individual based on these plots. The lowering of both the clavicle and humerus joint centers by the appropriate amount allowed for the entire side sweep to coincide with the measured data.

Modifications to Model Parameters The dependence of the clavicle elevation on arm elevation was established by Otani by fitting regression equations to empirical data collected by Inman. The clavicle elevation angle in degrees is

$$C_{el} = \cos(ab) * \beta_1 + (1 - \cos(ab)) * \beta_2 - 90.0 \quad (1)$$

where

$$\beta_1 = 0.2514 * e_l + 91.076 \text{ for } 0 \leq e_l \leq 131.4 \quad (2)$$

$$\beta_1 = -0.035 * e_l + 128.7 \text{ for } e_l > 131.4 \quad (3)$$

and

$$\beta_2 = 0.21066 * e_l + 92.348 \text{ for } 0 \leq e_l \leq 120.0 \quad (4)$$

$$\beta_2 = 120.0 \text{ for } e_l > 130.0 \quad (5)$$

Otani's model of the clavicle abduction angle was simply a linear dependence on the shoulder abduction, that is

$$c_{ab} = \text{coef} * ab \text{ (where coef} = 0.2) \quad (6)$$

As the arm is elevated or lowered from the horizontal position, the clavicle abduction angle decreases. This fact necessitates that the clavicle abduction equation also be dependent on shoulder elevation.

$$c_{ab} = \text{coef} * ab * \sin(e_l) \quad (7)$$

Equation 7 allows for smoother motions of the clavicle abduction to occur. As the shoulder moves through 0 or 180 degrees the clavicle abduction angle

moves through 0 without a discontinuous motion.

Modeling Stretched Versus Relaxed Motions

The clavicle angles (elevation, abduction) are important in the modeling of relaxed versus stretched motions of the arm. The parameters associated with these motions were studied in detail. The abduction of the clavicle (c_{ab}) was observed to be directly related to the coefficient term in equation 7. The coefficient (coef) term correlates to the physical ability of individuals to stretch their clavicle joints in the horizontal plane (abduction). Individuals can increase the clavicle abduction angle for a specific position by stretching. It is difficult to do this while maintaining a sweeping motion. But when a specified point in space is the goal, individuals can increase their clavicle abduction angle and hence increase their reach envelope. This parameter can be empirically determined for an individual and differs if the reaching characteristics are relaxed or stretched.

The elevation of the clavicle (c_{el}) is dependent upon β_1 and β_2 coefficients of the model equations 1 - 5. To model the stretching motion for extreme elevation angles, the β_1 and β_2 coefs were modified to include an extra term.³ These modifications to the clavicle abduction and elevation computations enabled the prediction of stretched and relaxed reach sweeps for any plane of motion.

Results

Excellent fits between the model data and the measured data were obtained. Over the range of subjects, the average error in fit was 0.96 cm and the average maximum error was 3.19 cm. The maximum error refers to the single data point with the largest deviation between model and measured values. The absolute average difference is an average over the entire range of motion (150 data points) of the sum of the absolute errors between model and measured values. In addition, a regression plot of model versus actual reach distances (shoulder to end-effector) revealed a correlation coefficient of 0.98. This represents a significant improvement over the previous reach model.

Parameter estimation for the model is central to achieving accurate reaching. Three parameters were examined in detail: joint center location, the coef term of the clavicle abduction equation (eq. 7) and the stretch coefficient of the clavicle elevation equations.

For all subjects, the horizontal relaxed and stretched sweeps were compared to determine the best range of values for the coef term in the clavicle abduction angle calculation (eq. 7). Over the 12 subjects, an average relaxed coef of 0.24 and an average stretched coef of 0.62 were calculated. Extreme elevation angles of the random sweeps were used to estimate the best fits for the stretch coefficient. Further validation of these parameters needs to be done in order to determine accuracy of predicting reach sweeps for any subject.

Conclusions

Reach sweep measurements taken with a magnetic tracking device have been used to validate and extend a computer model of the shoulder complex. This model describes the shoulder complex with two joints (clavicle and humerus) which have complex dependent motion. This model can predict "relaxed" reaches within an error of 1 cm over the entire range of motion of the shoulder complex. The clavicle elevation and abduction equations can be adjusted to model stretched reaches. Based on our model, we can generate accurate reach volumes either for relaxed or stretched arm motion.

Preliminary results indicate that it may be possible to relate the amount of joint center lowering to a standard anthropometric measure. The amount of joint center lowering for each individual was plotted versus the height of the subject. A linear fit to this data provides a method for approximating the adjustment of the shoulder joint centers. More data needs to be collected and other anthropometric measures need to be correlated in order to solidify this result.

References

- ¹Inman, V. T., Saunders, M., and Abbott, L., "Observations of the Function of the Shoulder Joint," *The Journal of Bone and Joint Surgery*, Vol. 26, No.1, Jan. 1944, pp. 1-30.
- ²Otani, E. M., "Software Tools for Dynamic and Kinematic Modeling of Human Motion," Master Thesis, Department of Computer and Information Science, University of Pennsylvania, July 1989.
- ³Aldridge, A. M., Panyda, A., and Maida, J., "Validation of the Clavicle/Shoulder Kinematics of a Human Computer Reach Model," Proceedings of the International Simulation Technology Conference, Nov. 1992.
- ⁴National Aeronautics and Space Administration, *Man-System Integration Standards, NASA-STD-3000*, Vol. 1, 1987.

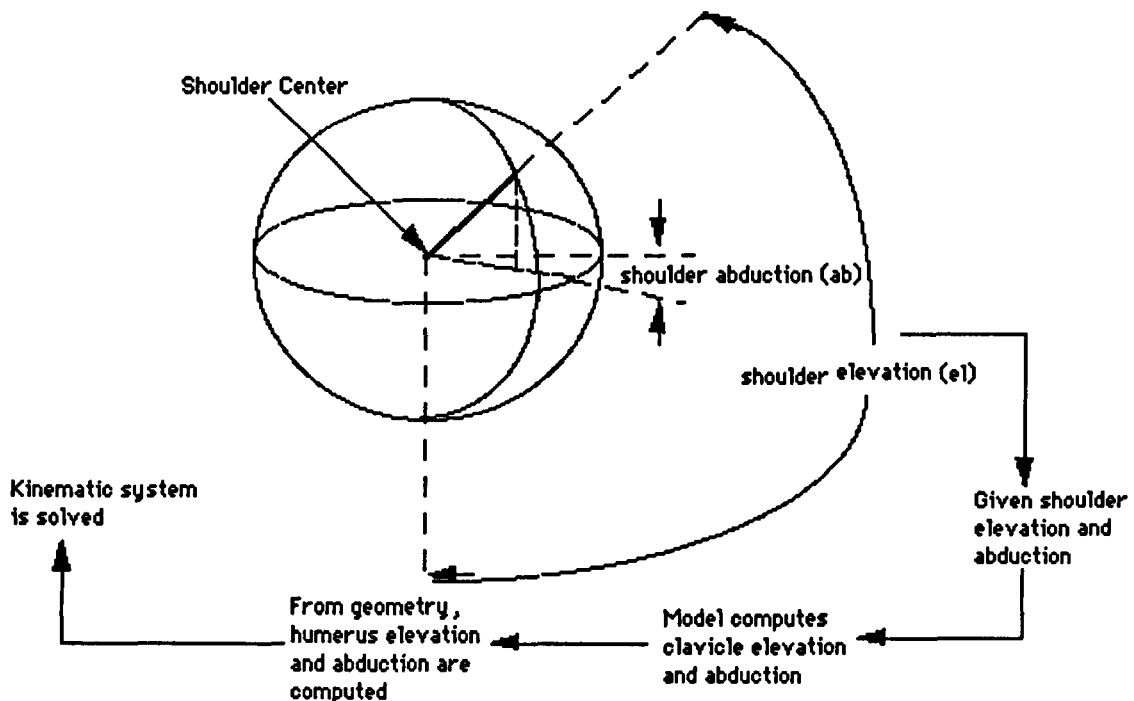


Figure 1. Shoulder Kinematic Model Overview.

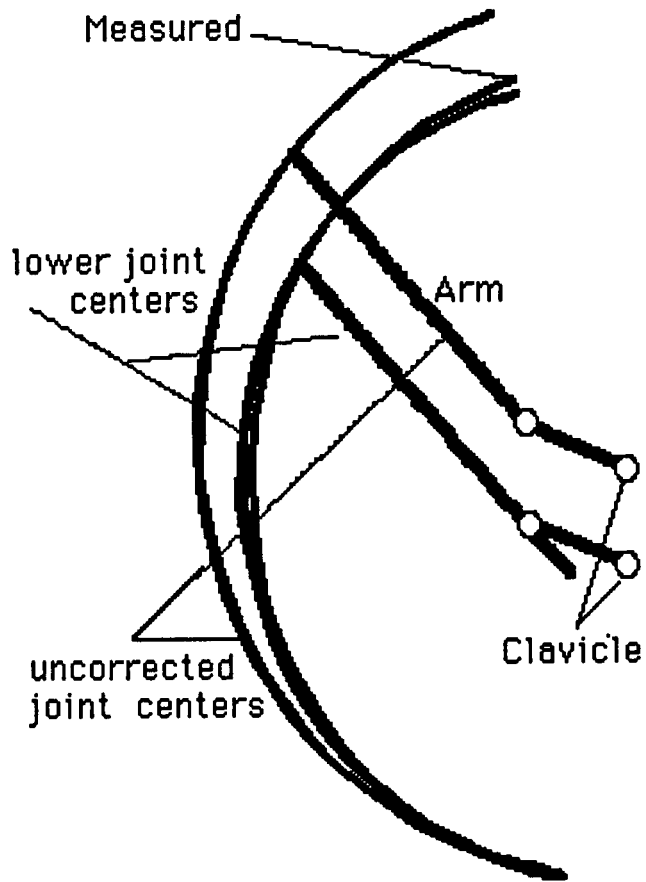


Figure 2. Measured Versus Computed Reach Sweeps (With and Without Joint Axis Correction).

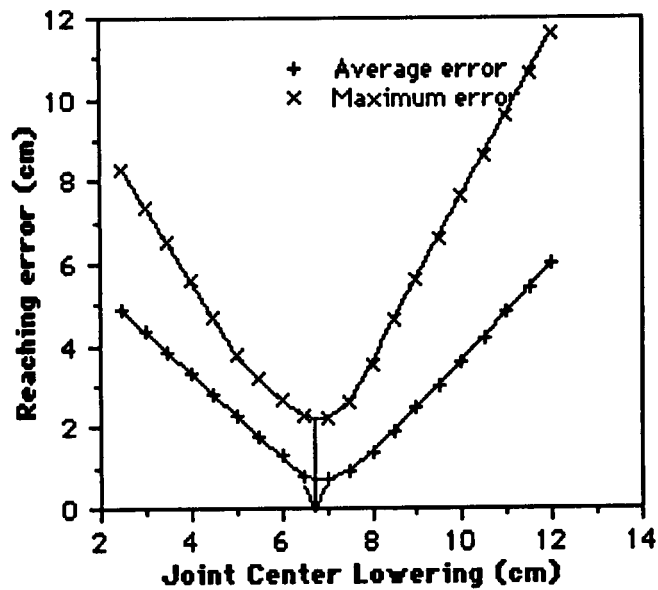


Figure 3. Location of Optimal Joint Center.

A Preliminary Comparison and Validation of Computer Lighting Simulation Models for Space Applications Using Empirically Collected Data

James C. Maida, Abhilash K. Pandya,* and Ann M. Aldridge*

Johnson Space Center/SP34

*Lockheed Engineering and Sciences Company

Abstract

Extravehicular activities performed in space require proper lighting conditions. The placement and properties of lights and materials used are highly constrained by factors which include power consumption limits, heat dissipation issues, and available space. An accurate lighting model capable of simulating complex 3-dimensional environments would be a valuable tool for space applications. This model could be used to deal with complex visibility issues and aid in the optimum selection of lights, materials, and viewing perspectives for space operations.

A variety of lighting simulation packages are available. This report describes the limitations and validity of three of these models: "standard" ray tracing, "Radiance," and radiosity. Using empirically collected data on material/light properties, a controlled experiment and an accurate geometry were set up both in the graphics environment as well as in NASA's Lighting Environment Test Facility. Luminance at various points in the environment was measured with a photometer and also computed in the graphics environment. Modeled versus measured values agree to within the limitations of the photometric procedures used. This report describes the details of the validation study.

Introduction

Geometric modeling and viewing of structures is commonly used in aerospace engineering. The analysis of lighting conditions is the next logical extension for realistic viewing analysis. When determining the lights, viewing perspective, and materials used for a particular mission, many issues including power consumption limits, heat dissipation issues, and available space are carefully considered. Recently, computer graphics lighting models have been used by the Space Station and Shuttle community. Design decisions have been recommended based on these studies. If these models are employed without understanding the basic assumptions and approximations used by the simulation and without validation of the results that they produce, some potentially serious problems could arise. This concern has provided the thrust to research and validate computer models used for these lighting applications.

Three classes of models were chosen for validation: standard ray tracing, "Radiance," and radiosity. The standard ray tracing (Rshade) program by Craig E. Kolb (Princeton, New Jersey) traces light from the eye point to

the light sources in the environment while reflecting the rays in accordance with surface properties. Radiance by Greg J. Ward (Lawrence Berkeley Laboratory, California) extends the ray tracing method by using a Monte Carlo technique to compute interreflections between surfaces. Radiosity by Min-Zhi (University of Pennsylvania, Pennsylvania) computes a view-independent lighting solution, which balances the energy flux of each surface with respect to every other surface in the environment.

Major issues of concern for realistic space applications were the modeling of interreflections between surfaces, the handling of large complicated geometry, and the ability to compute luminance values at any point in the environment. A simple geometric experiment was set up both in the graphics environment and in NASA's Lighting Environment Test Facility to investigate the problems associated with these lighting models. Luminous flux at direct and interreflected surfaces was measured with a photometer and also computed in the graphics environment. The ray tracing and the radiosity algorithms were found to be inadequate for realistic space applications. The Radiance algorithm computed the interreflections to within the accuracy of the measuring device and could also handle complex environments. The results presented here show that lighting can be accurately simulated for space applications with the Radiance model.

Methods

Phase 1

The three lighting models were compiled on a Silicon Graphics VGX machine. A set of programs was developed to output geometry, transformation information, material properties, and light information from an in-house geometry modeler (DMC) into formats specific to each of the light modeling programs. A simple geometry, consisting of a room with two cubes and a light source, was then created and used as input to the various model formats. Figure 1 shows the geometry that was created. This top view illustrates the arrangement of the cubes, the light source, and the viewing vector. The light source was pointed directly at cube 1. Cube 1 was rotated towards cube 2 at a 45 degree angle such that the directly illuminated surface of cube 1 would reflect light onto cube 2 as illustrated by the dotted light path in figure 1. The view was adjusted so that both the directly and indirectly illuminated surfaces were visible.

Phase 2

An experimental setup similar to the one run in phase 1 of the methods was set up in NASA's Lighting Environment Test Facility. The setup included a well collimated, small, uniform light source; two 30x30x60 cm white boxes; a black curtain; a video camera; and a Model 301 photometer (Photo Research, Burbank, California). A light source was set up 90 cm from box 1, which was tilted at a 45-deg angle facing box 2 at a distance of 150 cm. The video camera was located to view the setup at locations all along the perimeter of the experiment. The photometer was used to measure the surface reflectance of the boxes, the floor, the wall, and the luminance of the light source. In addition, photometric measures were taken at both the directly and indirectly lit surfaces. Careful attention was paid to the geometry of the scene and to the view point. The same scene was created in the graphics environment and was converted to the Radiance format.

Phase 3

A test was set up at the Systems Integration Facility's Shuttle Mockup where all lights in the facility were shut off except for the Shuttle's mid and forward payload bay lights. Camera views of the payload were recorded on a Panasonic video recorder. The Shuttle, with the various structures present during the mockup session, was created in the graphics environment and outputted to the Radiance format. Payload bay light and material parameters for the computer model were estimated based on published results.¹

Results

Phase 1

Of the three modeling packages, radiosity is least suited for space applications for the following reasons. Radiosity required that the lighting simulation be contained within a closed environment due to the methodology of the energy flux equilibrium computation. In addition, this computation was highly memory intensive and was unreasonable for the large detailed structures modeled in space applications (i.e., Space Station). Moreover, specular reflections could not be modeled with the radiosity program.

Figure 2 shows the output of the other two models. In theory, light rays emanating from the source should strike cube 1, and depending on the reflectance properties of cube 1, illuminate the surface of cube 2. In the ray trace image, it is clear that the interreflections are not present. The ray trace algorithm can use an arbitrary constant term to approximate the indirect lighting of the scene. In realistic applications, this term is not constant and needs to be computed and not arbitrarily set. On the other hand, Radiance output shows the expected result

without any arbitrary ambient terms. In the Radiance view, cube 2 does in fact show the reflected light from cube 1. Also, the back right side of cube 1 (away from the light) is also illuminated from interreflections off of the floor and the walls.

Phase 2

Phase two was developed to determine exactly how accurate the Radiance program was in its estimation of both direct and indirect lighting. Two measures of luminance were made, one on box 1 (direct light) and one on box 2 (interreflected light). Table 1 shows the light and material values measured for the experimental setup. Measured versus predicted values are listed in table 2. Figure 3 is a comparison of the output of the Radiance model with the video camera view of the experiment. Radiance output can convert luminance values into a color coded image. This allows for a visual analysis of the distribution of luminance in the image (fig. 3d).

Conclusions

Based on the results in phase 1 of the experiment, it was concluded that ray trace and radiosity were not suitable for space applications. Radiosity modeled the diffuse interreflections, but not the specular, and could not handle the large geometry in a nonclosed environment. Ray tracing did not handle the interreflections. Light striking cube 1 in figure 2 should illuminate cube 2. For ray tracing, it does not. Radiance behaved as expected in that cube 2 was lit by the reflection from cube 1. Phase 2 of the experiment was designed to test exactly how close the Radiance computation could come to a measured value at the direct and indirect surfaces. Table 2 shows that the measured and modeled values agreed to within the experimental error. The measurement accuracy of the light meter is about 10% calibrated for a specific wavelength of light. In addition, there are a number of simplifying assumptions that have been made in the experiment. In order to model the materials in the environment correctly, it was required that the bidirectional reflectance curves of each material be measured.² Because the precise equipment necessary for that measure was not available, only one measure of reflectance, at one angle and at one point, was made. This simplification negates the angle dependence of the reflectance. For instance, in figure 3 the model view has a highly specular reflectance shown at the floor coming directly from the light; the actual view is not nearly as pronounced. Moreover, assumptions of uniform material surfaces, uniform light source, video camera distortions, effects of atmosphere, interference from other more distant objects in the room, like the ceiling, and the persons taking the measurements only add to the error expected. After considering all the assumptions and the error of measurements involved the computed luminance results and the corresponding views from Radiance are a

very reasonable estimate of light in the environment.

Phase 3 of the experiment was an attempt to provide a means to extend this work to realistic applications. Figure 4 shows model versus actual Space Shuttle view of a low lighting situation. Before considering this view, it is important to realize that, again, there are even more simplifying assumptions used. The material and lighting parameters in this environment were estimated from Ref. 1. Some of the uncertainties, in addition to the ones mentioned in phase 2, were related to the following: light intensity distribution data used in the model were based on detailed measurements of one bay light; this data did not correspond exactly to the lights used in the mockup; the effects of the rest of the high bay area (ceiling, walls, etc.) were not considered; and the view from the camera that we used was attenuated by the iris control mechanism (its own gamma correction). Considering all these assumptions, the views generated from the model are very reasonable.

Future work needs to focus on validation of even more complex lighting situations where the material and light properties are more accurately defined.

In addition, it is imperative that a more rigorous data collection effort to extend the data base of light and material properties for Space Station Freedom be initiated.

References

- ¹Wheelwright, C., "Orbiter Solar/Artificial Illumination During STS Flights," JSC 20541, May 1985.
- ²Ward, G. J., Rubinstein, F. M., and Clear, R. D., "A Ray Tracing Solution for Diffuse Interreflection," *Computer Graphics*, Vol. 22, No. 4, August 1988, pp. 85-92.

Acknowledgments

We would like to thank Jennifer Toole, Chuck Wheelwright (Lockheed ESC), and Dean Jensen (NASA JSC) for assistance with data collection and the use of the Lighting Environment Test Facility.

Table 1. Material Reflectance for Experiment

Materials	Illuminance (footcandles)	Luminance (footlamberts)	%Reflectance
Box	39.3	26.0	66%
Floor	235.0	3.0	1.3%
Wall	255.0	6.1	2.4%

Light source luminance - 136,800 footlamberts.

Table 2. Validation Results

	Box 1(direct light) (footlamberts)	Box 2 (indirect light) (footlamberts)
Measured range	6.5-7.9	0.10-0.12
Computed range	3.0- 7.0	0.05-0.30

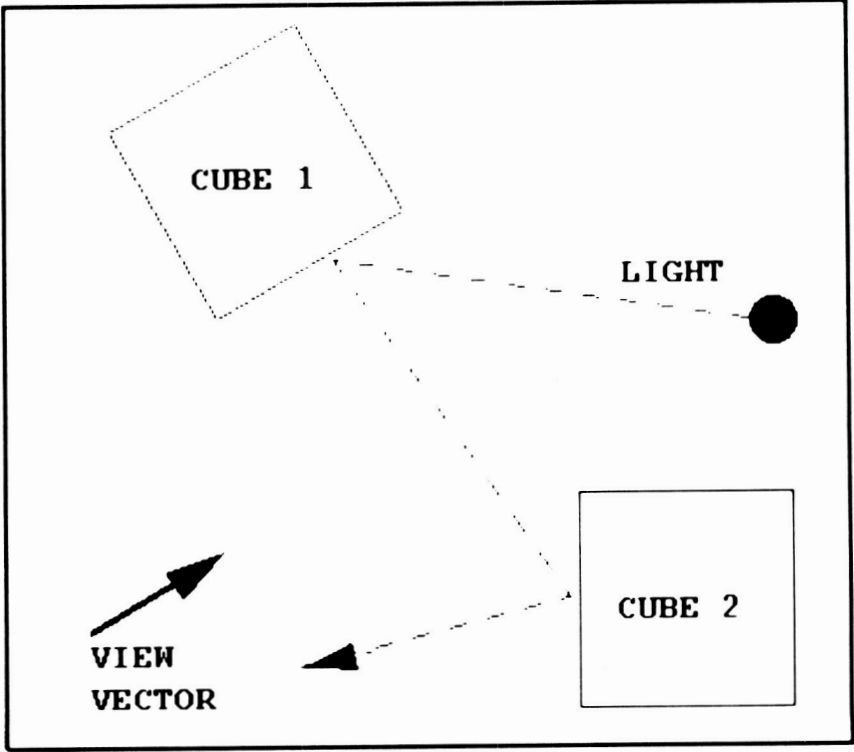


Figure 1. Top View of Experimental Scene Geometry.

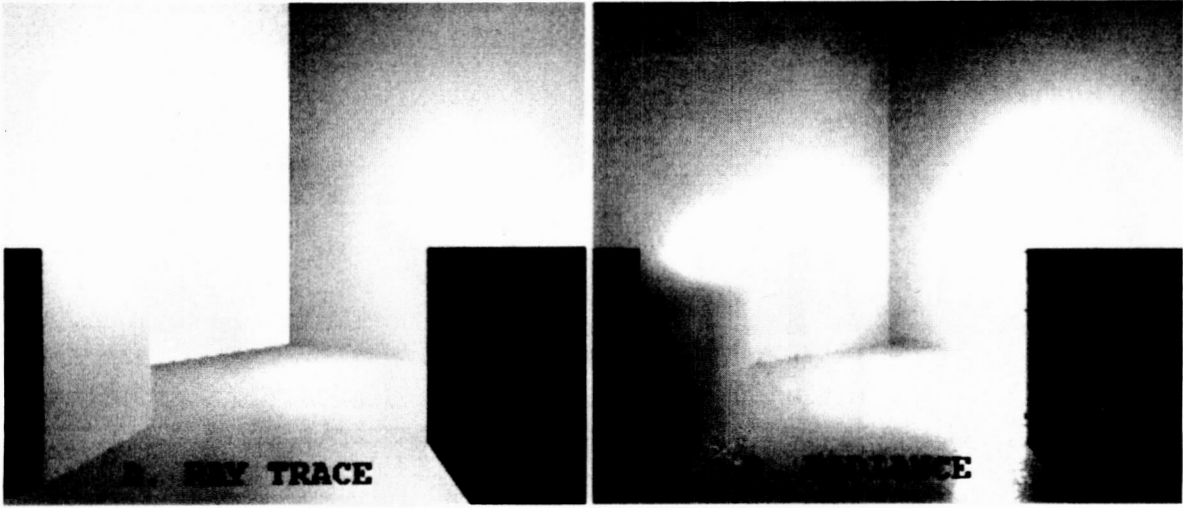


Figure 2. Comparison of Ray Trace and Radiance.

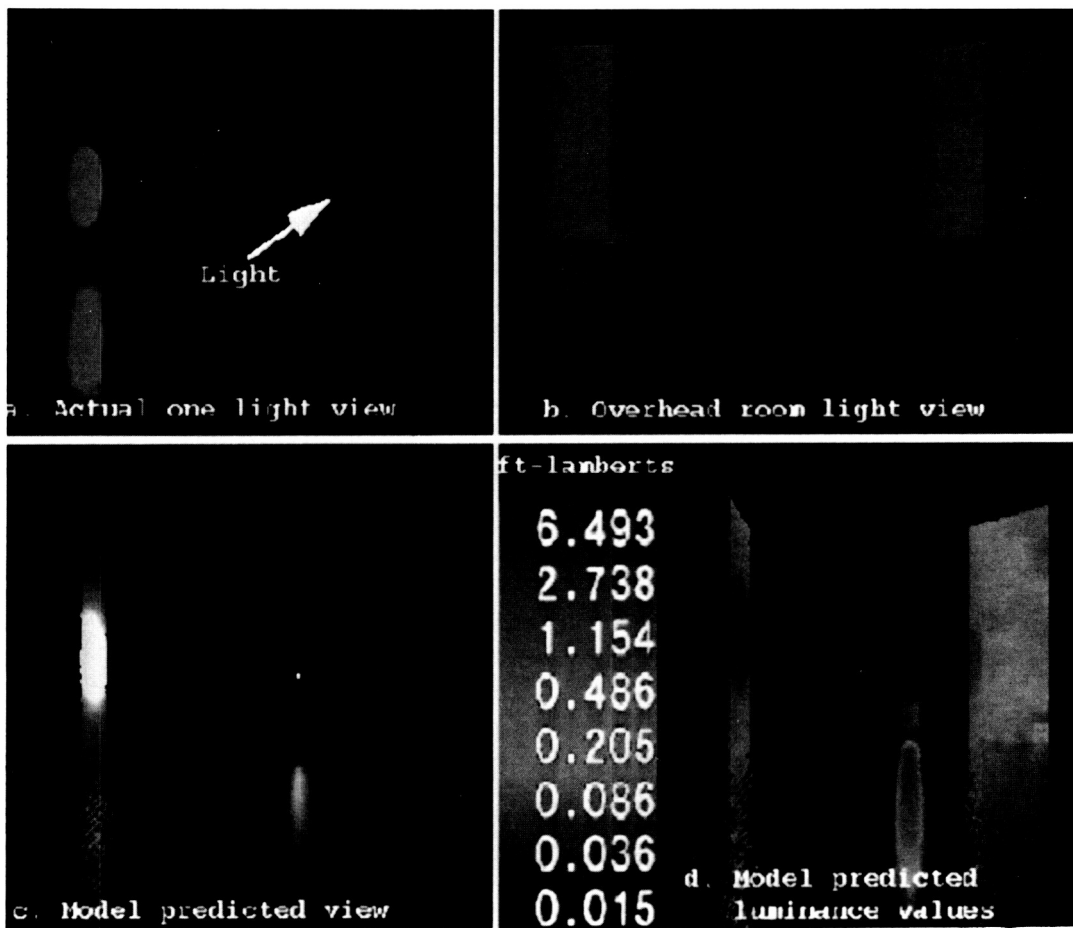


Figure 3. Model Versus Actual View of Lighting Experiment.

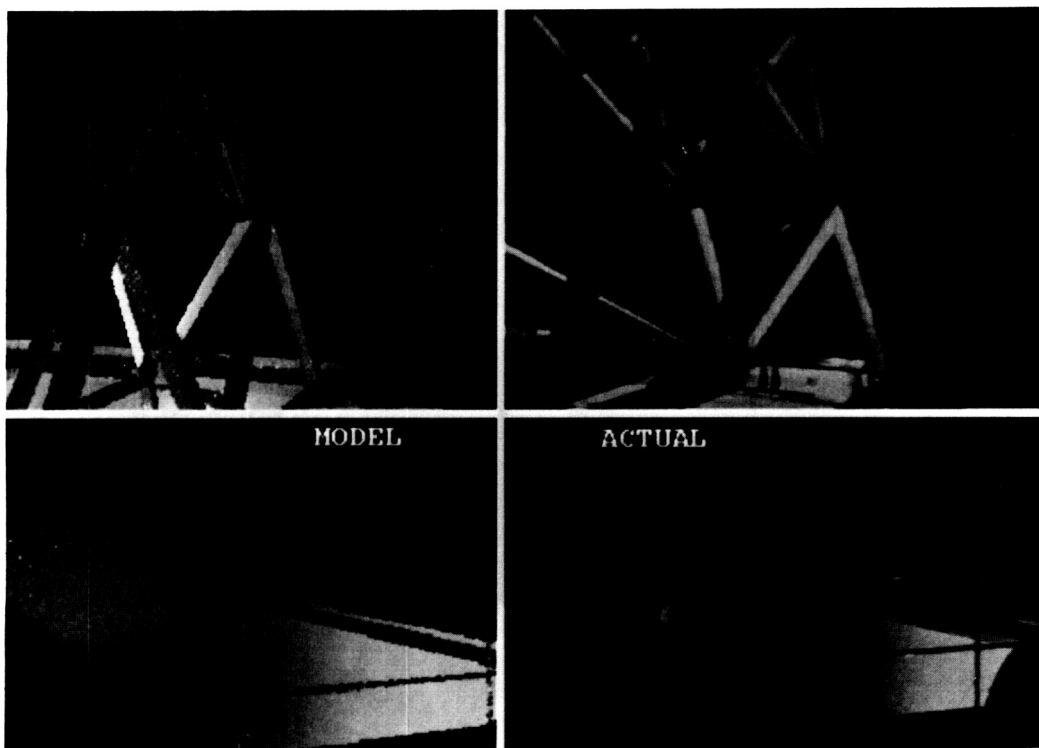


Figure 4. Model Versus Actual View of Space Shuttle.

Habitation Development Tool

Laurie A. Weaver and Paul D. Campbell*
Johnson Space Center/SP33

*Lockheed Engineering and Sciences Company

Abstract

As part of the JSC Director's Discretionary Fund Program, a computer-based tool was developed to aid in the estimation of the mass and volume of habitable elements for advanced spaceflight missions. The tool allows its user to define mission and system constraints and generates estimates of the mass and volume of a habitable element required to support the defined mission.

Introduction

The Flight Crew Support Division (FCSD) at JSC supplies the agency's expertise in the integration of human crews into spaceflight missions. In this role, FCSD provides requirements definition, conceptual design, and system development for habitable elements which support space crews.

Advanced missions to the Moon and Mars have been under study by NASA for a number of years. The Habitation Development Tool (HDT) was created by FCSD to support these and future efforts by aiding in the definition of flight crew habitation systems.

Problem Statement

The definition of advanced spaceflight missions is sensitive to the mass and volume of the systems necessary to accomplish them. The habitat for a human crew often represents one of the largest nonpropulsion elements to be launched from Earth; therefore, its mass and volume must be estimated early in the mission definition phase in order to provide information necessary for sizing launch systems.

Approach

The HDT was defined as a means for systematic, consistent estimation of habitable element mass and volume.

A process was defined for the description of a human space mission and the generation of integrated mass and volume estimates for the habitable elements necessary to support that mission. Figure 1 illustrates this process. User and software functions were allocated to define the extent of the automated tool.

Data gathering consisted of a survey of NASA experts in the areas of habitable element design and a literature search for data needed in the HDT. Experts at JSC and other NASA centers were asked to provide data

which describe the mass and volume of the various subsystems of a generic habitable element. These data were collected in the form of data bases and algorithms which relate subsystem sizing to various mission parameters such as crew size, mission duration, and resupply interval.

Detailed data bases of crew accommodations equipment and consumables were derived from the Apollo, Skylab, Space Shuttle, and Space Station Freedom Programs. Refs. 1 and 2 were used as sources of Apollo data. Refs. 3 and 4 were used as sources of Skylab data. Ref. 5 was used as a source of Shuttle data. Ref. 6 was used as a source of Space Station Freedom data. A subset of the Apollo data base is shown in figure 2.

Recent technology development was used as the basis for definition of additional concepts beyond those of past spaceflight programs.

Data describing thermal control, life support, extravehicular activity, health care, structural and mechanical, information management and communications subsystems were provided by experts at JSC.

Data describing the radiation shielding subsystem were extracted from refs. 7-10. This data was used to create a data base of shielding material thickness versus human dose equivalent. Algorithms were defined to interpolate values from the data base dependent on various user inputs and to calculate a shield mass estimate.

Software development of the HDT included integration of the collected data sets and development of the user interface. The data collected were formatted as Microsoft™ Excel tables and macros. The Aldus SuperCard™ application was used to build the user interface. The resulting HDT software is executable by the Apple™ Macintosh™ series of personal computers. Lockheed Engineering and Sciences Company personnel provided all software development. Figure 3 illustrates part of the HDT user interface.

After development, the HDT was tested by users within the JSC Flight Crew Support Division. This testing included simulation of various lunar and Mars mission scenarios.

Results

The HDT has been found to be useful in early, rapid estimation of habitable element mass and volume when used by a person knowledgeable about human support requirements and previous spaceflight programs. This

knowledge is essential in making judgements in the selection of user inputs to the tool and interpretation of its outputs.

The HDT has also been found to be useful for parametric study of the effects of mission parameters on habitable element sizing.

Conclusions

Systems engineering tools such as HDT are valuable in the early phases of program and mission definition. It is expected that the HDT will be used in future studies of advanced human spaceflight.

Several areas of the HDT should be developed further to increase its value. Some of the current subsystem data should be updated to improve its fidelity. Additional user selection options should be provided for alternate technologies in some subsystems. Integration of some subsystem algorithms to improve the simulation of interaction effects should also be performed.

References

- ¹Apollo 16 Stowage List: List A CM Launch Stowage List, 1972. [JSC Internal Report]
- ²Apollo 16 Stowage List: List B LM Earth Launch Stowage List, 1972. [JSC Internal Report]
- ³Skylab Stowage List Command Modules 116, 117, 118 Skylab Missions 1/2, 1/3, 1/4," Jan. 11, 1974.
- ⁴Skylab A Orbital Workshop Mass Properties Status Report Model No. DSV-7," MDC G26445M, McDonnell Douglas, March 1973.

⁵*Shuttle Flight Operations Manual*, Johnson Space Center, Crew Systems, MOD Training Division, JSC-12770, Vol. 12, Rev. A, Aug. 16, 1985.

⁶"Man-Systems Architectural Control Document," SSF Program Office, SSP 30257, Rev. D, Sept. 1991.

⁷*Guidance on Radiation Received in Space Activities*, National Council on Radiation Protection and Measurement, NCRP Report No. 98, July 31, 1989.

⁸Simonsen, L. C., Nealy, J. E., and Townsend, L. W., "Concepts and Strategies for Lunar Base Radiation Protection: Pre-Fabricated Versus In-Situ Materials," 22nd International Conference on Environmental Systems, SAE 921370, July 1992.

⁹Simonsen, L. C., Nealy, J. E., Townsend, L. W., and Wilson, J. W., "Space Radiation Dose Estimates on the Surface of Mars," *Journal of Spacecraft and Rockets*, Vol. 27, No. 4, July-August 1990.

¹⁰Simonsen, L. C., and Nealy, J. E., "Radiation Protection for Human Missions to the Moon and Mars," NASA TP 3079, January 1991.

Acknowledgments

This task was funded by the JSC Center Director's Discretionary Fund. The principal investigator was Laurie A. Weaver of the JSC Human Factors Project Office. Work was performed by Eleanor Cizek, Martha Evert and Jay Hill of the Lockheed Engineering and Sciences Company.

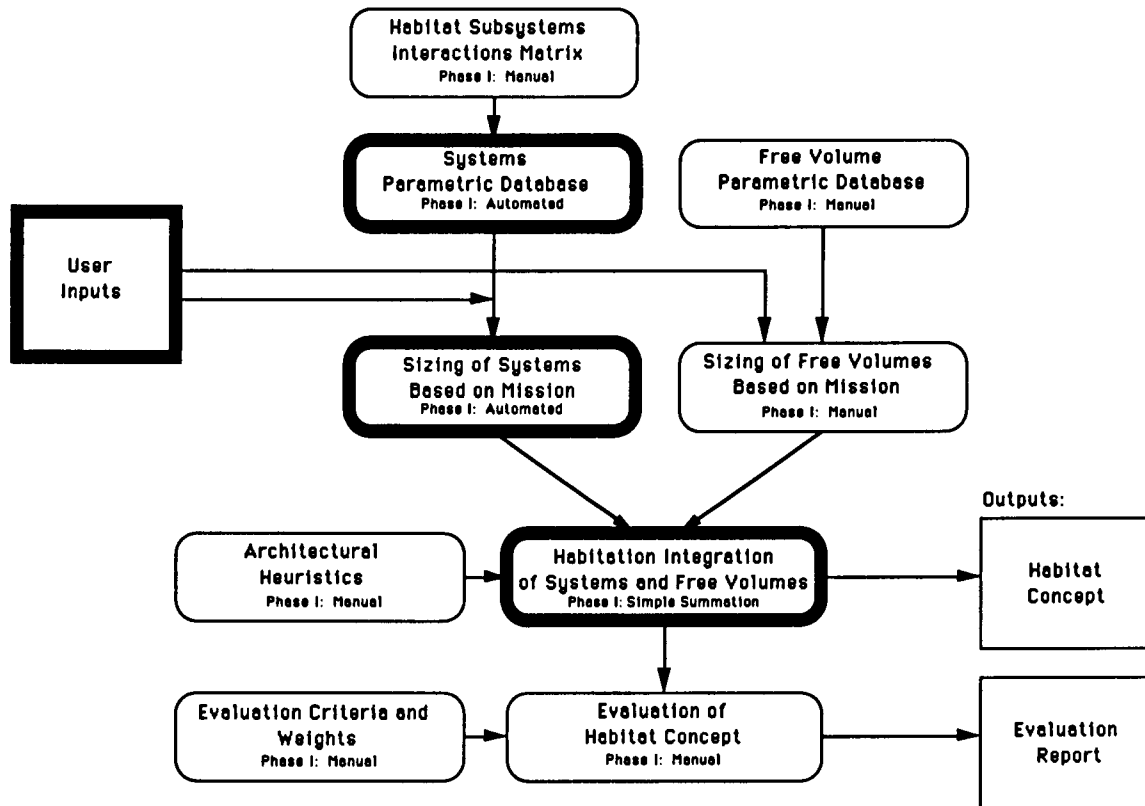


Figure 1. Habitation Development Tool Process.

ITEM	USE RATE ITEMS	PERS	DAY	Unit Size	Wt (lb)	Vol (in ³)
CREW QUARTERS						
CM - Restraint, sleep rope tiedowns	3	0	0	1	0.70	109.96
CM - Restraint assy, sleep right and left	2	0	0	1	3.80	596.95
CM - Restraint assy, sleep center	1	0	0	1	2.30	361.31
CM - Pad, headrest	3	0	0	1	1.10	172.80
CM - Heel restraint	3	0	0	1	1.10	172.80
CM - Container, heel restraints	1	0	0	1	0.10	15.71
CM - Cushion	1	0	0	1	6.00	942.55
CM - Strap, couch, restraint	2	0	0	1	0.30	47.13
LM - sleeping restraint assy	2	0	0	1	2.30	361.31
LM - strap assy for sleeping restraint	2	0	0	1	0.10	15.71
LM - Hammock assy	1	0	0	1	4.00	628.36
LM - Hammock assy	1	0	0	1	3.90	612.65

Figure 2. Subset of Apollo Crew Module Database.

Number of Crew Members	6
Mission Length (days)	500
Resupply Length (days)	250
Safe Haven Length (days)	0
NumberDays of Consumables Stowed in Habitat	14
Free Volume (m3)	108
Residual Volume (m3)	50
Location	Mars

Next Screen **Print Screen** **Quit**

Figure 3. Part of the HDT User Interface.

Human-Computer Interaction Issues In Geographic Information Systems

Frances Mount, Kevin O'Brien,* Steven E. Chrisman,* and Benjamin Beberness,*
Johnson Space Center/SP34

*Lockheed Engineering and Sciences Company

Abstract

Geographic information systems (GISs) are an electronically based means for recording, storing, manipulating, and presenting information tied to geographic coordinates. In interacting with the GIS, the user is confronted with a sample of the information available in the real world and with a computer medium for manipulating that information. It is critical that the information be presented in a meaningful manner and that the communication with the computer be consistent with the task demands of the user. The Human-Computer Interaction Laboratory (HCIL) at JSC is examining GIS user interface issues from the vantage point of developing a working system for JSC's Space Shuttle Earth Observation Project (SSEOP). A description of the development of a prototype system and lessons learned are reported.

Introduction

The HCIL at JSC is currently involved in exploring information processing and computer interface design in GISs. GISs are computer-based tools for gathering, storing, retrieving, analyzing, and presenting geographical information. While the GIS concept has been around for over 20 years, advancements in computing systems have resulted in dramatic increases in the number of users and commercial products in recent years. In a survey of GIS software producers, the 1991-92 International GIS Sourcebook¹ reports a nearly fivefold increase in the number of installed systems since 1985. GIS capabilities include joining information from sources as varied as satellite images, radar, weather reporting stations, and seismic data collection sites with records from direct human observation.

A specific GIS application described by Star and Estes was used to evaluate water availability and the effect of irrigation on crop production in Africa.² The data considered included rainfall amounts, groundwater levels, soil types, and surface slope. Models defining water availability and soil potential were applied to the available data. The results were mapped on an electronic display of African political boundaries. The map distinguishes regions requiring irrigation from those not needing irrigation, and the expected benefit of irrigation, by region. Once the needed data was gathered, these activities could be performed on a single system in a matter of minutes.

The GIS buys the user access, time, and flexibility. Access to information is increased as a result of linking the user to an endless variety of geographically registered data. This data can be filtered, sorted, and parsed according to the users' interests. Automated data access and management not only save the user time in selecting meaningful information, they free the user from time spent gathering appropriate paper-based sources from reference centers or libraries. The user also enjoys the flexibility to revise the selected data set and the information displayed.

Problem Statement

Human-Computer Interaction Concerns for GIS

Given what appears to be an ideal system for data management, analyses, and display, one might ask what remains to be explored? There are two critical interface issues that contribute to the productivity of the GIS user. The first focuses on the information used in a geographical task. The second focuses on the computer as the medium through which the information is viewed.

The information contained in a GIS is a "representation." It is a representation because the information is only a sample or subset of the information available in the real world. Sampling results in changes of scale, reduction of a 3-dimensional object to a 2-dimensional image, reduction of context, and limitation to a finite set of object characteristics. When a map is drawn at a one pixel to one thousand meter scale, each pixel somehow summarizes all the information about the surrounding thousand meter area. That pixel may be defined as having an elevation of 500 feet, while the true elevation in the area represented may range from 300 to 700 feet. In sampling, information is lost and the user is left with questions as to the quality of the sample. Spatial and statistical analysis methods have been developed to provide summaries of sample data and estimates of the error associated with the summary. These methods aid the user in determining whether what can be "known" from the sample is in agreement with what can be "known" from the whole set of information. Geographers and statisticians have dedicated careers to developing optimal ways of sampling and analyzing data.³ GISs can and should provide information about sampling error as demonstrated by An, Moon, and Bonham-Carter.⁴

The second critical GIS interface issue relates to the medium through which the information is presented, the

computer. Computer-based information systems have a great number of differences from paper-based text and picture formats. The differences do not automatically favor the computer version. For instance, if a city planner is using a map of one resolution and decides that not enough area is covered by the map, two options are available: change the map scale or get a bigger sheet of paper. Computer users are limited by the maximum screen size that the system will support and therefore must change the map scale. The reduction in scale and the concomitant loss of information may be undesirable. Other computer-related difficulties arise with defining the language by which work is coaxed out of the computer and in determining ways to optimize data storage and access.

Approach/Method

Prototype and Evaluation of a GIS Implementation

The strategy employed in the HCIL to increase NASA's understanding of GIS interface and application issues involves three activities: literature review, experimentation, and iterative GIS design. Through review of the relevant literature, we have developed a broad understanding of issues, theories, and potential solutions regarding GIS interface design. Experimentation allows us to test theories and solutions in a controlled setting.

Iterative GIS design is an approach in which we learn by developing, testing, and redesigning a system. Specifically, we are working with the Space Shuttle Earth Observation Office at JSC on the implementation of a GIS to support the SSEOP. SSEOP provides support to Space Shuttle Earth-looking photography. SSEOP activities to be supported by the GIS include selecting and describing photographic targets, providing the Shuttle crew with photograph acquisition training, and cataloguing the mission photographs.^{5,6} In order to meet these needs, the GIS development must go through the steps of task analysis, prototype development, system implementation, and user/system performance evaluation.

The information gained from a task analysis of SSEOP tasks was incorporated in three GIS prototypes. The first prototype is geared toward supporting real-time photograph target selection for missions (fig. 1). The information is displayed in both pictorial and text format to aid the user in selecting optimal targets. Pictorial images of the Shuttle orbit are overlaid on variable scale world maps. Access is provided to data sets, including day/night cycles, previous photography, current world events, and incoming requests for photography. The prototype also includes a word processing form on which messages are prepared for delivery to the Shuttle crew.

The second prototype addresses SSEOP's cataloging and indexing (C&I) activities (fig. 2). A large part of the C&I task involves pattern recognition on the part of the

SSEOP staff. The Earth observation photographs are examined and the photograph's center point matched to map coordinates. The coordinates, as well as descriptive information about the photograph are then entered into the data base. The prototype provides access to existing data bases containing flight parameter information and surface pattern information in the form of maps and previous photographs. Functions for altering the map scale, orientation, and geometry aid in the pattern matching task.

The third prototype incorporates training information prepared by SSEOP personnel in a mission specific tutorial for the Shuttle crew. Training information is grouped in four general areas. World maps with orbit track overlays, approach photos from the Shuttle, and an animated Earth horizon view are grouped in one screen to provide information about flight path and viewing perspective (fig. 3). Another screen provides text descriptions of preselected photography sites along with fly-over views and detailed geographical reference information. The third screen presents a timeline of fly-over times of preselected photography sites displayed side-by-side with the mission activity timeline. The final screen contains text descriptions of important geological, meteorological, and oceanographic features; techniques for photographing these features; fly-over information; and a selection of classic Shuttle photographs of the features. Initially, this tutorial package will provide needed preflight reference and pattern recognition materials to crewmembers and in the future could become an onboard package for new and refresher training.

Results

Summary of the Prototype

The prototype GIS has undergone a number of reviews by the HCIL and SSEOP technical personnel. In keeping with the iterative approach, these reviews have resulted in improvements of the prototype. Having achieved broad approval for the concepts and functions demonstrated in the prototype GIS, we are currently in the process of developing the components of the working system. In that process, components will be implemented, usability testing conducted against a baseline measure of task performance, and revisions made to the GIS as warranted.

Conclusions

Preliminary Lessons Learned

While they must be considered preliminary, some statements can be made regarding lessons learned from the GIS project. Perhaps the most basic lesson is that a GIS is conceptually little more than a data base and a graphical means of displaying selected data. It must be remembered that the magic associated with a GIS is not in the image quality of the display. If there is any magic, it

resides in the quality of the information entered into the system and the judicious understanding of information analysis and presentation on the part of the user.⁷ As with statistical packages, the admonition “garbage in, garbage out” applies to the use of a GIS.

The second lesson, following from the first, is that data bases are difficult to construct. The difficulty lies in the formalization of knowledge. When a data base is constructed for some land area, each sample point has a fixed set of characteristics associated with it. Data analysis and presentation is limited to these characteristics or to some combination of them. On the other hand, the human observer confronted with an on-the-spot analysis of the same area may introduce or discard, and combine or separate information in ways limited only by the capacities of the senses and immediate memory. This distinction is nothing new, nor is the study of what characteristics constitute true knowledge about objects. While the world of GIS implementation may not be expected to solve the problem, good GIS implementation will benefit from understanding the issues surrounding concept formation. Xiao and Raafat and Zhang and Giardino have demonstrated how thoughtful use of data structure can be used to verify and structure new data.^{9,10}

The final lessons that have taken form at this point in the project relate to the focus in the GIS world on graphical, or more specifically, pictorial images. The emphasis is placed on the pictorial because GIS graphics rarely consist of bar graphs, pie charts, or x, y coordinate functions. The emphasis is placed squarely on pictures in color and with iconic representation of objects. The difficulties with graphic and pictorial displays are described in detail by Bertin, Tufte and Cleveland.^{11,12,13} While cartographers can provide extensive information on optimal map creation, the assumption that mapmaking is the exclusive benefit from GIS is misguided.^{14,15,16} In the case of the proposed SSEOP GIS, most of the expected productivity gains are related to centralized access to information and implementation of needed data bases. Examples of innovative graphical techniques in GISs include Urban's use of 3-dimensional data representations (not to be confused with 3-dimensional perspective pictures) and Welch's use of stereographs to present elevation and distance data.^{17,18} In general, the user who takes into account the breadth of information display techniques will be much more successful than those who fixates on pictures.

References

- ¹Parker, H. D. (ed.), *1991-92 International GIS Sourcebook*, GIS World, Inc., Fort Collins, CO, 1991.
- ²Star, J., and Estes, J., *Geographic Information Systems and Introduction*, Prentice-Hall, Inc., Englewood Cliffs, NJ, 1990.
- ³Frank, A., and Goodchild, M., “Two Perspectives on Geographical Data Modeling,” Univ. of California, Santa Barbara, National Center for Geographic Information and Analysis, Report No. 90-11, Santa Barbara, CA, 1990.
- ⁴An, P., Moon, W., and Bonham-Carter, G., “On Knowledge-Based Approach of Integrating Remote Sensing, Geophysical and Geological Information,” *Proceedings of the International Geoscience and Remote Sensing Symposium '92*, Vol. 1, 1992, pp. 34-38.
- ⁵Nelson, R., Willis, K., Daley, W., Brumbaugh, F., and Bremer, J., “Cataloging and Indexing: The Development of the Space Shuttle Mission Database and Catalogs from Earth Observations Hand-Held Photography,” *Proceedings of the International Geoscience and Remote Sensing Symposium '92*, Vol. 1, 1992, pp. 155-157.
- ⁶Chambers, M., Jaklitch, P., Helms, D., and Whitehead, V., “Ground Support for Space Shuttle Earth Observations by the NASA Environment Remote Sensing Analysis Facility (EARSAF),” *Proceedings of the International Geoscience and Remote Sensing Symposium '92*, Vol. 1, 1992, pp. 158-160.
- ⁷National Center for Geographic Information and Analysis, *Annual Report*, Univ. of California, Santa Barbara, Santa Barbara, CA, 1991.
- ⁸Smith, E., and Medin, D., *Categories and Concepts*, Harvard Univ. Press, Cambridge, MA, 1991.
- ⁹Xiao, Q., and Raafat, H., “Remote Sensing Image Classification by a GIS Guided Spatial Analysis,” *Proceedings of the International Geoscience and Remote Sensing Symposium '92*, Vol. 2, 1992, pp. 1606-1608.
- ¹⁰Zhang, K., and Giardino, J., “Expert System Based on Knowledge Extraction From a GIS,” *Proceedings of the International Geoscience and Remote Sensing Symposium '92*, Vol. 1, 1992, pp. 319-321.
- ¹¹Bertin, J., *Semiology of Graphics*, Univ. of Wisconsin Press, Madison, WI, 1983.
- ¹²Tufte, E., *The Visual Display of Quantitative Information*, Graphics Press, Cheshire, CT, 1983.
- ¹³Cleveland, W., *The Elements of Graphing Data*, Wadsworth Advanced Book Program, Monterey, CA, 1985.
- ¹⁴McCleary, G., Jr., “An Effective Graphic ‘Vocabulary’,” *IEEE Computer Graphics & Applications*, Vol. 3, No. 2, 1983, pp. 46-53.
- ¹⁵McCleary, G., Jr., Jenks, G., and Ellis, S., “Cartography and Map Displays,” *Pictorial Communication in Virtual and Real Environments*, edited by S. Ellis, M. Kaiser, and A. Grunwald, Taylor and Francis, London, 1991, pp. 76-96.
- ¹⁶Price, K., and Hodgson, M., “Onward and Forward,” *Photogrammetric Engineering & Remote Sensing*, Vol. 58, 1991, pp. 1553-1555.
- ¹⁷Urban, R., “Space Exploration Mapping: The Use of GIS to Chart Our Best Course to First Contact,” *Proceedings of the International Geoscience and Remote Sensing Symposium '92*, Vol. 1, 1992, pp. 41-43.

¹⁸Welch, R., "Desktop Mapping With Personal Computers," *Photogrammetric Engineering and Remote Sensing*, Vol. 55, 1989, pp. 1651-1662.

JSC, Houston, Texas. The work was conducted in the Flight Crew Support Division's Human-Computer Interaction Laboratory at JSC. The authors wish to thank the members of the Space Shuttle Earth Observations Project for their cooperation in this work.

Acknowledgments

This work is supported by contract NAS9-17900 from the National Aeronautics and Space Administration,

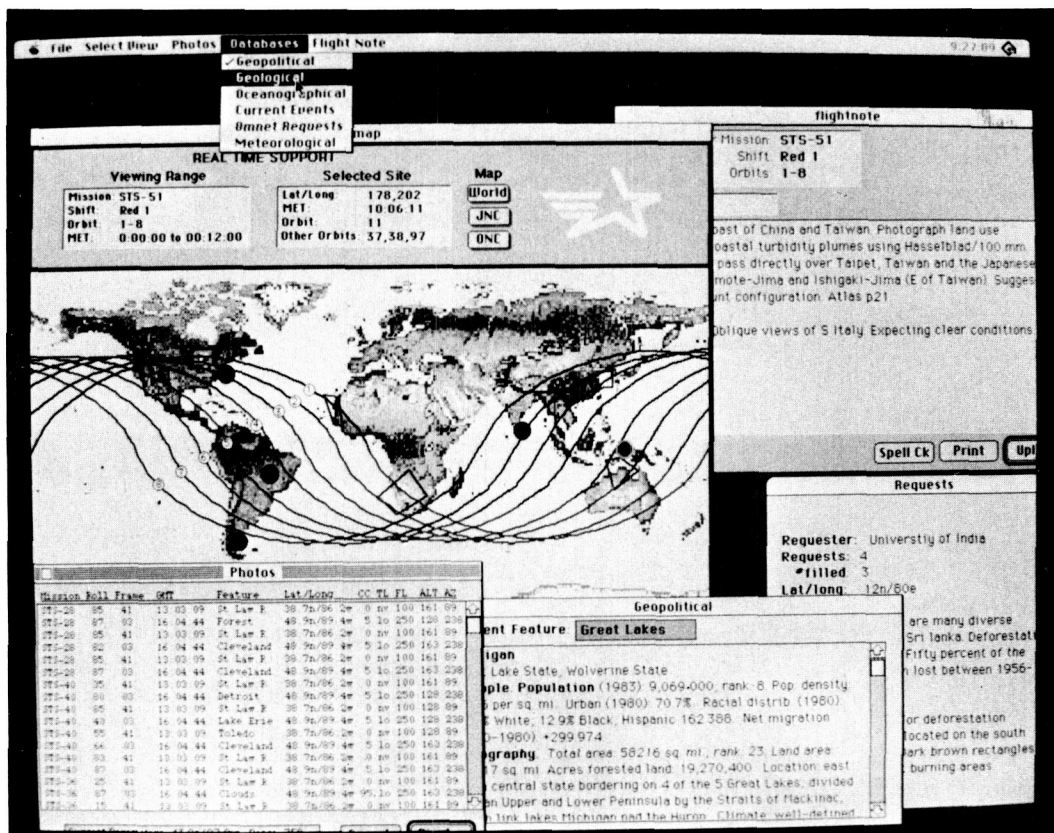


Figure 1. GIS Prototyping for SSEOP Real-Time Photograph Target Selection. Windows Include Reference Map, Flight Note Form, and Data Bases, Including Previous Photographs, Geopolitical Information, and Outside Photograph Requests.

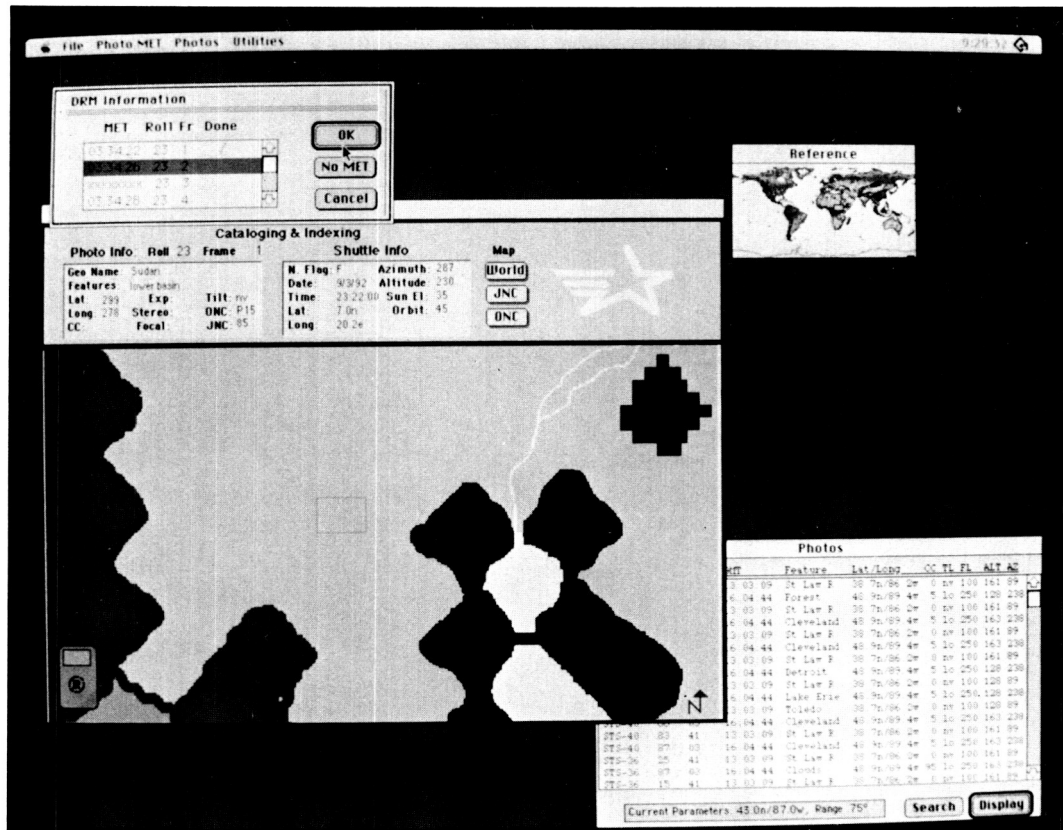


Figure 2. GIS Prototype for SSEOP Cataloging and Indexing. Windows Include Film/Mission Reference Information, Map Reference, World Reference, and Previous Photograph Data Bases.

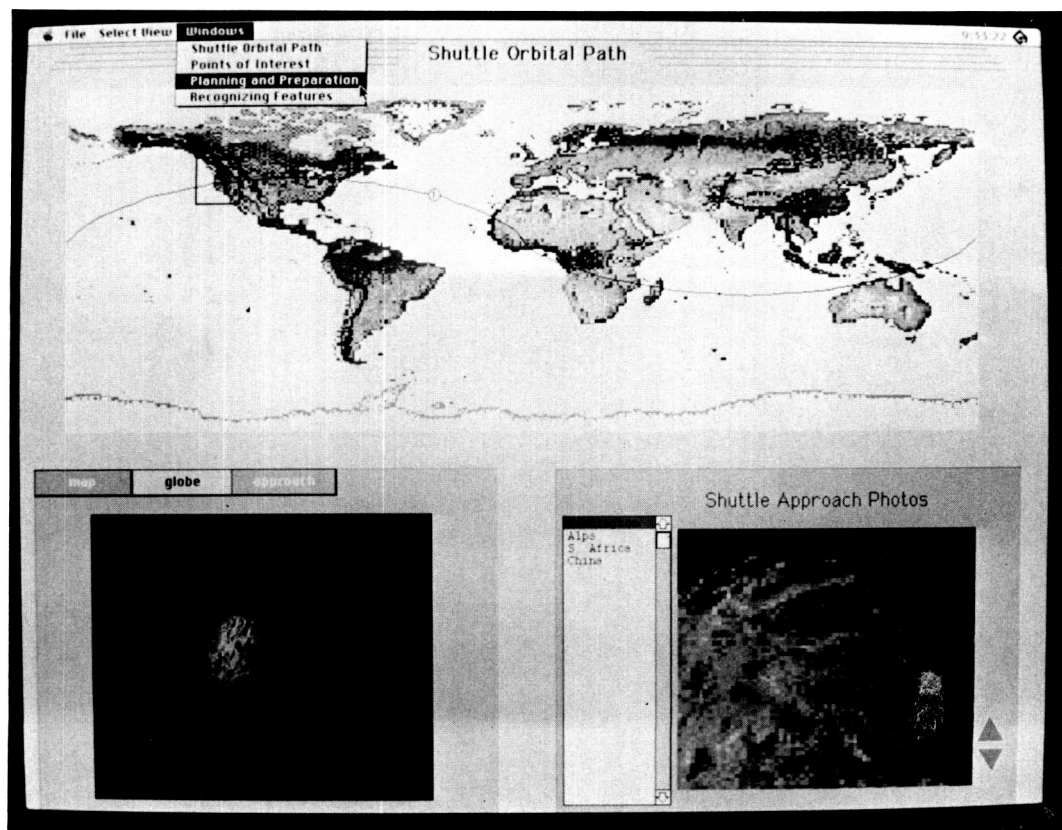


Figure 3. GIS Prototype for Crew Training. Windows Include Mission Orbital Paths as Represented on a World Map, 3-Dimensional Globe and in Previous Earth Observation Photographs.

Loads Produced by a Suited Operator Performing a Tool Task Without the Use of Foot Restraints

Glenn K. Klute, Jeff Poliner,* and Sudhakar Rajulu*
Johnson Space Center/SP
*Lockheed Engineering and Sciences Company

Abstract

The space program is seeing an increased number of extravehicular activities (EVAs); thus, it is of interest to NASA to know the capabilities that astronauts have in performing their EVA tasks. Also of interest are the requirements on equipment used during the EVAs. Some EVAs do not allow for the use of foot restraint devices to hold the astronaut's body in position; rather, handrails are used. This study documented the loads produced by subjects performing a tool task without the use of foot restraints. Six subjects, all wearing a Shuttle extravehicular mobility unit (EMU) space suit, participated in this study aboard an aircraft flying parabolic trajectories, which produces brief periods of weightlessness. The task was to perform a maximal effort with one hand holding a 25 cm wrench. The subject's other hand grasped an EVA handrail. The torque on the wrench was measured, as well as the forces and moments transmitted to the handrail. Peak torques during the wrenching task were on the order of 70-80 Nm. Peak forces were on the order of 100 N normal to the surface and 200 N in a tangential direction. Greater torque and loads were produced when using the tool in a direction toward the midline of the subject's body than were produced away from the midline. These results can be applied to the development of tasks and equipment for use during EVAs.

Introduction

Because of an increase in the number of EVAs that astronauts will be performing in the coming years, NASA is interested in determining the capabilities of a suited astronaut working in a weightless environment.

Traditionally, an astronaut involved in EVA tasks is held in position by a portable foot restraint (PFR). The PFR provides adequate restraint to counter the forces generated from the use of a wide variety of powered and nonpowered EVA tools. In certain situations, it may be advantageous to perform operations while free floating. This would eliminate the need for a PFR setup. In those situations, the astronaut would have to grasp the EVA handrail in one hand and perform the task with the other.

Some work has been done at NASA investigating the capabilities of suited astronauts to perform certain tasks while in foot restraints. However, very little information is available concerning their abilities to perform duties without the use of foot restraints. In addition, there is interest in gathering information concerning the loads

transmitted to the EVA handrail when performing this type of task.

Many of the tool tasks which astronauts are expected to perform can be classified as torquing tasks, in which they must use a wrench or similar tool to apply a torque to a fitting or fastener.

This study was intended to examine the loads produced by a suited subject performing a torquing task with a single EVA handrail and no foot restraints.

Specifically, the purposes of this investigation were to

- Determine the amount of torque which can be produced by a suited subject in a weightless environment without the use of foot restraints
- Measure the loads applied to the supporting hand while performing a torquing task in zero g without the use of foot restraints
- Determine differences in the loads produced while performing a torquing task between individuals' dominant and nondominant sides, and between different directions of tool rotation (clockwise versus counterclockwise)

Methods

Six male subjects participated in this study including four astronauts and two nonastronauts. All of them were experienced in performing tests while wearing pressurized suits. The subjects had each passed an Air Force Class III physical examination and had met the requirements for the physiological training program, as prescribed by NASA. Their heights ranged from 162 cm to 180 cm with a mean of 175 cm and their masses varied from 61 kg to 77 kg with a mean of 70 kg. While all of them were right-handed, both hands were tested in the study.

Tests were conducted aboard NASA's KC-135 aircraft. This is a modified jet which is capable of flying parabolic arcs, during which the passengers and equipment within the plane experience virtual zero g. Each parabola lasts approximately 25 s.

Figure 1 depicts the work site arrangement. A unistrut framework, approximately 190 cm by 55 cm, was attached to the aircraft floor. An AMTI (Model #OR6-6-1000, Advanced Mechanical Testing, Inc., Newton, Massachusetts) force platform was placed at the center of the frame. An EVA handrail was bolted to the center of the force platform. On one side of the EVA handrail was a fixed 7/16 in bolt head, located 61 cm (24 in.) from the center of the forceplate. An instrumented torque wrench (Model #1150-200, GSE, Inc., Farmington Hills, Michigan) was used to measure the torque output. The

wrench had a padded handle located 24.8 cm (9.8 in.) from the tool end.

Amplifiers (Model #2120A, Measurements Group, Raliegh, North Carolina) from the four tri-axial load cells in the force platform gave outputs of three orthogonal components of force and three orthogonal components of moments. The coordinate system of the forceplate was such that with the subject positioned as in figure 2, the Y-axis was parallel to the longitudinal axis of his body, the X-axis corresponded to the mediolateral axis of his body, and the Z-axis was perpendicular to the coronal plane of his body. The six force platform signals, along with the analog output from the instrumented torque wrench, were sampled digitally by a data acquisition system at a rate of 250 Hz.

During the flight, prior to the start of the zero-g parabolic arcs, the subject donned the Shuttle EMU with the help of suit technicians. The suit was then pressurized to 4.3 psi. At the onset of zero g, the subject was assisted to the work site by two people where the torque wrench was attached to the fixed bolt fitting with the arm of the wrench parallel to the longitudinal axis of the subject's body. The subject was instructed to produce as much torque in the wrench as he could, using the handle 24.8 cm (9.8 in.) from the end. His other hand held onto the handle mounted on the force platform. He first rotated the torque wrench in one direction and held it there for several seconds; he then rotated the wrench in the opposite direction and held it there for several seconds. Forceplate and torque wrench data were collected during the zero-g interval.

A repeated measures design was used in this study. The independent variables included the hands (dominant versus nondominant) and the directions in which the force was applied (inward versus outward rotation). Each subject performed two trials for each hand/direction combination. The dependent variables included the three axial components of force, the three components of the moment, the resultant shear force magnitude and direction, and the torque output from the wrench.

Raw data were in the form of seven channels of time-based data for each parabola (three forces and three moments from the forceplate, and the torque from the torque wrench) for the duration of the zero-g interval. The window of data corresponding to the actual performance of the task was determined from plots of the data and from the video recordings. Within each window, the peak magnitude for each of the seven channels was obtained. The two components of force parallel to the direction of movement (X and Y) were combined to calculate a resultant shear force magnitude and direction. Thus, there were a total of nine dependent variables. For comparison purposes, necessary manipulation of the data was performed in order to change the coordinate system from one based on the forceplate to one based on the subject.

From the two trials for each conditions, the larger value for each of the nine dependent variables was taken

as representative for that subject. Statistical analyses focused on eliciting the differences between the dominant and nondominant hand (left versus right) as well as between different directions of movement. The responses of each dependent variable to the test variables (hand dominance, direction) were first examined descriptively. Next, the dependent variables were tested for statistical significance using various statistical tests. A multivariate analysis of variance (MANOVA) was performed to determine the collective response of the dependent data to changes in each one of the test variables. Each MANOVA was followed by an univariate analysis of variance (ANOVA) to determine the influence of all test variables and their interactions. Finally, the Ryan-Einot-Gabriel-Welsh test criterion was used to determine whether there were significant variations within the levels of each test variable. A significance level of 0.05 was chosen to determine whether the analyses were significant or not.

Results/Discussion

Table 1 below presents the group results from the experiment. The column labels indicate the test conditions: side and direction of rotation. "Left" and "Right" indicate the arm that was used to generate the torque with the wrench. Recall that all subjects were right-dominant. "In" and "Out" indicate the direction of rotation, relative to the midline of the subject's body. An inward movement with the right arm was a clockwise rotation; outward was counterclockwise. Similarly, an inward movement with the left arm was a counterclockwise rotation; outward was clockwise.

The first row presents the maximum applied torque (in Newton-meters) from the tests as measured by the instrumented torque wrench. The remaining data are from the forceplate connected to the handrail.

Statistical analysis of the data revealed that there was no significant difference between using the left and right hands. However, the two directions of rotation were significantly different in the measures of: X force, X moment, Z moment, torque output, and the resultant shear force. All of these variables were found to be significantly greater during inward motion than during outward motion. With regard to the Y force and moment and the Z force, there were no significant differences between the inward and outward directions.

The greatest component forces were in the X direction along the mediolateral axes of the subjects' bodies. This was expected since the X axis was the axis along which the force was applied to the wrench. Magnitudes of the X component of force were approximately 171 N for outward rotations and 223 N for inward rotations. The peak components of force in the Y and Z directions were relatively low and fairly consistent across the test conditions. The peak Y force, which was parallel to the operator longitudinally, ranged between 68 and 111. The peak Z force averaged around 68 N.

As expected, the greatest moment occurred around the Z axis (30 Nm) and the lowest moment occurred around the X axis (9 Nm). The peak Y moment remained fairly constant around 18 Nm. The peak X and Z moments were significantly affected by the direction of rotation. On an average, the peak X moment dropped from 16.7 Nm to 9.9 Nm when the direction changed from inward to outward rotation (decrease of 41%); the peak Z moment dropped from 29.2 Nm to 14.6 Nm (50%). The shear force was also significantly higher during inward rotation than during outward rotation. The shear force averaged about 226 N and 169 N during inward and outward rotations, respectively (decrease of 25%). Finally, the maximum amount of torque was about 72 Nm during inward rotation and about 46 Nm during outward rotation.

Conclusions

In summary, suited operators performing a wrenching task in a weightless environment without the use of foot restraints generated approximately 72 Nm of torque. During this task, the loads transmitted by the other hand

to the supporting structure were approximately 78 N in a normal direction and 226 N in a tangential direction. Torques and loads were significantly less when pulling the wrench inwards than pushing outwards. These results can be applied to the development of tasks and equipment for use during EVAs.

In summary, suited operators performing a wrenching task in a weightless environment without the use of foot restraints generated approximately 72 Nm of torque. During this task, the loads transmitted by the other hand to the supporting structure were approximately 78 N in a normal direction and 226 N in a tangential direction. Torques and loads were significantly less when pulling the wrench inwards than pushing outwards. These results can be applied to the development of tasks and equipment for use during EVAs.

Acknowledgments

This study was supported by contract NAS9-17900 from the National Aeronautics and Space Administration, and was conducted by the Anthropometry and Biomechanics Laboratory.

Table 1. Averaged Subject Data for the Torquing Experiment. Force Values are in Newtons; Moments and Torques are in Newton-Meters. Standard Deviations are Given within the Parenthesis. Values are the Average of the Six Subjects' Greatest Efforts.

<u>VARIABLE</u>	<u>LEFT - IN</u>	<u>LEFT - OUT</u>	<u>RIGHT - IN</u>	<u>RIGHT - OUT</u>
Peak Torque	67.4 (10.0)	42.5 (13.0)	75.6 (18.3)	48.8 (22.1)
Peak Force X	209.8 (19.3)	170.2 (72.7)	236.1 (26.5)	172.3 (67.1)
Peak Force Y	110.7 (20.4)	98.5 (42.6)	90.0 (35.3)	68.2 (31.5)
Peak Force Z	90.4 (57.6)	51.2 (13.8)	65.7 (45.7)	65.8 (38.9)
Peak Shear Force	212.4 (16.4)	164.7 (78.0)	240.1 (24.8)	173.9 (66.8)
Angle at Peak Shear	19.4 (4.1)	22.6 (7.3)	11.9 (4.5)	9.4 (12.3)
Peak Moment X	18.2 (5.4)	8.8 (2.5)	15.1 (3.0)	10.9 (6.5)
Peak Moment Y	17.0 (1.9)	16.4 (8.3)	20.5 (2.0)	18.8 (11.8)
Peak Moment Z	29.7 (4.1)	15.0 (8.1)	28.7 (6.3)	14.2 (6.7)

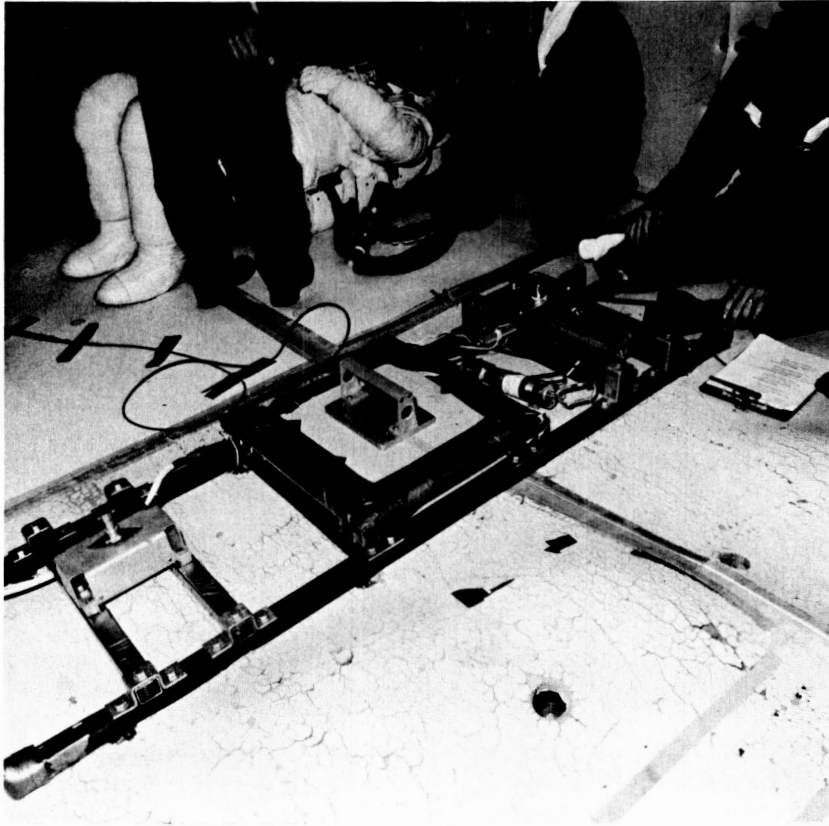


Figure 1. Work Site Arrangement.

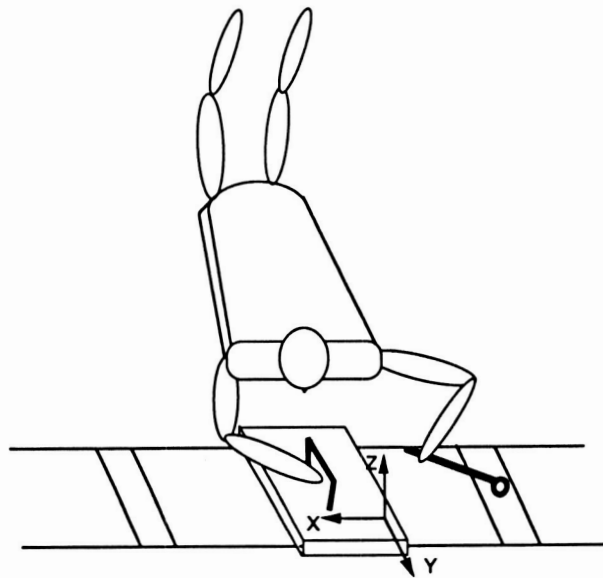


Figure 2. X, Y, and Z Axes.

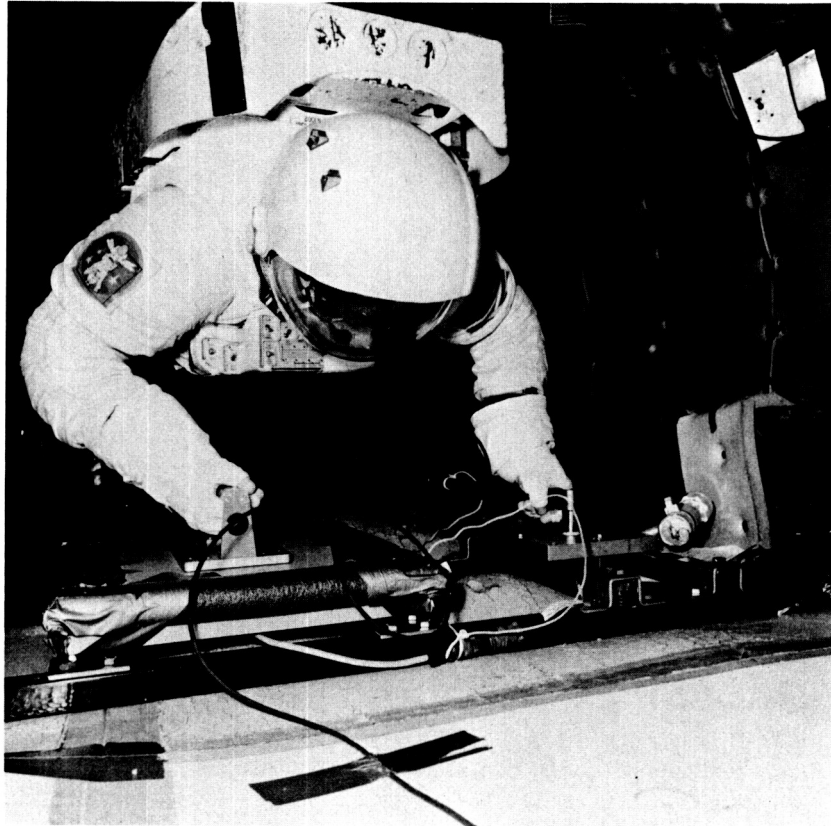
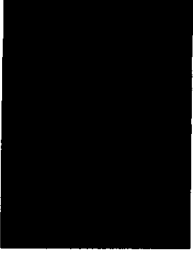


Figure 3. Picture of Subject Performing Torquing Task.



*Space
Systems
Technology*



Tunable Plasma Rockets with RF-Heating and Superconducting Thrust Chambers

Franklin R. Chang Diaz and T. F. Yang*
Johnson Space Center/CB
*M.I.T. Plasma Fusion Center

Abstract

Theoretical and experimental research in tunable plasma propulsion (variable specific impulse/thrust at constant power) has been carried out over the last decade. Important developments of this research include: the demonstration of an increased radio frequency (RF)-to-plasma coupling efficiency (68%) as a result of antenna design and relocation, as well as wave launching techniques; the theoretical demonstration of plasma-field detachment at the rocket exhaust; and the experimental validation of predicted performance parameters. Other results include the estimation of attractive power specific mass or "alpha" values of 8 kg/kW, including the power system, and the use of off-the-shelf components. Substantial improvements to these values are expected with emerging technologies in high-temperature superconductivity and RF-confinement.

Introduction

One of the most important issues in connection with human interplanetary travel is the crew's prolonged exposure to weightlessness as well as the high radiation dosage that accrues during long voyages. From this point of view, it becomes crucial to achieve a minimum trip-time and to extend the ship's acceleration schedule consistently with human and power plant limitations. Flexibility in these well-known "trajectory variables," however, remains limited by the capabilities of conventional (constant specific impulse (I_{sp})) chemical engines. Trip-times remain "high" and are severely restricted by payload and fuel constraints while acceleration time is negligibly short compared to total trip-time. Intensive research in the development of higher power and I_{sp} electric and thermal rockets (including nuclear rockets) has ameliorated the payload-to-fuel limitation while somewhat reducing the trip-time. These advances have also prompted this present reexamination of variable propulsive "schedules" in the operation of "power-limited" rockets; these advances promise still better performance, with extended beneficial acceleration profiles and consequent reductions in trip-time.

Problem Statement

It is well known that, when a rocket engine is limited by power, the attainment of high I_{sp} does not necessarily give the best results.¹ Under such conditions, a high I_{sp}

comes only at the expense of thrust. While the fuel requirement to achieve the trip may be drastically reduced over a low I_{sp} case, the trip-time rapidly increases. Actually, for a power-limited rocket, the best compromise between thrust and I_{sp} is one where the two quantities are allowed to vary and be continuously "tuned" to the conditions of flight; such is the case in the present approach.

In a typical case, the rocket starts from orbit around the planet of origin at a high thrust/low I_{sp} . As the vehicle moves away from the gravity well, I_{sp} increases while thrust decreases at constant power. At some intermediate point, the profile reverses and the rocket decelerates, under power, and is captured by the destination planet. Optimum I_{sp} variations can be very high (tens of thousands of seconds), depending on the particular mission. If these conditions are achieved, trip-times on the order of 3 months can be achieved for missions to Mars. Additionally, optimization of the acceleration profile leads to gains in payload fraction over the conventional chemical or nuclear thermal rocket. These results (Irving and Blum¹) are reproduced in figure 1.

New Technologies

Hitherto unattainable exhaust properties are now possible with the advent of new technologies in plasma heating and containment that were developed for the Controlled Thermonuclear Fusion Program. Moreover, recent developments in high-temperature superconductivity have pushed these embryonic concepts even further into the realm of engineering design and field test.²

To this end, over the past decade our group has been engaged in the development of a variable I_{sp} , RF-heated electrothermal rocket based on the technology of tandem mirrors.³ The particular approach considered here, because it is not a fusion concept, has permitted a substantial relaxation in the physics requirements on plasma density and temperature as compared with its fusion counterpart. In fact, the tandem mirror—an open-ended linear device that suffers from end-loss limitations in fusion—becomes particularly well suited as a variable I_{sp} rocket by virtue of such innate "leakage." Moreover, experiments performed in the closing years of the U.S. mirror program revealed an intrinsic axial asymmetry and plasma flow in these devices that we have sought to exploit.

PRECEDING PAGE BLANK NOT FILMED

Approach

In the present system (shown schematically in figure 2), thrust is produced in a three-stage process of: (1) cold plasma injection at high density, (2) high power amplification via ion cyclotron resonance heating, and (3) plasma expansion and magnetic field detachment in a two-stage hybrid (magnetic/conventional) nozzle. The magnetic system itself is an asymmetric, superconducting derivative of the tandem mirror but with greatly relaxed technical requirements over those of its predecessor (i.e., being able to confine plasmas radially that are not thermonuclear in nature) and, hence, is completely attainable with present technology. This particular configuration offers several advantages over more conventional plasma propulsion schemes; among these are:

- Variable thrust and I_{sp} at constant jet power: allows continuous exhaust optimization over the entire mission. This reduces the transit time for a given fuel/payload allocation over that obtainable with a constant I_{sp} at the same power.
- Electrodeless design: Relaxes many of the material constraints imposed on plasma devices where the fluid is heated or accelerated by means of physical electrodes that are immersed in the hot plasma. This relaxation, in turn, allows a greater power density.
- Magnetic and gas-dynamic insulation: Also relaxes materials requirements on the first wall of the thruster and is consistent with very high ($> 1 \text{ kW/cm}^2$) power densities. In addition, the established hypersonic coaxial gas layer provides a mechanism for collisional detachment of the plasma flow from the guiding magnetic field at the exhaust.

Results

One of the main experimental results has been the demonstration of a high RF-to-plasma coupling efficiency (68%). This efficiency is a result of relocating the main antenna to a point at the inboard side of the central cell magnetic mirror. This location allows the RF wave to undergo maximum damping as the wave travels to the center of the device. The effect, which is called Beach heating, was theoretically predicted and experimentally confirmed in our laboratory.⁴ These results are shown in figure 3.

In terms of the dynamics of plasma exhaust, extensive theoretical and numerical work has been carried out.⁵ Studies show that the presence of a well-established coaxial, hypersonic, neutral boundary layer can induce the plasma to detach from the guiding magnetic field. Detachment efficiency is expected to be a function of the "pitch angle" of the neutral jet with respect to the main plasma flow. Numerical plume dynamics for three cases are shown in figure 4: (1) free plasma expansion along the field with no gas injection; (2) plasma flow that is limited by the presence of purely axial gas flow; and

(3) plasma flow that is limited by the injection of a radial jet. A modification of the third option will be used during experimental verification.

Additional laboratory experiments are also providing data on the operating characteristics of this device. These data fit very well with predicted performance curves. For example, a low-density, low-power (9.4 kW) case study is shown in figure 5 for hydrogen at 68% efficiency; the three discrete points are experimental values. Additional measurements at higher densities and lower temperatures need to be carried out to validate fully the predicted performance envelope. The rocket performance envelope scales linearly with power; hence, thrust values of thousands of Newtons are obtainable for the multimewatt systems proposed for Mars.

Careful engineering studies and implementation of new technologies in magnetic vectoring and expansion nozzles have demonstrated that these systems can be made competitive in terms of their power specific mass or "alpha." Values of 8 kg/kW or less, including the nuclear power system, can be predicted.⁶ Additionally, new developments in monolithic superconducting systems and in the use of high voltage and regenerative liquid hydrogen designs may reduce this value further.^{7,8}

Finally, two emerging technologies are also being examined for potential application to this system: high-temperature superconductivity and RF-plasma confinement. New developments in these areas would strongly influence the success of this rocket. For example, the use of newly developed monolithic "magnetic replicas" to trap intense (> 2 tesla) static magnetic fields are being explored, because they would greatly simplify the superconducting coil design and further reduce the total weight. Our group is also investigating the use of RF energy-not just to heat the plasma, but to introduce additional radial confinement with consequent increases in the available plasma pressure. This is a collaborative effort led by Drs. Roger Remy and Jean Luc Cambier of ACC Inc., Dr. Steven Howe of the Los Alamos National Laboratory, and technical personnel from the Phillips Laboratory and the University of New Mexico.

Conclusions

Ongoing research in this new propulsion technology has produced several advances that open the path for a flight demonstration experiment. First, experimental results of RF-to-plasma power coupling show a much greater plasma power coupling efficiency than was previously estimated (68% vis-a-vis 55%). This is a result of refinements in the theory of RF plasma heating as well as in modifications in antenna positioning within the magnetic chamber. Second, engineering estimates of specific power or "alpha" of the system point to an attractive scaling at 8 kg/kW, of which the thrust system represents a negligible fraction. These conservative estimates, which use off-the-shelf equipment, may be

further improved for longer systems through the use of new technologies in superconductivity and RF confinement as well as through the use of power at high voltage. Finally, experimental measurements of plasma properties at high I_p follow the predicted values.

Despite these advances, further experiments need to be performed to validate the theory at lower I_p . Also, measurements need to be carried out that are designed to demonstrate the successful detachment of plasma from the guiding magnetic field at the exhaust. These experiments are being planned at this time.

References

- ¹ Irving, J. H., and Blum, E. K., Comparative Performance of Ballistic and Low-Thrust Vehicles for Flight to Mars, an unpublished lecture, 1958.
- ² Chang-Diaz, F. R., "Performance of an RF-Heated, Superconducting Plasma Rocket, INSTEP Experiment Proposal," NASA/Johnson Space Center, Houston, TX, submitted Jan. 14, 1993.
- ³ Logan, B. Grant, "Summary of the Mars Tandem Mirror Reactor Design," Lawrence Livermore National Laboratory, UCRL-89296, Sept. 1983.
- ⁴ Peng, Scott, "ICRF Wave Propagation and Plasma Coupling Efficiency in a Linear Magnetic Mirror," Ph.D. Dissertation, M.I.T., Cambridge, MA, 1991.
- ⁵ Krueger, W. A., "Plasma and Neutral Gas Jet Interactions in the Exhaust of a Magnetic Confinement System," Ph.D. Dissertation, M.I.T., Cambridge, MA, 1990.

⁶ Chang-Diaz, F. R., and Yang, T. F., "Design Characteristics of the Variable I_p Plasma Rocket," IEPC-91-128, Oct. 1991.

⁷ Ignatiev, Alex, and Chu, Paul, University of Houston, private communication, 1993.

⁸ Bromberg, L., Bobrov, E. S., and Williams, J. E. C., Superconducting Bitter Magnets, M.I.T. Plasma Fusion Center, private communication, 1990.

Acknowledgments

The authors would like to acknowledge the valuable contributions from Mr. Harvey Lander of the M.I.T. Plasma Fusion Center in gathering experimental data and in the operation of the device. Also, our gratitude goes to Dr. Kumar Krishen of the NASA New Initiatives Office for his valuable insight in planning the space-test experiment. Our special thanks are extended to Mr. Aaron Cohen and Capt. John W. Young of JSC, Dr. Robert Vondra of the Phillips Laboratory, and Mr. G. W. S. Abbey and Steven Harrison of the National Space Council for their continuous encouragement and support. The uninterrupted research we have enjoyed has been owing to the timely work of Mr. Earl VanLandingham and Mr. Donald Puddy of NASA and of Drs. Len Caveny and Mitat Birkan of the AFOSR. This work was funded by NASA and the United States Air Force Office of Scientific Research.

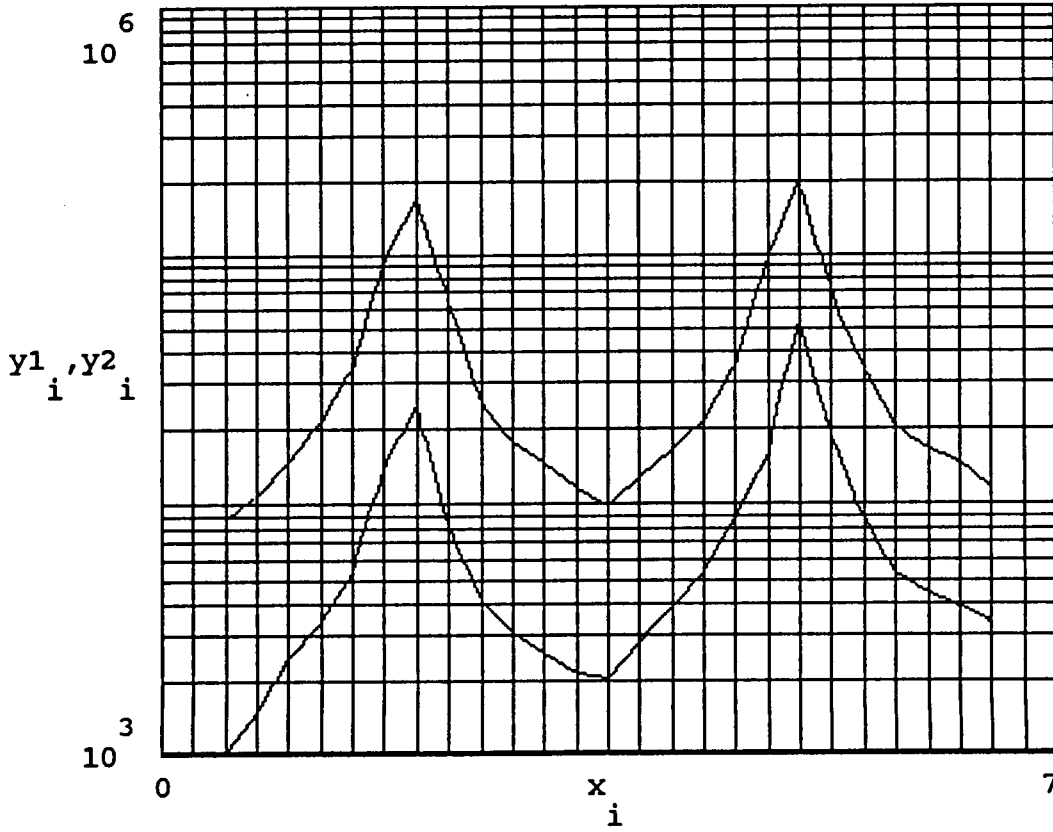


Figure 1. I_{sp} (seconds) as functions of trip-time (months) for round-trip mission to Mars. Upper curve is for “alpha” = 1 and lower curve is for “alpha” = 10.

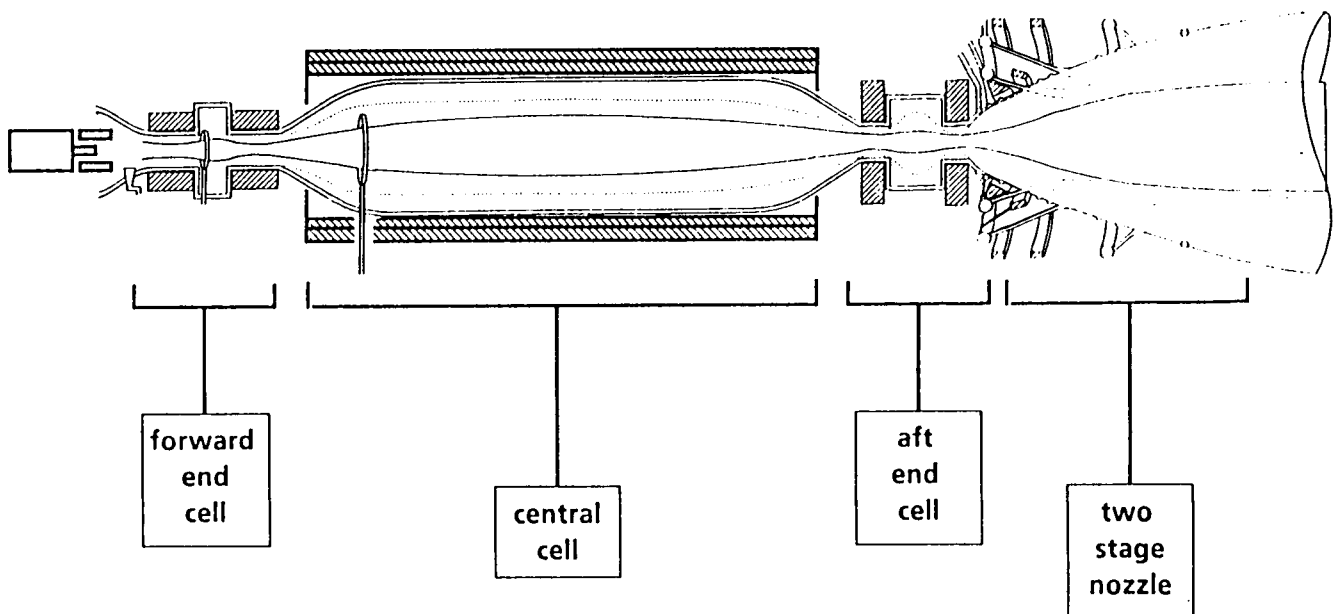


Figure 2. Thrust is Produced in a Three-Stage Process.

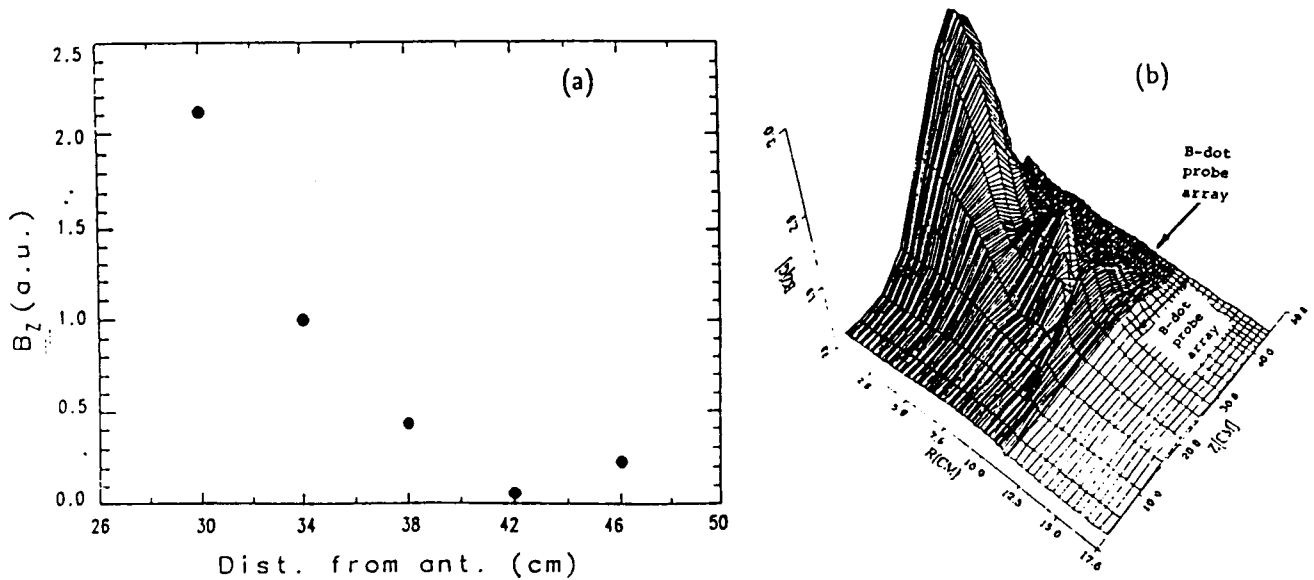


Figure 3. Axial B_z Profile at a Fixed Radius for Type II Discharge (a) and the Trimetric View of B_z from Beach code (b). The Wave is Damped (or Absorbed) as It Is Approaching the Resonance Plane.

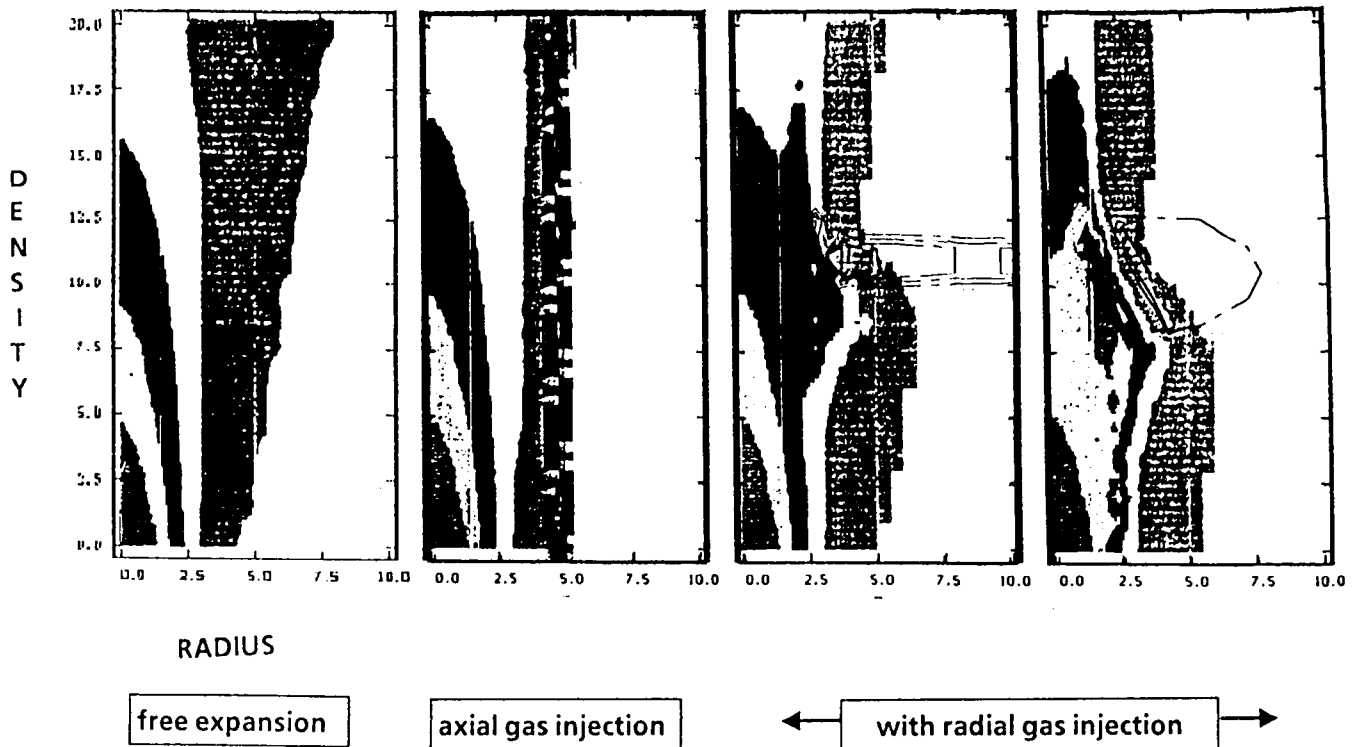


Figure 4. Plume Dynamics and Magnetic Field Detachment.

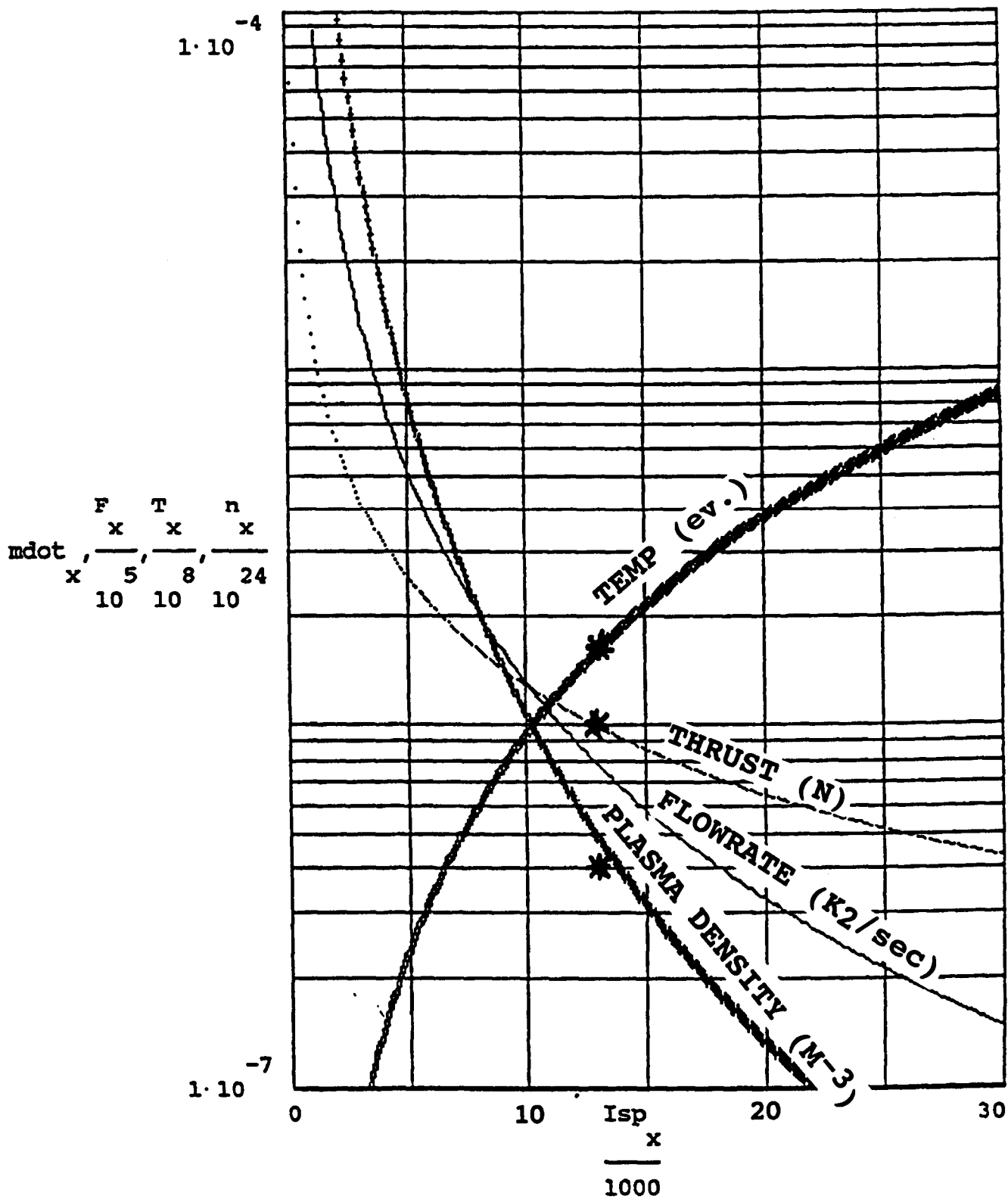


Figure 5. Performance Parameters for 9.4 kW at 68% Efficiency, Hydrogen.

Improved Power Tool Development

Ralph J. Marak
Johnson Space Center/EC

Abstract

The program described in this report was initiated to develop a prototype power tool to replace the unit now in the National Space Transportation System (NSTS) Program. The unit developed under this program is a hand-held, battery-powered unit that has simultaneous torque and revolution controls. A digital readout provides a visual indication to the operator regarding desired torque/number of revolutions that the unit is set to provide and actual torque/number of revolutions produced. Torque accuracies of 10% over the full range of 10 to 200 in-lbs were obtained. The unit uses a strain gauge system to measure the actual torque output and provides a feedback to a magnetic particle clutch to limit the torque produced from the motor.

Introduction

A significant number of tasks performed by an extravehicular activity (EVA) crewmember during the maintenance and repair of a payload or satellite require the removal of various types of threaded fasteners. A crewmember fatigues rapidly while performing these multi-rotational tasks in the Weightless Environment Training Facility. During Shuttle mission Space Transportation System (STS)-41B, a power tool was developed to demonstrate its usefulness in performing the types of tasks that were required for STS-41C, the Solar Max Mission. This tool was used again during the WESTAR/PLAPA retrieval mission (STS-51A) and the LESAT repair mission (STS-51I).

The tool that was selected for these missions was a commercial tool. The unit was a reversible, two speed (50/100 revolutions per minute (RPM)) with five selectable torque ranges. Modifications were made to the brushed direct current motor to make it compatible with the vacuum environment in which it was to operate. An additional gear system has been added to the tool to decrease the speed of the motor to 20/50 rpm and raise the torque output for use during the Hubble Space Telescope maintenance and repair mission.

The major problem with this tool has been maintaining the tolerances on the torque settings between uses. This tool uses a slip clutch comprised of a spring, two plates, and a quantity of small ball bearings to regulating the torque output. Because of wear and temperature variations during the mission, it has been necessary to perform calibration tests at temperature extremes on the tools prior to their use on a mission.

Other tools have been developed that use a feedback circuit to limit the current to the motor when the proper torque is reached. Owing to efficiencies of the gears and inertia of the overall system, units of this type are susceptible to overshoot of the desired torque.

Problem Statement

The problem is to develop a self-contained, hand-held power tool that can be operated in an EVA environment. The tool will have a range of 10 to 200 in-lbs with an accuracy of $\pm 5\%$. Also, the tool will be capable of being set by the EVA crewmember and will provide a visual indication of the set/actual torque and number of revolutions. After the desired torque is reached, the tool will be programmed to provide a gradual release of the torque.

Approach/Method

The program established for the development of the power tool was separated into two phases. First, a brass board was to be developed to determine if a system could be assembled that would provide the desired torque accuracy and tolerance and would verify the program necessary to provide feedback to the components. We reasoned that a high level of accuracy could be obtained by the system with the use of a magnetic particle clutch. Based on the accuracy of the sensing device, the clutch could limit the amount of output torque by limiting the current to the clutch. A "ramp-down" feature could also be programmed into the unit that would provide a residual torque until the motor is shut off.

Catalog searches were made to select the major components for the brass board. Selection of components was based on the requirement that the components could be used in the prototype power tool as is or with only minor modifications made to the prototype power tool. Preliminary software algorithms and integrated circuits were developed while awaiting receipt of the hardware components from the suppliers. A block diagram of the system is shown in figure 1. The brass board was assembled and demonstrated. A 2% accuracy was obtained for the full range of 10 to 200 in-lbs. Verification of accuracy was made using a calibrated torque meter on the output of the shaft.

The second phase of the program was to design and manufacture a hand-held, self-contained unit that would be used for demonstration purposes. The unit was to be capable of selecting either the torque/revolution and the

level set by the operator. An indication of the levels set/ actual was also to be visible to the operator.

A packaging design was initiated based on the utilization of components from the brass board. The layout assembly giving dimensions of the unit is shown in figure 2. The original plan was to have the electronic package separated from the power tool, and circuit boards were designed based on that requirement. We decided to integrate the electronics into the tool after the boards were completed. This configuration would present a greater fidelity to the design of the final flight item.

The final assembly was completed and demonstrated. Owing to manufacturing problems with the torque sensor, torque accuracies of 10% over the range of 10 to 200 in-lbs were obtained. The "as-built" power tool is shown in Figures 3 and 4.

Results

Based on tests performed with the brass board and the demonstration unit, a power tool can be manufactured that uses a magnetic particle clutch to provide a high degree of accuracy over a range of 10 to 200 in-lbs. The power tool is capable of adjusting "real time" in 5 in-lb increments and of providing visual indications of set/ actual levels of both torque and number of revolutions.

Conclusions

Designs of a proto-flight power tool are to be prepared and a tool manufactured that can be used in an

orbital environment. In accordance with the NSTS requirement for Government-furnished equipment hardware ground testing, additional testing will be performed on the proto-flight power tool to verify its operational characteristics at temperature extremes and in a vacuum environment. After testing is completed, the proto-flight power tool would be used as part of an EVA flight experiment.

Acknowledgments

It is with sincere appreciation that the author acknowledges the cooperation and effort of the following personnel in the development of the basic concept for the power tool:

ILC - Space Systems

Mike Withey
Viet Truong-Cao
Robert Pham
Dale Daugherty

and of the following personnel for the excellent effort in the software development, circuit designs, and final packaging and demonstration of the power tool:

Lockheed Corporation

Louis Li
Chen Chen
Larry Walters

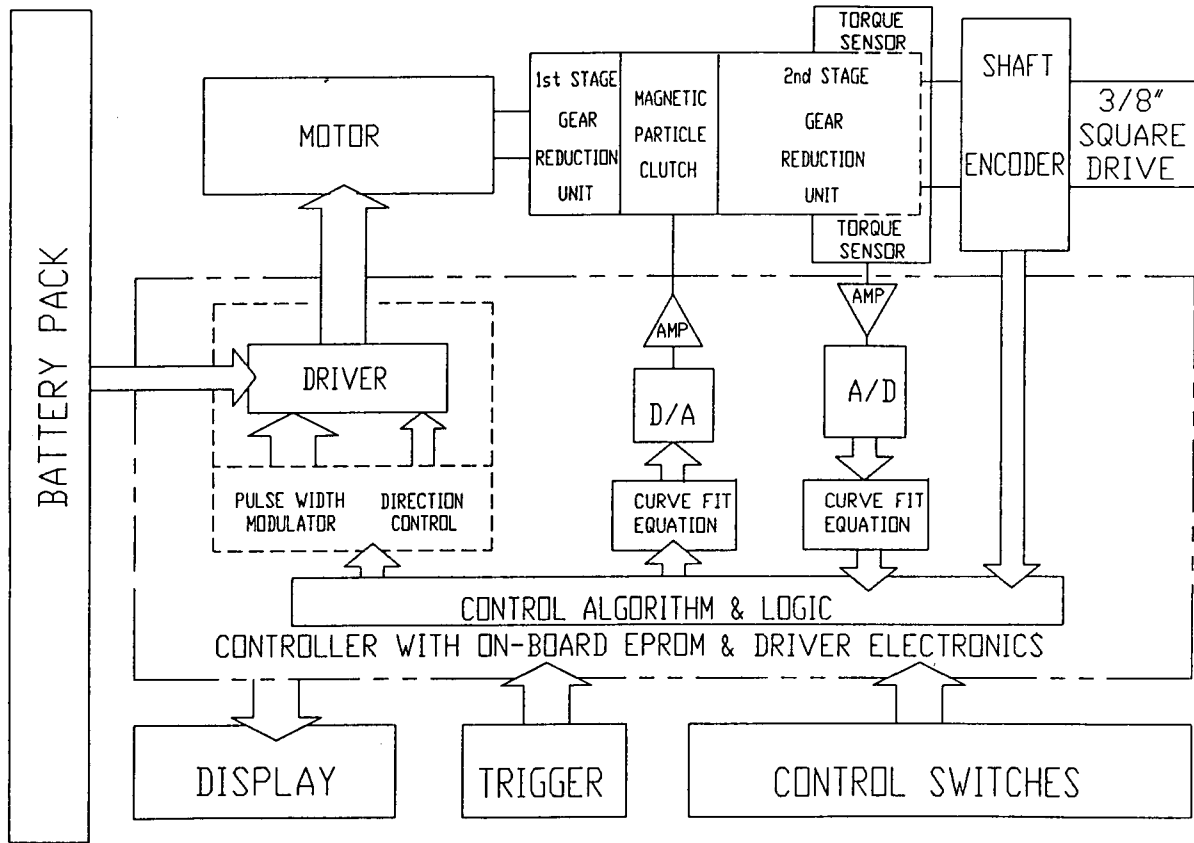


Figure 1. Programmable Power Tool System Block Diagram.

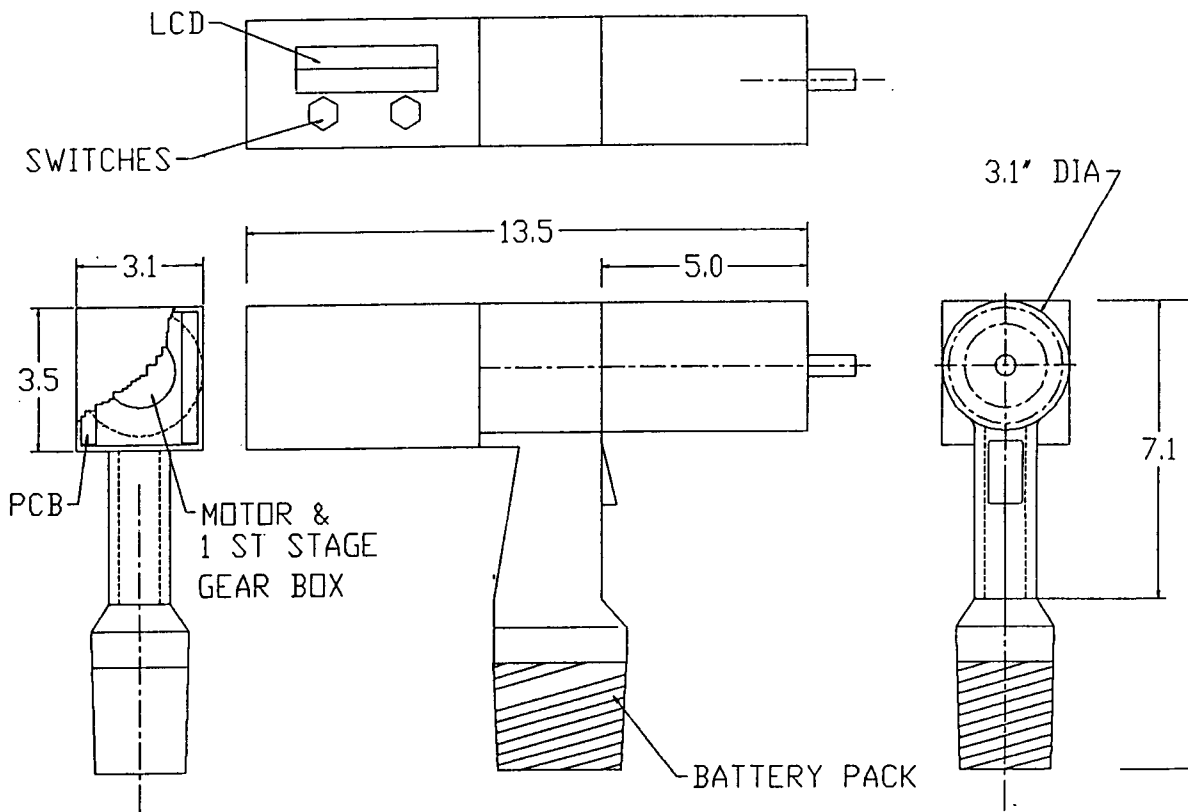


Figure 2. Layout Assembly.

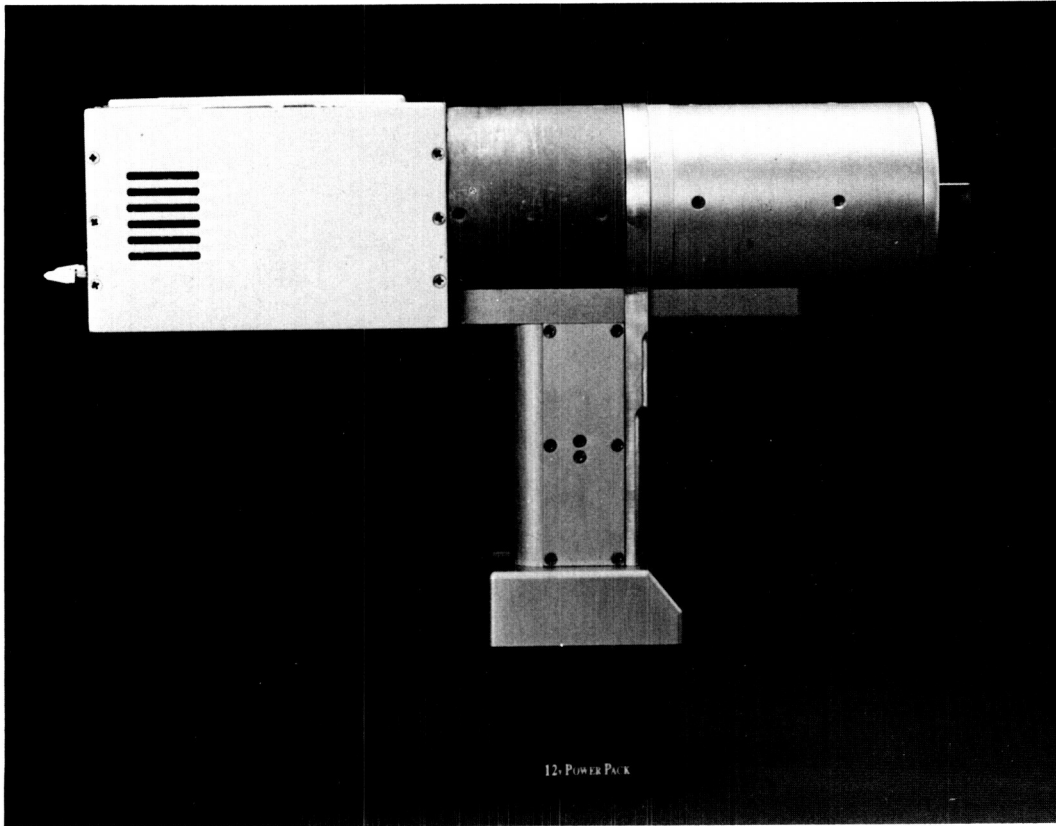


Figure 3. The "As-Built" Power Tool.

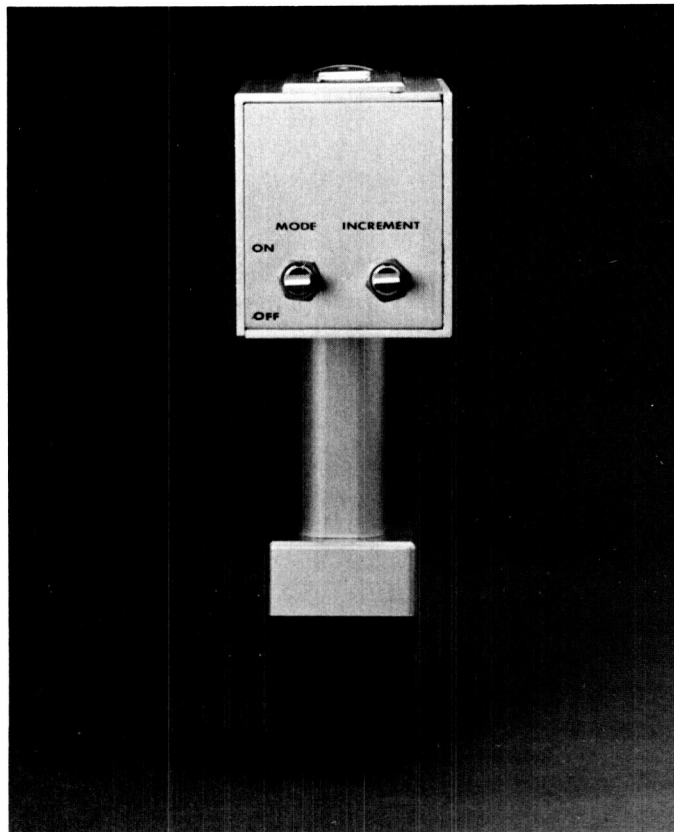


Figure 4. The "As-Built" Power Tool.

EMU Fuel Cell and Metal Hydride Hydrogen Storage System In-House Evaluation

Jose A. Marmolejo
Johnson Space Center/EC5

Abstract

In this paper, we will give an update on recent testing of an advanced development effort carried out on an extravehicular mobility unit (EMU) fuel cell energy storage system that was initially developed for the Space Station Freedom (SSF) EMU. This concept, which is fueled by oxygen and hydride-stored hydrogen, is being considered as an alternative to the Shuttle EMU's zinc-silver oxide battery. The main consideration drivers in choosing a newer technology are superior cycle life and quick recharge. Our test article was comprised of selected test points from an earlier test series. This test article was retested to identify any discrepancies resulting from a period of nonuse that may exist with this technology (such as limited life).

Introduction/Background

The limitations of the zinc-silver oxide battery that is currently used in the Space Shuttle EMU are a serious concern for SSF, where a much greater number of extravehicular activities (EVAs) will be required. (It is anticipated that EVA pairs will be performed from the Station up to 52 times a year.) In the Shuttle Program this battery technology has demonstrated a short wet-life (120 days), a limited cycle life (only 8 cycles), and a slow recharge time (> 20 hours). Its usage would be impractical on SSF because of cost, volume, logistics, logistics bookkeeping, crew interface for servicing/replacement, and storage. Unfortunately, the mature technology of the zinc-silver oxide battery does not offer much potential for improvement.

On the other hand, the oxygen-breathing proton exchange membrane fuel cell that is fueled by hydride-stored hydrogen presents an attractive alternative to the zinc-silver oxide battery for Space Station or for other program applications. It has the potential of matching the operational simplicity of the battery while overcoming its shortcomings in performance. Even at this early stage of development, an attractive performance future can be projected for this technology. The goal of the NASA development program was to demonstrate the fuel cell/hydride technology pair as an alternative EMU power supply by meeting the following objectives: high energy/volumetric density (comparable to that or smaller than that of batteries), high cycle capability (> 500 cycles), quick recharge capability (< 25 minutes), and safety (with hydrogen stored within metal hydrides).

Fuel Cell Energy Storage System (FCESS) Design

The FCESS is comprised of a 32-cell proton exchange membrane stack, a metal hydride storage vessel, and a control subsystem. The cell stack design features passive water removal, thermal and physical integration with the hydride vessel, and waste heat removal by means of the EMU water-cooling system. The metal hydride storage vessel contains enough hydrogen to fuel the FCESS for up to 5 hours. Although metal hydrides have demonstrated a hydrogen storage ability that is superior to liquefaction, a metal hydride is being used in the EMU application primarily for safety reasons. The control subsystem provides reactant pressure and flow regulation, automatic start-up and shutdown, and electronic circuitry for protection of the power source against malfunctioning. A functional schematic of the FCESS breadboard unit is shown in figure 1. A fuel cell with thermally linked metal hydride hydrogen storage cylinders is shown in figure 2.

The FCESS, which was designed and fabricated under NASA Contract NAS 9-17775, is a freestanding power source that is suitable for bench testing at atmospheric pressure (fig. 1). Under a previous test series, it was shown that the FCESS design surpassed contractual statement of work (SOW) requirements in several areas. Noteworthy are a significantly lower volume, a faster recharge, and a substantially longer projected cycle life. Design specifications and operational features are summarized in tables 1 and 2. SOW requirements, where applicable, appear in brackets.

Previous Testing

Prior to NASA delivery, baseline and acceptance tests were performed at the vendor to verify performance of the FCESS design. A total of 78 test hours were logged, including numerous FCESS start-ups and shutdowns that were intentionally induced to check out the protective circuitry, and loads were induced that ranged from 4.5 to 15.7 amperes. Results of the tests have confirmed proper electrical performance, rated capacity, good thermal efficiency, adequate hydride performance, and no operational purge requirements (as predicted).

Upon NASA delivery, an additional 197 hours of operation over 38 cycles, including regenerations, were performed on the FCESS unit during September 1989 and January 1990. At that time, the unit had met or surpassed all SOW requirements.

Latest Testing

Approach. The objective of the latest test series was to revisit selected test points from the earlier NASA test series to evaluate any discrepancies resulting from a period of non-use that may exist with this technology (such as limited life). It was expected that degraded cell voltages (and total stack voltage) would be observed as well as a degraded water collection capability that is primarily owing to the FCESS not being operated in nearly 2 years.

The approach was to test the FCESS in an ambient environment over a range of operational test conditions including: a current demand of 7 amps, and coolant flow rates to maintain the stack temperature between 140°F and 158°F with coolant temperatures maintained between 50°F and 80°F. Regeneration test conditions included: coolant flow rates of 240 lbs/hr with coolant temperatures maintained between 45°F and 75°F and a hydrogen supply feed pressure of 250 pounds per square inch gauge (psig).

Results. A power functional test of the FCESS was held the day after a standard hydrogen recharge. During the functional test, an open circuit voltage of 30 volts was measured as expected (28 ± 4 volts). When a minimum load of 3 amps was applied, however, the stack voltage dropped to 12.2 volts. The only plausible explanation for the poor performance of the FCESS was that the fuel cell stack had become dehydrated during storage. A procedure was implemented that consisted of applying a minimum load for 30 seconds followed immediately by the application of no load (0 amps). By the end of the functional test, the FCESS was providing 24.7 volts at 7 amps. Although the FCESS was run for a period of

nearly 5 hours, only 50 cc of water were produced, which supported the theory that the fuel cell stack was dehydrated. Nonetheless, operation was within item specifications.

Two additional recharge and discharge cycles were performed on the FCESS. Voltages of 24.6 volts at 7 amps over 5:01 hours and 25.8 volts at 7 amps over 5:10 hours were recorded, respectively, for those 2 test days. In addition, a water production of 360 cc and 350 cc, respectively, was also measured and was as expected.

Conclusion/Summary

Since delivery of the FCESS in April 1989, numerous test hours over numerous charge and discharge cycles have been recorded by NASA on the FCESS, thus proving the viability of this technology as an alternative to the zinc silver-oxide battery technology currently in use by NASA. During the latest test series, it was shown that the FCESS could operate within its design specifications even after being stored for a period of nearly 2 years. This last exercise also demonstrated a procedure for "rewetting" the fuel cell stack that may be experienced during this storage time period, thus allowing the system to become activated safely and to operate well within its design specifications.

Acknowledgments

I would like to thank the crew for their excellent support which contributed to the smooth development of this project.

Table 1. FCESS Design Specifications

Capacity:	34 A-hrs (app. 1000 W-hrs)
Voltage:	28 + 4 volts
Current rating:	7A
Ambient temperature:	122°F
Volume(1):	415 in ³ [<1000 in ³]
Weight:	35 lbs
Hydrogen storage:	Metal hydride
Oxygen storage:	Compressed gas
Product water:	Potable, zero-g removable
Venting of gases:	None, start-up purge only
Heat release:	<200 British thermal unit (Btu)/hr [<300 Btu/hr]
Cycle life:	5000 [>120]
Charge time:	<15 minutes [30 minutes]

(1)Exclusive of controls

Table 2. FCESS Operational Features

- No venting of gases; start-up purge only
- Dead-end reactant flow regulation
- Product water removal by pressure-enhanced wicking
- Passive waste heat removal
- In-place hydride recharge
- Start-up and regeneration by multiple purge

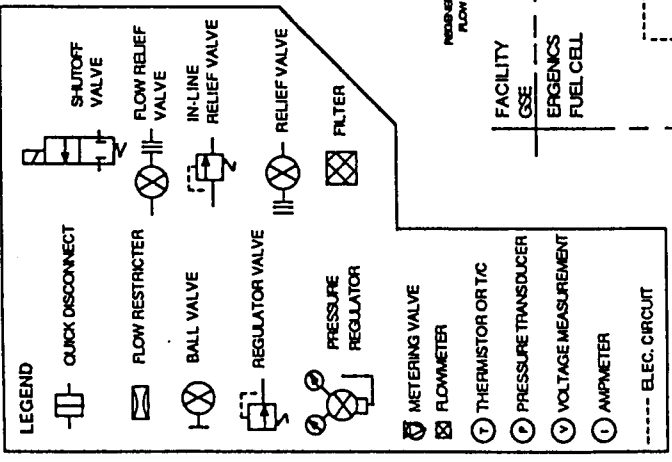
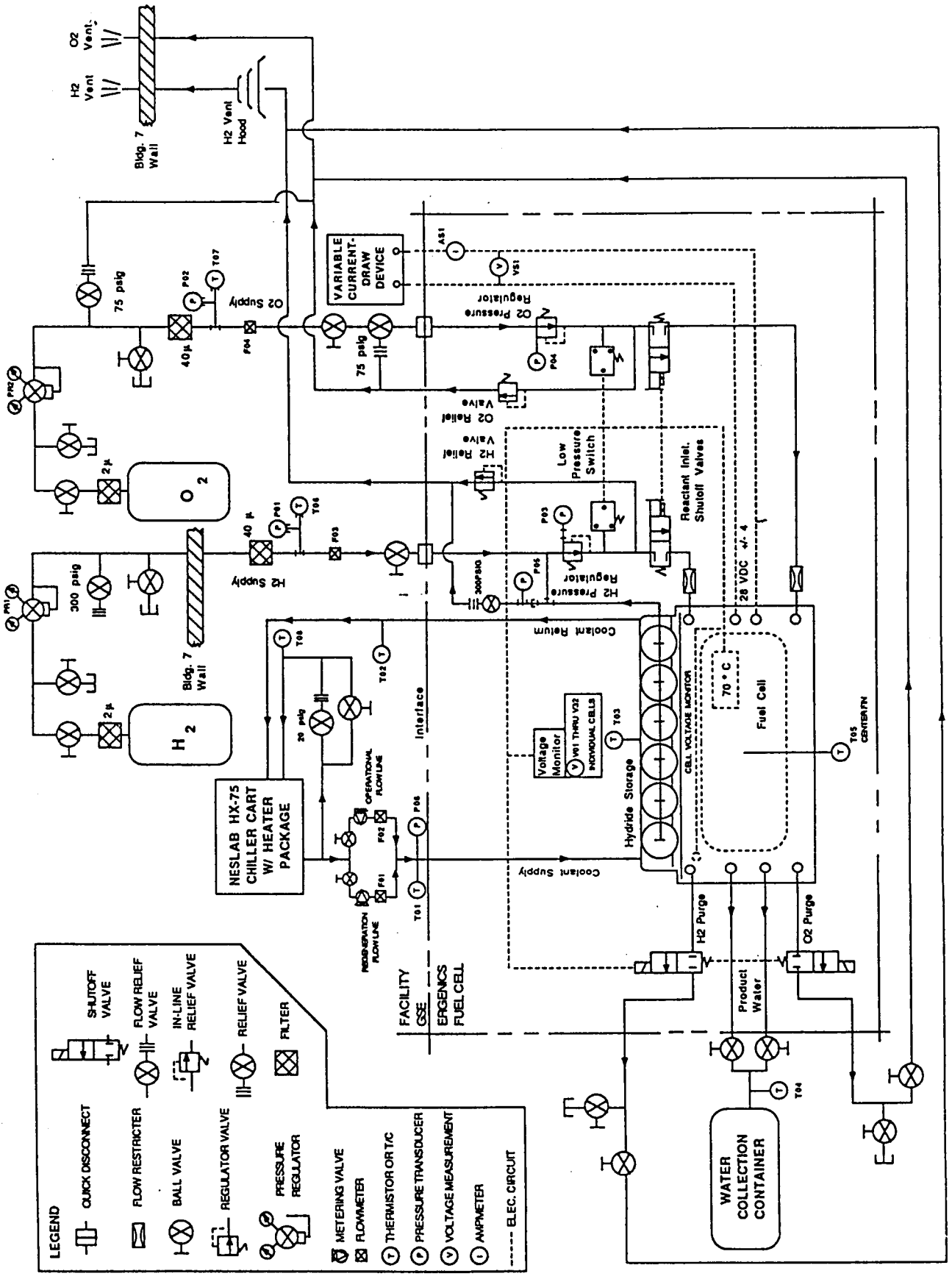


Figure 1. FCESS Integrated Test Article and Instrumentation Schematic.

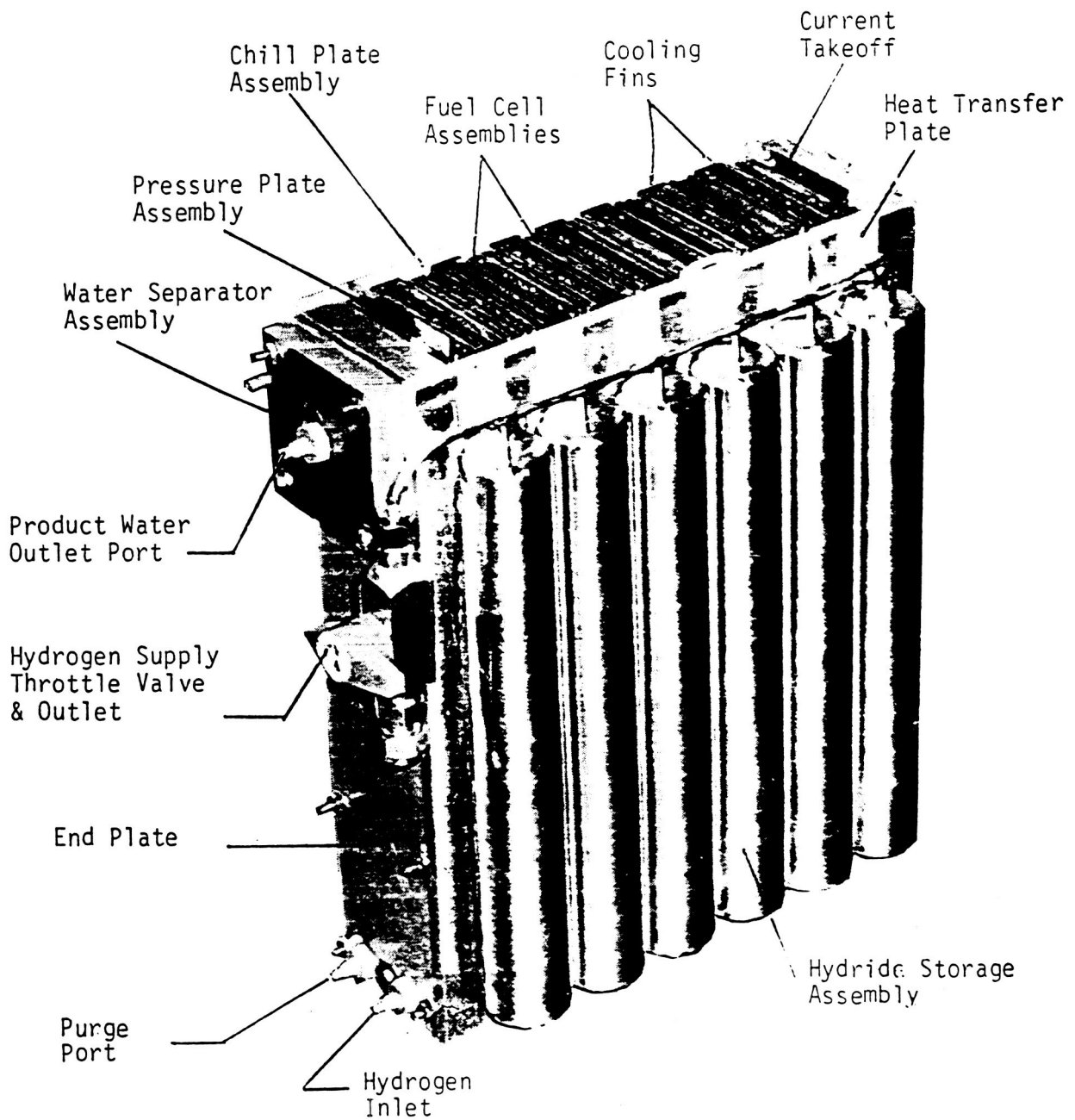


Figure 2. FCESS Breadboard Unit.

Metal Oxide CO₂ and Humidity Remover

Gretchen Thomas
Johnson Space Center/EC

Abstract

The metal oxide CO₂ and humidity remover (MOCHR) is an advanced life support technology that will provide atmospheric control for an advanced extravehicular mobility unit (AEMU). The system was developed by the AiResearch Los Angeles Division of Allied-Signal Aerospace Company, and uses a bed of silver/zinc oxide pellets to absorb CO₂ and H₂O vapor. The MOCHR is regenerable by blowing hot air through the canister at ambient pressure. Testing was performed at JSC to demonstrate MOCHR performance over a period of time while it was being cycled between extravehicular activity (EVA) and regeneration modes and to assess system performance characteristics under nominal and off-nominal metabolic CO₂ and H₂O loads. In this report we will briefly describe the MOCHR system and summarize the results of the testing conducted by the Crew and Thermal Systems Division at JSC. Testing was performed in the EVA test-bed portable life support subsystem breadboard (PLSSBB), located in building 7, room 2007, from April 29 to July 21, 1992.

Introduction

The MOCHR was developed by the AiResearch Los Angeles Division of Allied-Signal Aerospace Company and is a candidate CO₂ and humidity removal subsystem for an AEMU. This technology uses a bed of silver/zinc oxide pellets to absorb CO₂ and H₂O vapor. The MOCHR is regenerable by blowing hot air through the canister at ambient pressure. In actual use, absorption would take place in the extravehicular mobility unit (EMU) while on an EVA and regeneration would be performed in the airlock.

The MOCHR was tested using a simulated PLSSBB design. The integrated system is designed to provide different metabolic rates by applying corresponding heat loads to the metabolic heaters in both vent and coolant loops, as well as by injecting the appropriate amount of CO₂ and H₂O vapor into the simulated vent loop. CO₂ and H₂O injection rates for each metabolic rate were determined using an array of past Shuttle EMU/crewmember test and analysis results. MOCHR inlet vent loop temperature, humidity, and CO₂ concentration were varied correspondingly with the respective metabolic rate. The MOCHR was tested over a range of fixed and variable metabolic profiles.

The MOCHR regeneration phase required transferring the test article from the absorption test stand

to the regeneration unit. The regeneration unit was provided by the vendor and is located in building 7, room 2007, adjacent to the PLSSBB test stand. The MOCHR was then regenerated by blowing hot air through the canister at ambient pressure following the vendor-supplied regeneration profile.

Description

The MOCHR consists of a bed of pellets made up of a matrix of silver-zinc oxide. Each of these pellets is approximately 1/16 in. in diameter, with an aspect ratio of 1 to 1.5. Through absorption of CO₂ and H₂O vapor, the resulting reacted compounds consist of metal carbonates and bicarbonates, metal hydroxides, hydrates, and complex compounds. The absorption process is exothermic and the MOCHR uses an active cooling loop to carry off waste heat and to facilitate water vapor absorption. The MOCHR test article is shown in figure 1. As illustrated, the overall dimensions of the canister are approximately 15.4 in. X 12.0 in. X 4.7 in., giving the subsystem an overall volume of approximately 868.6 in³ (0.5 ft³). Once the MOCHR completed an EVA mode operational test run, it was disconnected and placed on the vendor-supplied regeneration test stand.

Approach/Method

The test series was conducted in the EVA test bed PLSSBB, located in building 7, room 2007. This lab is maintained and operated by EC4, the Systems Test Branch of the Crew and Thermal Systems Division.

Vent loop pressure was maintained at 8.3 psia during testing. The composition of the vent loop was initially standard breathing air—20.5% oxygen (O₂) and 79.5% nitrogen (N₂) gas. A bubbler was used for water vapor addition, while CO₂ injection was supplied by a K-bottle. Because the MOCHR pellets cannot tolerate liquid water, the inlet dew point was always held a minimum of 2°F above the cooling water temperature to prevent condensation in the canister.

Regeneration of the MOCHR takes place in two distinct phases. In the first phase, laboratory room air is heated to 190°F and is circulated through the MOCHR canister in an open loop mode to drive off the absorbed water vapor. In the second phase, air temperature is ramped up until it reaches 525°F. Again, the air is circulated in an open loop through the canister to drive off absorbed CO₂. Upon completion of regeneration, the canister can either be actively cooled, closed loop, or

allowed to cool passively. The total regeneration process takes approximately 13 to 16 hours, with 9.5 hours for regeneration and 3 to 6 hours for cool down (passively cooled).

Contract design provisions required that the MOCHR be able to absorb adequately metabolic CO₂ and H₂O vapor corresponding to a 1000 British thermal unit (Btu)/hr mixture ratio (MR) (0.2 and 0.3 lbm/hr, respectively) for 6 hours, plus a 500 Btu/hr MR (0.1 and 0.18 lbm/hr, respectively) for 2 hours for a minimum of 40 cycles, while maintaining a vent loop pressure drop less than or equal to 1.0 in H₂O. This canister was delivered to JSC by the vendor after the vendor performed 5 cycles. These cycles were taken into account when evaluating the performance. All absorption test points were run to either CO₂ (7.6 mm Hg) or to H₂O (60°F dew point) breakthrough, whichever occurred first.

Results

The MOCHR completed a total of 40 EVA/regeneration cycles. Five of these were at AiResearch and 35 were at JSC.

Throughout the course of testing, the gas flow pressure drop through the canister increased from 0.7 to 5.5 in H₂O. This pressure drop is significantly higher than that called for in the specification of less than or equal to 1.0 in H₂O.

Good CO₂ removal was demonstrated, and the over-design for CO₂ capacity was evident early in the test series when CO₂ absorption quantities significantly exceeded the 1.4 lbm specification. The maximum CO₂ capacity of the MOCHR observed over all test points was ~2.33 lbm. Although the capacity for the final test points was only 1.48 lbm, which is a 36% reduction from the maximum, it was still above the requirement. Elapsed time to CO₂ breakthrough and CO₂ absorption capacity both decreased ~2% per test cycle.

The maximum H₂O absorption capacity of the MOCHR, as observed in one of the early cycles, is ~2.12 lbm. This value meets the 2.1 lbm requirement. The capacity at cycle 38, however, was only 1.08 lbm, a 49% reduction from the maximum and also 49% below the requirement. The H₂O removal capacity specification (2.1 lbm) was met or exceeded in only one test point (2.12 lbm in cycle 14). Cycles 12, 16, and 18 achieved quantities of 2.05, 2.02, and 2.02 lbm, respectively. Elapsed time to H₂O breakthrough decreased 1 to 1.5 percent per test cycle. Water absorption capacity to breakthrough decreased ~2% per test cycle.

Conclusions

The MOCHR unit has demonstrated the capability for concurrent CO₂ and H₂O removal for 40 absorption/desorption cycles (35 of which occurred at JSC). The

MOCHR performed equally well under a variety of steady-state and transient metabolic load conditions. However, unlike the Shuttle EMU LiOH canister and sublimator, which provide near-constant vent gas CO₂ and dew point levels (i.e., P_{PCO₂} ~0.3 mm Hg and dew point ~40°F) to the suit, the MOCHR CO₂ and dew point levels increase substantially over time and cycle number.

CO₂ breakthrough (7.6 mmHg) only occurred at high metabolic rate levels (i.e., 1400 and 2000 Btu/hr steady state). At the more moderate activity levels (i.e., 1000 Btu/hr average or less), testing was stopped because of either water breakthrough (60°F outlet dew point) or time and personnel constraints. Therefore, EVA time should not be limited by the CO₂ removal performance.

Although elapsed time to H₂O breakthrough exceeded 8 hours for much of the test series, H₂O injection rates were not constant and actually decreased over time and cycle number because the H₂O injection rate was limited by a MOCHR inlet dew point constraint (to prevent water condensation). H₂O breakthrough did occur in less than 8 hours in the latter portion of the test series (as low as ~5.5 hours for a 1000 Btu/hr average metabolic rate at cycle 37). Therefore, EVA time may be limited by H₂O removal performance.

MOCHR testing showed a decreasing capacity with an increasing cycle number. Therefore, the final design must account for this reduced capacity to ensure that the capacity requirements continue to be met.

References

- ¹Smith, G., "Metal Oxide CO₂ and Humidity Remover (MOCHR) Test Plan Document," CTSD-SS-531, March 31, 1992.
- ²Allied-Signal Aerospace Company AiResearch Los Angeles Division, "Operations, Maintenance, and Repair Manual and Interface Control Document," 92-64909, March 3, 1992.
- ³Thomas, G., and Lovine, J., "Metal Oxide CO₂ and Humidity Remover (MOCHR) Final Test Report," CTSD-SS-591, December 1992.

Acknowledgments

The following organizations were involved in the design, development, test, and evaluation of the Metal Oxide CO₂ and Humidity Remover:

Allied-Signal Aerospace Company AiResearch Los Angeles Division
NASA Johnson Space Center Crew and Thermal Systems Division
EVA Branch
Systems Test Branch
Systems Engineering Analysis Office
Lockheed Engineering and Sciences Company

Air-Bearing Fan

Mike Lawson
Johnson Space Center/EC

Abstract

During advanced space suit studies, we determined that a nonintegrated fan with air bearings could contribute significantly to enhancing the robustness and reliability of a space suit life support system. AiResearch has built a small 2 lb fan that can operate from 4 to 23 psia, with variable speed from 4 to 8 actual cubic feet per minute, running at 95K to 215K rpm. Performance is very good, but further development is needed to prove long life and reliability.

Introduction

In May 1988, NASA started an effort to develop a small, efficient fan for extravehicular activity applications. The next-generation space suit differed in two major ways from the previous generations of suits. New space suit concepts were required to operate at pressures as high as 8.3 psi compared to the 4.3 psi of the existing Shuttle suit. Advanced water removal concepts for the suit did not require the integral water separator that the present space suit requires. Additionally, reliability studies indicated that the fan was one of the lowest mean time between failure (MTBF) components which suggests the need to separate the fan, pump, and water separator that are driven by a common motor on the Shuttle extravehicular mobility unit. The requirement was for a small volume and weight air mover that had a high MTBF. The fan needed to be more efficient and to draw less power for the higher operating pressures of the advanced suit.

Approach/Method

The approach to solve these new requirements was to use air bearing technology to reduce bearing wear and to design the aerodynamics of the impeller for the 8.3 psi condition. Additionally, the fan was to operate from 4 to 8 actual cubic feet per minute (ACFM) from 6 to 23 pounds per square inch absolute (psia). The design point was 5 inH₂O at 6 ACFM at 8.3 psia vent loop pressure. Since space suits often operate in a 100% oxygen environment, materials for the fan were carefully selected for fire resistance in this environment. The oxygen contacting surfaces are made of Inconel 625, 718, and 750. Several nonmetallics are used, but the largest nonmetallic is the stator winding support that is made from Vespel SP-1.

The permanent magnet motor is a two-pole toothless with a three-phase winding. Three Hall-effect sensors are used as position sensors for electrical commutation by the motor controller. The controller was built using off-the-

shelf electronics. A flight version will reduce the 8x10x2-in prototype box to a 2x2x0.5-in box that uses an application specific integrated circuit (ASIC).

Results

The fan and its controller are shown in figure 1. A line drawing of the portable life support system (PLSS) is shown in figure 2. It occupies 19 in³ and weighs 2 lb. Tests were initially run by the contractor at 23, 19.5, 14.7, 8.3, and 6.0 psia. The results of these tests are shown in figure 3. At the design point, the fan provides 5 inH₂O pressure rise at 6 ACFM at 8.3 psia that is drawing 23.6 w spinning at 166,000 revolutions per minute (rpm). Performance was as expected, except it has a slightly higher power requirement. Most of this is because of a lower aerodynamic efficiency than was expected. It is believed that some of this higher requirement is owing to inlet disturbances on the nose cone. The fan was also tested over a wider range at JSC. Test results are shown in figure 4. These results agreed well with the initial contractor results. In-house testing was also done at 4.0 psi and at a variety of different vent loop pressure drops.

Conclusions

The air-bearing fan has been a very successful technology program. The next step is to build another fan that will improve the inlet nose cone aerodynamics and reduce the electronics to the ASIC chip. A life cycle test program should then be set up to characterize the life of the foil bearings and of the electronics. After thousands of hours have been demonstrated, a robust fan design will be demonstrated that can be used for zero-g, lunar, and Mars applications.

References

- ¹AiResearch Los Angeles Division, "Final Report—Development of an Air Bearing Ventilation Fan," 92-65151, August 14, 1992.
- ²Abdallah, A., Lovine, J., Lawson, M., and Trevino, L., "Air Bearing Fan—Final Test Report," JSC-37707, CTSD-SS-608, December 18, 1992.

Acknowledgments

Paul Fukumoto and Roger Murry of AiResearch are to be acknowledged for the work they performed in the conceptualization, design, and testing of this high-speed air bearing fan.

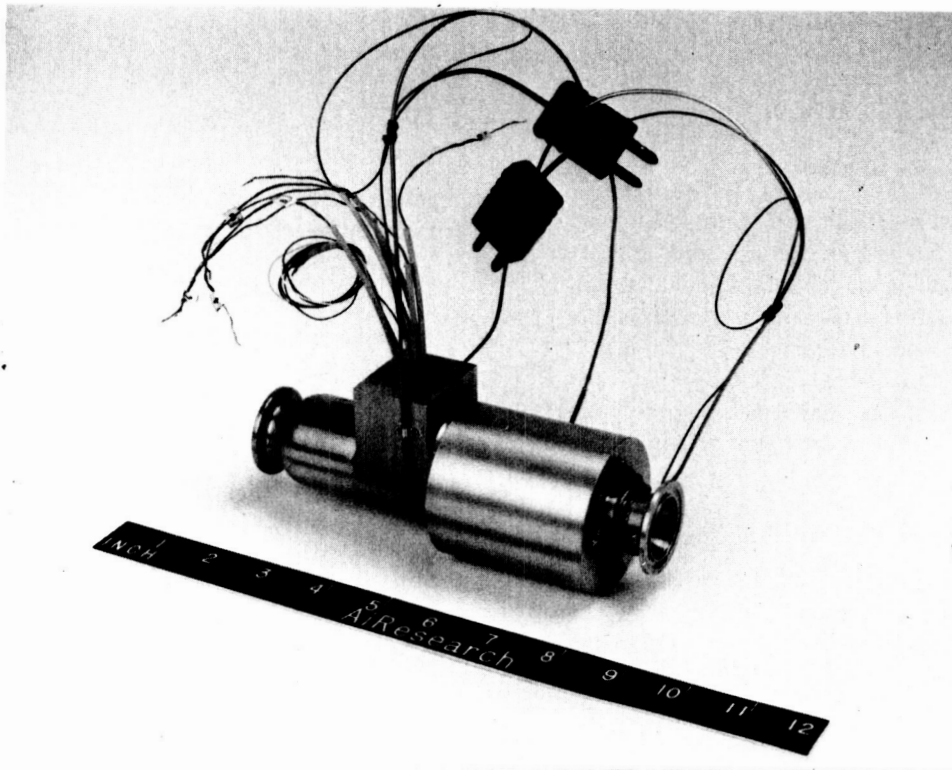


Figure 1. Air Bearing Fan.

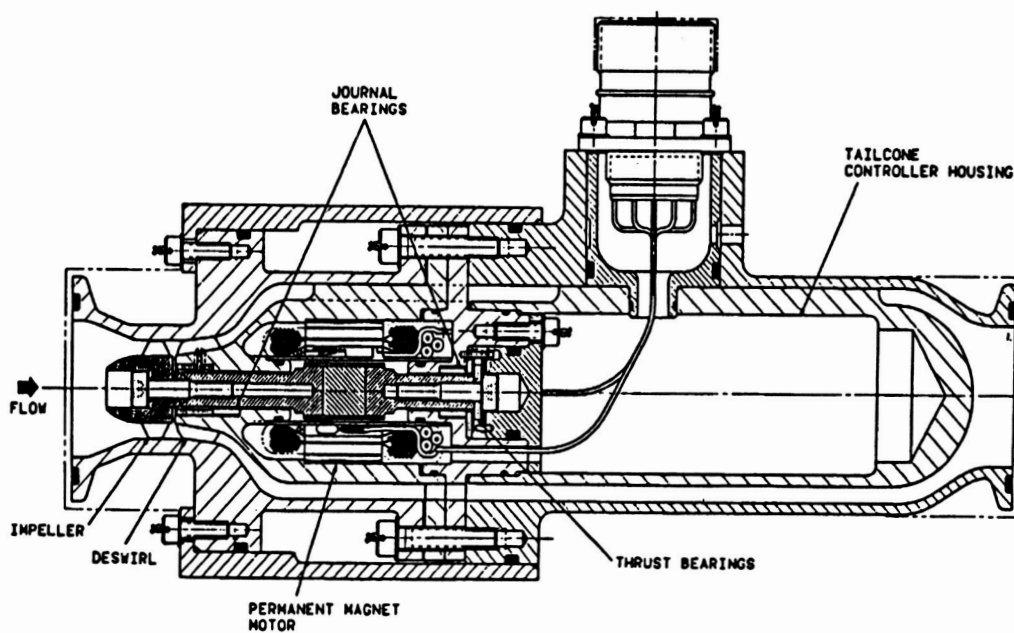


Figure 2. PLSS Air-Bearing Ventilation Fan.

A Hybrid Regenerative Water Recovery System for Lunar/Mars Life Support Applications

Charles E. Verostko and Marybeth A. Edeen
Johnson Space Center/EC

Abstract

Long-duration manned space missions will require integrated biological and physical/chemical processes to recover resources from wastes. In this report, we will discuss a hybrid regenerative biological and physical/chemical water recovery system that was designed and built in the Crew and Thermal Systems Division. The system is sized for a four-person crew and consists of a two-stage, aerobic, trickling filter bioreactor; a reverse osmosis system; and a photocatalytic oxidation system. The system was designed to accommodate high organic and inorganic loadings and a low hydraulic loading. The bioreactor was designed to oxidize organics to CO_2 and H_2O ; the reverse osmosis system reduces inorganic content to potable quality; and the photocatalytic oxidation unit reduces residual organic content (part per million range) to potable quality and provides in situ disinfection.

Introduction

For long-duration exploratory space missions, the reclamation of water for potable and hygiene uses from waste water is of vital importance. Approximately 230 kg of waste water are generated by a four-person crew during the course of normal daily activities. Efforts to recover this water have focused primarily on physical/chemical methods such as phase change and/or membrane processes. It is likely, however, that because of the additional waste components generated in a lunar/Mars habitat, some biological method may have sufficient advantages (low temperature, low pressure operation, etc.) over physical/chemical methods. The decision was therefore made to investigate a hybrid biological and physical/chemical system for water reclamation.

The hybrid regenerative water recovery system (HRWRS) is housed in the building 241 facility at JSC. It has been funded primarily from Center Directorate Discretionary funds since start-up in December 1991.

Problem Statement

The objectives of the HRWRS are to investigate the efficiency of a hybrid system to reclaim potable water from waste waters; to determine the chemical characteristics of individual sources of waste water; and to assess water usage amounts by using current Space Station Freedom (SSF) water allotments¹ and to determine the feasibility of a hybrid system for water recovery for long-duration missions (greater than 1 year).

System Description

The system is comprised of two major components: the waste water collection and transport system (WWCTS) and the three treatment processes (a two-stage aerobic trickling filter bioreactor, a reverse osmosis (R.O.) unit, and a photocatalytic oxidation system). A schematic of the system is shown in figure 1. The components of the system are described in detail below.

Waste Water Collection and Transport System

The WWCTS is comprised of the five production sources (shower, hand wash, urinal, laundry, and dishwasher), the facility use control system, the waste water production measurement system, and the transport system. Although each component of the waste water production source was a commercially available item, every effort was made to modify the components for limited water usage. The operation of the HRWRS is under complete computer control. Volunteers provide waste water from shower, hand wash, and urinal sources and also provide clothes for laundry. Dish wash waste water is provided every other day by using dinnerware from the JSC cafeteria. The volumes and frequency of collection of waste water from each production source are shown in table 1.

Bioreactor

Bioreactor design goals were to (1) replace pretreatment chemicals required for urine and waste water stabilization; (2) stabilize volatiles, such as ammonia, to prevent carryover to the R.O. system; and (3) accomplish organic removal down to 50 mg/l or less. The reactor was sized for a four-person crew.

Bioreactor Design

A fixed-film, aerobic reactor was chosen. The design of the bioreactor was based on the mass flow rate of water in the system, the expected organic carbon loading of the system, and the municipal design criteria. The mass flow rate of water in the system was based on Space Station water requirements for urine flush, shower, hand wash, and laundry water.¹ A two-stage reactor was designed in which most of the organic carbon would be removed in the first stage and the remainder of the organic carbon would be removed in the second stage, with the second reactor also accomplishing the nitrification of ammonia.

PRECEDING PAGE BLANK NOT FILMED

PAGE 24 INTERNATIONAL JOURNAL

Reactor Fabrication

Reactors were fabricated from high-strength plastic. The first stage is acrylic and has a cross-sectional area of 335 cm². The second stage is a standard polyethylene tube with a cross-sectional area of 190 cm². Both reactors were fitted with sample ports and thermocouplers at the inlet and the outlet and at depths of 0.30, 0.91, and 1.52 m into the bed. Flow distribution plates were designed to ensure distribution of the flow over the entire cross-sectional area of the reactor. Underdrains collected effluent water and directed the water to small settling tanks at the bottom of the reactors. Feed for the downstream processes and for recycle around the reactors is drawn from the middle of these settling tanks. Air is forced through the reactors from the bottom to the top with a blower.

Reactor Inoculation and Acclimation

Bioreactors were inoculated with effluent water from the Vince Bayou Waste Water Treatment Plant in Pasadena, Texas, on December 12, 1991. That plant was chosen because it uses a rock-trickling filter as one of the initial treatment steps for the waste material, so the residual microflora should have been well-adapted to fixed-film growth. Also, it is a municipal system with some industry effluent feeding into it, which means the microflora were expected to be very diverse. The waste concentration was slowly increased to full strength.

Two cartridge filters (35 and 8 microns, respectively) were placed in the line between the effluent from bioreactor two and the reverse osmosis system to remove large particulates and biomass from the water stream. An additional 5-micron filter was included on the reverse osmosis system itself.

Reverse Osmosis System

A commercial reverse osmosis system was procured from Applied Membranes (San Marcos, California). The system uses two Filmtec seawater-type membranes (spiral wound) that are 11.4 cm in diameter, are 101.6 cm in length, and are run in series. Unlike most applications for R.O., a requirement of 85% recovery of water from the bioreactor was imposed. Additionally, the water quality requirement for the permeate was less than 100 mg/l total dissolved solids (TDS). At flow rates of 0.76 l/m (concentrate), 22.71 l/m (recirculate), and 6.06 l/m (permeate), and with the above requirements met, the result is a concentrate of approximately 10,000 to 12,000 mg/l TDS. Typical operating pressures are 2070-2760 kPa. No chemical additives are injected into the system to avoid biofouling and/or chemical deposition (as in normal operations). Instead, a daily 5-minute flush of the system with deionized water is performed. Plans to recover the 15% water lost as concentrate are now being developed.

Photocatalytic Oxidation System

The photocatalytic oxidation system was developed by Photocatalytics, Incorporated, under a Phase II small business innovative research program.⁵ The principle of photocatalysis of residual organic material is well known. The catalyst material is TiO₂, which is made into a slurry with deionized water and poured into a 12-liter batch reactor. The solution under test is then added to the reactor. Ten ultraviolet (UV) lamps (germicidal, 30 W each) are concentrically spaced around a central stirrer in the reactor. Typical initial total organic carbon (TOC) levels are in the 30 to 100 mg/l range (which is the range of TOC values from the reverse osmosis permeate). The UV lamps are then energized, the stirrer is activated, and a head pressure of 69 kPa of oxygen added to the system. Interaction of the UV with TiO₂ particles produces hydroxyl radicals from the surrounding water molecules. This activated hydroxyl radical is then able to oxidize the residual organic material in the water matrix to produce CO₂ and H₂O. Depending on the initial concentration of organic material, the lamps are energized for a period of between 1 and 3 hours. The high UV flux also enhances rapid disinfection of the water.⁵

After a period of illumination, the lamps and stirrer are switched off, the head pressure of oxygen is removed, and the resulting purified water is removed from the reactor. The finely divided catalyst particles are removed from the product water by cross-flow filtration. The principle of cross-flow filtration is the mechanical removal of particles through a fine mesh filter using a back pressure on the filter to obtain filtrate (product water). As catalyst material builds up on the filter, however, the head pressure becomes insufficient for efficient filtration. At this stage, the filter is back-flushed with a burst of 172.5 kPa water. The result is that catalyst is flushed off the membrane and back into the reactor.

Results

Bioreactor

The WWCTS became operational on March 5, 1992. Subsequently, the feed to the reactors was collected from the urinal, shower, hand wash, laundry, and dishwasher. Additional make-up urine or soap was added if there were insufficient test subjects to obtain the equivalent of a 4-person use in 1 day.

Bioreactor performance was determined based on reduction in TOC from inlet to outlet, reduction in ion concentrations from inlet to outlet, the dissolved oxygen profile of the system, and visual observation of the biomass. Other parameters that were measured occasionally included pH, total dissolved solids, and inorganic carbon (IC) content.

Bioreactor performance over the 2 months of October and November, when the system water allotments were reduced to SSF allocations is shown in figure 2. As can be seen, the effluent TOC from the second reactor was

consistently below 50 mg/l although the influent TOC ranged from 80 to 650 mg/l. This indicates that the microorganisms are robust and that they rapidly respond to changes in influent concentration. The reactors have achieved an average TOC reduction of 90% since water allotments have been at SSF levels and a total reduction of 81.4% since start-up in December 1991. The molar ratio of nitrate to ammonia for the influent and effluent streams and the sulfate concentration for the same two streams during the 2-month period from October to December are shown in figure 3. The increase in the ratio of nitrate to ammonia in the effluent indicates that the reactors are nitrifying ammonia to nitrate and then to nitrogen gas. Accomplishing this conversion was one of the objectives of the system. The increase in sulfate concentration from influent to effluent is evidence that the soap used in the shower and hand-wash is being degraded by the microbial population. Overall, the TOC and ion chromatography results indicate that the reactors are performing as designed.

Reverse Osmosis System

Analysis of R.O. performance is based on two factors: percent recovery and percent rejection. In terms of percent recovery, during long-term testing, the system continually operated at between 85 and 87% recovery and at a permeate quality of below 75 mg/l TDS. During functional checkout of the system, however, several tests were performed on standard solutions up to 2200 mg/l TDS, at varying recovery percentages. Results of these preliminary tests are given in table 2.

Photocatalytic Oxidation System

A typical organic carbon profile as a function of time is shown in figure 4. It can be seen that the availability of organic material for oxidation becomes rate limiting at concentrations of 3 to 4 mg/l. The increase in IC is because of the buildup of CO₂ (in equilibrium with the carbonate ion). At a limiting concentration (~14 mg/l) of dissolved CO₂ and with the reactor temperature increasing, the level of IC decreases to ~10 mg/l. To date, no carryover of catalyst in the product water has been observed. The principle of operation has been proved.

Conclusions

It has been demonstrated that a hybrid biological and physical/chemical system is capable of treating waste water from shower, urinal, hand wash, laundry, and dishwasher sources and can produce potable water from such waste water.

A facility now exists that is automated to collect and process waste water. The system has flexibility for testing and evaluating biological and physical/chemical water recovery system processes.

The bioreactor has been in operation for 13 interrupted months and is removing organic impurities from the waste

water. The reverse osmosis system is demonstrating the ability to remove dissolved solids.

The major difficulties encountered during this period of investigation have been mechanical in nature. Specifically, mechanical difficulties are associated with pump design for low flow rates with high suspended solids levels.

The batch operational features of the photocatalytic oxidation system makes it unsuitable for complete system integration. This system will be replaced with an improved posttreatment system that is currently in fabrication.

System closure will be maximized by (1) the recovery of the 15% brine from the reverse osmosis system; (2) the closure of the gas loop from the bioreactor effluent; and (3) the development of a methodology for the treatment of bioreactor solids.

No expendable materials have been used in the HRWRS except for infrequent change out of cartridge filters between the bioreactors and the reverse osmosis system. This represents a substantial advantage over past and present water recovery systems.

Acknowledgments

We would like to acknowledge the following individuals at the Crew and Thermal Systems Division, JSC: A. F. Behrend, Manager, Advanced Programs; H. E. Winkler, Chief, Life Support Systems Branch; C. D. Thompson, Deputy Chief, Life Support Systems Branch; C. H. Lin, Chief, Systems Engineering Analysis Branch; C. E. Verostko, Aerospace Technologist, Life Support Systems Branch; M. A. Edeen, Systems Analysis Engineer, Systems Engineering Analysis Branch; and D. L. Henninger, Chief Scientist for Regenerative Life Support Systems, Life Support Systems Branch. We would also like to acknowledge the following individuals in the Crew Systems Department at Lockheed Engineering and Sciences Company: R. J. Gillen, Manager, Crew Systems Department; N. J. C. Packham, Senior Scientist, and M. S. Johnson, Engineering Assistant.

References

- ¹Environmental Control and Life Support System (ECLSS),” Revision D, NASA, Space Station Program, Architectural Control Document SSP 30262, Reston, VA, 1991.
- ²Verostko, C. E., Edeen, M. A., and Packham, N. J. C., 22nd International Conference on Environmental Systems, Seattle, WA, July 1992.
- ³Webb, P., ed., “Bioastronautics Data Book,” NASA SP-3006, NASA, Washington, D.C., 1964.
- ⁴Tchobanoglous, G., and Burton, F. L., Wastewater Engineering; Treatment, *Disposal and Reuse*, McGraw-Hill, Inc., 1991.
- ⁵Cooper, G., and Ratcliff, M. A., Photocatalytics, Inc., Boulder, Co., Final Report, June, 1990.

Table 1. Production Sources Use Mass and Frequency

Production Source	Mass per Use (kg)	Uses per Day
Shower	10.89	4
Urinal*	0.50	16
Hand Wash	2.04	16
Laundry	99.80	1
Dishwasher	45.72	0.5
Total Mass per Day (kg)	206.86	-

* Includes 0.125 kg per use flush water

Table 2. Reverse Osmosis Performance on Standard Test Solution

Ion	Feed (mg/l)	Permeate 1 27% Recovery (mg/l)	Rejection (%)	Permeate 2 53% Recovery (mg/l)	Rejection (%)	Permeate 3 85% Recovery (mg/l)	Rejection (%)
Cl (-)	556.50	1.50	99.73	2.65	99.52	5.40	99.03
PO ₄ (3-)	500.00	0.25	99.95	0.40	99.92	0.85	99.83
SO ₄ (2-)	355.00	0.15	99.96	0.25	99.93	0.60	99.83
Na (+)	512.50	0.80	99.84	1.55	99.70	3.10	99.40
Mg (2+)	30.00	0.05	99.83	0.05	99.83	0.10	99.67
Ca (2+)	1.75	0.05	97.14	0.10	94.29	0.10	94.29
K (+)	251.50	0.27	99.89	0.49	99.81	1.09	99.57
TDS (mg/l)	2207.25	3.07		5.49		11.24	

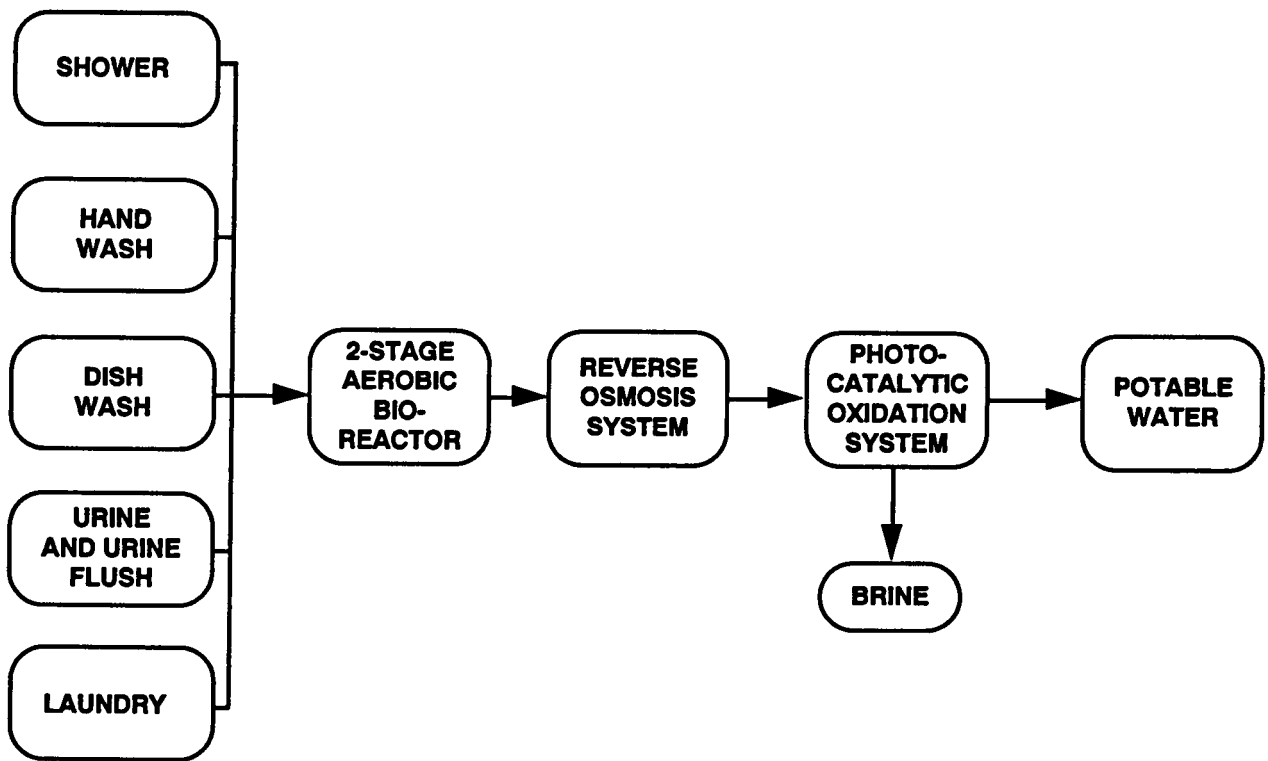


Figure 1. Hybrid Regenerative Water Recovery System Schematic.

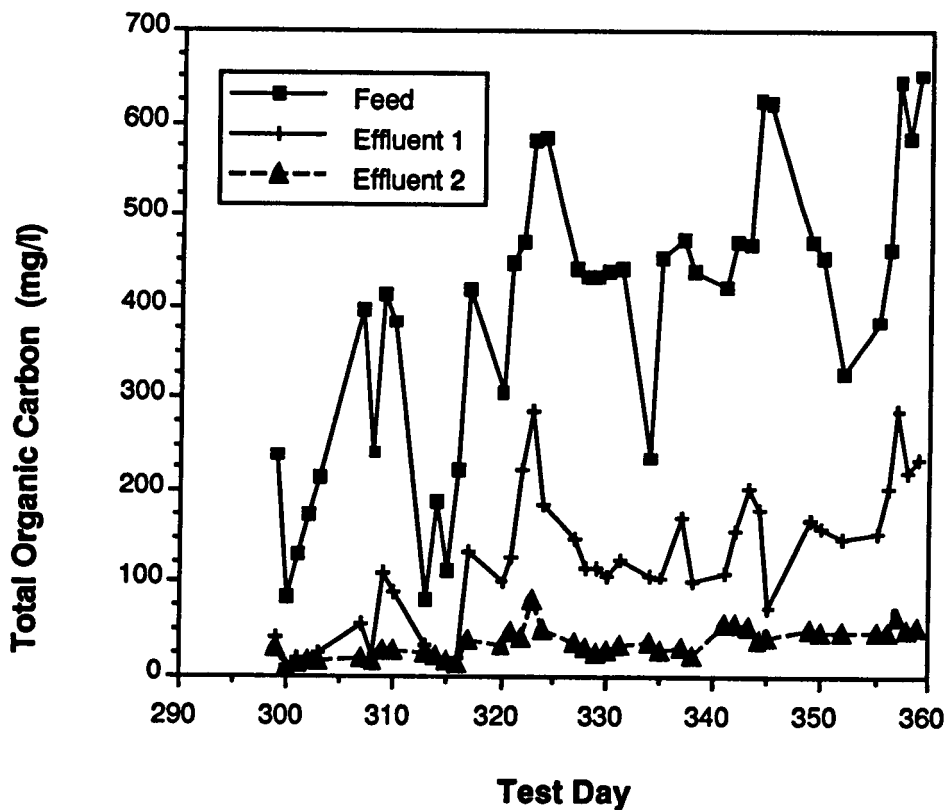


Figure 2. Total Organic Carbon Bioreactor Performance During Long Duration Testing.

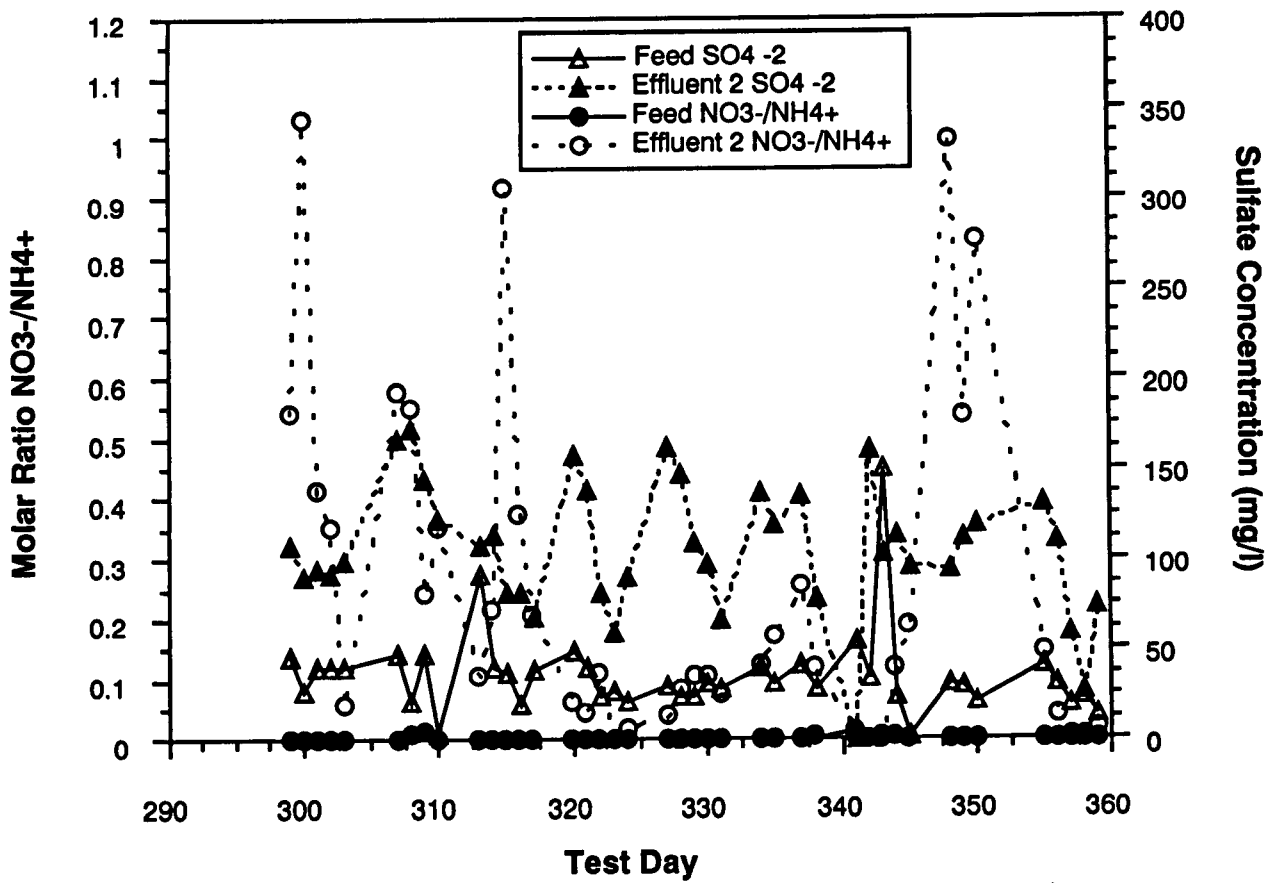


Figure 3. Ion Chromatographic Characterization During Long Duration Testing.

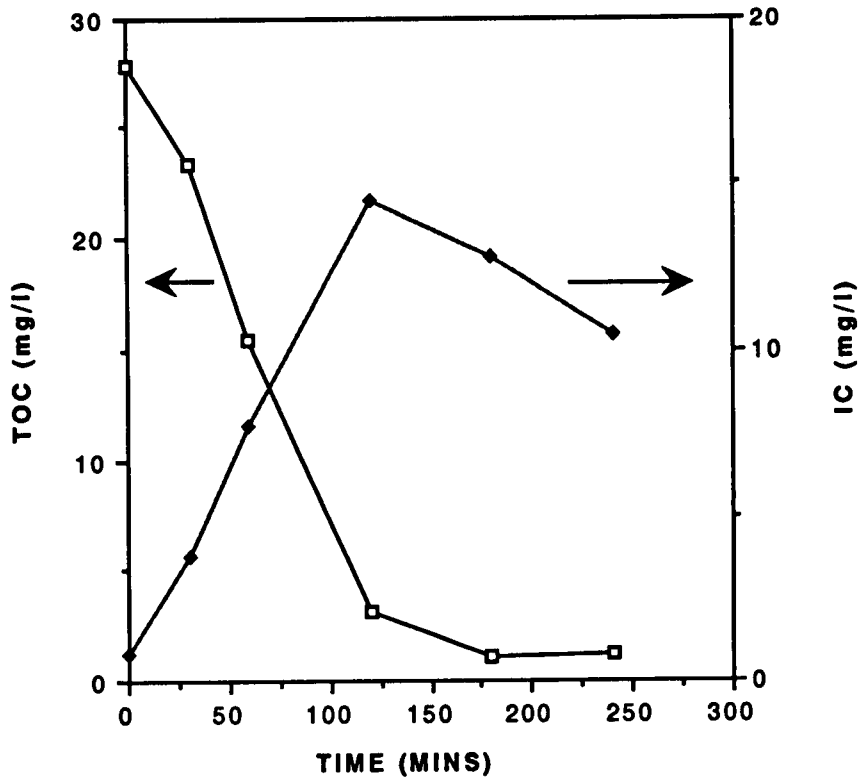


Figure 4. Profile of Organic Oxidation using the Photocatalytic Oxidation System.

Two-Phase Pressure Drop of Ammonia In Small Diameter Horizontal Tubes: Experimental Results

Eugene K. Ungar and John D. Cornwell
Johnson Space Center/EC

Abstract

Data for pressure drop in adiabatic two-phase ammonia flows in small diameter horizontal tubes are presented. The data has direct application to the sizing of the flow-through radiator tubes in the Space Station Freedom heat rejection system. The data are compared to existing correlations for pressure drop and are found to be significantly lower than the most commonly used correlations. However, several of the less commonly used correlations predict the data accurately. A recommendation is made for a method to accurately predict the pressure drop in two-phase ammonia flows in small horizontal tubes.

Nomenclature

A	cross-section area of tube, $(\pi/4)d^2$	(ft ²)
d	diameter	(ft)
	mass flow rate	(lbm/s)
Re _f	Reynolds number of the liquid as if it were flowing alone, $\rho_f u_f d / \mu_f$	
Re _g	Reynolds number of the vapor as if it were flowing alone, $\rho_g u_g d / \mu_g$	
u _f	superficial velocity of the liquid, $(1-x)/(\rho_f A)$	(ft/s)
u _g	superficial velocity of the vapor, $x/(\rho_g A)$	(ft/s)
x	quality	
μ_f	absolute viscosity of the liquid phase	(lbm/ft s)
μ_g	absolute viscosity of the vapor phase	(lbm/ft s)
ρ_f	density of the liquid phase	(lbm/ft ³)
ρ_g	density of the vapor phase	(lbm/ft ³)

Introduction

The Space Station Freedom (SSF) will be assembled on-orbit between November 1995 and December 1999. The SSF Active Thermal Control System (ATCS) acquires waste heat from the manned modules and the outboard electric components and rejects the heat through radiation to space (figure 1). The ATCS consists of three two-phase ammonia flow loops, one with a setpoint of 58°F, the other two with setpoints of 35°F. In each flow loop, liquid ammonia is partially vaporized at multiple heat acquisition sites and is returned to the pump module. Here the liquid and vapor are separated. The liquid is returned to the heat acquisition sites and the vapor is transported to the radiator array, where it is condensed and slightly subcooled. The condensed liquid is then returned to the pump module.

The ATCS heat rejection system consists of two arrays of three flow-through radiator orbital replacement units

(ORUs) each. The starboard wing contains the heat rejection for the two 35°F setpoint flow loops. The port wing contains the heat rejection for the 58°F setpoint flow loop. Each ORU contains eight panels as shown in figure 2, each 10.08 ft by 8.67 ft. Each panel contains 22 evenly spaced flow tubes as is shown in figure 3. The flow tubes are 10.5 ft long and are connected in parallel by manifolds that run the length of each ORU. The three ORUs in each array are connected in parallel.

The SSF ATCS imposes strict requirements on the radiator array pressure drop. A total of 1.4 psi is available for pressure drop through the ORUs. In order to maintain as even a flow distribution as possible, 1.0 psi is allocated for the pressure drop in the flow tubes, with the remainder allocated for the manifolds, other plumbing, and fittings.

Knowledge of the pressure drop in the flow tubes is of critical importance. If the allocated pressure drop is exceeded at the design point (maximum load), the total allocated radiator array pressure drop will be exceeded, which would cause difficulty in maintaining the ATCS setpoint. If the pressure drop at maximum load is significantly less than the 1 psi allocated, the flow distribution in the radiator ORU will suffer, which would lower the total heat rejection capability of the array.

Using the two-phase flow pressure drop prediction methods in the literature, a tube size of 0.093 in was provisionally selected to yield the desired pressure drop. However, there was a great deal of concern over the accuracy of this sizing because the pressure drop prediction methods in the literature were developed for large tubes (diameter on the order of 1 in). Also, a literature search showed that only minimal experimental work in the low quality range had been performed on two-phase flows in small diameter tubes.^{1,2} Therefore, it was decided to perform a series of tests to investigate the pressure drop for two-phase ammonia flows in SSF radiator-sized tubes. The adiabatic pressure drop tests performed at NASA Johnson Space Center that are reported here were complemented by tests of the pressure drop in condensing ammonia flows in SSF-sized tubes that were performed concurrently at LTV Missiles and Space Company³ (now Loral Vought Systems Co.).

Together the two tests were designed to yield sizing information for the SSF radiator tubes and information to allow prediction of the on-orbit performance of the SSF radiator array. As a result of these experiments, a final tube size of 0.067 in was selected to provide the required pressure drop in the flow-through radiators.

Test Rationale

The pressure drop in the SSF flow-through radiators consists of the frictional pressure drop minus the pressure recovery owing to condensation. The frictional pressure drop at any point should be identical to the pressure drop in adiabatic two-phase flow owing to the small quality gradient in the tubes (the tube length is approximately 2000 diameters). In the SSF radiators, the pressure recovery is only a few percent of the frictional pressure drop and can be easily estimated. Therefore, predicting the two-phase adiabatic pressure drop is the first and most important step in predicting the pressure drop in the SSF flow-through radiator tubes.

Ground tests were performed to measure the adiabatic two-phase pressure drop because, owing to the small tube size and the fairly high vapor velocity for the SSF radiator tubes, it was expected that the flow regime and thus the pressure drop in Earth-normal gravity (1-g) would be the same as in the microgravity (0-g) of flight. Possible two-phase flow regimes in horizontal tubes at 1-g are annular, stratified, intermittent (slug), and dispersed bubble. For our case, as long as the flow regime is not stratified, the flow regimes and the pressure drops are expected to be the same in 1-g as in 0-g.

The 1-g operating conditions for SSF flow-through radiator-size tubes for SSF flow rates were compared to Taitel and Dukler's⁴ prediction for the transition between the annular and stratified flow regimes. The limits indicate that annular flow will exist for qualities above approximately 10% in Earth-normal gravity. That is, the pressure drop in 90% of the two-phase length should be the same in 1-g and in 0-g. Because the pressure gradient is largest by far in the high quality region of the radiator tube, using a 1-g based prediction that is accurate from 100% to 10% quality will provide a pressure drop prediction with an error significantly less than 10%.

Based on these arguments, it was decided that adiabatic ground testing of the appropriate tube size, quality, and ammonia mass flow rates would provide pressure drop information directly applicable to the SSF radiator design.

Literature

There are many predictions of the pressure drop in two-phase flow available in the literature. Some of the most commonly used predictions are briefly described below:

- Homogeneous predictions treat the two-phase flow as a single fluid with mixture properties. All the mixture properties except viscosity can be easily found. The most commonly used mixture viscosity representation is that of McAdams et al.⁵
- Lockhart and Martinelli⁶ proposed a prediction based on a large number of pressure drop measurements for one- and two-component two-phase mixtures. Their correlation is generally considered to be accurate for the case of annular flow.
- Asali, Hanratty, and Andreussi⁷ proposed an annular flow

correlation that includes the effects of the thickness and roughness of the liquid film on the pressure drop.

- Crowley and Izenson⁸ extended Wallis's⁹ liquid/vapor interface Darcy friction factor correlation to allow the prediction of pressure drop in annular flow.
- In the smooth annular prediction, the Darcy friction factor for the liquid/vapor interface is taken to be the same as if the vapor were flowing alone in the tube. In comparison, the Darcy interfacial friction factor in Crowley and Izenson's model is typically an order of magnitude higher than it is for a smooth interface.

Experiment

A series of adiabatic two-phase ammonia pressure drop tests were performed at NASA/Johnson Space Center in October 1991. In these tests, a known mass flow rate of two-phase ammonia at a known quality was passed through horizontal tubes of 0.0575, 0.0701, 0.1017 and 0.1240 in diameter. The test sections were each 10 ft long with 3 ft inlet and 1 ft outlet sections of the same diameter as the test section. A precision differential pressure transducer sensed the pressure drop across the 10 ft length. A more complete description of the experimental apparatus, as well as the experiment methodology and the test results can be found in ref.¹⁰

Results

A total of 134 steady-state two-phase flow pressure drop data points were obtained for the four tube sizes at various mass flow rates and qualities. The superficial liquid Reynolds numbers (Re_l) for all the data were less than 700. The superficial vapor Reynolds numbers (Re_v) ranged from 450 to 11,000. Also, a limited number of pressure drop data points for subcooled liquid and superheated vapor flows were obtained. These data verified that the instrumentation was accurate. Representative two-phase pressure drop data are compared with the various predictions for the same nominal conditions in figures 4, 5, 6, and 7. The figures show a trend that is consistent in all the data obtained in this test. The Crowley and Izenson prediction and the Lockhart-Martinelli prediction both consistently overpredict the data by a significant amount. In contrast, the McAdams et al. homogeneous prediction, the smooth annular prediction, and the prediction of Asali et al. all match the data very well. Table 1 contains a summary of the RMS errors for the more accurate predictions when applied to the present data.

Figures 8 and 9 show comparisons between all the present two-phase data and the McAdams et al. prediction, and the prediction of Asali et al. The data is predicted equally well by both methods.

The Lockhart-Martinelli prediction is the standard for predicting pressure drop for annular flow in large tubes. Previous ammonia testing at JSC has indicated that for horizontal tubes of 0.620 and 0.706 in diameter the two-phase pressure drop is well predicted by the Lockhart-Martinelli correlation.¹¹ However, the Lockhart-Martinelli

correlation does not fit the present data for small diameter tubes. This unsuitability is not surprising considering that the Lockhart-Martinelli prediction was developed mainly from steam and air/liquid data in tubes with diameters on the order of one inch. Surface tension has a much stronger influence on two-phase flow in smaller tubes. Here surface tension effects could tend to smooth the liquid/vapor interface and hence reduce the pressure drop in annular flow. This explanation is supported by the good correlation of our data with the smoothannular model and by the accuracy of the correlation of Asali et al. which, for our data, has interfacial friction factors approximately equal to the Darcy friction factor if the vapor were flowing alone. Duschatko's et al.³ concurrent condensing flow experiments yielded results in excellent agreement with our own.

Conclusions

The pressure drop for two-phase ammonia flows in small diameter tubes cannot be predicted with acceptable accuracy using the techniques normally used for large tubes. The pressure drop data obtained in the present work is equally well predicted by the McAdams et al. homogeneous prediction and by the Asali et al. annular flow prediction. Because of its ease of calculation, the McAdams et al. homogeneous pressure drop prediction has been recommended for use in sizing the SSF ATCS flow-through radiator tubes to yield an acceptable pressure drop.

References

¹Barnea, D., Luninski, Y., and Taitel, Y., "Flow Pattern in Horizontal and Vertical Two-Phase Flow in Small Diameter Pipes," *The Canadian Journal of Engineering*, 61, 1983, pp. 617-620.
²Suo, M., Griffith, P., "Two-Phase Flow in Capillary Tubes," *Trans. ASME, Journal of Basic Engineering*, 1964, pp. 576-582.
³Duschatko, R. J., Flores, R. R., and Wolfe, G. W., "Pressure Drop Experiments in Ammonia Flow in Small Diameter Tubes, AIAA 92-2908, 27th Thermophysics Conference, Nashville TN, July 6-8, 1992.
⁴Taitel, Y., Lee, N., and Dukler, A. E., "Transient Gas-

Liquid Flow in Horizontal Pipes: Modelling the Flow Pattern Transitions," *AICHe Journal* 24 (5) 1978, pp. 920-934.

⁵McAdams, W. H., et al., "Vaporization Inside Horizontal Tubes - II - Benzene-Oil Mixtures," *Trans. ASME*, 64, 1942, pg. 193 (as cited in ref. 8).
⁶Lockhart, R. W., and Martinelli, R. C., "Proposed Correlations for Isothermal Two-Phase Two-Component Flow in Pipes," *Chem. Eng. Prog.* 39, 1949, pp. 39-48.
⁷Asali, J. C., Hanratty, T. J., and Andreussi, P., "Interfacial Drag and Film Height for Vertical Annular Flow," *AICHe Journal*, 31 (6), 1985, pp. 895-902.
⁸Crowley, C.G, and Izenson, M. G., "Design Manual for Microgravity Two-Phase Flow and Heat Transfer," Final report from Creare Inc. to Air Force Astronautics Laboratory, Report no. AL-TR-89-027, 1989.
⁹Wallis, G. B., One-Dimensional Two-Phase Flow, McGraw-Hill, New York, 1969.
¹⁰E. K. Ungar and J. D. Cornwell, "Two-Phase Pressure Drop of Ammonia in Small Diameter Horizontal Tubes," presented at 17th AIAA Ground Testing Conference, Nashville, TN, July 6-8, 1992, AIAA-92-3891.
¹¹Sifuentes, R., "Ground Test Article (GTA) Phase I Quick Look Report," JSC 25084, NASA/Johnson Space Center, 1991.

Acknowledgments

This test was conducted by McDonnell Douglas Space Systems Company (MDSSC) for the Crew and Thermal Systems Division of NASA Johnson Space Center. The authors wish to acknowledge the contributions of two MDSSC engineers, John V. Fussell and Jody R. Augustine, who performed an outstanding job both during the test buildup and throughout the performance of the test. The authors also wish to thank Loral Vought Systems Co. for allowing the use of figures 1, 2, and 3.

Table 1 - Comparison of Existing Prediction Methods for the Present Data

Prediction Type	RMS error		
	Re _g <1500	Re _g >1500	all
Lockhart-Martinelli	70.6%	100%	95.9%
Smooth Annular	160%	23.5%	34.4%
McAdams et al.	33.3%	21.2%	23.8%
Asali et al.	30.7%	18.5%	21.2%

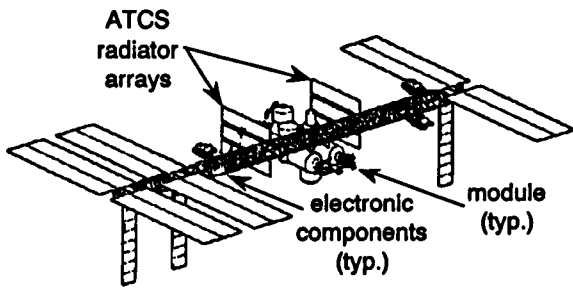


Figure 1. Space Station Freedom.

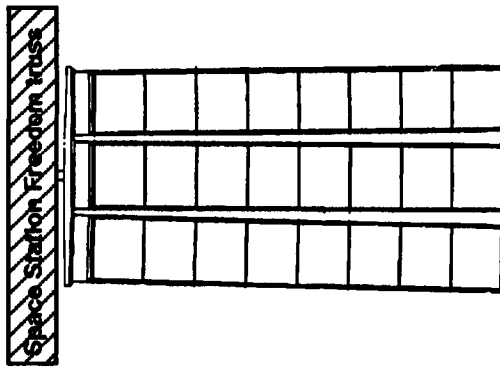


Figure 2. Radiator Panel Array (typ.).

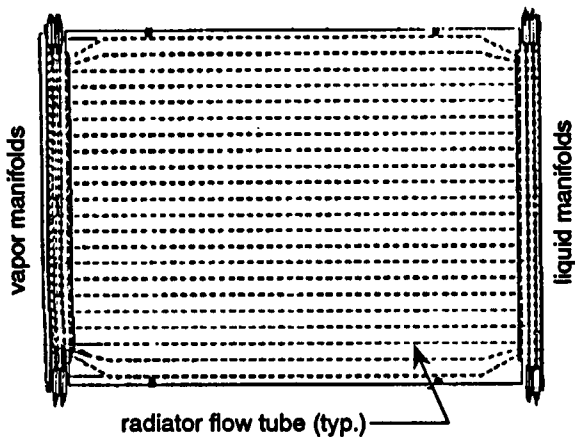


Figure 3. SSF Flow-Through Radiator Panel.

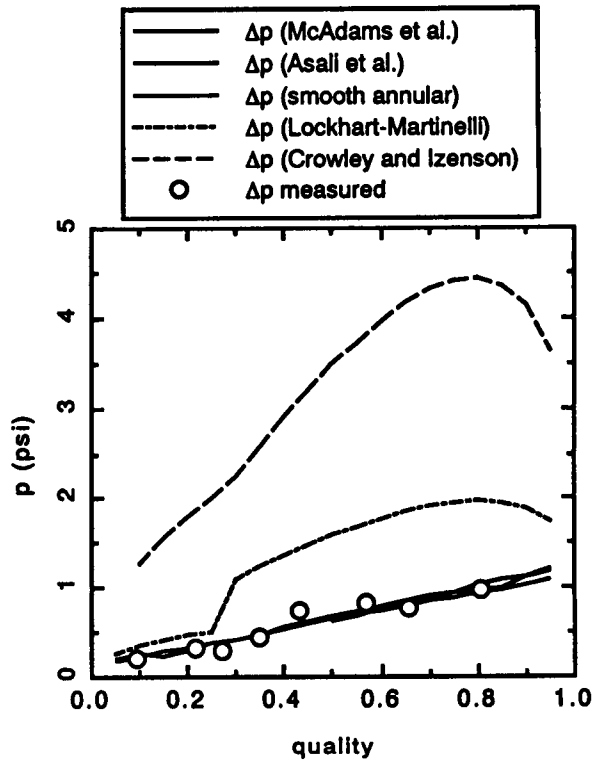


Figure 4. Data and Predictions for 0.0575 inch tube, 0.55 lbm/hr, 76°F.

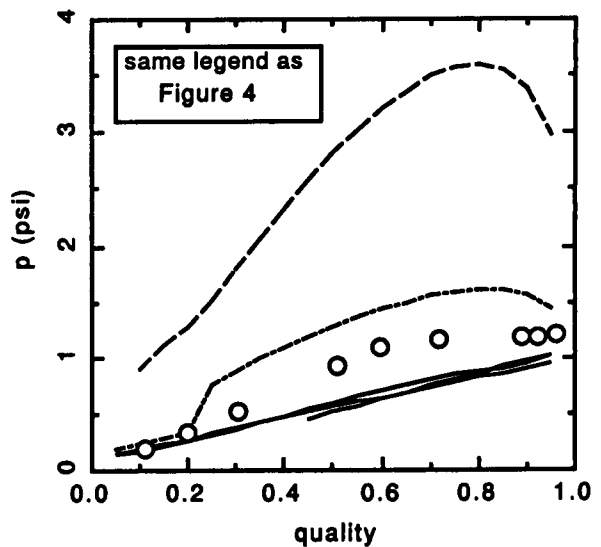


Figure 5. Data and Predictions for 0.0701 inch tube, 0.86 lbm/hr, 76°F.

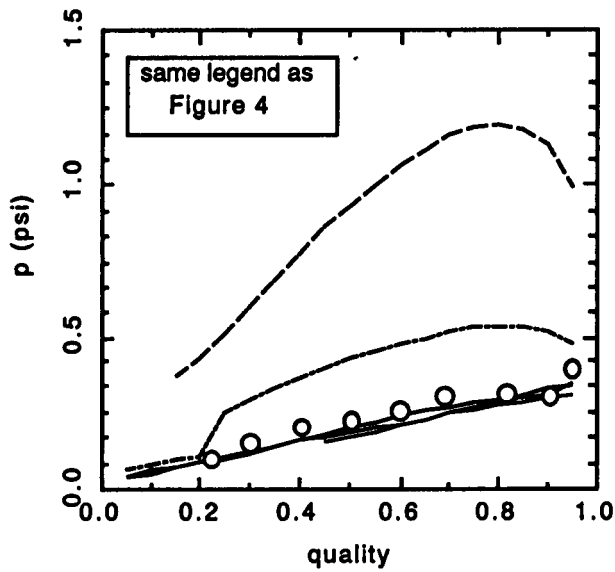


Figure 6. Data and Predictions for 0.1017 inch tube, 1.24 lbm/hr, 74°F.

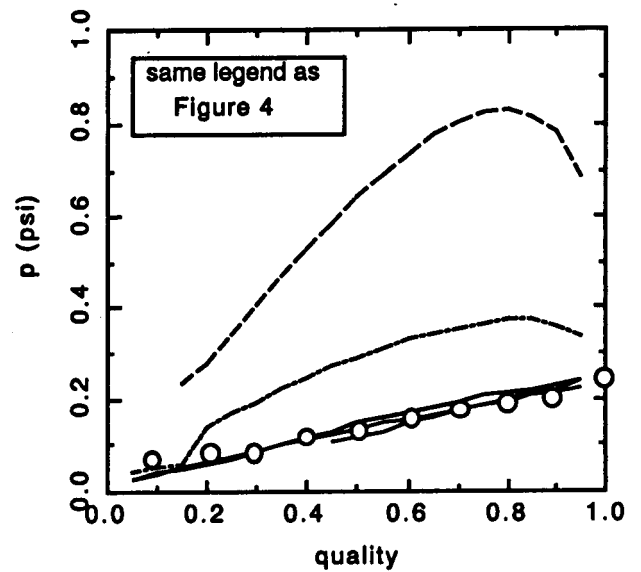


Figure 7. Data and Predictions for 0.1240 inch tube, 1.75 lbm/hr, 74°F.

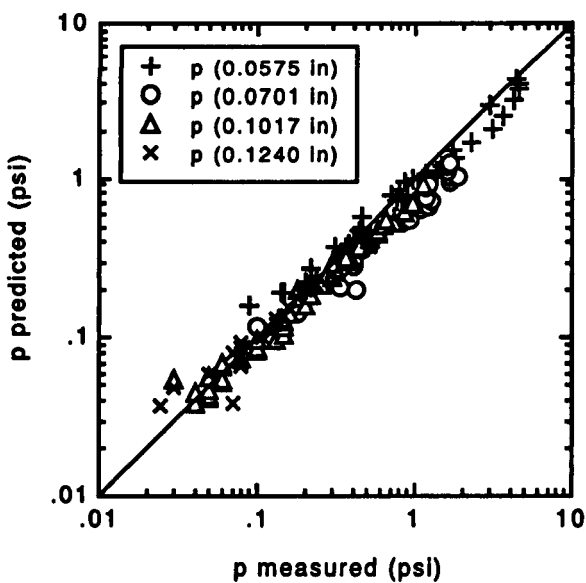


Figure 8. Comparison of Present Data with the McAdams et al. Prediction.

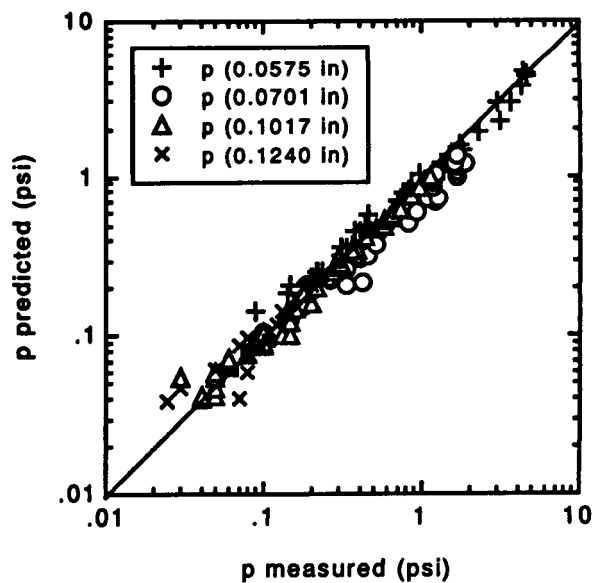


Figure 9. Comparison of Present Data with the Asali et al. Prediction.

Two-Phase Flow Characterization for Fluid Components and Variable Gravity Conditions

Kathryn M. Miller
Johnson Space Center/EC

Abstract

The program entitled "Two-Phase Flow Characterization for Fluid Components and Variable Gravity Conditions" was initiated by JSC to investigate vapor-liquid flow regimes and pressure drops in pipe components under variable gravity conditions. The program supports the Space Station Freedom (SSF) external active thermal control system (ATCS) and utility distribution system designs as well as future space missions, including the proposed Moon/Mars missions. Objectives for the program include studying two-phase flow behavior in fluid components (smooth pipes, bellows lines, quick-disconnect fittings), expanding the two-phase data base for zero-g conditions, developing a data base for low-g conditions (Moon g, Mars g), and validating models for two-phase flow analyses. Zero-g and low-g data were gathered using a Freon-12 flow loop during five test series on the NASA KC-135 aircraft.

A large flow regime data base was developed for smooth tubes in four gravity levels (zero g, 1/6 g (Moon), 1/3 g (Mars), one g). More limited pressure drop data were also obtained for the smooth tubes and component test sections for zero-g and low-g conditions. This program produced the first published, low-g, two-phase data and also provided data to support the SSF Program.

Introduction

Programs that require increased waste thermal power levels caused an evolution in space system thermal control from conduction paths to single-phase working fluid loops. The SSF will employ the next step in that evolution because its higher power levels and longer transport distances have led to the use of a two-phase ammonia working fluid system, the ATCS. This system will provide a virtually isothermal energy sink at lower mass and pump power than would be possible with a single-phase system. Future space missions, such as the proposed Moon/Mars missions, will have even more demanding thermal management requirements. The full potential of two-phase systems will be used to make these missions more viable. The highly complex phenomena of two-phase flow often requires empirical treatment, however; and at the time this program was initiated, zero-g data were sparse and there were no published low-g data.

JSC has had previous experience in the research and development of two-phase space systems, including: reduced-gravity flight experiments on the KC-135

aircraft^{1,2}; ground and Shuttle flight experiments of heat pipes^{3,4}; and, most notably, ground evaluation and development of two-phase thermal control systems for SSF.

The JSC project described in this report was a KC-135-based experimentation effort initiated in fiscal year 1991 (FY91). The following sections present the problem statement, program overview, and some available results.

Problem Statement

As stated previously, the highly complex nature of two-phase flows, the sparsity of associated microgravity data, and the lack of any low-g, two-phase data were all drivers for initiating the program. Objectives for the program included studying two-phase flow behavior in fluid components (smooth pipes, bellows lines, quick-disconnect fittings), expanding the two-phase data base for zero-g conditions, developing a data base for low-g conditions (Moon g, Mars g), and validating models for two-phase flow analyses.

Program Overview

The following paragraphs provide a brief overview of the program. This overview includes a description of the test package, brief sections on the flow regime and pressure drop testing, and a summary of the test flights.

Experiment Package Description

The experiment package, shown schematically in figure 1, was developed by Foster-Miller Inc. as part of a Phase II small business innovative research contract performed for the United States Air Force (USAF) Phillips Laboratory at Kirtland Air Force Base. The Phillips Laboratory/Foster-Miller package was selected for this program because of its history of KC-135 flight testing during 1990.⁶ The USAF agreed to loan the test package to the JSC for the 2-year project.

The experiment package was delivered to the Thermochemical Test Area at JSC in April 1991 to undergo modifications. Alterations were made to the package to enable different components' testing and to allow for a wider range of flow rates of both the liquid and vapor phases. After modifications, the experiment package contained two adiabatic test sections that had 1.2-m (48-in.) length and a straight inlet length of ~0.6 m (24 in.). The smooth pipe test sections had 10.4-mm

(0.41-in.) and 4.6-mm (0.18-in) inner diameters. Vapor flow measurements were made with a low-range or a high-range venturi meter. Liquid flow measurements were taken with a low-range or a high-range turbine-type meter. Combining the minimum measurable flows with the pump upper limit allowed flow rates of roughly 0.001 to 0.090 kg/s (713 lbm/hr) of liquid and 0.001 to 0.010 kg/s (79 lbm/hr) of vapor. A more detailed description of the package after modifications can be found in the report by Best.⁷

In addition to being well proven on the KC-135, this test loop offered a unique characteristic by employing a Foster-Miller two-phase pump, which could process inlet mixtures of any quality. Freon-12 was selected for the working fluid because of its low toxicity, heat of vaporization, low surface tension, material compatibility properties, and high vapor density at acceptable pressures. Nominal operating conditions were 588.4 kPa (85 psia) and 294 K (70°F).

Flow Regime Testing

Flow regimes are the spatial distributions of liquid and vapor phases flowing in a pipe. The prediction of other parameters, such as pressure drop and heat transfer coefficient, is specific to the flow regime experienced. The project's goal for predicting flow regime transitions and, thus, characterizing two-phase flows was to develop a model that could be used for a wide range of fluids and environmental conditions, including the reduced gravity of the Moon or Mars and the zero g on orbit.

Pressure Drop Testing

Pressure drop can profoundly affect pipe and pump sizing—and, hence, the mass and power—of two-phase thermal control systems. These effects are particularly critical for space systems, where penalties for under- or over-designing are significant. The pressure drop testing of this project had two thrusts: to provide one- and zero-g two-phase pressure drop data through fluid components to verify design procedures for the Space Station external ATCS and utility distribution system, and to provide pressure drop data for smooth pipes at different gravity levels.

Flight Series

Zero-g and low-g, two-phase flow data were gathered on five flight series onboard the NASA KC-135 aircraft during FY91 and FY92. More than 500 parabolas were flown. A picture of the experiment package in its test configuration onboard the KC-135 is shown in figure 2.

The following list summarizes the time frame and gravity levels of the flight tests completed:

- Flight Series I, August 19-23, 1991, four zero-g flights
- Flight Series II, November 19-21, 1991, three zero-g flights

- Flight Series III, December 17-20, 1991, one zero-g and three Moon-g flights
- Flight Series IV, January 22-31, 1992, two zero-g, one Moon-g and one Mars-g flights
- Flight Series V, July 7-10, 1992, two zero-g and two Mars-g flights

Results

A large flow regime data base has been developed for smooth tubes in four gravity levels (zero g, $1/6$ g (Moon), $1/3$ g (Mars), and one g). Results indicate the existence of a unique flow regime for low-g conditions, a regime that is presently named stratified/annular. This regime is similar to the annular regime normally seen in zero g with the exception that the fluid film coating the tube is much thicker on the bottom than on the top because of low gravity effects. Flow regime data obtained for Mars-g are shown in figure 3.

Approximate regions are shown (fig. 3) for the major flow regimes as seen under Mars-g conditions (stratified, plug, stratified/annular, and annular). Some overlap of the data is evident, and this overlap is representative of the transition zone for flow regimes. Work is continuing on comparison of these data to existing and developed flow regime models.

More limited pressure drop data were also obtained for the smooth tubes and component test sections for zero-g and low-g conditions. Analyses are continuing to interpret these data for the final report.

Conclusions

This program has produced the first published, low-g, two-phase flow regime and pressure drop data, and has also provided data to support the SSF Program. Project results will be documented in an internal JSC report, "JSC-32261 Two-Phase Flow Characterization for Fluid Components and Four Gravity Levels," which is expected to be published in early 1993. The Crew and Thermal Systems Division at JSC is currently pursuing an orbital flight experiment through the INSTEP program as the next major technical step in the advancement of two-phase flow systems and modeling.

References

- ¹Kachnik, L., Lee, D., Best, F. R., and Faget, N., "A Microgravity Boiling and Convective Condensation Experiment," in *Trans. ASME Winter Annual Meeting*, ASME Paper 87-WA/HT-12, held in Boston, MA, December 13-18, 1987.
- ²Chen, I-Y., Downing, R. S., Parish, R., and Keshock E., "A Reduced Gravity Flight Experiment: Observed Flow Regimes and Pressure Drops of Vapor and Liquid Flow in Adiabatic Piping," *AIChE Symposium Series*, Vol. 84, No. 263, pp. 203-216, 1988.
- ³Rankin, J. G., "Integration and Flight Demonstration of a

High-Capacity Monogroove Heat-Pipe Radiator," in *AIAA 19th Thermophysics Conference*, AIAA-84-1716, 1984.

⁴Kosson, R., Brown, R., and Ungar, E., "Space Station Heat Pipe Advanced Radiator Element (SHARE) Flight Test Results and Analysis," in 28th Aerospace Sciences Meeting, AIAA-90-0059, 1990.

⁵Brady, T., "Summary of Results from the Testing of Three Prototype Thermal Bus Systems for Space Station Freedom," in AIAA/ASME 5th Joint Thermophysics and Heat Transfer Conference, AIAA-90-1740, 1990.

⁶Hill, W. S., and Best, F. R., "Definition of Two-Phase Flow Behaviors for Spacecraft Design," in Final Report, Contract No. F29601-88-C-0062, Air Force Phillips Laboratory, Kirtland AFB, NM, 1991.

⁷Best, F. R., "NASA JSC Microgravity Two Phase Flow Project," in Test Equipment Data Package July 1991, Texas A&M University, College Station, TX, 1991.

Acknowledgments

This work was performed at JSC as a cooperative effort among the Propulsion and Power Division, the Crew and Thermal Systems Division, and the New Initiatives Office. Space Station funding was provided through the divisions for the components studies and by the JSC Center Director's Discretionary Fund for the advanced low-g studies.

The author wishes to acknowledge Dr. Frederick Best and his staff at Texas A&M University and Dr. Wayne Hill of Foster-Miller Inc., subcontracted to Texas A&M, for providing expertise in both two-phase flow analyses and KC-135 testing. In addition, the cooperation of the NASA KC-135 support staff was greatly appreciated. The author would also like to thank the USAF Phillips Laboratory on behalf of NASA for loaning the equipment package for the duration of this program.

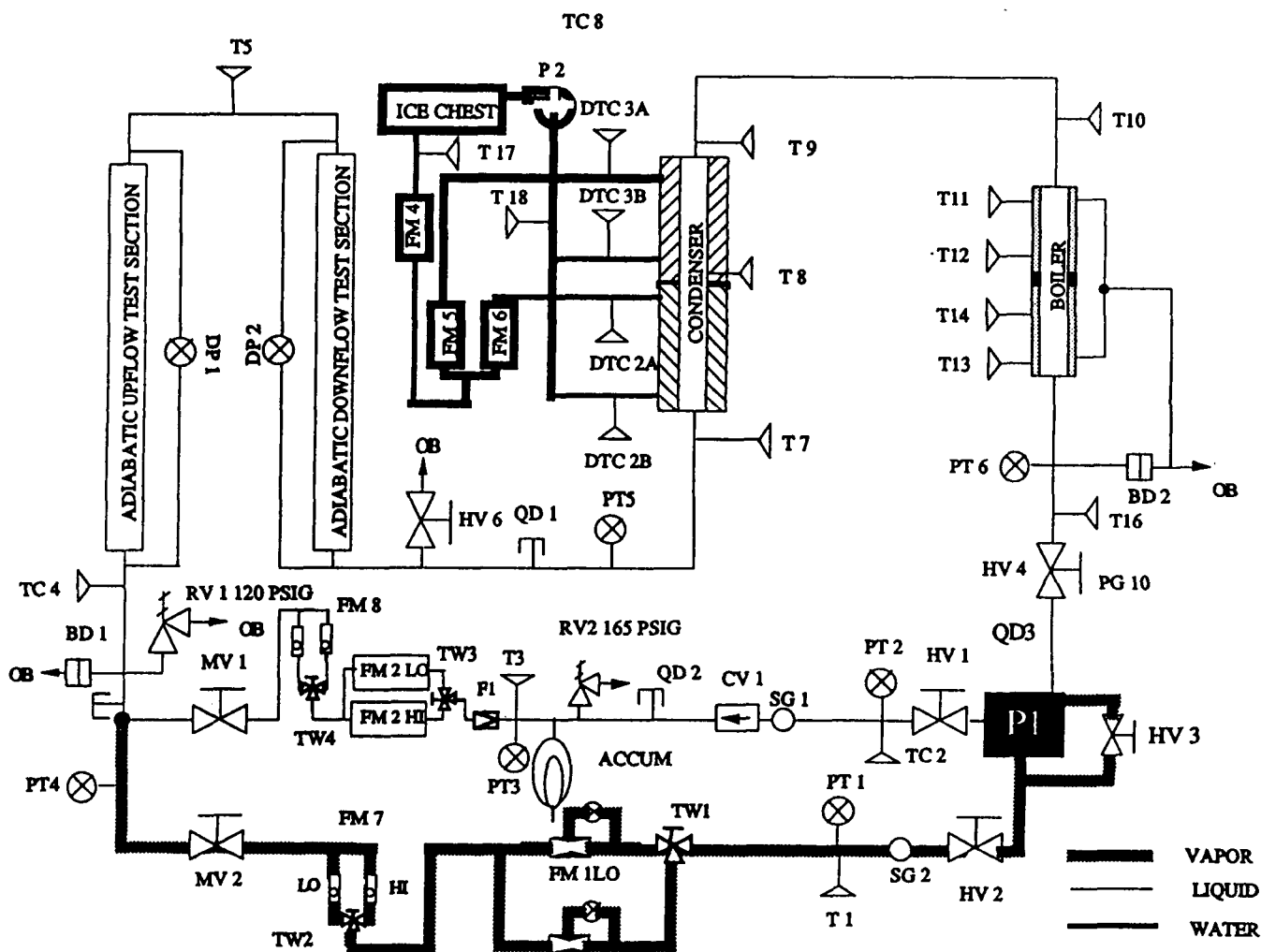


Figure 1. Two-Phase Experiment Loop Schematic, Post-Modifications (Best 1991).

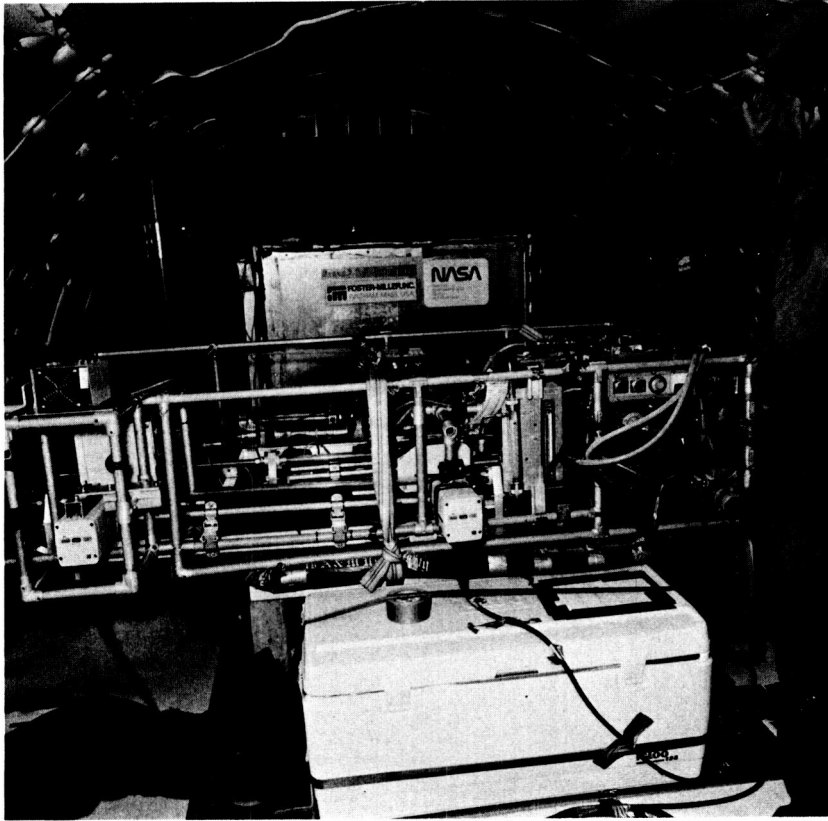


Figure 2. Phillips Laboratory/Foster-Miller Experiment Package Aboard the KC-135.

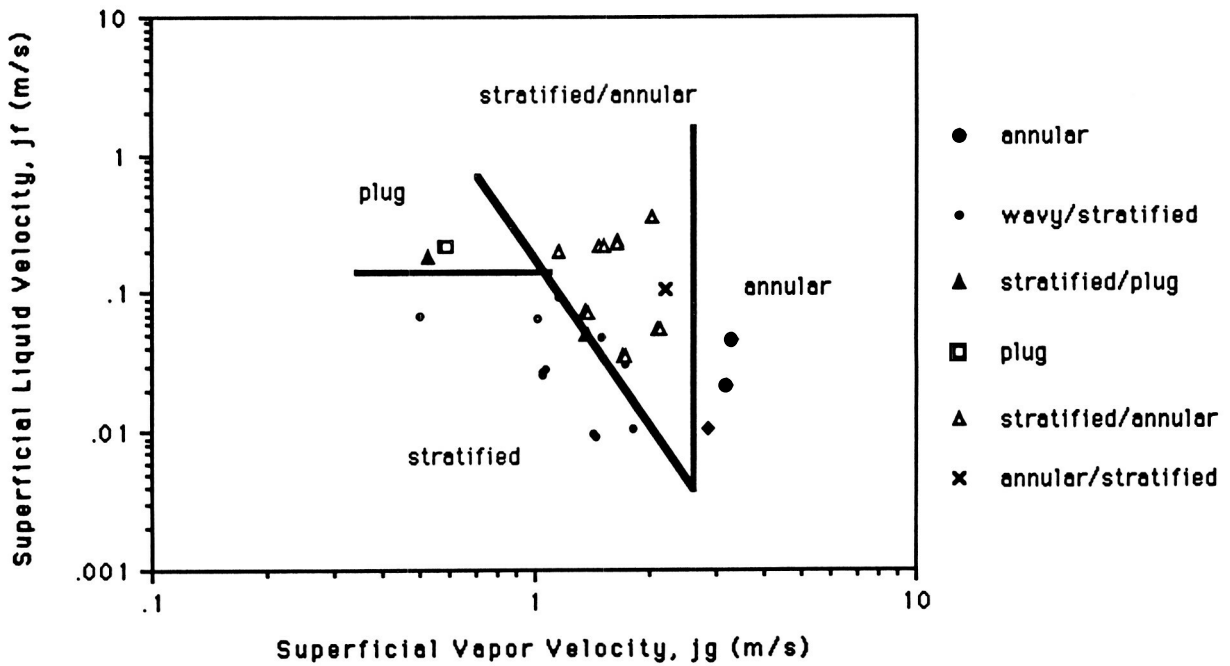


Figure 3. Flow Regime Data for $1/3$ g (Mars) with a Tube ID = 0.0105 m.

Electromagnetic Probe Development for Fluid Flow Measurements

G. D. Arndt, Jim Carl,* and W. W. Koepsel**

Johnson Space Center/EE

*Lockheed Engineering and Sciences Company

**Mutronics System

Abstract

A simple, nonintrusive electromagnetic probe has been developed that can measure instantaneous changes in the flow rates of two fluids or two states of a single fluid. This technique makes the measurements by distinguishing between the differences in the dielectric constants of the two liquids or gas/liquid phases of the same fluid. Possible NASA applications include measurements of helium/hydrazine flow during rocket tests at White Sands Test Facility, liquid/gas flow in hydrogen or oxygen lines in Orbiter engines, and liquid/gaseous Freon™ flow in zero g tests with the KC-135 aircraft at JSC.

Introduction

Ground testing of reaction control system (RCS) thrusters at the White Sands Test Facility (WSTF) are constrained by not being able to measure helium and hydrazine flowing through inlet pipes to the thruster engine. A microwave technique has been developed that can measure instantaneous flow rates of two liquids or two states of a single fluid. This technique, which is sensitive to the dielectric constants of two liquids or liquid/gas phases, has numerous NASA applications:

- monitoring of the aforementioned helium and hydrazine flowing through inlet pipes to RCS thrusters
- monitoring of Freon conditions in zero g
- monitoring of liquid/gaseous conditions in cryogenic hydrogen or oxygen flow lines
- monitoring of water/gas flow in flapper valve tests at JSC
- determining the existence of bubbles on a flow line

System Description

In this system, a microwave coaxial transmission line is inserted through the wall of the pipe into the fluid(s). The center pin of the small probe has minimal extension into the fluid inside the pipe. The fluid acts as a load impedance on the transmission line, and this load varies with the changes in the effective dielectric constant of the fluids changes as the fluids flow past.

A microwave signal is continuously transmitted down the coaxial line into the pipe, and a reflected signal travels back. This reflected signal is dependent upon the S_{11} parameter as defined by

$$S_{11} = \frac{Z_0 - Z_L}{Z_0 + Z_L} = P e^{-j\Theta}$$

where

Z_0 is the characteristic impedance of the coaxial line (50 Ohms)

Z_L is the load impedance on the coax due to the fluid within the pipe

Θ is the angle of the complex S_{11} parameter, which is dependent upon the effective dielectric constant of the fluid in the pipe.

The system essentially measures the instantaneous phase angle of the reflected signal from the terminated probe within the pipe. The amount of the phase shift measured when the flow changes from all liquid 1 to all liquid 2 is dependent upon the dielectric constants of the two liquids. Similarly, measurements of the liquid/gas phases of the same fluid are dependent upon the dielectric constants of the liquid and the gas. It is a simpler task to measure changes in two liquids flowing through a pipe than it is to measure differences in the flow rates of liquid and gas states of the same fluid. This is because the dielectric constants of the liquid and gas states of cryogenic fluids are usually very close to the same values.

The electronic circuitry used to measure the instantaneous changes in phase as a function of time is shown in figure 1. In this system, a dual phase detector is used to measure the inphase component (I-channel) and quadrature component (Q-channel) of the instantaneous phase of the reflected signal. The "I" and "Q" channel outputs make the system easier to calibrate and to minimize long-term phase drifts within the electronics.

The DC output voltages from the phase detector are converted to digital data using an A/D converter as part of a data acquisition board integrated with a personal computer. The software has been customized to control the measurement rate and scaling of the data to maximize the frequency shifts for the individual dielectric constants of the fluids under measurement. The data for a single measurement run can be placed in a file for display in graphical form for immediate analysis or transferred to a disc for later processing. A block diagram of the complete electromagnetic probe system (hardware and software) is shown in figure 2.

Software has also been written to calculate the average value of the measurement run or any portion of the run. This calculation allows a valve for the average relative dielectric constant to be obtained.

Proof-of-Concept Tests

A complete system was built and tested in a field environment at the JSC. A Shuttle Program "flapper valve test" was conducted in building 356 in February 1992 in which deionized water and gaseous nitrogen were pumped at various flow rates through a specific flapper valve. The purpose of the tests was to determine the spring wear dynamics on the valve. For each flow rate (10 gal to 50 gal per min), the percentage of N_2 was varied from 10% to 75%.

All measurement runs for the microwave sensor were for a period of 10 sec. During this period, 6000 measurements were made and reported. A sample measurement run of the instantaneous nitrogen gas and water through the inlet pipe to the flapper valve is shown in figure 3. In this data collection, the percentage nitrogen is referred to as the void fraction. The data in figure 3 show the effects on large gas bubbles (little or no water present) as well as small bubble perturbations within the water flow. Visible observations of the water/gas flow through the clear tube confirmed this flow characteristic.

Summary

When fluids are flowing rapidly through a pipe, a flush-mounted or a short probe may be necessary so as not to disturb the flow. For the test programs to date, a probe length into the fluid of 0 to 2 mm has been used. The short probe "sees" fluid only a short distance away. If necessary to see farther into the media, an increase in probe length is needed to increase the effective fluid volume that influences the probe load impedance. A higher resonance frequency for the probe may also increase the effective volume.

To summarize, a microwave technique has been developed and tested that measures the change of phase of a reflected signal from a transmission line probe terminated within a fluid inside a pipe. The hardware and software can be optimized to enhance the measurement sensitivity of a system that measures a particular fluid. This system, which can be used in both NASA and commercial applications, is considered unique and will be patented.

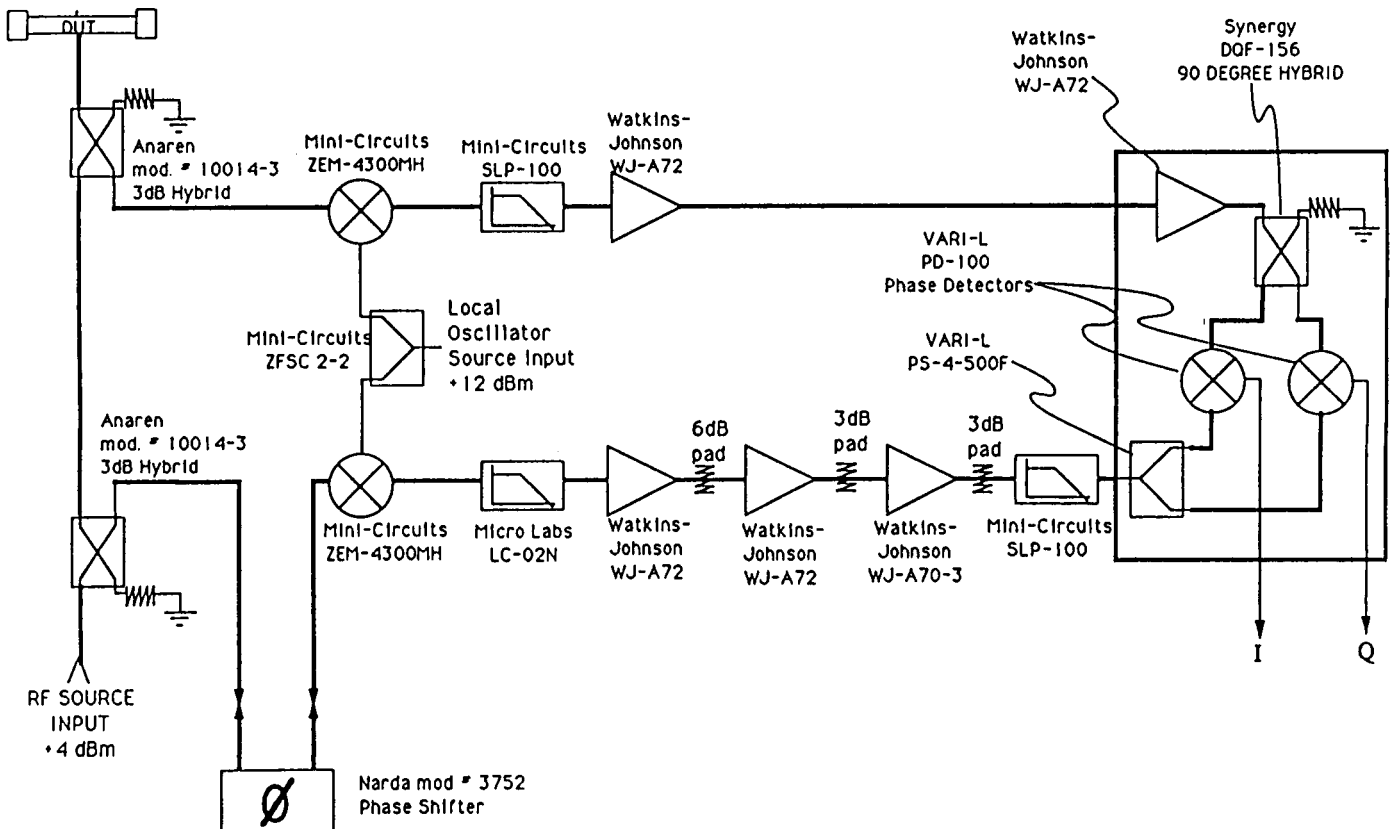


Figure 1. Phase Detector Block Diagram.

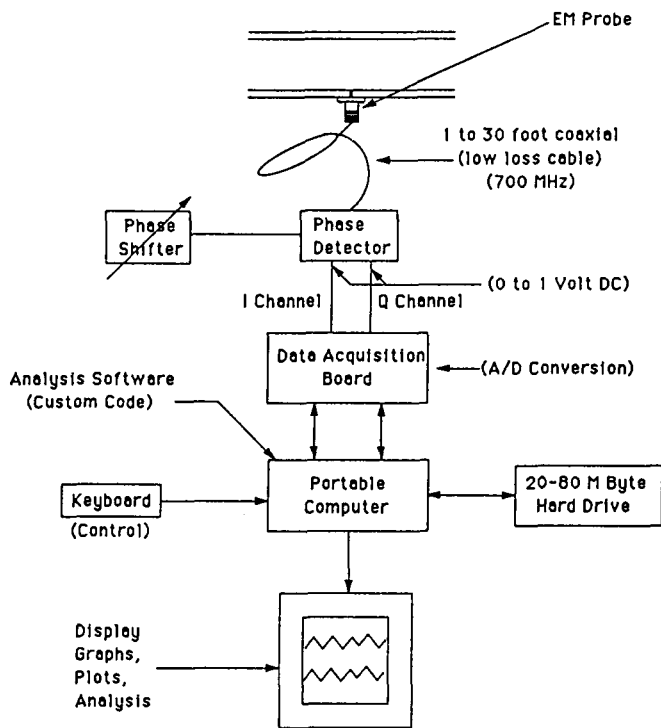


Figure 2. EM Probe System Block Diagram.

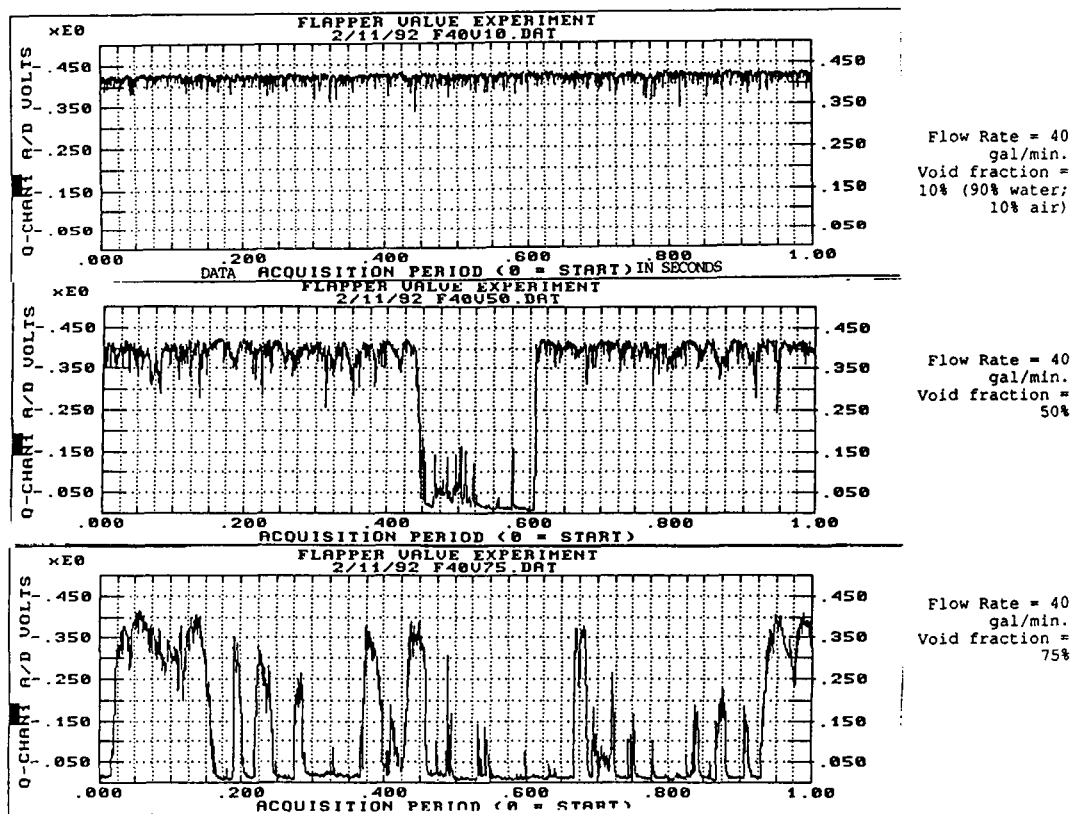


Figure 3. Flapper Valve Experiment Using Distilled Water and Air.

High Temperature Superconductivity Communications Flight Experiment

P. Ngo, K. Krishen, D. Arndt, G. Raffoul,* V. Karasack,*

K. Bhasin,** R. Leonard**

Johnson Space Center/EE/IA/EE

*Lockheed Engineering and Sciences Company

**Lewis Research Center

Abstract

A high temperature superconductivity (HTSC) flight experiment from the payload bay of the Space Shuttle Orbiter to the advanced communications technology satellite (ACTS) is being breadboarded. This proposed experiment, a joint project between JSC and the Lewis Research Center, would use a Ka-band (20 GHz) HTSC phased array antenna and front-end electronics (low noise amplifier) to receive a downlink communications signal from the ACTS. A conventional receiver demodulates the encoded telemetry signal, which is then turned around and transmitted back to ACTS and the ground.

The HTSC phased array has nine 4x4 microstrip patch antenna subarrays, which, when properly phased, provide approximately 24 dB of boresight gain. An 8x8 HTSC microstrip patch array has been built and tested. A Ka-band receiver, transmitter, modem, encoder, decoder, etc., are now being built and tested. Link analyses and interface problems with the Orbiter are addressed in the paper in addition to the design, fabrication, and testing of various subsystems used in the communication link.

Introduction

The recent discovery of high temperature superconductivities (HTSCs) has focused attention on the search for applications that will enhance the performance of communications systems. With the natural cooling abilities of space under certain conditions, potential space applications are attractive. One application is the use of HTSC materials in microwave and mm-wave feed networks for large antenna arrays. This application could enhance the communications system performance, primarily by reducing front-end losses, but by also allowing bulky waveguide feed structures to be replaced with smaller, high performance planar structures.

This paper describes a proposed HTSC mm-wave communications flight experiment between a Shuttle Orbiter in low Earth orbit (LEO) and the advanced communications technology satellite (ACTS) in geosynchronous orbit. The experiment involves a Ka-band, superconducting phased array antenna with the front-end electronics developed by the Lewis Research Center (LeRC) and the receiver, with appropriate interfaces in an Orbiter payload bay, developed by JSC personnel. Breadboard hardware for the various subsystems are

being built and tested. The expected timeframe for the experiment is 1996. The advantages of such an experiment include

- the first use of a complete HTSC communications system operating in a manned spacecraft environment,
- an evaluation of the thermal interfaces, cooling rates, and interfaces required for an HTSC system to work in an operational space environment,
- provides direct distribution of data from the ground to a spacecraft without the additional hops involved in the present communication links through the Whites Sands Test Facility, and
- the first utilization of the 19.7 GHz forward link from the ACTS to an orbiting spacecraft.

System Configuration

The ACTS is an experimental, geosynchronous satellite scheduled to be launched in February 1993 with a 4-yr expected operational lifetime. This satellite, which has been designed and developed by the LeRC, provides spot beams to fixed ground locations within the United States. It also has a 1.1m, computer steerable antenna that can communicate with LEO spacecraft. The system configuration, as shown in figure 1, has an uplink signal at 29.5 GHz, which is transmitted from the Electronic Systems Test Laboratory (ESTL) at JSC or from the LeRC to the ACTS. The signal is received by the 2.2m antenna on the ACTS, routed via a matrix switch to the 1.1m antenna, which transmits the signal at 19.7 GHz to the Orbiter. This is a bent-pipe mode within the ACTS with a 900 MHz IF bandwidth. The maximum Doppler shift during the experiment is approximately 500 MHz, which exceeds the capability of the ACTS baseband processing mode (demodulation/modulation).

The experiment program includes development of the space hardware for the Orbiter as well as ground transmitting equipment needed in the ESTL. In addition, the program includes certification testing and documentation required for flight on the Orbiter, integration into the payload bay, and the interfaces with the other Orbiter equipment. Certification testing includes four areas: thermal vacuum, vibration, structural loads, and electromagnetic interference (EMI). The experiment is categorized as a Class C payload (economically re-flyable or repeatable) with no Orbiter impacts in the event of an experiment failure.

A detailed block diagram of the spacecraft equipment is given in figure 2. The HTSC antenna could be a circular polarized phased array with nine subarrays; each subarray has 4x4 microstrip patch antennas. This antenna will be discussed in detail later in the paper. The antenna has approximately 25 dB of gain with a 10° half-power beamwidth. Each of the nine subarrays feeds a low-noise amplifier, followed by a monolithic microwave integrated circuit (MMIC) phase shifter. The phase shifters are controlled by a dedicated antenna controller that takes the state vector of the Orbiter from the payload interface panel and calculates the required phase shifter settings to point the beam electronically. Mechanical pointing requirements, as determined by the 3 dB beamwidth of a subarray, are approximately ±15° for boresight alignment.

Ground Equipment

The ground terminal at JSC has a 1.2m parabolic antenna, which is manually pointed to the ACTS. A baseband signal, 100 Kbps to 300 Kbps with convolutional encoding, is biphase modulated onto uplink carrier. The type of modulation data has not been determined.

Spacecraft Receiver

The spacecraft receiver requires either a large sweep bandwidth to acquire the Doppler shifted signal of ±500 MHz with a maximum rate of change of 0.6 KHz/sec, or the ground transmitter must have a preprogrammed ephemeris to compensate for the Doppler shift. It will probably be easier and less costly to Doppler compensate on the ground. Also, it has not been decided whether to record the uplink data for postmission evaluation or to turn around the data and transmit back to the ground via the normal Ku-band tracking data relay satellite system link or to use the Ka-band return link of the ACTS.

Link Performance

The circuit margin calculations for the forward link are shown in table 1. There is a 3 dB polarization loss in the ACTS/Orbiter link because of the linear polarized ACTS antenna and the circular polarized Orbiter antenna. The ACTS is operating in a bent-pipe configuration with a 900 MHz bandwidth; signal suppression could occur in the satellite's limiter, and a power sharing loss could occur in the output power amplifier. However, recent test data taken on a prototype ACTS system indicated little or no power sharing losses or signal suppression (private communications). Accordingly, these losses are zero in the calculations. A coding gain of 5 dB for the data is used to provide 2.9 dB of link margin for 300 Kbps of data.

Thermal Loading

Several thermal loading configurations were calculated for payloads located in the Orbiter payload bay. The analyses were performed using the thermal radiation analyzer system (TRASYS) model to produce radiation conductors and heating rates for various orbit attitudes; the TRASYS output is used as an input for the systems improved numerical differencing analyzer model to calculate temperatures for 136 nodes (points) within the Orbiter payload bay. A payload bay temperature of -250°F (113 K) could be achieved with even colder temperatures by using thermal isolator between the equipment and the payload bay structure. Regardless, a small cooling refrigerator will be necessary for the HTSC equipment.

Superconducting Antenna Array

The use of HTSC materials in antenna designs will increase the radiation efficiency of any antenna by reducing the ohmic losses in the structure. This appears as an increase in the gain of the antenna, since gain and radiation efficiency are in direct proportion. The use of HTSC materials will have a negligible effect on the shape of the antenna radiation pattern.

Although the gain of all normal-metal antennas can be increased to some extent via the use of superconductors, mm-wave arrays appear to have the greatest potential for practical improvement. For a corporate-fed array with a uniform excitation across its aperture, the gain of the array is

$$G(\text{dB}) = 10 \log(4\pi A/\lambda^2) - \alpha L \quad (3)$$

where A is the aperture area, λ is the wavelength of operation, α is the attenuation (dB/unit length), and L is the length of the transmission line from the array feed point to any radiating element. Figures 3 and 4 show how the length of the feed lines increases with greater array size and how the feed network losses affect the gain of the array, respectively. As can be seen, if losses can be neglected ($\alpha=0$), an arbitrarily large gain can be obtained if the physical size of the array is not limited by other constraints. However, as the length of the array side increases linearly, the length of the path from the array feed point to any element increases exponentially. Eventually, any losses in the feed network become large enough to limit the maximum available gain of the structure. These calculations were done at a frequency of 20 GHz, with lossless radiating elements separated by 1/2 λ . The loss value of 0.25 dB/in. is typical for room-temperature CU/PTFE microstrip or stripline transmission lines at this frequency. Often, waveguide feed networks are used to reduce loss at the expense of physical size.

Researchers at NASA/LeRC have fabricated and tested a 64-element thallium-film superconducting

microstrip array operating at 30 GHz.¹ The array is fabricated on a 10 m in. lanthanum aluminate substrate, and both the radiating elements and the microstrip corporate-fed network share the same side of the substrate. At 77 K, the device has shown a 2 dB higher gain than an identical antenna pattern with gold metallization at the same temperature, and 4 dB higher gain than the room temperature gold antenna.

In the antenna described above, both the feed network and the radiating elements were fabricated from HTSC material. It is known that superconducting patch radiators show only a modest increase in efficiency over that of normal-metal designs unless the patches are fabricated on relatively thin or high-dielectric substrates.² In fact, microstrip patch antennas are usually fabricated on thick ($\sim 1/20$), low dielectric constant ($\epsilon_r < 10$), low-loss ($\tan\delta < 0.001$) substrates. The substrates that are

presently compatible with HTSC films do not meet all of these criteria. A design, presently under way at JSC, that combines a HTSC stripline feed network and normal-metal patch radiators fabricated on a relatively thick, low dielectric constant substrate, is shown in figure 5.

References

- ¹L. L. Lewis, G. Koepf, K. B. Bhasin, and M. A. Richard, "Performance of TlCaBaCuO₃₀GHz 64 Element Antenna Array," presented at Applied Superconductivity Conference (Chicago, IL), 1992.
- ²V. G. Karasack, "High-Temperature Superconductor Antenna Investigations," *Superconductivity Applications for Infrared and Microwave Devices*, Kul B. Bhasin, Vernon O. Heinen, eds., Proc. SPIE 1292, 93-106 (1990).

Table 1. ACTS-to-Orbiter Link Calculations (300 Kbps)

Parameters	Values	Remarks
1. ACTS transmit power, dBW	16.3	43 watts
2. ACTS transmit circuit loss, dB	-3.0	
3. ACTS transmit antenna gain, dB	42.0	1.1m antenna
4. ACTS transmit EIRP, dBW	55.3	Sum 1 thru 3
5. ACTS power sharing loss due, dB to 900 MHz bandwidth	0.0	
6. Spaceloss, dB	-210.5	40744 Km, 19.7 GHz
7. Polarization loss, dB	-3.0	Linear to Circular
8. Pointing loss, dB	-5	Estimate
9. Orbiter antenna receive, gain, dB	25.0	9 subarrays; 16 microstrip patches/sub-array
10. Orbiter receive circuit loss, dB	-0.5	HTSC lines to input LNA
11. Orbiter total receive power, dBW	-134.2	Sum 4 thru 10
12. System noise temperature, dBK	29.6	NF = 5 dB, T _a = 290 K
13. Noise spectral density (N ₀)	-228.6	Boltzmann's Constant dB/KHz
14. Received C/N ₀ , dBHz	64.8	Lines 11 - (12+13)
15. Bit rate bandwidth, dBHz	54.8	300 Kbps
16. Received S/N, dB	10.0	Lines 14-15
17. Theoretical required S/N, dB	9.6	1.E-5 BER
18. Coding gain	5.0	(R = 1/2, K = 7)
19. Implementation loss, dB	-1.5	Estimate
20. Demodulation loss, dB	-1.0	Estimate
21. Required S/N, dB	7.1	Lines 17 - (18+19+20)
22. Link circuit margin, dB	2.9	Lines 16-21

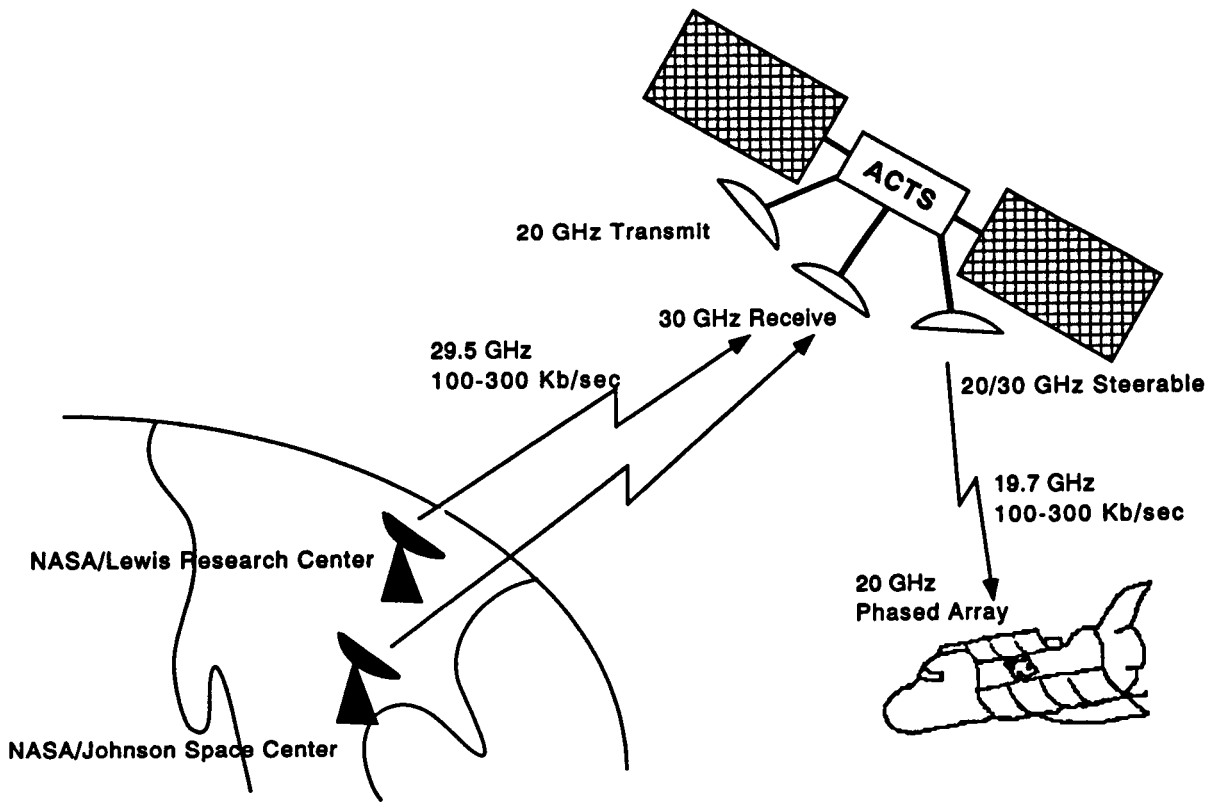


Figure 1. ACTS 20/30 GHz Flight Experiment.

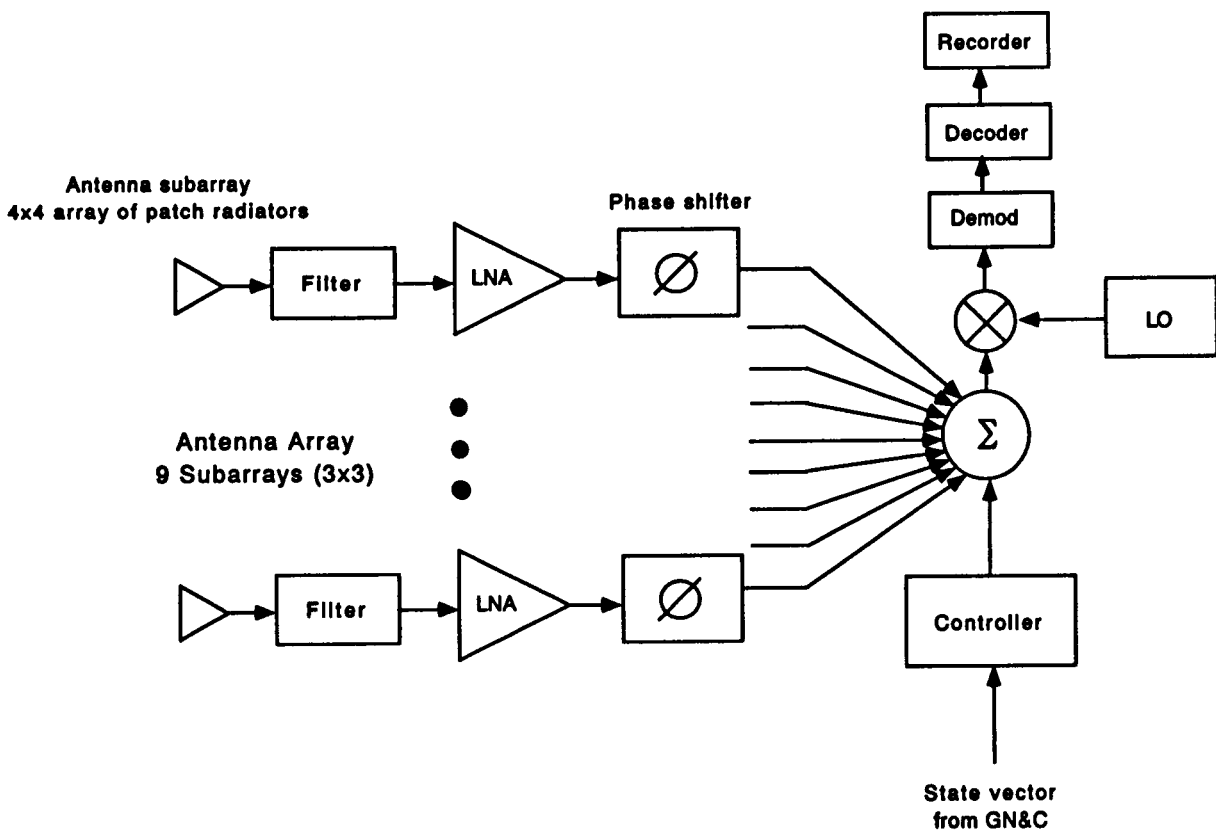


Figure 2. Electronic Equipment On Board the Orbiter.

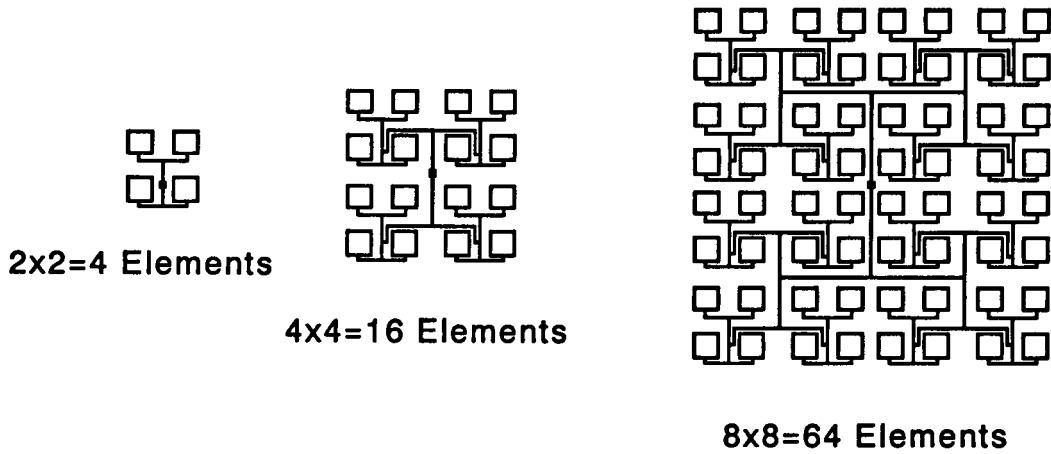


Figure 3. Feed Network Complexity Increases Exponentially as Corporate-Fed Array Side Length Increases Linearly.

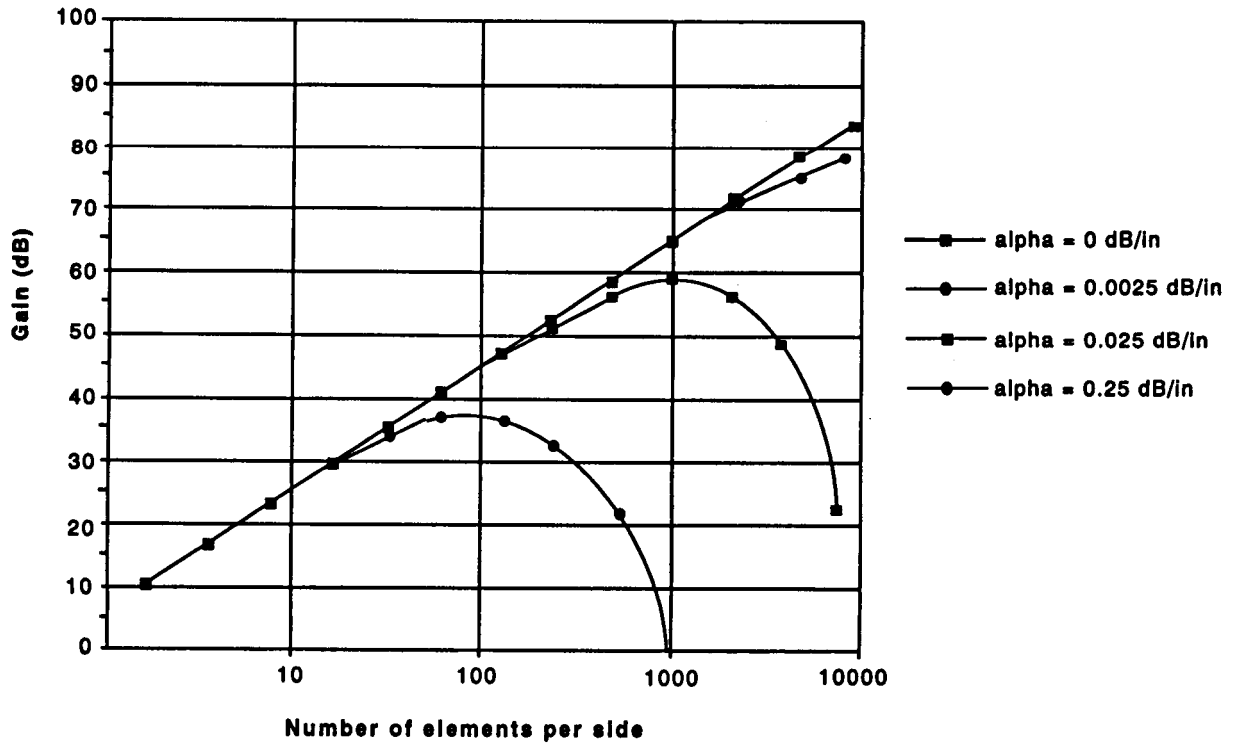


Figure 4. Array Gain Versus Size as a Function of Feed Line Losses.

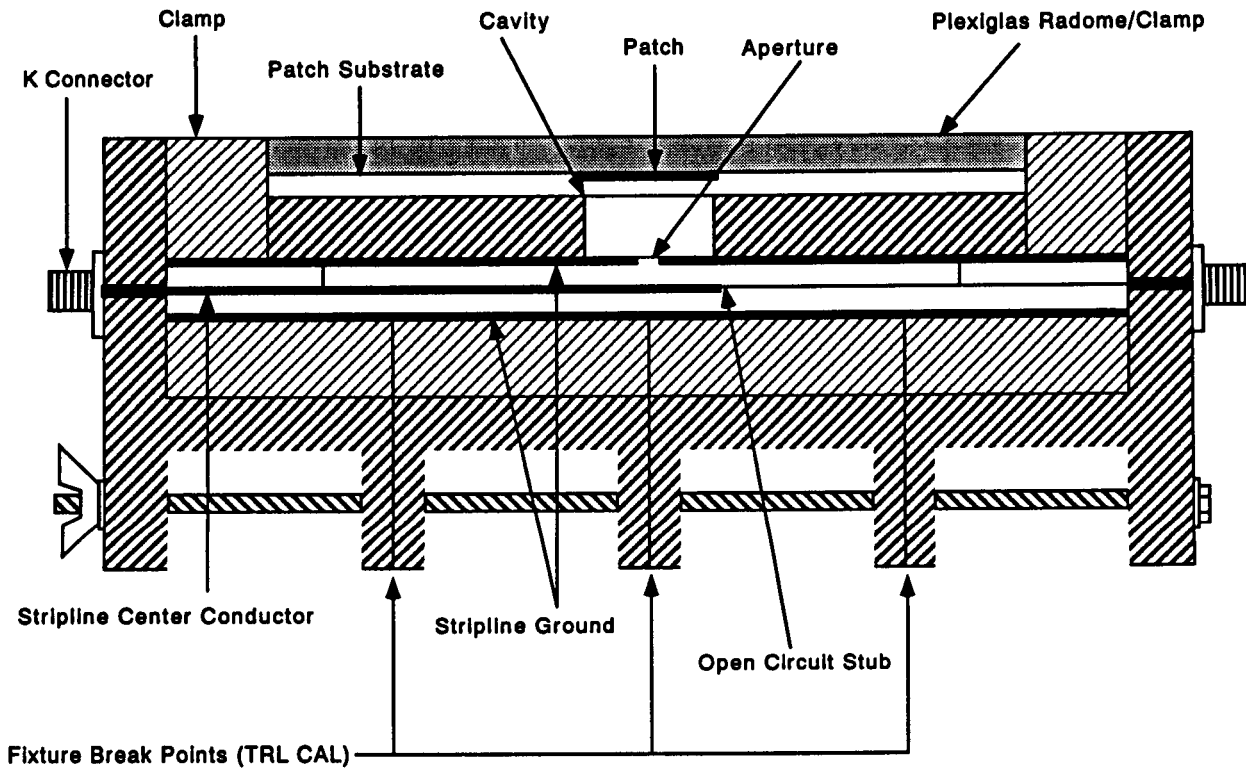


Figure 5. Single Aperture-Coupled Patch Antenna and Test Fixture - Cross Section.

Computer Antenna Pointing for Space Station Freedom

G. Dickey Arndt and Brian Bourgeois*
Johnson Space Center/EE
*National Research Council Fellow

Abstract

A Kalman filter, using rate gyro information from the Space Station Freedom high-gain antenna and observation unit pointing vector to target satellite, is introduced to compensate for pointing errors due to structural oscillations of the long, flexible boom on which the antenna is mounted.

Introduction

The proposed design of Space Station Freedom (SSF) places its high-gain antenna (HGA) on a long, flexible tower. This introduces the possibility of antenna pointing errors due to structural oscillations of the tower. Our solution to the problem consists of mounting a rate gyro assembly (RGA) on the HGA base and using RGA output and software to compensate for the structural dynamics. A detailed description of the concept is given below, but the basic idea is as follows. Guidance, navigation, and control (GNC) provides, at periodic intervals, the position vectors of SSF and the target tracking data and relay system (TDRS) satellite. Were the tower rigid, this information would suffice to point the antenna (open-loop pointing). Because of oscillations of the tower, however, the pointing vector computed from GNC differs from the actual pointing vector to the target. The two vectors are related by a linear transformation, which is computed by using the rate gyro information and is improved by using the observed pointing vector while the antenna is locked on the target.

A computer simulation was implemented to demonstrate proof of concept. In the program, the HGA is modeled as a 6-ft diameter parabolic dish that radiates in the Ku-band. The flexible tower has a total length of about 10 ft. Gaussian noise on the measurements of the antenna gimbal angles, and rate gyros are taken into account. The pointing accuracy goal for this design was chosen to be one-half of the 3-dB beamwidth, or approximately 6 milliradians (mrad). The simulation results demonstrate that this objective can be met.

The idea of mounting an antenna on a long, flexible boom is a novel one that has not been attempted. To the best of our knowledge, literature on this topic is nonexistent. J. Suddath determined that there is indeed a potential pointing problem and gave a preliminary analysis of a possible solution.¹ The present work is an outgrowth of those seminal ideas.

Theoretical Development

At periodic time intervals, GNC provides the unit pointing vector u from antenna to target. The vector u is the pointing vector measured in the inertial frame and then transformed to the coordinate frame of the known SSF orbit, denoted here as the orbital frame. The translational motion of the orbital frame is that of the SSF orbit. The rotational motion of the orbital frame is about the axis perpendicular to the plane of the SSF orbit with constant angular velocity equal to that of SSF. In this coordinate frame, the x-axis is always parallel to the radial vector from Earth to SSF. Because of the random oscillations of the tower, the antenna coordinate frame differs from the orbital frame. Failure to account for this may result in severe pointing errors. One approach is to calculate the transformation R from the orbital frame to the antenna frame; that is,

$$a = R u,$$

where

a = unit pointing vector in antenna frame
 u = unit pointing vector in orbital frame.

Because of the large distances involved, we may ignore translational motion and assume that R is purely rotational. It is well known² that R is an orthogonal matrix; that is, $RR^t = I$, where I is the identity matrix and where R^t is the transpose of R . Also, the set of orthogonal matrices (that preserve orientation) is a 3-dimensional space; that is, it can be parametrized by three variables. We use the Euler angles $(\phi, \theta, \psi)^2$ and write

$$R = \begin{pmatrix} \cos\theta \sin\psi & \cos\theta \cos\psi & -\sin\theta \\ -\cos\phi \sin\psi + \sin\phi \sin\theta \cos\psi & \cos\phi \cos\psi + \sin\phi \sin\theta \sin\psi & \sin\phi \cos\theta \\ \sin\phi \sin\psi + \cos\phi \sin\theta \cos\psi & -\sin\phi \cos\psi + \cos\phi \sin\theta \sin\psi & \cos\phi \cos\theta \end{pmatrix}.$$

Here,

- ϕ = the perturbation angle of rotation about the axis in the plane of the SSF orbit, which is parallel to the radial vector to the Earth
- θ = the perturbation angle of rotation about the axis in the plane of the SSF orbit, which is parallel to the radial vector to the Earth
- ψ = the perturbation angle of rotation about the axis perpendicular to the plane of the SSF orbit.

Let $x = (\phi, \theta, \psi)$ represent the state vector, an unknown function of time to be determined to calculate the transformation R . We now develop a system of

ordinary differential equations satisfied by the components of the state vector.

Rate gyros at the base of the antenna provide the instantaneous angular velocity vector ω of the antenna frame. The ω is related to the time derivative of the state vector of Euler angles $\mathbf{x}' = (\phi', \theta', \psi')$ by

$$\omega = \begin{pmatrix} \omega_x \\ \omega_y \\ \omega_z \end{pmatrix} = \begin{pmatrix} 1 & 0 & -\sin\theta \\ 0 & \cos\phi & \sin\phi \cos\theta \\ 0 & -\sin\phi & \cos\phi \cos\theta \end{pmatrix} \begin{pmatrix} \phi' \\ \theta' \\ \psi' \end{pmatrix} = \mathbf{A} \mathbf{x}'.$$

$\mathbf{A} = \mathbf{A}(\mathbf{x})$ can be inverted to give

$$\mathbf{x}' = \mathbf{A}^{-1}(\mathbf{x}) \omega = \mathbf{f}(\mathbf{x}, \omega)$$

with

$$\mathbf{A}^{-1}(\mathbf{x}) = \begin{pmatrix} 1 & \sin\phi \tan\theta & \cos\phi \tan\theta \\ 0 & \cos\phi & -\sin\phi \\ 0 & \sin\phi \sec\theta & \cos\phi \sec\theta \end{pmatrix}.$$

This is a nonlinear system of three ordinary differential equations, which, from given initial conditions, determines the state of Euler angles and, hence, the orthogonal transformation \mathbf{R} from inertial to antenna coordinate systems for all time. In components, the system can be written

$$\begin{aligned} \phi' &= \omega_x + \omega_y \sin\phi \tan\theta + \omega_z \cos\phi \tan\theta \\ \theta' &= \omega_y \cos\phi - \omega_z \sin\phi \\ \psi' &= \omega_y \sin\phi \sec\theta + \omega_z \cos\phi \sec\theta. \end{aligned}$$

This system of equations serves as the state propagator in a Kalman filter which, along with the observation of the unit pointing vector \mathbf{a} in the antenna coordinate frame, provides a best estimate of the state at time $t + Dt$, given a best estimate of the state at time t .

Results and Conclusions

One scenario envisioned for using the concept discussed in this paper is the following. The SSF HGA is locked onto the target TDRS satellite for one-half of its orbit around the Earth; that is, for approximately 46.5 min. The antenna is out of contact with TDRS for the other half of the orbit. When it comes back out of the Earth shadow, contact must be reestablished.

GNC will inform SSF where to point the antenna, giving the pointing vector \mathbf{u} discussed above. The SSF onboard computer will use the best estimate of the state \mathbf{x} of Euler angles to calculate the transformation \mathbf{R} , which will be applied to \mathbf{u} to give the unit pointing vector \mathbf{a} in the antenna frame of reference. The antenna gimbal angles will be adjusted to point in this direction. If the pointing error is within the design goal of 6 mrad, which is one-half the 3-dB beamwidth of the HGA, the antenna

should be able to lock on the target. If acquisition is unable to be established, a scanning mode is entered. In this case, the scanning procedure should be much simpler than if the antenna were pointed using the GNC vector \mathbf{u} .

A computer program was implemented to simulate this scenario. The three Euler angles were given arbitrary initial phases, representing the point in time at which SSF has just moved from behind the Earth shadow and into the view of the TDRS satellite. It is assumed that target acquisition has been accomplished by unspecified means. For 46.5 min, the state vector \mathbf{x} is propagated and updated using observations of the actual pointing vector. For the next 46.5 min (in the shadow of the Earth), \mathbf{x} is propagated only, assuming no observations of the actual pointing vector. When this is completed, a calculation of the pointing error is made and is compared with the pointing error that would be obtained using only the GNC vector \mathbf{u} .

The results of the simulation indicate that the 6 mrad pointing error goal can be met, provided that noise on the measurement of the antenna gimbal angles and of the tower angular perturbation rates is not too significant. Tolerable noise levels are 2 mrad for the gimbal angles and 10 deg/hr (0.05 mrad/s) for the rate gyros. Improved noise levels result in improved system performance. An increase in rate gyro sampling frequency also results in a decrease in antenna pointing error.

The pointing error was observed to be a rapidly oscillating function of time with a frequency of approximately 1 Hz, reflecting the simulated frequency of the tower oscillations. With a sampling frequency of 80 Hz, the mean pointing error was approximately 1.5 mrad with a maximum of 3.5 mrad over the 93 min orbit and with a given 30 mrad initial error. A sampling frequency of 120 Hz reduced the mean pointing error to approximately 1 mrad with a maximum of 2.25 mrad under the same conditions.

In conclusion, the study shows that the concept of using rate gyro information for propagation with observed pointing information for improvement to aid in target reacquisition is a viable one. The concept has potential applications to SSF or to any large space vehicle where an HGA must be positioned at some minimum distance from the vehicle to avoid interference during reception and damage to onboard electronics during transmission. One such application for this technology is to the proposed onboard orbital debris radar antenna. One use of this radar is as a last resort warning signal that SSF is in imminent danger of collision with a debris particle. The decision as to whether or not to execute a costly maneuver may depend crucially on the accuracy of the radar measurement. The techniques espoused in this paper provide an aid to obtaining the required accuracy.

References

- ¹Suddath, J. H., *An Approach to Compensating for the Effects of Structural Dynamics on Pointing Space*

Station High Gain Antennas, NASA Johnson Space
Center Memorandum, March 9, 1989.

²Goldstein, H. *Classical Mechanics*, Second Edition,
Addison-Wesley, 1980, pp 137-148.

³Cheney, W. and Kinkaid, K., *Numerical Mathematics
and Computing*, Second Edition, Brooks/Cole, 1985, pp
394-396.

⁴Brogan, W., *Modern Control Theory*, Second Edition,
Prentiss-Hall, 1985.

Acknowledgment

We would like to acknowledge posthumously Jerry
Suddath's contributions to the basic research on this
project.

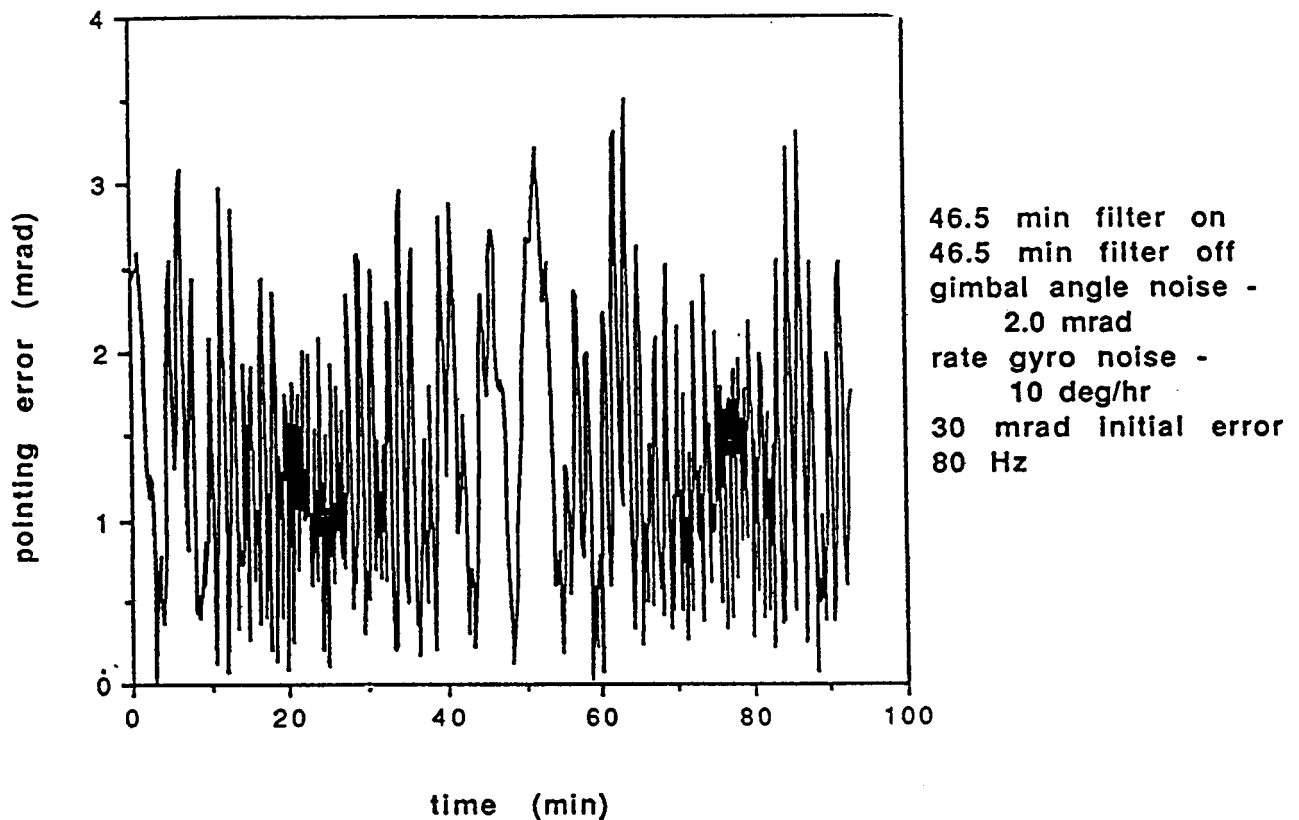


Figure 1. Pointing Error Versus Time (Sampling Frequency = 80 Hz).

A Mobile Communications Space Link Between the Space Shuttle Orbiter and the Advanced Communications Technology Satellite

Patrick Fink, G. D. Arndt, M. Chavez, R. Robinson,
P. Bondyopadhyay,* S. Kim,* and Roland Shaw**
Johnson Space Center/EE

*Lockheed Engineering and Sciences Company
**Shason Microwave Corp.

Abstract

A communications link between the Space Shuttle Orbiter and the advanced communications technology satellite is described. The prime objectives are to demonstrate a Ka-band low-Earth orbit to geostationary orbit (LEO-GEO) link as well as to provide a test-bed for a high-definition television video compressor. Both 20 and 30 GHz hardware for the experiment have been breadboarded, including a 144-element, circularly polarized phased array antenna and a 1-W hybrid power amplifier, both at 29.5 GHz.

Introduction

A Ka-band, mobile communications link between the Space Shuttle Orbiter and the advanced communications technology satellite (ACTS) has been proposed as a joint effort of JSC, Jet Propulsion Laboratory, and Honeywell, Inc. The Orbiter will communicate with JSC by low bit-rate, convolutional encoded data. A compressed, high-definition television (HDTV) signal constitutes the source.

The objective for the Orbiter/ACTS flight experiment (OAFE) is several-fold. First, the experiment will demonstrate the utility of ACTS technology in future commercial LEO-GEO satellite relays. Second, the experiment will serve as a test-bed for an HDTV compression algorithm developed by Honeywell, Inc. Also, monolithic microwave integrated circuit (MMIC) and Ka-band hybrid solid-state technologies used in the transmitter will further advance the application of these technologies in a space environment. Future satellite systems expanding on ACTS technology would benefit greatly by extended use of MMICs, which are often regarded as unproved in a space environment. Other objectives of the experiment are to evaluate a moderate gain antenna using computer steering in the dynamic environment of a maneuvering Orbiter and to evaluate multi-beam communication links for direct distribution of experiment data for manned space applications.

The OAFE definition has been modified several times as a result of budgetary constraints. This paper will address the hardware as it was originally conceived and developed for the experiment: a return link, transmitting from the Orbiter to JSC via the ACTS satellite. Most of this hardware will be used in the revised experiment (a ground-ACTS-ground propagation study).

Orbiter/OAFE: Return Link

This version of the OAFE was conceived as a return link from the Orbiter to JSC via the ACTS satellite. Low bit-rate data are radiated through a phased array antenna to the ACTS 1-m steerable antenna. The ACTS, configured in the microwave switch matrix mode, relays the signal to JSC, where the signal is received by a 1.2-m dish antenna.

Link Performance

A 4.32 dB link margin exists for the return link experiment. The phased array consists of 9 subarrays, each driven by a 1-W amplifier, to provide a transmit power of approximately 9 dBW. With an array antenna gain of 25 dBi and circuit losses totaling 2 dB, the EIRP is 32 dBW.

The received signal is demodulated by a long phase-locked loop with 2.5 dB implementation/demodulation loss. A 5.0 dB coding gain is necessary to close the loop with a 4.3 dB margin for a bit rate of 16 kbps. The link margin is determined primarily by the uplink (Orbiter to ACTS) since the gain of the ACTS 1-m antenna is considerably less than that of the isolated spot beams.

Antenna and Doppler Considerations

The ACTS 1-m steerable antenna will have an instantaneous maximum angular rate of 0.20 mrad/sec when tracking the Orbiter. The Doppler shift and Doppler rates reach a maxima of ± 750 kHz and ± 1 kHz/sec, respectively. Since the Doppler profile is well known, the shift is readily precompensated.

The onboard phased array receives pointing data from the Orbiter guidance, navigation, and control (GN&C) to determine the phase shifter bits. The Orbiter payload bay is pointed to the ACTS within 10° , and the array points, open-loop, to $\pm 8^\circ$ in steps of 1.3° (element spacing = 0.7 l).

Flight Hardware

A block diagram of the transmitter for the OAFE return link is shown in figure 1. Audio data at 16 kbps is rate 1/2 convolutionally encoded. The signal is biphase shift keying (BPSK) modulated and upconverted to 29.5 GHz. A more recent design allows for Doppler

precompensation by replacing the BPSK modulator with a direct digital synthesizer. Although the receiver is capable of tracking through the ± 750 kHz of Doppler shift, precompensation allows for a narrower noise bandwidth in the receiver.

The 29.5 GHz signal is preamplified before a 9-way power divider routes the signal to nine subarrays. Each subarray is preceded by a 1-W phase shift/amplifier module. The phase shifter is a 4-bit MMIC developed by Honeywell. Input power to each module is +12 dBm. A 10 dB insertion loss associated with the phase shifter and 30 dB of amplifier gain results in 1 W being delivered to each subarray.

Ka-Band Antenna Array

The transmitting antenna at 29.5 GHz consists of a 144-element circularly polarized microstrip phased array arranged as a 3x3 array of 16-element subarrays. Each subarray consists of a 2x2 array of a 4-element cluster designed as a single feed, circularly polarized microstrip compound radiating element. One version of the 4-element cluster is shown in figure 2. A 4-bit phase shifter in each of the 3x3 arrays will provide electronic scanning in a conical space of approximately 10° .

This design of the compound radiating element employs dual-feed, square microstrip patch elements in conjunction with sequential feeding and rotation technique to enhance the axial ratio bandwidth. Impedance and axial ratio bandwidths of over 1 GHz at the center frequency of 29.5 GHz are very easily achieved. The typical radiation pattern of the 16-element subarray (fig. 3a) consisting of a 2x2 array of the 4-element cluster is shown in figure 3b.

The wide bandwidth for this version comes at the expense of a small loss in the subarray gain. For this particular experiment, the bandwidth required is less than 200 MHz. This will permit us to use a more efficient version where single feed, structurally perturbed square microstrips are used to design the 4-element cluster. The receiving antenna at 19.78 GHz is a similar 144-element, circularly polarized microstrip phased array antenna.

Phase Shift/Power Amplifier Module (PSPA)

Mechanical

The prototype phase shift/power amplifier (PSPA) module is shown in figure 4.

The second revision is similar in form, although shorter, and was designed with a mating heat sink. This unit has dimensions 7.0 in. x 1.1 in. x 1.1 in. (not including the heatsink).

The PSPA module shown in figure 4 is, in form, an identical predecessor to a flight unit with the exception of the flange on the input side. This flange would be absent on the flight unit to allow for a front-loading array structure. For ground use, the dual flange is a convenient method of locking the module in a heat sink. The final

revision is shown in figure 5 inside a mating heat sink designed for ground use.

Both ends of the module have a K-connector interface that accepts either a two-hole flange SMA female or flush mount female-female interconnect. The SMA female connector is used on the output for lab testing, while in operation a 1.1 in. x 1.1 in. x 0.25 in. antenna carrier plate mounts flush onto the PSPA flange. In addition to the K-connector interface, a miniature D-connector resides on the input side. The D-connector accepts regulated power at +12V and -5V as well as 4 transistor-transistor logic phase shift bits.

Voltage regulation for the PSPA resides in a recess in the heat sink. The heat sink also mounts a 1.2 W miniature fan over the output side of the PSPA. The fan draws 5.30 ft³ of air per min along the sides of the PSPA module and through holes between the bottom heat sink fins. An additional air channel runs aft to the regulator compartment.

Electrical

The design specifications of the PSPA are as follows:

Gain	30 dB
1 dB compression	30 dBm
Bandwidth	≥ 500 MHz
Harmonic Distortion	TBD
Prime DC Power	≤ 30 W

The PSPA is comprised of a 4-bit MMIC phase shifter followed by eight hybrid metal semiconductor field-effect transistor (Toshiba™) stages. The first prototype PSPA exhibited gain in excess of 30 dB at 1 W of output power. However, the driving stages were narrowly tuned for gain above 6 dB, which proved to be too thermally sensitive. The prototype is being refitted with stages matched for broader bandwidth. Also, to increase reliability, the second revision PSPA has been designed to operate at a lower temperature.

Ground Station

A 19.78 GHz superheterodyne receiver (fig. 6) is being developed for the JSC ground station. An existing MMIC 20 GHz receiver developed by Harris Corporation will be used to downconvert the signal to 3.58 GHz. A long phase locked loop will track the Doppler shift to maintain a constant IF of 70 MHz. The quadrature phase detector then demodulates and produces the voltage controlled crystal oscillator (VCXO) control voltage. The demodulated data are then input into an ASIC bit synchronizer to establish a clock and recover the data. Finally, the data are decoded. To improve acquisition time, the VCXO is swept when the loop is not phase locked. The acquisition time, without Doppler compensation, is approximately 3.5 sec.

With the current BPSK system, performance is degraded by the phase jitter produced by the phase noise of the ACTS local oscillators. Figure 8 shows the effect

of phase jitter on bit error rate performance.¹ The minimum calculated root mean square phase jitter for the experiment is 11.4° , which results in a degradation of 3 dB. A study is currently being performed to determine whether differential phase shift keying (DPSK) will improve system performance. DPSK has a greater immunity to phase jitter, but is not as efficient as BPSK.²

²Spilker, J. J. *Digital Communications by Satellite*, Prentice-Hall, 1977.

Acknowledgments

The authors would like to extend thanks to Shason Microwave Corp. for their help in the development of the PSPA.

References

¹Holmes, J. K., *Coherent Spread Spectrum Systems*, Krieger Publishing Co., 1990.

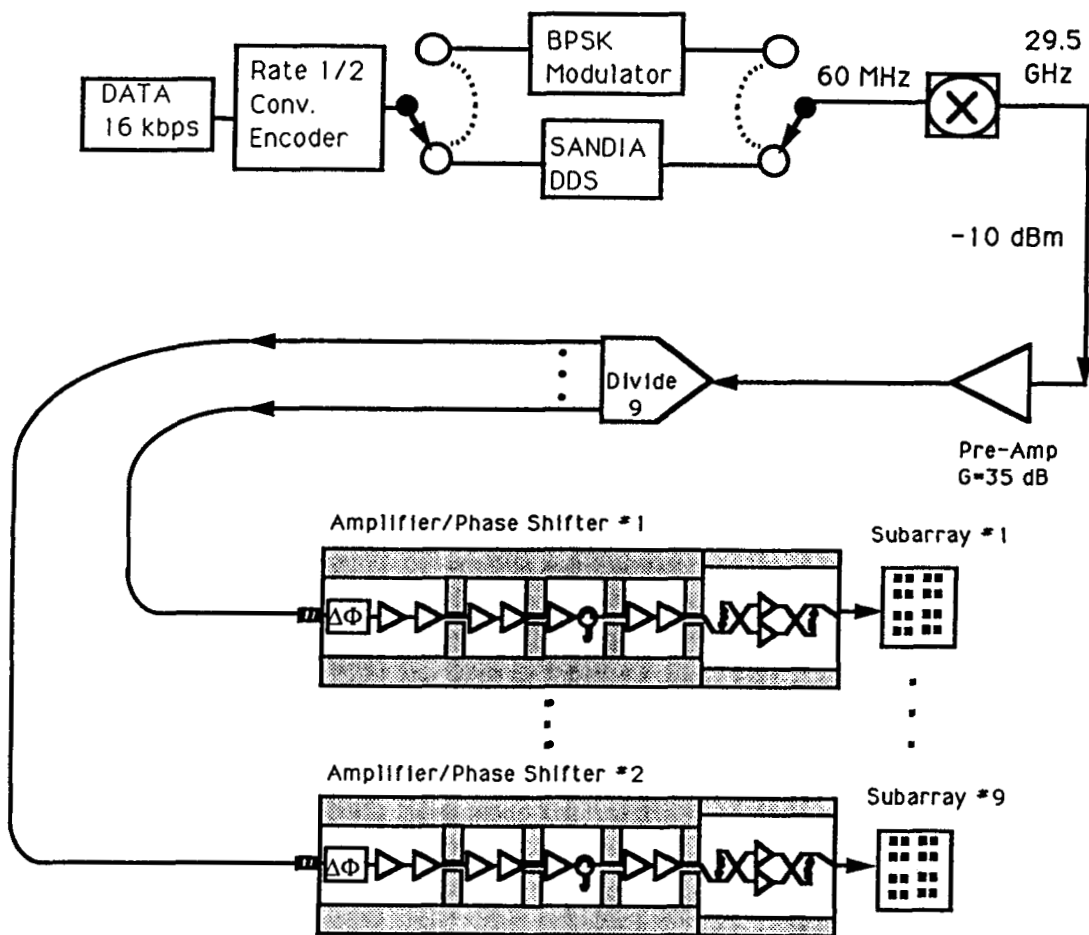


Figure 1. OAFE Transmitter.

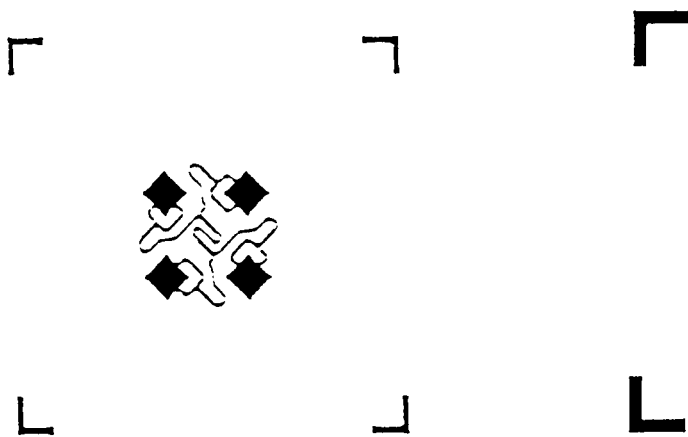


Figure 2. A 4-Element Cluster.

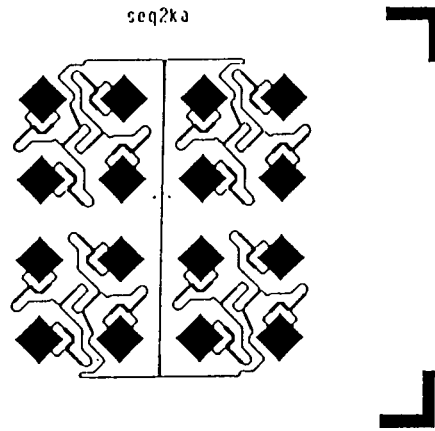


Figure 3a. A 16-Element Subarray.

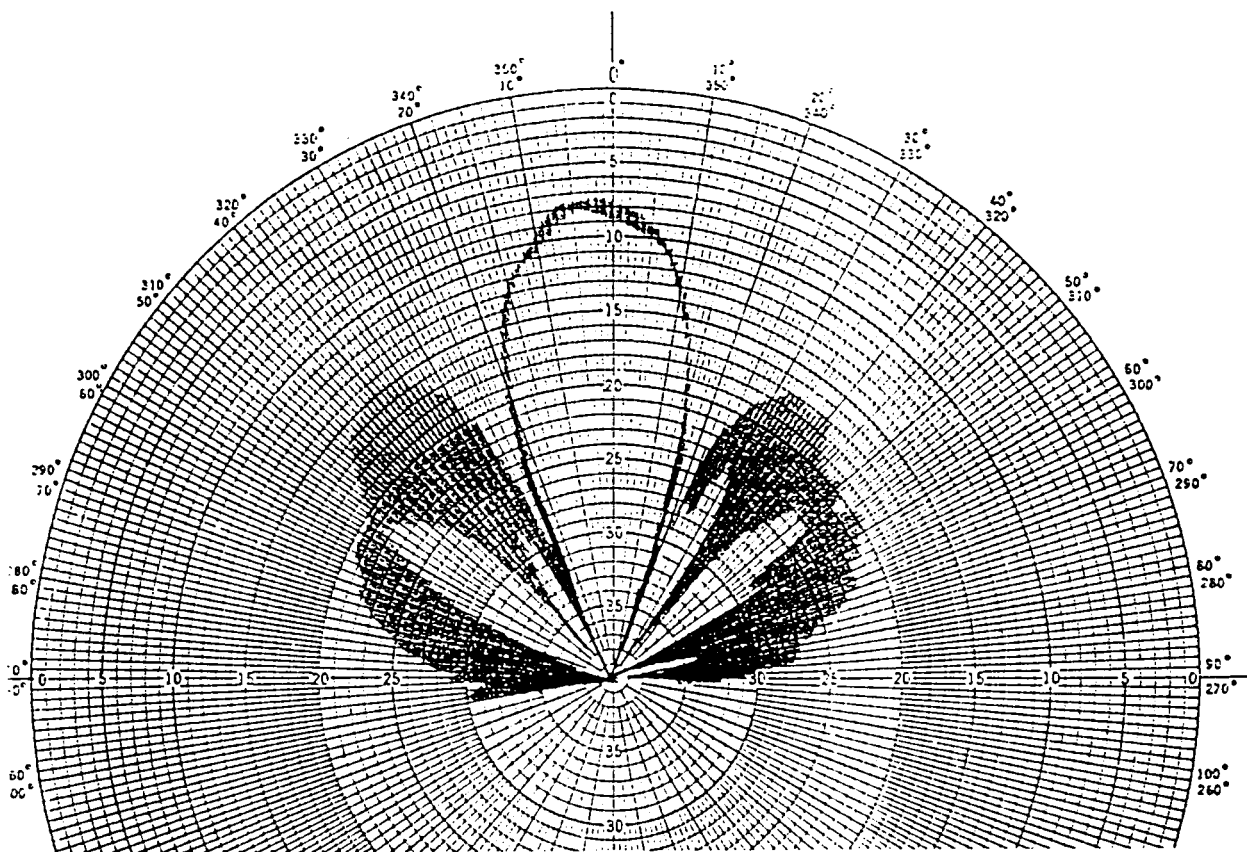


Figure 3b. Subarray Radiation Pattern.

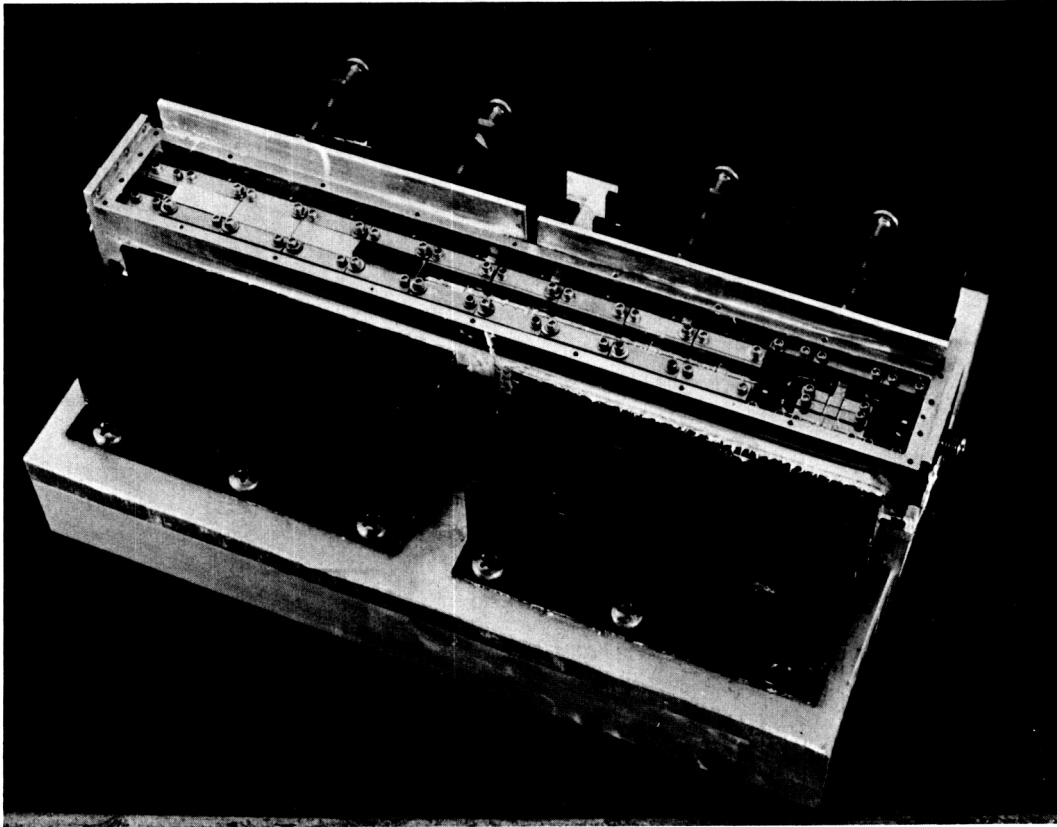


Figure 4. The Prototype Phase Shift/Power Amplifier (PSPA) Module.

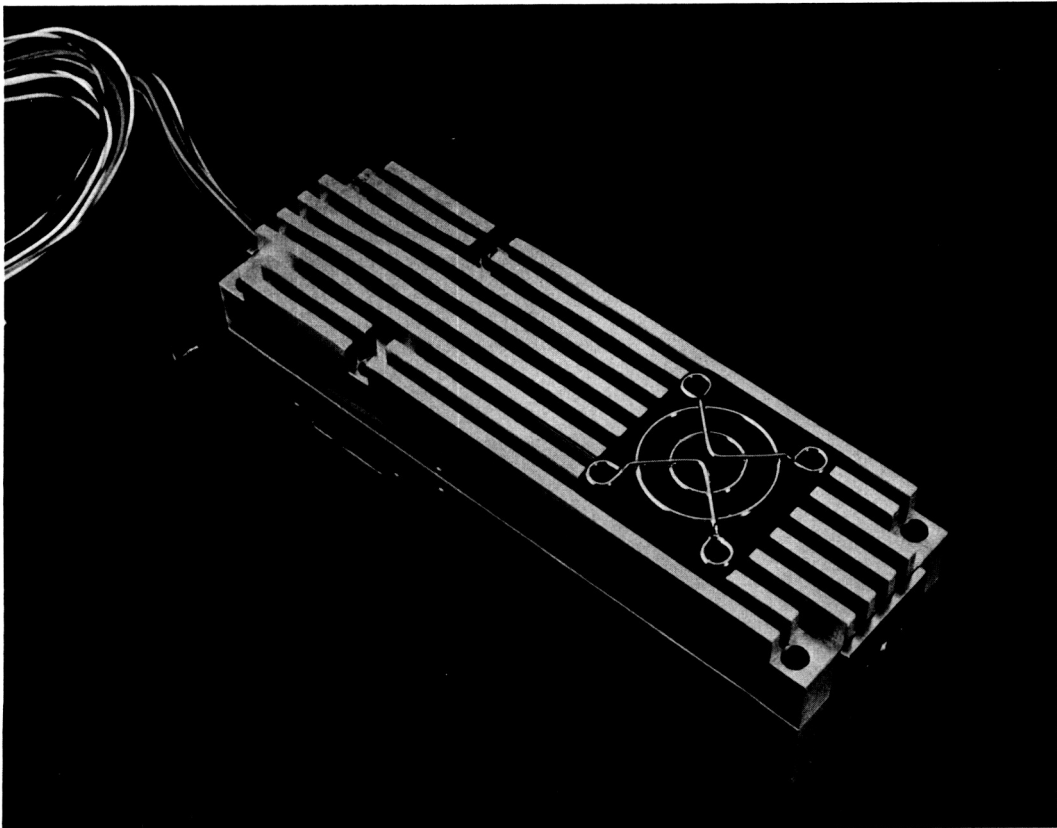


Figure 5. The Final Revision of the PSPA Inside a Mating Heat Sink.

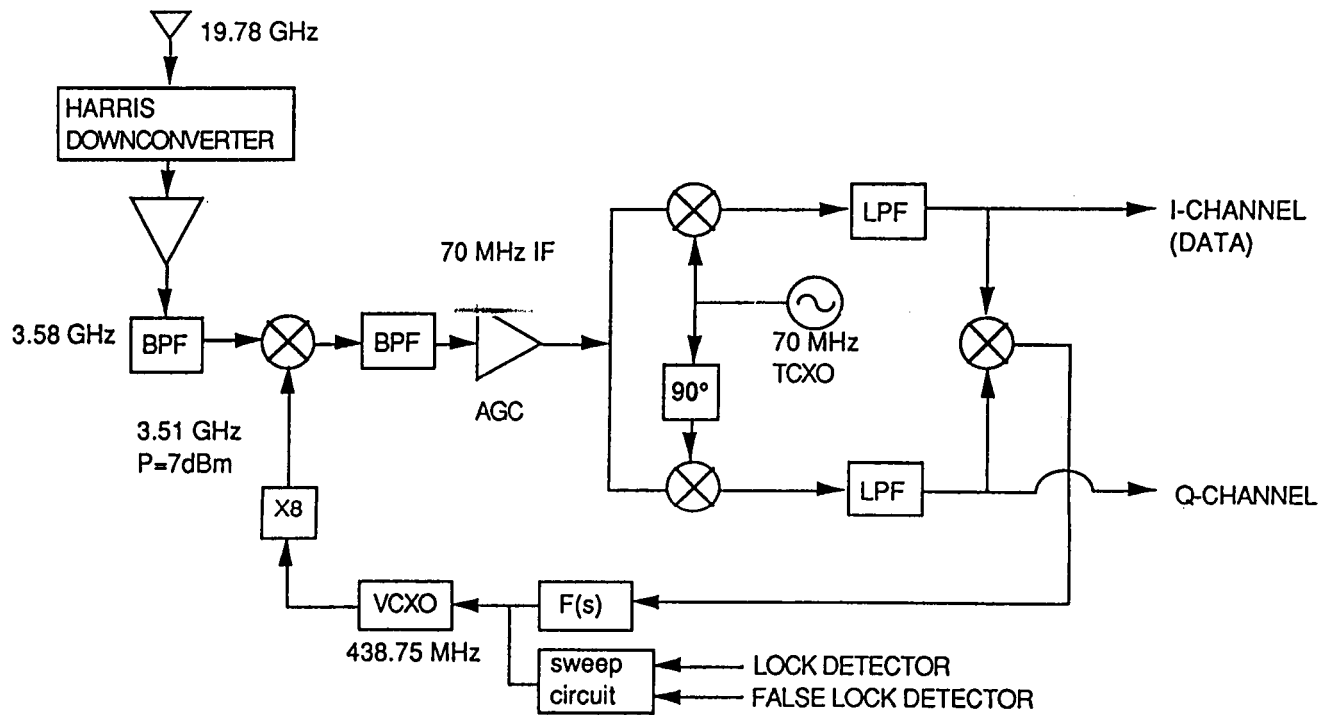


Figure 6. 19.78 GHz Superheterodyne Receiver.

Hybrid Vision's Eye Tracking

Richard D. Juday
Johnson Space Center/EE

Abstract

The Johnson Space Center Hybrid Vision Program is developing hardware for a medical purpose. It is a high-speed image processing device, an optical joint Fourier transform correlator, that JSC has patented for use in retinal laser treatment.

Introduction

The Hybrid Vision Program at the Johnson Space Center combines optical and digital image processing for various purposes. Among the optical processing elements under development are optical correlators, spatial light modulators, and optimal filter theory. Among digital processing elements are digital stereo, video rate geometric image warping, and space variant image sensing. One method we recently patented¹⁻⁴ is a method of processing an unmodeled image of a surface so that the apparent motion of the surface can be rapidly tracked. The effect as seen from the sensor is that the surface is stabilized. Its potential space applications include navigation for autonomous planetary landing, detection of previously unmodeled landing hazards, and autonomous rendezvous and capture. We are also pursuing Earth-bound applications for our techniques, significantly in human vision. Two such are most significant. The first is prosthetic image warping for field defect problems such as maculopathy and retinitis pigmentosa, a program we have active among NASA, the University of Houston, and the University of Pennsylvania. The second is surface tracking by means of the optical joint Fourier transform, as described above, for tracking the motion of surface features. We have patented its application to tracking the motion of the retina for use in laser photocoagulation of diseased retinal structures. In this application, we have allied ourselves formally with the Army's Missile Command (MICOM) and with Pinnacle Imaging. The military is interested in developing a passive identification system that would be able to quickly identify friend or foe and thereby reduce fratricide in battlefield situations. MICOM is contributing funding and practical correlator technology.^{5,6} Pinnacle is supplying a test-bed for the concept described in the next section. Figure 1 is reproduced from the patent.

Problem Statement/Description

The need for the image stabilization method arose in the need to land an autonomous vehicle on a planetary

surface in the presence of unknown obstructions. JSC proposed image stabilization based on the optical joint Fourier transform and led a proposal, including Ames Research Center and the Jet Propulsion Laboratory (JPL), for the development of a highly sophisticated vision system. It would fully model the visible obstructions based on optic flow, the differing motions of elements in the field of view as the viewpoint translated. The joint transform correlator (JTC) would provide the gross tracking, and the digital image processing modules developed by Ames and verified by JPL would analyze the second-order image motion for the underlying 3-dimensional basis. Although the fully competent vision system was not funded, the various pieces continue in separate development, including the joint transform correlation stabilization. Juday described the image analysis method to the University of Alabama's H. John Caulfield, who knew of a medical practitioner who had need of the technique. Caulfield put Juday in touch with Steve Charles of Pinnacle Imaging, and the project is now under way. In the retinal laser treatment, there is a need for landing the laser onto only the desired portions of the retina.

Approach/Method

The method of the optical joint Fourier transform¹⁻⁶ offers a fast, reliable, and inexpensive method to correlate images with reference images. In the medical field, the laser eye surgeon needs rapid registration of retinal images to facilitate hitting exactly the spot on the retina that the surgeon wishes to photocoagulate. Pinnacle Imaging has shown the medical practicality of a digital method for rapid registration; however, the digital method is too expensive for commercialization. The optical image processing method using the joint Fourier transform correlation promises to be sufficiently inexpensive to be commercially attractive. The digital method was technically confounded by torsion of the eye—a problem JSC thinks can be solved by digital processing of the reference image.⁷

JSC developed the JTC method of image stabilization for automated planetary applications, notably the extraction of shape-from-motion owing to translation of the sensing platform with respect to a 3-dimensional structure. The JTC method can remove the image motion that originates in camera position jitter, rather than in differing perspective points on the object, and thus is regarded as noise to the process. The method has been substantiated in laboratory measurements.²⁻⁶

Results

Significantly, Rocketdyne (a division of Rockwell International) has presented results⁸ in which their prototype of an eye surgery JTC met the system requirements for speed, linearity, capture radius, etc. Draft specifications for the processing speed and latency are shown in figure 2. The prototype ran at 700 Hz with a lag time from conclusion of electronic image to provision of error signal of just over 2.5 msec. Our medical partner, Pinnacle Imaging, has formed a technical alliance with OCA Applied Optics to construct the optical processor of a surgical system that would embed the JTC technology to track the retina.

Conclusions

The technique is proven in the laboratory and in prototype. Organizations have committed to implementing the method in practice and appropriate actions are being taken.

References

¹U. S. Patent 5,029,220; Optical Joint Correlator for Real-Time Image Tracking and Retinal Surgery; July 2, 1991.

²Jerome Knopp and Richard D. Juday, "Optical Joint Transformation Correlation on the DMD," Proc. SPIE 1053, 1989, pp. 208-215.

³Jerome Knopp, "Spatial Weighting of Synthetic Reference Objects for Joint Correlation by Random Pixel Mixing," Proc. SPIE 1295, 1990.

⁴Eddy C. Tam, Francis T. S. Yu, Don A. Gregory, and Richard D. Juday, "Autonomous Real-Time Objects Tracking With an Adaptive Joint Transform Correlator," Optical Engineering, April 1990, pp. 314-320.

⁵Don A. Gregory, Jeffrey A. Loudin, and F. T. S. Yu, "Illumination Dependence of the Joint Transform Correlation," Appl. Opt. Vol. 28, no. 15, 1989, p. 3288.

⁶F. T. S. Yu, Suganda Jutamulia, and Don A. Gregory, "Adaptive Real-Time Pattern Recognition Using a Liquid Crystal TV Based Joint Transform Correlator," Appl. Opt., Vol. 26, No. 8, 1987, p. 1370.

⁷Richard D. Juday and Brian Bourgeois, "Convolution-Controlled Rotation and Scale Invariance in Optical Correlation," Proc. SPIE 938, 1988, pp. 198-205.

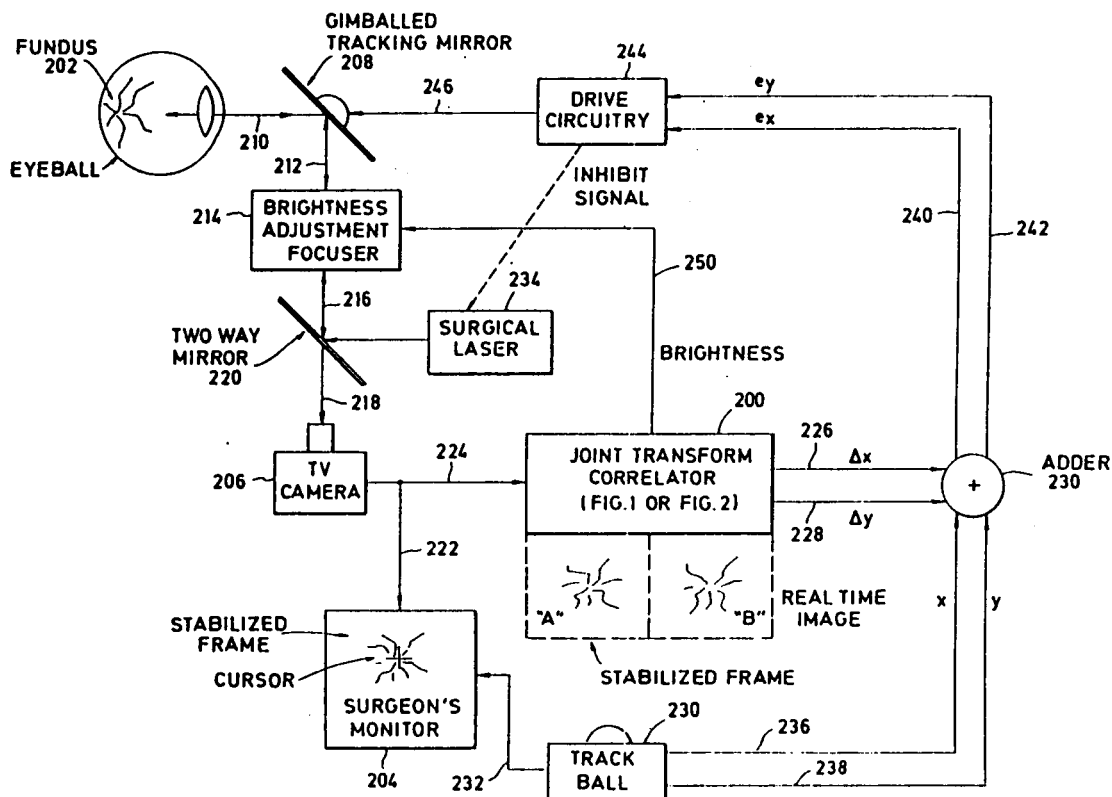


Figure 1. Optical Joint Correlator for Real-Time Image Tracking and Retinal Surgery.

Input image format and system timing diagram... joint transform correlation for eye tracking

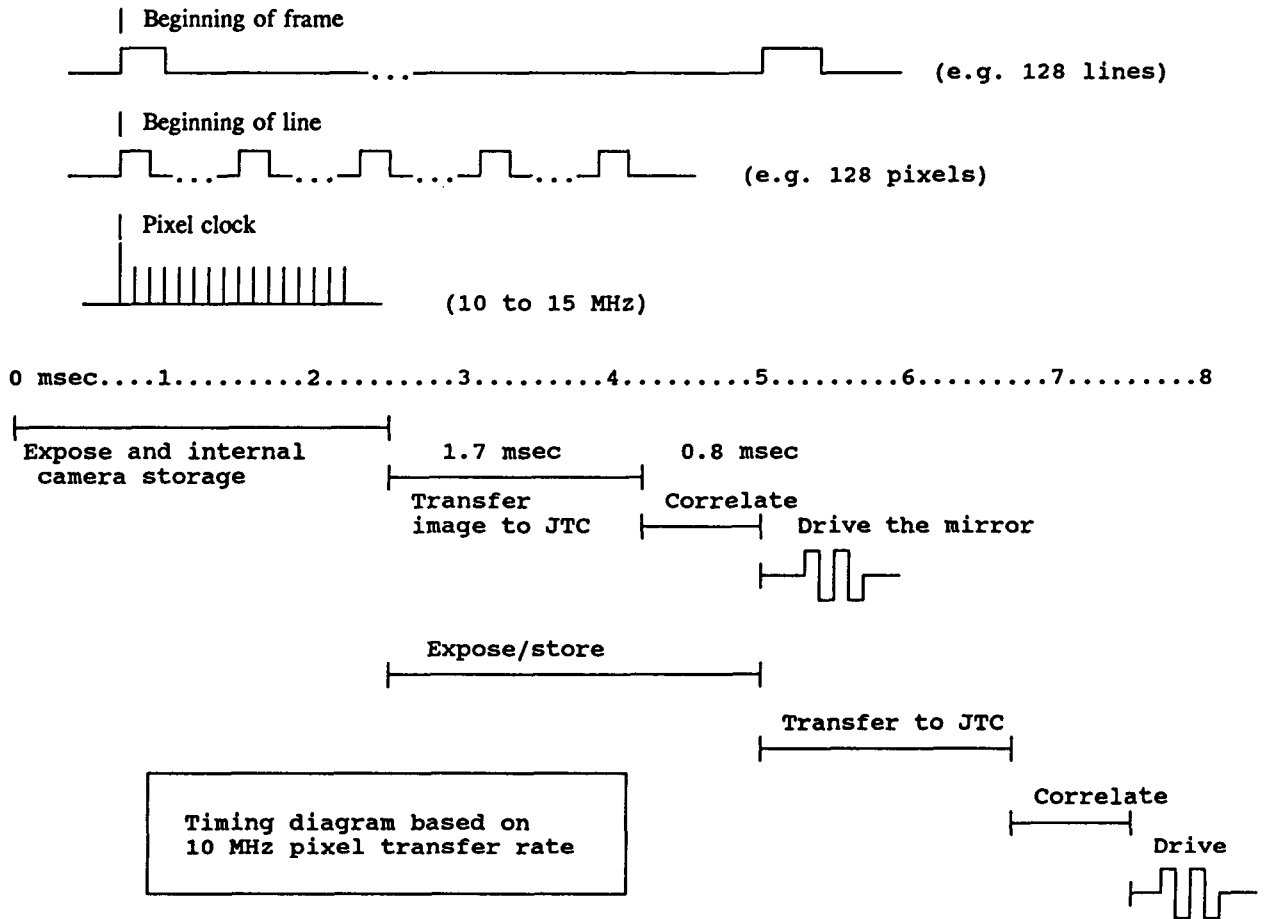


Figure 2. Example Timing Diagram as Necessary for Retinal Tracking for Photocoagulation.

Spacecraft Gliding Parachute Autoland Project - Status

R. E. Meyerson, A. Sim,* J. Murray,* D. Neufeld,* and R. D. Reed*
Johnson Space Center/EG
*NASA Dryden Flight Research Center

Abstract

A joint NASA Dryden Flight Research Facility/JSC program is being conducted to determine the feasibility of an automatic recovery of a spacecraft using a ram-air inflated parafoil recovery system for the final stages of entry from space. The feasibility was studied using a 150 lb model of a flat-bottomed biconic spacecraft flown with a man-rated parafoil. Key elements of the vehicle include global positioning system navigation, a flight control computer, sonar sensing for terminal altitude, and onboard data recording. A flight test program was used to develop and refine the vehicle. Development included several ground tests and manual flight using a radio uplink. The vehicle demonstrated automatic flight from 8,000 ft above ground level and a 1-mile lateral offset that resulted in a precision flared landing at a predetermined spot. Test results and future program objectives are also discussed in this paper.

Introduction

NASA is currently studying a variety of vehicles for the return of humans and cargo from space. Although the configuration of these vehicles is not yet confirmed, a number of capsule shapes are currently under consideration for several proposed NASA missions. Among them are the assured crew return vehicle (ACRV), which will be a "lifeboat" for the Space Station Freedom. The Lunar Transportation System (LTS) is an element of the Space Exploration Initiative (SEI) that will transport crewmembers to the lunar surface and return them to Earth. The Mars Environmental Survey is an SEI precursor mission that will map portions of the surface of Mars. The Personnel Launch System and Lifesat mission will return crewmembers and biological experiments from low-Earth orbit.

Several approaches are being considered for landing and recovery of advanced spacecraft. The ACRV mission is currently studying both land and water landing options, using parachutes and a landing attenuation system. The LTS study managers have baselined land landing to provide operational flexibility. For a capsule vehicle, all of the above named missions could benefit from the use of a deployable precision landing system.

Problem Description

The use of deployable ram-air inflated gliding parachutes for spacecraft recovery has been proposed since the mid-1960s. Studies for the Gemini and Apollo

Programs included the use of Parasails, Sailwing, and Rogallo Parawings for spacecraft recovery. The primary problems with these systems were inflation performance and reliability. While the performance of these systems was promising, the lack of a large experience base hurt chances for their use in a large recovery program. An inability to control the high horizontal velocities developed during flight also made these systems unacceptable. The emergence of the ram-air inflated Parafoil as the parachute of choice among sport jumpers has brought the issue of gliding parachutes for spacecraft recovery back to the forefront.

The Advanced Recovery Systems Program, managed out of the NASA Marshall Space Flight Center, focused on the development of a large-scale gliding recovery system. Although canceled after nine flight tests, the program was successful in developing a unique inflation loads management system for large Parafoils. Reliability issues that raised concerns during the 1960s have been reduced because of the high number of systems in sport use today. The major issue that remains with the use of these systems is the development of a highly reliable, autonomous landing flare system. Engineers at NASA Dryden Flight Research Center, under the sponsorship of JSC, have been flight testing a system that uses global positioning system (GPS) guidance and a sonar altimeter to perform this task.

The purpose of this paper is to summarize the results of phase 1 of the Spacecraft Autoland project. A description of the vehicle, its design, and control concepts are presented. The steps leading to the final flight demonstration are detailed. The flight results, lessons learned, and a sample of the flight data are included. Future program objectives are also included.

Potential customers for this technology within NASA include all of the manned space programs listed above as well as unmanned vehicles, including planetary probes and booster recovery systems. Potential customers for this technology outside of NASA include the U.S. Navy, who is studying the use of automatic gliding parachute systems on aircraft ejection seats, and the U.S. Army/Air Force, who prefer offset delivery of cargo to minimize danger to aircraft and crews of the airlift community.

Approach/Method

Vehicle Description

The philosophy adopted for this project was to use off-the-shelf equipment whenever possible to keep costs low and reduce development time. The flight test article

consisted of a flat-bottomed biconic vehicle, flight control system, and a Parafoil recovery system. The biconic vehicle was constructed of tubular steel with a plywood bottom and removable aluminum upper and side skins. The Parafoil used for this phase is a 288-ft² wing built by Glide Path Company (model name, Manta™). The docile flight characteristics, low wing loading (near 0.5 psf), and proven design allowed the project to concentrate on the development of the autonomous flight system rather than the parachute itself. The project concept was to substitute a smaller, higher performance (higher wing loading) Parafoil once the vehicle is developed. The flight vehicle, parachute, and harness are depicted in figure 1.

The flight control system consisted of both manual and autonomous modes. The vehicle was controlled using two control line actuators to perform turns and the landing flare maneuver. The control actuators, widely used in unmanned air vehicle systems, provide 13.75 ft-lb of torque.

The manual mode used a radio control model receiver and transmitter to uplink signals through a 15 W power booster. This mode was used primarily in the early stages of the program to develop confidence in the deployment and flight characteristics of the vehicle.

The autonomous mode was the primary mode used for the demonstration flight program and allowed the vehicle to guide itself back to the programmed target using GPS data for navigation.

The following hardware items were included as part of the autonomous system:

<u>Hardware item</u>	<u>Use</u>
Sensym SMRTBAR01 Pressure Altimeter	Approach guidance waypoints
Polaroid Ultrasonic 6500 Sonar Altimeter	Landing Flare maneuver
Rockwell NavCore V GPS Receiver	Navigation
KVH C100 Magnetic Compass	Vehicle Heading
Flight Computer (Custom)	Flight Systems Processing

Ground Tests

A ground test approach was used to verify the performance and operation of the autonomous flight system hardware. A pickup truck and a fixed crane were used in two different test series to verify the steering control commands from the flight systems, the operation of the GPS receiver, and the performance of the sonar altimeter.

Validation of the steering commands was performed by placing the flight vehicle in the bed of a pickup truck and driving the vehicle over a surveyed course on the Edwards Air Force Base dry lakebed. After acquiring lakebed landing site coordinates into memory, the truck would be driven several thousand feet away at a speed similar to that of the vehicle in flight (20 mph). An observer riding in the truck would then translate the vehicle actuator position into a left or right turn for the

driver. This proved to be an effective way to obtain a crude zero-wind simulation of the operation of the GPS receiver and flight control computer.

A second ground test series used a crane to check the functionality of the sonar altimeter. The original vehicle concept involved downlinking the control computer data display to a ground-based video monitor. It was discovered, however, that the video downlink degraded the sonar altimeter range from 35 ft down to about 20 ft above ground level (AGL). Since a range of about 30 ft was needed, many variations of transmitter and antenna location were evaluated by hoisting the vehicle by crane to a height of 35 ft. After some limited success, we decided to eliminate the downlink and record the video signal on board. After this change was made, the crane was used to verify the operation of the altimeter.

Flight Tests

Numerous steps were taken toward the final demonstration of autonomous flight. Flight tests performed to demonstrate the vehicle capability included "slope soaring" and airdrop flights.

Early in the development, the vehicle was flown manually with only the uplink receiver and control servos installed. The first manual mode flights consisted of "slope soaring" the vehicle from a hillside in times of high winds (approximately 15 kn). These flights occurred prior to the development of the test-bed vehicle and provided a method for flying the vehicle without first having to validate parachute and harness deployment characteristics. Two flights were made with this technique and were used to evaluate with the general flight characteristics (including gentle turns), the landing flare, and control actuator capabilities.

To initially validate the parachute deployment and harness design, a second wedge vehicle was fabricated with the same external geometry and weight as the flight test vehicle. This test-bed was constructed at low cost and was considered expendable because it did not contain any internal electronics. The vehicle was air-launched several times, and the data produced provided significant confidence in the parachute deployment and harness design.

The autonomous (auto) flight mode could be selected from the ground transmitter. The vehicle typically would remain in the auto mode until it failed to perform as desired. Problems with the control logic were common during the early auto mode flights as several control algorithms were evaluated. To have the capability for immediate reversion to manual mode was considered mandatory. While in auto mode, the vehicle turn performance, navigation, and landing flare were evaluated. The height at which the flare maneuver was performed and turn performance parameters were often adjusted between flights.

Flight Operations

The majority of the flight tests were performed using a Cessna C206 aircraft with side door. After the completion of all flight checklists, the vehicle landing location and ground wind speed and direction were loaded into the flight computer. Prior to loading into the aircraft, GPS lock was achieved using the vehicle-mounted GPS antenna. The vehicle was then loaded into the aircraft and connected to the external (aircraft-mounted) GPS antenna. During launch, an umbilical cord was separated, and the vehicle was switched over to the vehicle-mounted antenna via an internal switch. The external GPS antenna was removed after Flight 22 (see Results). Following a successful launch and parachute deployment, it was necessary to manually command full brakes to release the control lines. Left and right turns would be performed to verify free controls and generally check the health of the system. Approximately 1 min after launch, the auto mode was selected.

The auto mode approach consisted of a direct approach to the landing site, loiter above the target, j-turn to final approach, and the landing flare. The geometry of the landing maneuver is included in figure 2. The first phase begins at the initiation of the auto mode, commanding the vehicle at a constant heading toward the target. At a point called waypoint 1 (WP1), the vehicle transitions to a loiter, during which the vehicle flies in an oval pattern until reaching an altitude A2 (300 ft). The initiation of the second turn in the loiter oval is called WP2. At the altitude A2, the vehicle flies downwind and transitions to the j-turn at WP4. The vehicle begins its final approach at 100 ft AGL. The sonar altimeter begins operation at about 35 ft AGL, and the flare maneuver is initiated approximately 25 ft AGL.

Results

A series of eight flights was performed in the auto mode during November and December 1992. The flight numbering system began at Flight 1 with the "slope soaring" tests. The auto mode tests are numbers 20 through 28. A summary of each of the tests is included below.

Flight 20 11/19/92 The vehicle was launched downwind of the target, and once GPS position was locked in, the vehicle performed several "figure 8" maneuvers. It appeared that the vehicle was having difficulty acquiring or maintaining a track to the landing site. The vehicle was then switched back to manual mode for the remainder of the flight, including the landing. Discussion with skydivers who had made jumps a few minutes later indicated the presence of high winds at altitudes above 2000 ft AGL. At the higher altitudes, the vehicle ground track was near stationary. This lack of a pronounced ground track confused the flight software because the velocity relative to the ground was nearly zero or negative.

Flight 21 11/24/92 This launch was again to the downwind side of the target, and the winds at altitude appeared low, judging by the lack of wind turbine activity at nearby Mojave. When put into the auto mode, the vehicle again performed the "figure 8" maneuvers as on Flight 20. The vehicle was then flown to the final approach in manual mode and returned to auto to perform the landing flare. Shortly before touchdown, the vehicle flew over a 5-ft deep ditch, which affected the final flare logic. The final rate of descent at touchdown was measured at 3.5 ft/s.

Flight 22 11/24/92 Upon loading the vehicle into the launch aircraft, a problem was discovered with the external (airplane mounted) GPS antenna. After some diagnostic checking and discussion, it was decided to fly without the use of this antenna. As a result of this problem, launch did not occur until 55 min after the wind information was programmed into the flight computer (as a point of comparison, the time between wind loading and flight is normally about 15 min). During this time, the wind direction changed and resulted in a 5-kn downwind landing. Launch was performed upwind of the target, and the vehicle was flown manually for approximately 90 sec to ensure good GPS lock and to establish a ground track prior to auto mode initiation. In auto mode, there were no "figure 8" maneuvers, and the vehicle remained in auto mode for the remainder of the flight. Several good holding patterns were flown. The landing was a bit harder, similar to a downwind landing in an aircraft. Postflight review of the data indicates that GPS lock was achieved about 45 sec after launch, compared with 35 sec on Flight 21 in which an external GPS antenna was used. Thus, it was decided to remove the external GPS antenna from the launch aircraft.

Flight 23 12/2/92 This flight was landed in the auto mode in the open desert. The landing flare maneuver was initiated at 25 ft AGL and was performed nearly perfectly with a vertical velocity near zero. It was noted that landings on the uneven desert surface produced significant scatter in the sonar altimeter readings.

Flight 24 12/2/92 This flight was landed on a smooth surface in the manual mode, with partial brakes, but no final flare. During Flights 23 and 24, ground winds were near zero, but the upper altitude winds were significant. This caused the navigation logic to input spurious maneuvers, including the "figure 8" maneuvers seen previously. The results of these two flights prompted the team to update the flight control system to hold magnetic heading whenever the GPS and magnetic compass readings differ by more than 45 deg.

Flight 25 12/10/92 This flight was a test of the software modification discussed above. The software gains were reduced on the navigation turns ("baby turns") and were increased on the large maneuvering turns. The oscillations were eliminated on this flight; however, the navigation turns were reduced too much, causing heading changes that took too long to return the vehicle to the desired heading. Also, the maneuvering turns resulted in

270 deg turns being required to accomplish a 180 deg heading change.

Flight 26 12/10/92 The gains for large maneuvering turns were reduced on this flight and produced satisfactory results.

Flight 27 12/10/92 The gains for small navigation turns were increased and produced a nearly perfect autonomous flight. The landing flare maneuver resulted in a vertical velocity at touchdown less than 1 ft/s at a point 662 ft from the target.

Flight 28 12/10/92 After performing five successful autonomous landing flares, it was decided to deploy Flight 28 at an altitude of 8500 ft AGL. To return the vehicle to the landing site, ground control had to be used at high altitude, because it was discovered that the GPS short-term guidance did not function properly when the vehicle drifts backward in high winds. As a result, the software was modified to use the magnetic compass heading for short-term corrections. An auto mode landing profile from sonar altimeter initiation to touchdown is included in figure 3.

Conclusions

Under JSC sponsorship, NASA Dryden Flight Research Facility has developed and demonstrated a fully autonomous approach and landing system for application to future spacecraft recovery. Using existing technologies, the autonomous system was demonstrated during the last 2 months of contract year 1992 in a series of eight successful flights. The program was successful in proving the concept of autonomous landing using simple open-loop methods, and additional work during the next year will improve the knowledge base. A final report is in progress. Additional work during the next year is discussed below.

Future Plans

This flight test activity is being continued in fiscal year 1993 in three areas: upgraded software to include wind sensing, evaluation of alternative landing flare techniques, and evaluation of various lift-to-drag gliding parachutes. Aerodynamic instrumentation will be included in the spacecraft to allow for postflight analysis of vehicle performance.

The first task will include the evaluation of a variety of parachutes including smaller, more maneuverable parachutes and high-glide paragliders. Measurements of turn rate, rate of descent, glide ratio, and flare performance will be recorded and compared. The addition of aerodynamic instrumentation including a "tattletale" type accelerometer and rate gyro package will also be included as part of this task to improve the quality of flight data received.

The second task will consist of an evaluation of alternative landing flare techniques using the second

vehicle modified with the addition of radio control. The trailing edge retraction flare using an actuator, while perfectly suitable for small models, will be difficult to incorporate into full-scale spacecraft because of weight and power requirements. A variety of methods for performing the landing flare maneuver will be investigated and their performance compared under a variety of wing loadings. Sensitivity to flare initiation altitude and vehicle dynamics at touchdown will be evaluated in the flights.

The third task consists of upgrading flight algorithms to include some method for compensating for wind during the descent. Data from the existing magnetic compass and the GPS receiver could be used to compute wind magnitude and direction in real time. Ground-based systems for measuring wind profiles will also be investigated to uplink to the vehicle.

References

- ¹Hinson, J. K., Application of Gliding Parachutes to the Space Station Crew Emergency Return Vehicle, JSC-22820, December 1987.
- ²Knacke, T. W., Parachute Recovery Systems Design Manual, NWC-TP-6575, 1992.
- ³Libby, Charles E. and J. L. Johnson, Jr., Stalling and Tumbling of a Radio-Controlled Parawing Airplane Model. NASA-TN-D-2291, July 1964.
- ⁴Maydew, R. C. and C. W. Peterson, Design and Testing of High Performance Parachute, AGARD-AG-391, November 1991.
- ⁵Naeseth, Roger L., An Exploratory Study of a Parawing High Lift Device for Aircraft, NASA-TN-D-629, 1960.
- ⁶Wailles, W. K., Advanced Recovery Systems for Advanced Launch Vehicles Phase 1 Study Results, AIAA-89-0881, April 1989.
- ⁷Ware, G. M. and J. L. Hassel, Jr., Wind Tunnel Investigation of Ram-Air Inflated All-Flexible Wings of Aspect Ratios 1.0 to 3.0, NASA TM SX-1923, December 1969.

Acknowledgments

The following organizations and personnel have been involved in the project:

- Principal Investigator: Robert Meyerson (EG3/NASA Johnson Space Center)
- Dryden Technical Program Coordinator: Alex Sim (Code XRA/NASA Dryden)
- Research Engineer and co-P.L.: James Murray (Code XRA/NASA Dryden)
- Project Engineer: R. Dale Reed (PRC Inc. at NASA Dryden)
- Research Model Engineer/Technician: Dave Neufield (Code XOI/NASA Dryden)

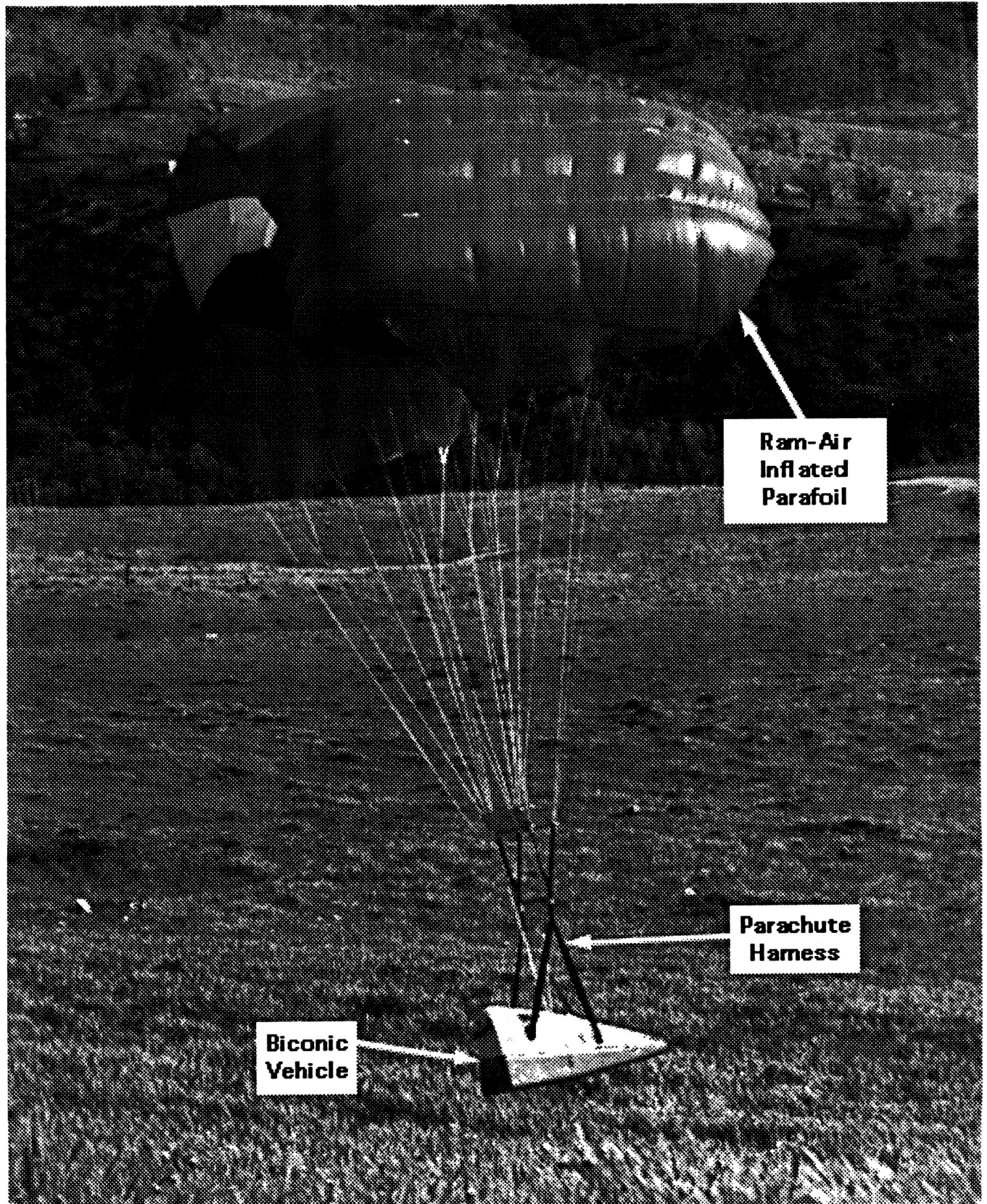


Figure 1. Flight Test Vehicle.

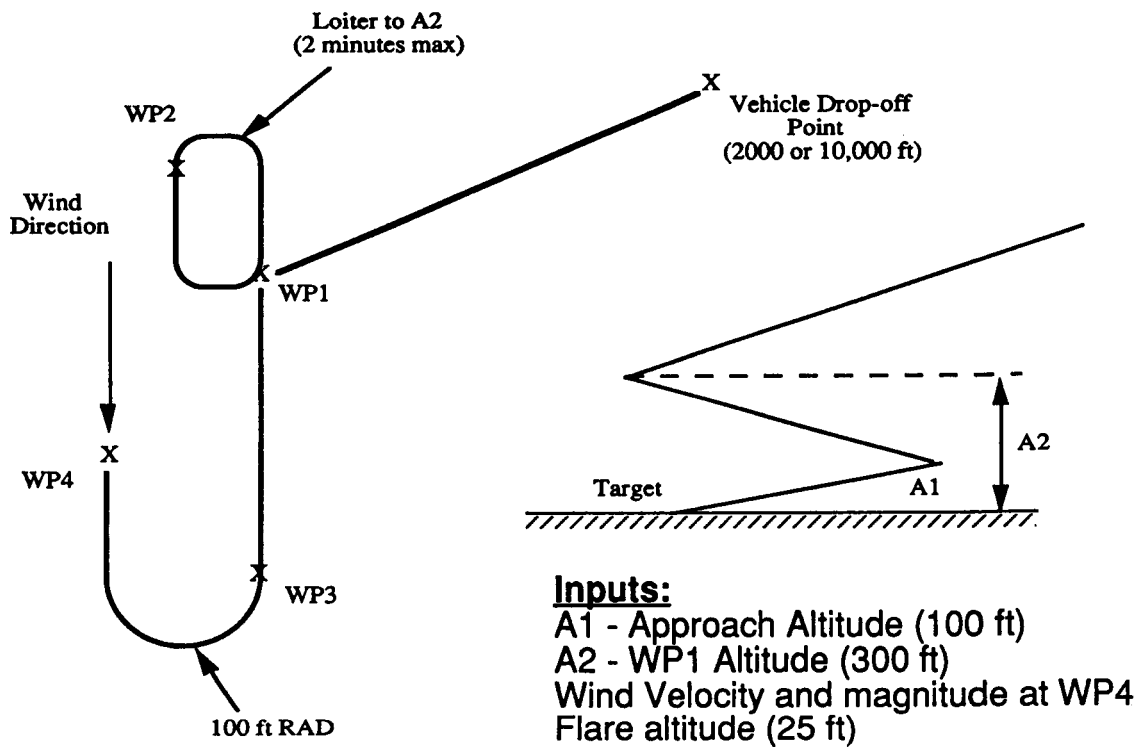


Figure 2. Approach and Landing Geometry.

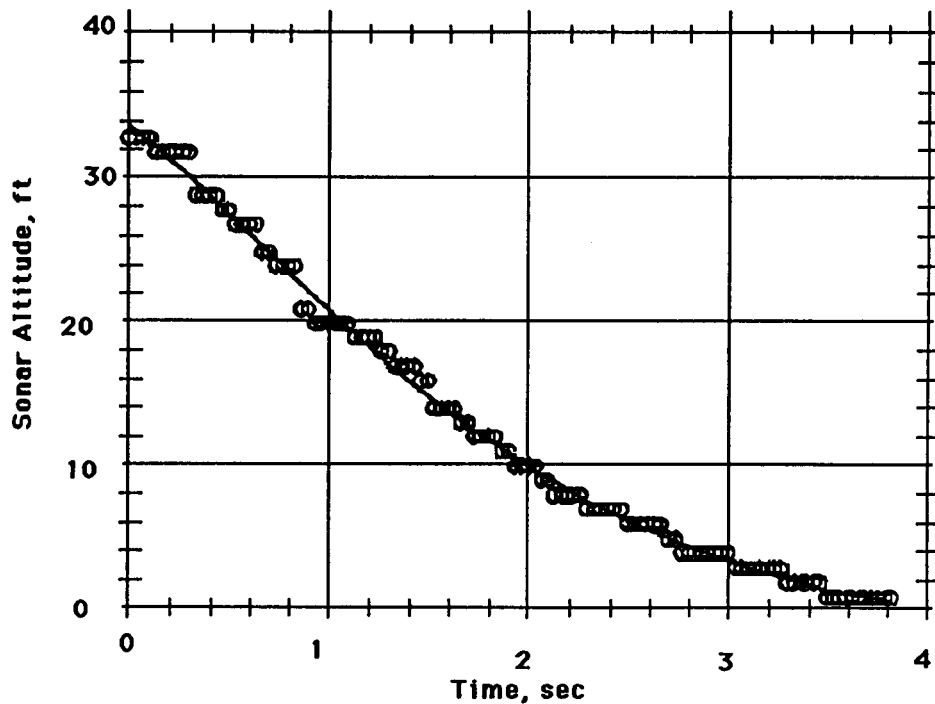


Figure 3. Auto Mode Landing.

Avionics Reference Model

David Pruett
Johnson Space Center/EK

Abstract

Current trends in avionics design and implementation are heading toward more extensive use of accepted standards in all areas of hardware and software design and implementation. Following development work over the last 5 years in the more general area of computer and information sciences standards work, a reference model for avionics has been developed compatible with the Institute of Electrical and Electronic Engineers (IEEE) P1003.0 reference model for application software portability and the International Organization for Standardization - Open Systems Interconnection (ISO OSI) reference model. This paper describes some of the aspects of the avionics reference model. This work was done over the last 2 years in a collaborative way between the Flight Data Systems Division and Lockheed Engineering and Sciences Company (LESC).

Introduction

The ISO established the first reference model for use with standards. Its purpose was to allow standards users and developers to work within a common framework. The developers would use the framework, or reference model, to define functionality and completeness of standard specifications. The users would use the reference model to develop profiles of selected and tailored standards that work together to meet specific program requirements.

Over the last 5 years, the IEEE, through the Portable Operating System Interface (POSIX) P1003 committee, has been working on a broader reference model targeted for the development of profiles that allow application software portability and interoperability across heterogeneous platforms. The P1003.0 reference model is sufficiently generic to apply to a wide variety of platform types represented within the P1003 standards activities.

The avionics reference model elaborates on the P1003.0 reference model to one more level of detail to identify significant interfaces and functions within the application platform that are not addressed by the P1003.0 reference model.

Problem Statement

Obvious trends are being followed within the avionics development and user communities that point to continued and increased use of standards in the development of flight systems. The trend will not be

aided by the ever increasing numbers of standards; it will only make it more difficult to select a compatible set. It was this same issue that forced the OSI community to adopt a reference model to provide a way of producing a compatible set of standards tailored for a specific application. Not only are network communications standards continuing to be developed, but the latest trends are in the definition of software interface standards or Application Program Interface Definitions. A reference model for avionics is needed that would provide a structure for developing profiles of standards that meet specific mission needs beyond network communications.

Approach

The work described here began with existing reference models within the standards communities, specifically, the OSI reference model [ISO7498] and the IEEE POSIX P1003.0 reference model [IEEEP1003.0]. The limitation of the OSI model to communications prevented its expansion to the needs of the avionics reference model. The scope of the P1003.0 model is very broad, encompassing information systems from real time to batch, but because it included real-time capabilities, it was inferred that further specifications within that model would lead to a workable avionics model. Additionally, by starting with the P1003.0 model, the avionics model was assured of incorporating the OSI model since they are compatible.

The relationships of the P1003.0 reference model to avionics has a long history. When the P1003.0 committee was formed, the first text presented to it consisted of extracts from a NASA Space Station Program Architecture Requirements document for the Space Station Information System. That document attempted to describe the overall Space Station command and telemetry information structure in terms of interfaces between the various elements from flight systems to ground systems and the standards that were to be utilized to effect communication interoperability. But, other requirements on the information system required software interoperability and portability. To architect such a requirement, another set of interfaces was defined having to do with the logical connectivity of software functions in flight systems and ground systems. This separation of physical communications interface standards requirements and software logical (i.e., nonphysical) connectivity formed the basis of the text presented to the P1003.0 committee. That concept has been carried out in the final P1003.0 reference model. The physical

connectivity interface is defined as the external entity interface (EEI), and the software logical interface is defined as the application program interface.

To determine the range of possible mission specific requirements on an avionics system, an attempt was made to quantify the avionics performance requirements, at a high level, for current and future spaceflight systems. These requirements were compiled but showed no significant needs that would impact the eventual reference model. It is in the selection of standards for a specific mission that these performance requirements would have impacted.

Because the work was performed within and for the Flight Data Systems Division, the reference model as it exists now is heavily oriented toward data system capabilities. We were limited in manpower to be able to expand the detail to other systems that are part of avionics in general.

Results

There are three components to the avionics reference model. The generic system architecture, which identifies high-level functional blocks and interfaces for the avionics along with operational systems, is not necessarily part of a vehicle. The generic functional architecture identifies generic atomic functions for Space Data Systems (additional functional architectures for other components of the avionics suite can and should be developed, but this was beyond the scope of our activity). The architecture interface model defines an interface class structure that is directly related to the P1003.0 reference model. This paper will describe the second two parts. All three are defined in the two documents produced from this project [WRAY1992-1] [WRAY1992-2].

Generic Functional Architecture

Past and future avionics systems for spaceflight vehicles were reviewed, and the essential functional components of the space data system were identified and categorized. Five major functional categories were identified along with detailed functionality to two levels within each category. Table 1 provides the details of the functional components. This information is useful in identifying which subfunctions are required, based on a given mission requirements statement, and was used successfully in the development of a data system design for the Artemis common lunar lander. No locality is implied for these functions; in fact, these functions can be performed on the ground as well as within the spacecraft, depending on mission requirements.

Architecture Interface Model

The architecture interface model is structured around the concept of classes of interfaces. The interface model identifies six classes of interfaces that describe

completely the connectivity within and external to an avionics system. The classes of interfaces are grouped by hardware-oriented interfaces, software-oriented interfaces, physical interfaces, and logical (or functional) interfaces.

The classes of interfaces are also mapped into the two interfaces of the P1003.0 model EEI (hardware interfaces) and API (software interfaces). Figure 1 is a graphical representation of the avionics reference model, which includes the relationship to the POSIX P1003.0 reference model.

Definitions

A hardware interface is an interface between two hardware components or between a hardware component and a software component.

A software interface is an interface between two software components.

A physical interface is defined as the routing requirements associated with passing data from the source of the data to the end user of the data. Data are used by an entity in a physical manner if it passes the data on without using or changing the data; for example, network operating systems are physical interfaces to applications because they package or unpack data and send it to another network node. Both hardware and software physical interfaces apply.

A logical interface is defined as the characteristic requirements associated with an interaction between a source of data and the end user of the data. For instance, a communications application that receives data from a global positioning system satellite formats the data into a package of information, and passes it to the guidance, navigation, and control (GN&C) application must define a "logical" interface with the GN&C application that defines the content and meaning of the data transferred. These data will pass through an arbitrary and mission-dependent number of "physical" interfaces. Logical interfaces normally exist only between software components; however, this is only because the functionality associated with logical interfaces is sufficiently complex to prohibit hardware implementation as yet.

Interface Class Descriptions

Class 1 hardware physical interfaces are the direct connections between different types of hardware such as those needed to enable buses and communications links between processors.

Class 2 hardware-to-system software physical interfaces are the direct connections between hardware registers and software drivers, such as those needed to enable address registers to move bit patterns from hardware to software, and service drivers that can respond to the bit patterns.

Class 3 system-software-to-system software physical interfaces are the direct connections between operating

system service code and local system services software code.

Class 4 system software-to-other-system software logical interfaces are the indirect connections that enable local system service software within two physically separated application platforms to interoperate.

Class 5 system-software-to-applications-software physical interfaces are the direct connections that enable software service code to access and process data from local application software code.

Class 6 applications-software-to-applications-software logical interfaces are the indirect connections that enable an application originating data to pass the data to an application that needs to use the data, or enable an application needing data to determine the source from which the data must be obtained. This interface provides the indirect connections that allow applications in different systems or in the same system to communicate, thus enabling applications software to interact across system boundaries or within system boundaries to accomplish a mutual purpose. These interfaces may be applicable to applications executing in the same processor, in different processors in the same node, or in different systems.

Use of Reference Model

To use this interface model, a system user or developer will define the functions of the system at the interfaces and then select relevant standards as necessary. This process is called "profiling" within the standards community. This process will also identify areas where standards are not defined that require definition work for the system.

Conclusions

The next step for the reference model is to have it reviewed and modified by an interested standards setting

body. That is currently in progress. The reference model was presented to the Society of Automotive Engineers in October 1992. They are currently reviewing the reference model and determining what action to take on it. We are continuing to pursue the expansion of the model in more detail within the flight data systems area and are beginning to develop a mode, state, and functional simulation model of a generic flight data system based on this work.

References

- ¹International Organization for Standardization, "Information Processing Systems - Open Systems Interconnection - Basic Reference Model," *Draft International Standard 7498*, October 1984.
- ²Institute of Electrical and Electronic Engineers, "Guide to The POSIX Open Systems Environment," *Draft Standard P1003.0*, (latest draft).
- ³Wray, Richard and Stovall, John, "Space Generic Open Avionics Architecture (SGOAA) Standard Specification," LESC-30354, December 1992.
- ⁴Wray, Richard and Stovall, John, "Space Generic Open Avionics Architecture (SGOAA) Reference Model Technical Guide," LESC-30347, December 1992.

Acknowledgments

This work was performed in a collaborative environment between NASA and Lockheed. The Lockheed participants were Dick Wray, John Stovall, and Ben Doeckel. Support of this effort was provided by the Strategic Avionics Technology Working Group (SATWG) chaired by Dr. Ken Cox, Chief Navigation Control and Aeronautics Division, JSC and the Strategic Avionics Architecture Panel of SATWG chaired by Ed Chevers, Deputy Division Chief, Information Sciences, Ames Research Center.

Table 1. Space Data System Services

Standard Data Services Manager	Data System Manager	Operating System	Data Base Manager	Network Services Manager
<ul style="list-style-type: none"> • Standard Services Data Acquisition Controller - Data Bus Services - Sensor and Effector Input/Output - Sensor Pre-Processing Services - Distributed Data Read/Write - Journal Manager • Standard Services Data distribution - Caution and Warning Processing - Telemetry Processing - History Processing • Reports Generator - tables - Forms - Outputs 	<ul style="list-style-type: none"> • Configuration Manager - Upload Software Tables Change Management - Reconfiguration HW/SW - Maintain System configuration • Timing Service Controller - Monitor Timing Service - Automatic Timing Reconfiguration - Manual Timing Reconfiguration - Update Timing - Resynchronize Timing • Data System Initialization, Startup and Reconfiguration - Identify SW to be loaded - Load and Initialize SW - Terminate Software - Process Initialization and Reload Requests • DSM Health, Status and FDIR Controller - Collect Health Status and Failure Data - Process Health Status and Failure data - Automatic Reconfiguration - Manual Reconfiguration - Update History Data Base 	<ul style="list-style-type: none"> • OS Kernel - Process Management and Control - Initialization and Configuration Management - I/O Management - Memory Management - CPU Management - Utility Services - Privacy and Security Management • ADA RTE - Ada Compiler Support - Ada/Non-Ada Mixed Environment • OS/RTE Extensions - Real-Time Applications Task Control and Communications - Ada Multi-Program Management - Inter-Process Communications - Internal Bus Management - OS/RTE Initialization and Self Test - Precision Time Distribution • Non-Standard Processor Services 	<ul style="list-style-type: none"> • File Service Controller - Sequential File Services - Structured File Services - Distributed File services - Resource Management (in mass store) • Distributed File Transfer Service Controller - Internal System Node Transfers - Recording Control - Ground Archives • File Transfer Access and Management Controller - External Node Transfers - Virtual/real file mapping (in mass store) 	<ul style="list-style-type: none"> • Network Services Controller - Network Command Verification - Network Stack Controller - Network Queue Management - Stack • Network Manager - Network Coordinator - Network Status Directory - Network Fault Detection - Stack Layer Management - Network Security Management - Network Performance Status • Remote Operator • Network Directory Service Controller - Directory User Agent - Directory System Agent - Directory Information Base - Directory Information Tree • Network Association Controller

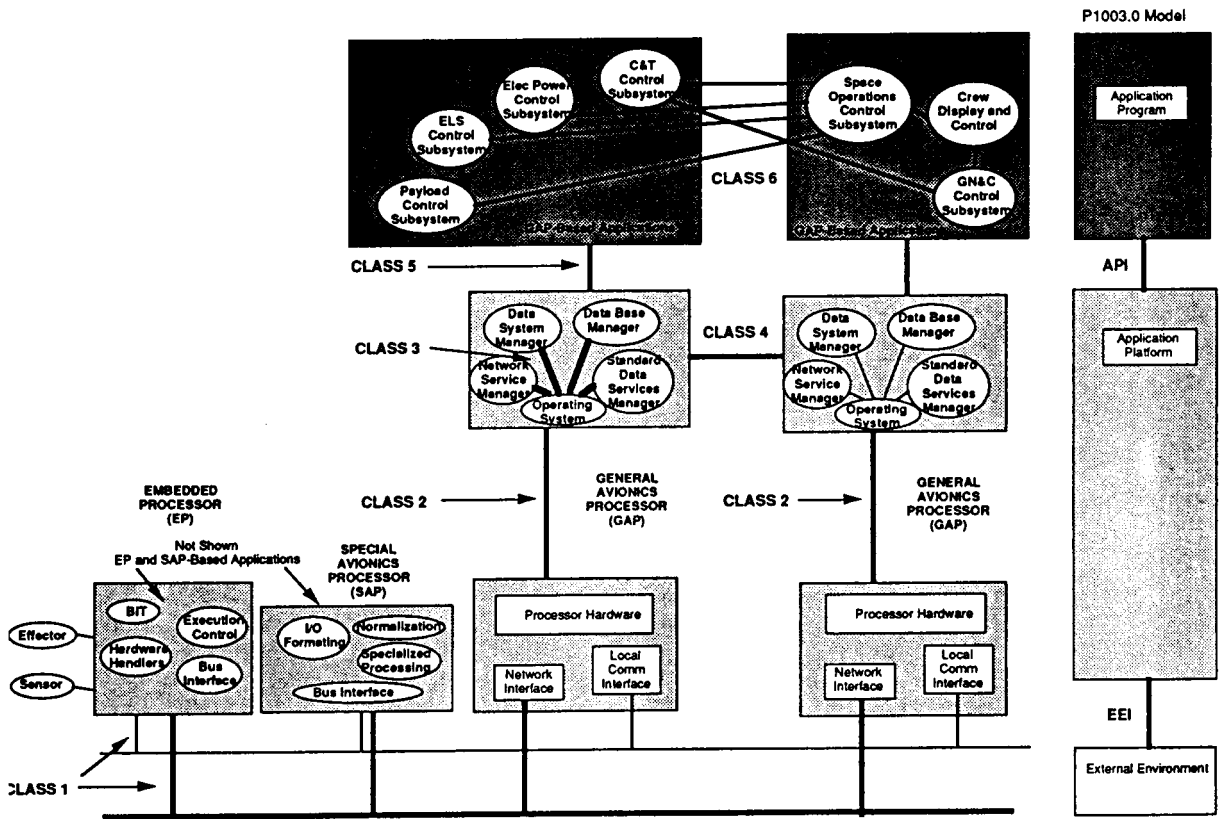


Figure 1. Representation of Avionics Reference Model and Its Relationship to the P1003.0 Reference Model.

REPORT DOCUMENTATION PAGE

Form Approved
OMB No. 0704-0188

Public reporting burden for this collection of information is estimated to average 1 hour per response, including the time for reviewing instructions, searching existing data sources, gathering and maintaining the data needed, and completing and reviewing the collection of information. Send comments regarding this burden estimate or any other aspect of this collection of information, including suggestions for reducing this burden, to Washington Headquarters Services, Directorate for Information Operations and Reports, 1215 Jefferson Davis Highway, Suite 1204, Arlington, VA 22202-4302, and to the Office of Management and Budget, Paperwork Reduction Project (0704-0188), Washington, DC 20503.

1. AGENCY USE ONLY (Leave blank)	2. REPORT DATE August 1993	3. REPORT TYPE AND DATES COVERED Technical Memorandum	
4. TITLE AND SUBTITLE The JSC Research and Development Annual Report 1992		5. FUNDING NUMBERS	
6. AUTHOR(S)		8. PERFORMING ORGANIZATION REPORT NUMBER S-731	
7. PERFORMING ORGANIZATION NAME(S) AND ADDRESS(ES) Lyndon B. Johnson Space Center Houston, Texas 77058		10. SPONSORING / MONITORING AGENCY REPORT NUMBER NASA TM 104777	
9. SPONSORING / MONITORING AGENCY NAME(S) AND ADDRESS(ES) National Aeronautics and Space Administration Washington, D.C. 20546-001		11. SUPPLEMENTARY NOTES	
12a. DISTRIBUTION / AVAILABILITY STATEMENT Unclassified/Unlimited Publicly Available Subject Category 99		National Technical Info. Service 5285 Port Royal Road Springfield, VA 22161 (703) 487-4600	12b. DISTRIBUTION CODE
13. ABSTRACT (<i>Maximum 200 words</i>) Issued as a companion to Johnson Space Center's Research and Technology Annual Report, which reports JSC accomplishments under NASA Research and Technology Operating Plan (RTOP) funding, this report describes 42 additional JSC projects that are funded through sources other than the RTOP. Emerging technologies in four major disciplines are summarized: space systems technology, medical and life sciences, mission operations, and computer systems. Although these projects focus on support of human spacecraft design, development, and safety, most have wide civil and commercial applications in areas such as advanced materials, superconductors, advanced semiconductors, digital imaging, high density data storage, high performance computers, optoelectronics, artificial intelligence, robotics and automation, sensors, biotechnology, medical devices and diagnosis, and human factors engineering.			
14. SUBJECT TERMS Research Projects, Research and Development, NASA Programs, Technology Utilization, Space Technology Experiments		15. NUMBER OF PAGES 246	16. PRICE CODE
17. SECURITY CLASSIFICATION OF REPORT Unclassified	18. SECURITY CLASSIFICATION OF THIS PAGE Unclassified	19. SECURITY CLASSIFICATION OF ABSTRACT Unclassified	20. LIMITATION OF ABSTRACT Unlimited